Regulation of the Ctf19^{CCAN} protein complex at the budding yeast kinetochore

Inaugural-Dissertation
zur Erlangung des Doktorgrades
Dr. rer. nat.

der Fakultät für Biologie
an der

UNIVERSITÄT DUISBURG-ESSEN

vorgelegt von
Miriam Böhm
(geb. Lutomski)
aus Duisburg

Dezember 2020

Die der vorliegenden Arbeit zugrunde liegenden Experimente wurden in der Abteilung für Molekulare Genetik I der Universität Duisburg-Essen durchgeführt.

1. Gutachter: Prof. Dr. Stefan Westermann
2. Gutachter: Prof. Dr. Doris Hellerschmied-Jelinek
3. Gutachter: -

Vorsitzender des Prüfungsausschusses: Prof. Dr. Hemmo Meyer

Tag der mündlichen Prüfung: 16.04.2021

DuEPublico
Duisburg-Essen Publications online

UNIVERSITÄT DUISBURG ESSEN
Offen im Denken

ub | universitäts bibliothek

Diese Dissertation wird via DuEPublico, dem Dokumenten- und Publikationsserver der Universität Duisburg-Essen, zur Verfügung gestellt und liegt auch als Print-Version vor.

DOI: 10.17185/duepublico/74290
URN: urn:nbn:de:hbz:465-20220628-121458-0

Alle Rechte vorbehalten.

In the context of this doctoral work, the following articles were published:

Killinger, K., **Böhm, M.**, Steinbach, P., Hagemann, G., Blüggel, M., Jänen, K., Hohoff, S., Bayer, P., Herzog, F. and Westermann, S. (2020). Auto-inhibition of Mif2/CENP-C ensures centromere-dependent kinetochore assembly in budding yeast. EMBO J *39*, e102938, doi: 10.15252/embj.2019102938

Böhm, M., Killinger, K., Dudziak, A., Jänen, K., Hohoff, S., Mechtler, K., Örd, M., Loog, M. and Westermann, S. (2021). Assembly-sensitive SCF-Cdc4 phospho-degrons regulate kinetochore stability in mitosis. *Manuscript submitted for publication*

SUMMARY

A correct chromosome-microtubule interaction is crucial for mitotic and meiotic divisions in every living eukaryotic organism. The proteinaceous structures that are responsible for the correct attachment of chromosomes to microtubules are called kinetochores. Kinetochores are large multiprotein complexes that create a binding interface for the dynamic spindle on centromeres to ensure a correct sister-chromatid segregation in mitosis or the segregation of homologous chromosomes in meiosis I. In the budding yeast *Saccharomyces cerevisiae*, a single microtubule attaches to a specialized nucleosome containing the protein Cse4/CENP-A in exchange for the histone protein H3 at the centromeric region. Kinetochore assembly in budding yeast has to be timely and spatially regulated, in order to allow bi-oriented microtubule binding as soon as the centromeric DNA is replicated. How efficient kinetochore assembly is coupled to cell cycle progression is not well understood.

This study provides new insights into mechanisms of phospho-regulation of the $Ctf19^{CCAN}$ protein complex through a detailed analysis of the essential inner kinetochore component Ame1/CENP-U, a subunit of the COMA subcomplex. Biochemical analysis in this study indicates that phosphorylation of Ame1 does not influence the ability to bind known interaction partners like the outer kinetochore complex Mtw1c, the essential CCAN component Mif2 or centromeric DNA. Biochemical and genetic experiments reveal that a major function of CDK phosphorylation of Ame1 is the regulation of protein levels, most clearly demonstrated after challenging cells with excess Ame1/Okp1. In particular Ame1 residues Ser41/Ser45 and Ser52/Ser53 were identified as Cdc28/Clb2 phosphorylation sites that constitute phospho-degron sequences which allow binding of the E3 ubiquitin ligase complex SCF with the F-Box phospho-adapter Cdc4. Cell cycle analysis of endogenous Ame1 revealed that degron motifs are activated stepwise in a cell cycle dependent manner, leading to full phosphorylation in M-Phase and subsequent degradation via SCF-mediated ubiquitination in mitosis. Phosphorylation and degradation are prevented upon interaction of Ame1 with the Mtw1 complex creating a safety mechanism to only remove free subcomplexes of Ame1/Okp1, that would otherwise favor ectopic kinetochore assembly. Artificially creating stronger Cdc4-degron sequences on Ame1 compromised viability in otherwise wildtype cells but was able to partially suppress the growth phenotypes of *cdc4* mutants. Apart from Ame1, also the COMA complex subunit Mcm21 is phosphorylated in a cell cycle dependent manner and

it is shown that the overexpression of COMA complexes is toxic for cells, explaining why protein levels need to be carefully controlled. In addition to this regulatory mechanism, a novel protein-protein interaction site on the Ame1 C-Terminus was identified, which is responsible for the binding of Ame1/Okp1 to the heterodimer Nkp1/Nkp2. In summary, a novel mechanism for a restricted kinetochore assembly is presented that requires a CDK-mediated phosphorylation and ubiquitination of kinetochore subunits by SCF^{Cdc4}.

CONTENTS

SUMMARY **5**

CONTENTS **7**

ABBREVIATIONS **11**

LIST OF FIGURES **13**

LIST OF TABLES **15**

I. INTRODUCTION **16**

1.1 Cell division is the basis of life **16**

1.1.2 The life cycle of budding yeast 17

1.1.3 Mitosis – how cells achieve their exact genetic reproduction 19

1.1.4 Checkpoints – the bodyguards of the cell cycle 20

1.1.5 The clockwork of the cell division cycle 22

1.2 The ubiquitin-proteasome system in *S. cerevisiae* **25**

1.2.1 The E3 ubiquitin ligase complex SCF^{Cdc4} ubiquitinates phosphorylated target proteins 28

1.2.2 E3 ubiquitin ligase complexes regulate protein levels during cell division 29

1.3 Kinetochores are structural and regulatory complexes for correct chromosome segregation **33**

1.3.1 Centromeres – the basis for kinetochore assembly 33

1.3.2 Kinetochores assemble on centromeric chromatin 35

1.3.3 Posttranslational modifications allow SAC function and error correction 38

1.3.4 Posttranslational modifications of Cse4 avoid ectopic kinetochore assembly 39

1.3.5 Inner kinetochore components specify kinetochore localization 40

1.4 Objectives **42**

II. MATERIALS AND METHODS **43**

2.1 Instrumentation and Software **43**

2.2 Chemicals **46**

2.3 Frequently used buffers and solutions **49**

2.4 Enzymes **55**

2.5 Kits **55**

2.6 *Saccharomyces cerevisiae* strains **56**

2.7 Generated and used plasmids **56**

2.8 Antibodies **57**

2.9 Recombinant proteins **58**

2.10 Plasmid generation in *E. coli* **59**

2.11 Bacterial expression in *E. coli* **60**

2.11.1 Purification of recombinant Ame1/Okp1 complexes 61

2.11.2 Purification of Nkp1/Nkp2 complex 61

2.11.3 Purification of Mtw1c and Mtw1/Nnf1 complexes 62

2.12 Protein expression in *S. cerevisiae* **62**

2.12.1 Purification of Cdc28/Clb2 kinase 63

2.13 Generation of *S. cerevisiae* strains **64**

2.13.1 Transformation of *S. cerevisiae* 64

2.13.2 Genetic crossing and mating of *S. cerevisiae* 66

2.13.3 Genomic DNA isolation from *S. cerevisiae* 67

2.13.4 Verification of newly generated strains 67

2.14 Cell cycle arrests of *S. cerevisiae* **68**

2.14.1 FACS analysis 68

2.15 GAL-Shift assay **68**

2.16 Serial dilution of *S. cerevisiae* **69**

2.16.1 The anchor-away technique 69

2.17 Colony sectoring assay of *S. cerevisiae* **69**

2.18 Preparation of whole cell lysates from *S. cerevisiae* **70**

2.18.1 Quick & Dirty method to prepare whole cell lysates 70

2.18.2 Extended method to prepare clear yeast cell extracts 70

2.19 Biochemical analysis of yeast proteins **71**

2.19.1 Polyacrylamide gel electrophoresis 71

2.19.2 Western Blotting 72

2.19.3 Electrophoretic mobility shift assay (EMSA) 72

2.19.4 Analytical Size Exclusion Chromatography 72

2.19.5 *In vitro* kinase assays 73

III. RESULTS 74

3.1 Biochemical analyses of Ame1-WT and phosphorylation mutants 74

3.1.1 Recombinant Ame1-WT and phosphorylation mutants have similar biochemical properties 74

3.1.2 Ame1-WT/Okp1 and Ame1 mutants bind DNA in a similar manner 76

3.1.3 Ame1/Okp1 wildtype and mutant complexes bind equally well to the outer kinetochore component Mtw1c in solution 77

3.1.4 The Ame1/Okp1 complex binds to the main inner kinetochore component Mif2 78

3.1.5 Purification of N- and C-terminal truncation mutants of AOc 79

3.1.6 Ame1/Okp1 complexes with truncated proteins bind equally well to DNA 81

3.1.7 Nkp1/Nkp2 binds to the C-termini of Ame1 and Okp1 82

3.1.8 Nkp1/Nkp2 and DNA bind to Ame1/Okp1 competitively 85

3.2 Ame1 is a target for the cyclin dependent kinase (CDK) *in vivo* 86

3.2.1 Generation of a non-phosphorylatable mutant of the essential CCAN component Ame1 86

3.2.2 Ame1 phosphorylation mutants do not alter the growth phenotype of budding yeast 87

3.2.3 Manipulation of the Ame1 phosphorylation status in cells 89

3.2.4 Cdc28 is at least partially responsible for the phosphorylation of Ame1 90

3.2.5 Phosphorylation of Ame1 changes during cell cycle progression 91

3.2.6 Ame1 phosphorylation mutants display similar localization in cells 92

3.2.7 Purification of Ame1/Okp1 complexes from budding yeast 93

3.2.8 The Ame1-7A mutant displays slightly reduced chromosome transmission fidelity 95

3.2.9 Internal truncations of the Ame1 N-terminus compromise cell viability 96

3.3 Analyzing CDK phosphorylation of Ame1 in more detail using an overexpression system 98

3.3.1 Ame1 phospho-mutants accumulate to increased protein levels after overexpression 98

3.3.2 The E3 ubiquitin ligases Psh1 and Mub1 are not responsible for Ame1 protein level regulation 100

3.3.3 Identification of phospho-degron motifs in Ame1 102

3.3.4 The E3 ubiquitin ligase SCF^{Cdc4} initiates Ame1 degradation 103

3.3.5 Overexpression of Ame1 compromises the growth of SCF mutants 105

3.3.6 Optimizing the phospho-degron sequence on Ame1 enhances its degradation via SCF^{Cdc4} 107

3.4 Phosphorylated forms of endogenous Ame1 accumulate over S-Phase and start to disappear in mitosis 109

3.4.1 Stepwise phosphorylation of endogenous Ame1 occurs at the identified phospho-degron sequences 109

3.4.2 Ame1 phosphorylation patterns change during the cell division cycle 111

3.4.3 Phosphorylated forms of Ame1 disappear in mitosis 112

3.4.4 SCF^{Cdc4} is responsible for degradation of phosphorylated Ame1 in mitosis 113

3.5 *In vitro* kinase assays with Cdc28/Clb2 reveal an Mtw1c binding-sensitive phosphorylation of Ame1 and Okp1 115

3.5.1 Ame1's seven-residue phosphorylation cluster is a target for Cdc28/Clb2 116

3.5.2 Ame1 phosphorylation by Cdc28/Clb2 is sensitive to Mtw1c binding 118

3.6 The COMA complex is a better target for SCF^{Cdc4} 120

3.6.1 Mcm21 is phosphorylated by CDK *in vivo* and *in vitro* 120

3.6.3 Mcm21 is phosphorylated in a cell cycle dependent manner 122

3.6.4 Increased levels of COMA are toxic to yeast cells 123

IV. DISCUSSION 126

4.1 A new role for the Ame1 C-terminus within kinetochore architecture 127

4.2 Ame1 can assemble into the kinetochore independently of its phosphorylation status 129

4.3 An overexpression system to study the consequences of increased AO/COMA levels in the cell 129

4.4 Ame1 phosphorylation by CDK promotes degradation via the E3 ligase SCF^{Cdc4} 130

4.5 CDK phosphorylation is required for regulation of Ame1 protein levels away from kinetochores 132

4.6 Kinases other than CDK might also be involved in COMA phospho-regulation 134

4.7 Kinetochore assembly is restricted to centromeres 135

4.8 COMA complex formation might create a high affinity binding interface for SCF^{Cdc4} 138

4.9 Incorporation into kinetochores prevents Ame1 degradation 140

4.10 CDK-mediated ubiquitination via SCF^{Cdc4} as a novel mechanism for a regulated kinetochore assembly 141

V. SUPPLEMENTARY DATA 143

VI. REFERENCES 159

AKNOWLEDGEMENTS 169

CURRICULUM VITAE 171

DECLARATIONS 173

ABBREVIATIONS

aa	amino acid
AO	Ame1/Okp1
APC/C	Anaphase Promoting Complex/Cyclosome
ATP	Adenosine TriPhosphate
bp	base pairs
BSA	Bovine Serum Albumine
CBF3	Complex of Cep3, Ctf13, Ndc10, Skp1
CCAN	Constitutive Centromere Associated Network
CDEI-III	Centromeric Determining Elements
CDK	Cyclin Dependent Kinase
CENP	CENtromere Protein
CKI	Cyclin dependent Kinase Inhibitor
CM	Ctf19/Mcm21
COMA	Ctf19/Okp1/Mcm21/Ame1
CPD	Cdc4-Phospho-Degron
CV	Column Volume
DIC	Differential Interference Contrast
DMSO	DiMethylSulfOxid
DNA	DesoxyriboNucleic Acid
doADE	dropout ADEnine
doHIS	dropout HIStidine
doLEU	dropout LEUcine
doLYS	dropout LYSine
doTRP	dropout TRyPtophan
doURA	dropout URAcil
EMSA	Electrophoretic Mobility Shift Assay
FACS	Fluorescence-Activating Cell Sorting
FPLC	Fast Protein Liquid Chromatography
FRB	FKBP12-Rapamycin-Binding
GAL-promoter	GALactose inducible promoter
GFP	Green Fluorescent Protein

GTP	Guanosine TriPhosphate
IPTG	IsoPropyl β-d-1-ThioGalactopyranoside
kb	kilo base pairs
KMN	Knl1/Mtw1c/Ndc80c
LB	Lysogeny Broth
MCC	Mitotic Checkpoint Complex
MN	Mtw1/Nnf1
MTOC	MicroTubule-Organizing Center
NN	Nkp1/Nkp2
PEST-rich	Proline, Glutamic acid, Serine, Threonine-rich
PTM	Post-Translational Modification
rpm	rounds per minute
SAC	Spindle Assembly Checkpoint
SCF	Complex of Skp1, Cullin, F-Box protein
SD	Synthetic medium with Dextrose
SDS-PAGE	Sodium Dodecyl Sulfate PolyacrylAmide Gel Electrophoresis
SEC	Size Exclusion Chromatography
SPB	Spindle Pole Body
SRG	Synthetic medium with Raffinose/Galactose
TCEP	Tris-(2-CarboxyEthyl)-Phosphin
TEV-protease	Tobacco Etch Virus-protease
YEPD	Yeast Extract Peptone with Dextrose
YEPRG	Yeast Extract Peptone with Raffinose/Galactose

LIST OF FIGURES

Figure 1.1: The life cycle of the budding yeast *S. cerevisiae*. 18
Figure 1.2: The cell division cycle of *S. cerevisiae* and kinetochore-microtubule attachments. 21
Figure 1.3: Oscillation of cyclin levels and CDK activity over the cell cycle. 24
Figure 1.4: Model of SCF^{Cdc4} bound to a phosphorylated substrate. 27
Figure 1.5: SCF degradation of Sic1 controls S-CDK activation. 30
Figure 1.6: The E3 ligase APC/C with two activator proteins induces late mitosis. 32
Figure 1.7: Overview of the budding yeast kinetochore. 36
Figure 1.8: Kinetochores are assembled from individual building blocks. 37
Figure 2.1: Purification of Cdc28/Clb2. 64
Figure 3.1: Ame1/Okp1 or Ame1 variants 7A and 7E behave similar in SEC. 75
Figure 3.2: Electrophoretic Mobility Shift Assay of AO complexes reveals similar binding to DNA. 76
Figure 3.3: Ame1-WT/7A/7E/Okp1 complex binding to Mtw1c is similar in SEC. 77
Figure 3.4: AO mutant complexes bind to Mif2 in SEC. 78
Figure 3.5: Purification of N- and C-terminal truncation mutants of Ame1/Okp1. 79
Figure 3.6: C- terminal truncation mutants of Ame1/Okp1 can be purified but show different behavior in SEC. 80
Figure 3.7: EMSAs of C- and N-terminal truncations of AOc reveal normal DNA-binding activity. 81
Figure 3.8: Okp1 C-terminus is partially responsible for interaction with Nkp1/Nkp2. 83
Figure 3.9: The C-terminus of Ame1 is essential for NNc interaction. 84
Figure 3.10: In EMSA NNc and DNA bind competitively to AOc full length but not to C-terminal truncation mutants. 85
Figure 3.11: Domain organization and mapped phosphorylation sites of the essential CCAN protein Ame1. 86
Figure 3.12: Phosphorylation mutants in Ame1 do not have a major effect on cell growth. 88
Figure 3.13: Ame1 phospho-mutants display different migration behavior in SDS-PAGE. 89
Figure 3.14: Ame1-WT phosphorylation is at least partially dependent on CDK. 90
Figure 3.15: The phosphorylation pattern of Ame1-WT changes over the cell cycle. .. 91
Figure 3.16: Ame1-WT and mutant proteins localize to kinetochore in a similar fashion. 92
Figure 3.17: Ame1-WT and phospho-mutants copurify a similar set of proteins. 94
Figure 3.18: Chromosome transmission fidelity experiment with Ame1-WT and Ame1-7A. 95
Figure 3.19: Ame1 truncation mutants show that protein length is important for viability. 97
Figure 3.20: Overexpression of Ame1 leads to an accumulation of the phosphorylation mutants relative to the wildtype protein. 99

Figure 3.21: Comparison of Ame1 expression levels in two E3 ubiquitin ligase complex mutants. 101
Figure 3.22: Identification of SCF^{Cdc4} phospho-degrons in Ame1. 102
Figure 3.23: SCF^{Cdc4} complex is responsible for Ame1 protein level regulation. 104
Figure 3.24: AOc overexpression inhibits growth in *skp1-3* or *cdc34-2* backgrounds. 106
Figure 3.25: Placing an optimal CPD into Ame1 counteracts the *cdc4-1* mutant..... 108
Figure 3.26: Two new Ame1 variants allow to follow CPD phosphorylation over the cell cycle. 110
Figure 3.27: Phosphorylated Ame1-3A appears at entry of S-Phase and disappears during mitosis as seen in western blot and FACS profiles. 111
Figure 3.28: Pds1-Myc staining reveals disappearance of Ame1 phospho-forms at anaphase onset. 112
Figure 3.29: Skp1 is necessary for Ame1 degradation in mitosis. 114
Figure 3.30: Overview of recombinant Ame1/Okp1 complexes. 115
Figure 3.31: Ame1 and Okp1 are phosphorylated by Cdc28/Clb2 *in vitro*. 117
Figure 3.32: *In vitro* kinase assays of Ame1 reveal binding-sensitive phosphorylation of Ame1/Okp1. 119
Figure 3.33: Domain organization of Mcm21 and COMA complex formation. 121
Figure 3.34: Mcm21-6xFlag is phosphorylated in a cell cycle dependent manner..... 122
Figure 3.35: Overexpression of either COMA wildtype or COMA phospho-mutants. 124
Figure 3.36: Overexpression of COMA diminishes growth in a wildtype and *skp1-3* mutant background..... 125
Figure 4.1 A new Ame1 structure highlighting the C-terminus as an interaction hub. 128
Figure 4.2: Ame1 and Okp1 are phosphorylated by CDK and show specific docking sites. 133
Figure 4.3: The COMA complex is only accessible for CDK-mediated ubiquitination when it is not incorporated into the kinetochore..... 139
Figure 4.4: Different E3 ligases regulate kinetochore function during cell division. .. 142
Figure S1: Serial dilution assay of integrated Ame1 phosphorylation mutants. 157
Figure S2: Cell cycle experiments with two additional Ame1 phosphorylation mutants to narrow down the important residues for slow migration forms..... 157
Figure S3: Combination of Ame1-WT or phosphorylation mutants with Cnn1-5A or Dsn1-6A does not compromise the growth. 158

LIST OF TABLES

Table 2.1: Instrumentation used in this study..... 43
Table 2.2: Software used in this study 46
Table 2.3: Chemicals used in this study 46
Table 2.4: Solutions and buffers used in this study..... 49
Table 2.5: Enzymes used in this study 55
Table 2.6: Kits used in this study 55
Table 2.7: *S. cerevisiae* background strains used in this study 56
Table 2.8: Plasmid backbones used for genetic experiments in *S. cerevisiae*..... 56
Table 2.9: Plasmid backbones used for expression in *E. coli* or *S.cerevisiae*..... 57
Table 2.10: Antibody solutions with the according dilution and incubation times used in this study. 57
Table 2.11: Recombinant proteins generated and used in this study. 58
Table S1: Extended list of all *S. cerevisiae* strains used in this study..... 143
Table S2: Extended list of plasmids used for genetic experiments in *S. cerevisiae*..... 153
Table S3: Extended list of plasmids used for expression in *E. coli* 156

I. INTRODUCTION

1.1 Cell division is the basis of life

One prerequisite of life is the ability of cells to reproduce themselves, which comprises the competence to undergo cell division. This allows reproduction of an entire unicellular organism like the eukaryote *Saccharomyces cerevisiae*, or maintenance of multicellular organisms like plants, higher vertebrates and humans. Generally speaking, the underlying mechanisms for cell reproduction are conserved from yeast to human and follow the same course of action. In order to allow cell division, the cell needs to duplicate its contents beforehand. The amplification and distribution of some components like organelles take place throughout the cell cycle, whereas others are highly regulated in time. This includes the duplication and segregation of the genetic material, which takes place in S- and M-Phase of the cell division cycle, respectively. In brief summary of the cell cycle, cells enter G1 phase in which they are primed for replication of their genetic material. In synthesis (S) Phase the genetic material gets duplicated, so that it can be separated in M-Phase with help of the mitotic spindle. M-Phase is separated from S-Phase through a phase called G2. Whereas in higher vertebrates and human cells the nuclear envelope has to be dissolved for microtubules to bind to the chromosomes, the nucleus in budding yeast stays intact and intranuclear microtubules are attached to DNA almost throughout the whole cell division cycle (Jaspersen and Winey, 2004). All eukaryotic organisms have in common that proteinaceous machines known as kinetochores serve as an attachment site for spindle microtubules on centromeric DNA (Biggins, 2013; Westermann et al., 2007). It is of uttermost importance that the newly generated cell contains an exact copy of the genetic material, otherwise this might lead to aneuploid chromosome numbers, which might result in irregular cell growth and development of cancer cells within a multicellular organism (Cahill et al., 1998; Sato et al., 2001; Saunders et al., 2000). The budding yeast *S. cerevisiae* is a well-studied eukaryotic model organism, in which many essential biological mechanisms were studied, including the cell division cycle and mitosis. With this study we like to attempt the investigation of kinetochore function and assembly over the cell cycle. Because many kinetochore proteins are conserved from yeast to human the new insights can be extrapolated to higher organisms (Westermann et

al., 2007). *S. cerevisiae* also inherits many different advantages especially for kinetochore research, which will be stated later in detail.

1.1.2 The life cycle of budding yeast

As its name suggests, the budding yeast *S. cerevisiae* is dividing through budding. The appearance of the bud and its gradual increase in growth can be experimentally used to evaluate the cell cycle stage and functions therefore as a marker for cell cycle progression (Figure 1.2).

At the beginning of the cell cycle yeast cells are round in shape and have a diameter of 2-4 µm. This unbudded shape is a marker for G1. As cells start with replication in S-Phase, a small bud emerges from the mother cell and grows until it reaches the size of the mother cell, which marks further progression into mitosis. In budding yeast, S-Phase merges into mitosis since no real G2 exists, because as soon as the centromeric region is replicated, mitosis can start (Kitamura et al., 2007; Morgan, 2007). Entry into mitosis is visible through bud growth to a large budded cell, where the newly emerging bud reaches almost the size of the mother cell. Cytokinesis separates the two cells physically and a new cell cycle in both cells can begin. Yeast can undergo the mitotic division as a stable haploid and a stable diploid cell, the only difference being that diploid cells are slightly bigger with a diameter of 4-6 µm. Two haploid cells can fuse and form a new diploid strain, a process which is known as mating. This can be used as a genetic tool to combine two or more mutated genes (Sherman, 2002). This is only possible because budding yeast is heterothallic and two haploid cells of opposing mating types (a and alpha) can fuse and form a diploid zygote, when they sense each other's pheromones. The cell shape changes into a pear-like asymmetrical form, which is called a shmoo and the cell cycle is halted in a G1-like state. Laboratory yeast strains are genetically altered so they cannot spontaneously change their mating type, which is known as mating-type switch. Naturally occurring yeasts can induce a mating type switch in order to form diploid strains that can undergo germination, which leads to the formation of four stress resistant spores. Also in the laboratory, under nutrient starving conditions diploid cells undergo sexual reproduction in order to produce four spores that are more robust against environmental stressors (Herskowitz, 1988). These tetrads can be dissected to form four individually growing strains. Budding yeast was used as a model organism to investigate sexual reproduction and meiosis, however, in this study meiosis is only used experimentally to

generate new strains or to analyze genetic defects. When diploid cells are in rich medium however, the asexual mitotic division can take place like in the haploid state (Figure 1.1).

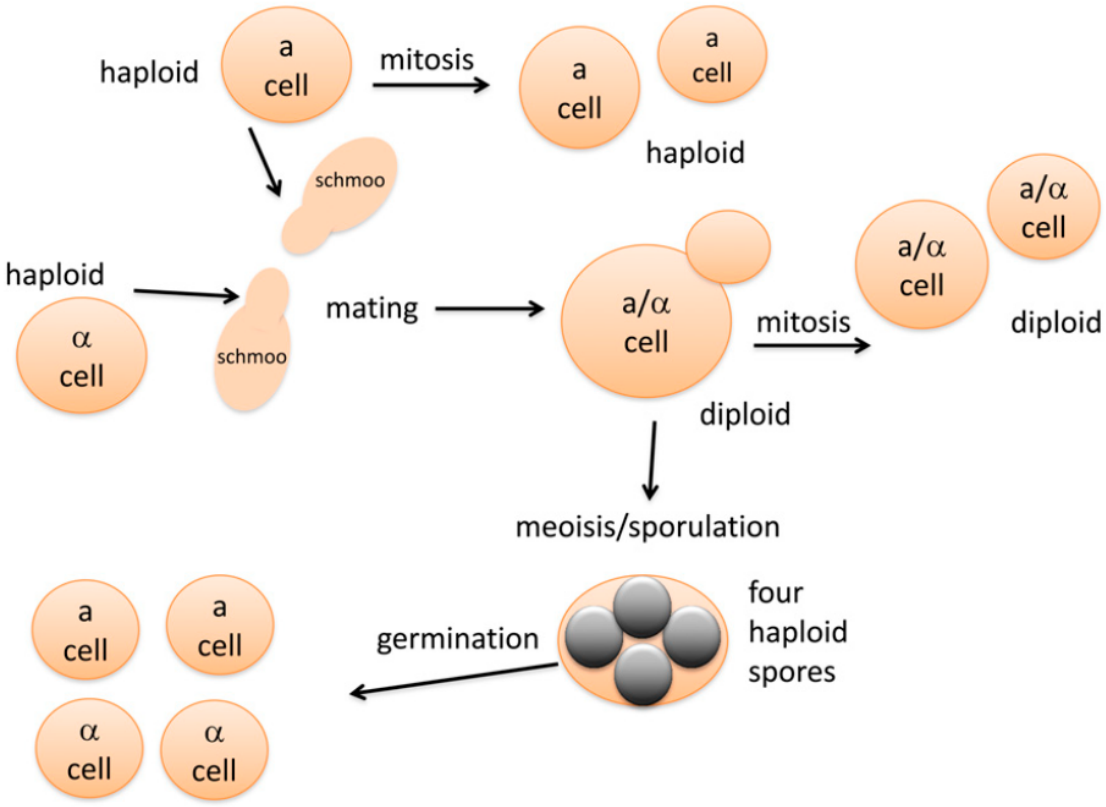

Figure 1.1: The life cycle of the budding yeast *S. cerevisiae*. Budding yeast can proliferate by mitosis or germinate through meiosis. Meiosis is restricted to diploid yeast cells. A huge advantage of budding yeast in the laboratory is that it can be cultivated in a stable haploid or diploid state. Haploid yeast strains of opposing mating types (a and alpha) can sense potential mating partners through pheromones and prepare for cell fusion by changing their cell shape into an asymmetrical pear like shmoo form. After cell fusion and zygote formation diploid yeast strains can either proliferate through mitosis or under starving conditions undergo meiosis and create four haploid spores that can be separated experimentally and grown as individual haploid strains (adapted from (Duina et al., 2014)).

1.1.3 Mitosis – how cells achieve their exact genetic reproduction

Mitosis is a tightly regulated process in which the previously duplicated genetic material of one cell is equally divided into the mother and a newly generated daughter cell. The interaction of chromosomes and the mitotic spindle is of great importance for chromosome segregation and a lot of important insights regarding this field of knowledge were made in the last decades (Biggins, 2013; Westermann et al., 2003; Westermann et al., 2007). Budding yeast mitosis is very similar to mitosis in higher eukaryotes and many conserved processes and key-players have been revealed using budding yeast as a model organism, although some important differences have been found. As a clear difference to higher eukaryotes, the nuclear envelope in budding yeast is not dissolved at mitotic entry, but instead *S. cerevisiae* undergoes what is called a close mitosis. The nucleus is positioned at the budneck during cell division and divided into two functional nuclei during cytokinesis (Howell and Lew, 2012). Microtubules emanate from the spindle pole body (SPB), the equivalent of higher eukaryotes' centrosome which is embedded in the nuclear envelope. This allows attachment of chromosomes to microtubules almost throughout the entire cell division cycle (Jaspersen and Winey, 2004; Sazer, 2005). Astral microtubules that reach out of the nucleus towards the cell wall help to position the nucleus within the cell, whereas nuclear microtubules grow into the nucleoplasm, and form the mitotic spindle and attach to chromosomes (Winey and Bloom, 2012). The proteinaceous scaffolds that constitute the attachment sites for microtubules on each chromosome are conserved from yeast to humans and are called kinetochores. In higher eukaryotes like humans, outer kinetochores can only assemble after nuclear envelope breakdown, allowing microtubules to attach to chromosomes (Bornens, 2002; Sazer, 2005). In budding yeast, the kinetochore is assembled already at the beginning of the cell cycle. Kinetochores assemble on centromeric chromatin and are large multiprotein machines, that create a binding platform for dynamic microtubule plus-ends (Biggins, 2013; Westermann et al., 2007). During S-Phase, when the second sister chromatid is replicated and the SPB is duplicated, microtubule-kinetochore attachment is transiently dissolved in order to assemble a new sister kinetochore onto centromeric chromatin (Kitamura et al., 2007). Assembly of the second sister kinetochore is still a subject of investigation, but it is clear, that the assembly has to be temporary and spatially regulated, because as soon as the centromeric region is replicated, microtubules have to attach to the second sister kinetochore. It was also shown that the number of kinetochore subcomplexes changes between S-Phase and mitosis (Dhatchinamoorthy et al., 2017;

Joglekar et al., 2006), but how excess subcomplexes that are not incorporated into the kinetochore are removed quickly, is still unknown. In this thesis we identified a possible mechanism, of how the cell deals with this problem. To ensure faithful sister chromatid segregation, the ultimate goal of kinetochore microtubule interaction is to achieve a state called bi-orientation in which both sister kinetochores and hence sister-chromatids are bound to microtubules emanating from opposing SPBs. This will lead to generation of tension which is required for chromosome segregation in anaphase (Tanaka et al., 2005) (Figure 1.2). As this is a highly complicated process, it is guarded by a so-called checkpoint, which only allows progression into anaphase, when all chromosomes are properly bioriented.

1.1.4 Checkpoints – the bodyguards of the cell cycle

Checkpoints have evolved in order to regulate cell cycle progression, which ensures integrity of the genetic material. Apart from the intra mitotic checkpoint mentioned above, the first checkpoint within the cell cycle is the G_1 checkpoint, which ensures that the cell only enters S-Phase when all required nutrients and growth factors are present and if the DNA is undamaged (Morgan, 2007). As this checkpoint marks the entry into the cell cycle, it is also known as "Start". During S-Phase, the Intra-S-Phase checkpoint controls for a correct replication, to exclude the existence of DNA damage before cell cycle progression (Pardo et al., 2017). Before cells enter mitosis, the G_2/M checkpoint controls for cell size and a correct replication of DNA. The genetic information has to be duplicated completely and only once, in order to allow subsequent equal division of the genetic information to the two emerging cells (Weinert and Hartwell, 1993). After entry into mitosis the last possibility where the cell cycle can be halted is the checkpoint mentioned above that arrests cells in metaphase until all chromosomes are bioriented. As this checkpoint ensures that all chromosome pairs are attached to microtubules of opposing poles, it is also known as the Spindle Assembly Checkpoint (SAC). The SAC detects failures in chromosomal attachment and blocks cell cycle progression into anaphase until all kinetochores are bound to microtubules correctly (Kadura and Sazer, 2005; Vleugel et al., 2012). This highly regulated process includes multiple proteins and one of the key players that regulate this checkpoint is the Mitotic Checkpoint Complex (MCC) together with the kinase Mps1. The MCC in budding yeast includes the proteins Mad2, Bub3, Mad3 and Cdc20, which are all highly conserved. Cdc20 is the coactivator

of the E3 ubiquitin ligase complex Anaphase Promoting Complex/Cyclosome (APC/C). Through the binding of Cdc20 to the MCC, it is prevented from inducing the APC/C mediated degradation of cyclins and Securin, which causes a prevention of anaphase onset (Matellan and Monje-Casas, 2020). As APC/C function, including degradation of cyclins and Securin are key events in mitotic progression, it will be explained in chapter 1.2.2 in detail. Taken together, these shortly described checkpoints are able to halt the cell division cycle at important steps, so that the cells can divide their genetic material into two exact copies. Although checkpoints ensure genetic integrity, the driving force for the cell progression is represented by the master regulator of the cell division cycle: the cyclin-dependent kinase (CDK).

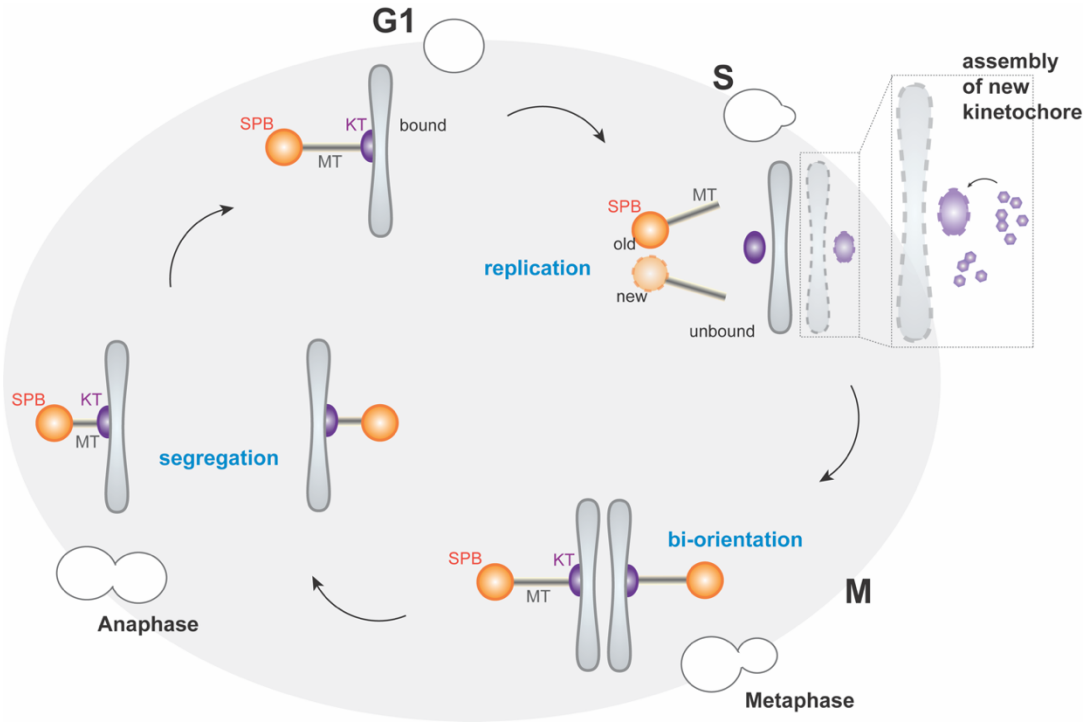

Figure 1.2: The cell division cycle of *S. cerevisiae* and kinetochore-microtubule attachments. The budding yeast *S. cerevisiae* reproduces asexually through budding. In G1, cells are round in shape and a small bud emerges when replication starts in S-Phase. In yeast, mitosis and S-Phase are overlapping, as mitosis begins as soon as the centromeric region is replicated. When cells enter mitosis, the bud is already grown to half the size of the mother cell and as mitosis progresses, the bud grows even further. Kinetochores are the attachment sites for nuclear microtubules and are assembled on centromeric chromatin. As in budding yeast a closed mitosis takes place, microtubules emanating from the spindle pole body (SPB; MTOC in yeast) are attached to kinetochores almost throughout the whole cell cycle. However, during a short period of time during S-Phase, microtubule-kinetochore attachments are transiently dissolved and a new kinetochore has to be assembled to achieve bi-orientation for proper chromosome segregation in anaphase. Cytokinesis separates the two cells and a new cell division cycle can start in both cells.

1.1.5 The clockwork of the cell division cycle

How exactly is the cell division cycle so tightly regulated and how does the cell deal with any kind of stress? In general, phosphorylation and dephosphorylation events of many proteins are essential for cell cycle progression or delay. This chapter addresses, how CDK itself is regulated through activating and inhibitory phosphorylations and how this affects cell cycle progression. In addition, it will be addressed which other effectors like kinases, phosphatases and inhibitory proteins are involved in the whole process and how correctly timed degradation of such is important for mitotic cell division.

Cyclin dependent kinases (CDKs) are family members of Proline directed Serine/Threonine kinases and fulfill regulatory actions through phosphorylation of substrates. They were first identified for their role in cell cycle regulation and much is known from studies in both budding and fission yeast (Morgan, 1997). CDKs are found in all eukaryotes and are also involved in transcriptional regulation, mRNA processing and the control of the mitotic cell cycle (Morgan, 2007). The structure of active versus inactive CDK and the conformational changes through binding of ATP to the active site were investigated through X-ray crystallographic studies from human Cdk2 (De Bondt et al., 1993; Jeffrey et al., 1995): CDK consists of two lobes and has a kidney like shape. The active site of every CDK is positioned between the smaller amino-terminal site and the larger carboxy-terminal site and is regulated through cyclin binding and conformational changes of flexible parts of the protein. Without cyclin binding, important side chains inside the active site are positioned in such a way, that they hinder proper ATP loading and therefore substrate phosphorylation. Additionally, a flexible T-loop (or activating loop) blocks the active site for substrate binding (Malumbres, 2014; Morgan, 1997), rendering the kinase inactive. Through an activating phosphorylation of this T-loop, the active site becomes accessible for substrates, which in turn effects cyclin binding, which additionally promotes correct ATP positioning in the active site for phospho-transfer reactions. Every active CDK/cyclin complex phosphorylates its substrates at a specific amino acid motif, also known as a consensus sequence: The minimal motif is a Serine or Threonine followed by a Proline (S/T-P). A more favorable motif has also a positive charge in form of an Arginine or Lysine at position +3 (S/T-P-x-R/K) (Endicott et al., 1999; Touati and Uhlmann, 2018). These substrate phosphorylation events can either activate the target protein, induce complex formation or lead to degradation of the protein. The phosphorylation of substrates can often be subducted from opposing phosphatases, of which examples will be stated later.

The master regulator of the cell cycle in budding yeast is the cyclin dependent kinase Cdc28 in budding yeast or Cdk1 and Cdk2 in higher eukaryotes (Malumbres, 2014). Although only such a limited number of CDKs exists for cell cycle progression, it must guide the cell through the various different events of every cell cycle in a timely and technically accurate manner. The single CDK in budding yeast deals with this challenge by the regulated expression and interaction with nine different cyclins, that can bind to Cdc28 and form stable heterodimeric complexes (Touati and Uhlmann, 2018). A dynamic and rapid expression and degradation of cyclins throughout the mitotic division cell cycle contributes to the timely order of cell cycle specific events. Cyclins are named after their oscillating concentration during the mitotic cell cycle. Figure 1.3 demonstrates CDK activity and oscillating levels of cyclins during the entire cell cycle. In budding yeast, the G1 cyclins Cln1, Cln2, and Cln3 target specific proteins, that are necessary for bud emergence and activate the master regulator of cell polarity Cdc42 (Howell and Lew, 2012; Simon et al., 1995). G1 cyclins are quite unstable proteins that contain PEST motifs and are degraded shortly after S-Phase transition (Salama et al., 1994). Cdc28/Clb5 or Cdc28/Clb6 are S-Phase specific complexes, that especially phosphorylate Sld2 and Sld3 which are important for initiation of replication (Bertoli et al., 2013), whereas Cdc28 together with Clb1 or Clb2 target mitotic proteins and therefore drive mitotic entry. The cyclin dependent kinase Cdc28/Cdk1 and the antagonistic protein phosphatase Cdc14 are the key players in cell cycle and mitotic progression (Howell and Lew, 2012; Manzano-Lopez and Monje-Casas, 2020), but also other kinases like Swe1/Wee1, Cdc5/Plk1, Ipl1/AuroraB, Mps1 or the phosphatase Cdc55/PP2A play important roles (Touati and Uhlmann, 2018).

In the next chapter the importance of the interplay of phosphorylation, dephosphorylation and phospho-induced degradation of cell cycle regulators is explained. As ubiquitin-driven protein degradation is the basis of many regulatory events during cell cycle progression, the ubiquitin-proteasome system of budding yeast will be addressed first.

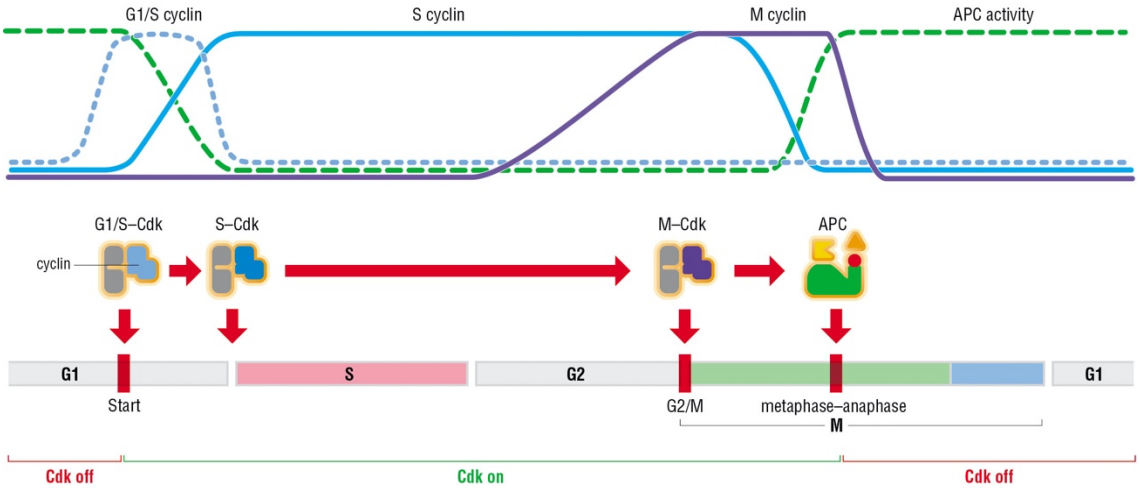

Figure 1.3: Oscillation of cyclin levels and CDK activity over the cell cycle. In budding yeast, a single mitotic CDK forms heterodimers with different cyclins to promote cell cycle progression. During G1, CDK is inactive. With the beginning of the cell cycle, CDK is activated until it gets turned off again at the metaphase to anaphase transition. Opposite to this CDK activity, APC/C activity is highest in G1 until it drops at the start of the cell cycle and rises again when CDK is inactivated at metaphase to anaphase transition (green dotted line). The different cyclins oscillate as well, as seen in colored lines (light blue: G1/S cyclins; dark blue: S cyclin; purple: M cyclin), leading to different substrate specificity of CDK at different stages of the cell cycle (adapted from (Morgan, 2007)).

1.2 The ubiquitin-proteasome system in *S. cerevisiae*

A very important posttranslational modification is the reversible transfer of the small and highly conserved protein ubiquitin to target proteins. Ubiquitin was first identified as a factor in proteolysis in rabbit reticulocytes and was called ATP-dependent proteolysis factor (APF-1) (Hershko et al., 1980; Wilkinson et al., 1980). It is essential in all eukaryotic cells and conserved from yeast to humans. It is preferably covalently attached to lysine residues in target proteins and needs to be activated at its C-terminus, but other sites including the N-terminus (Breitschopf et al., 1998), cysteine and serine residues were also shown to be ubiquitinated (Cadwell and Coscoy, 2005). Ubiquitin can be attached as a single molecule (mono-ubiquitination), as multiple single molecules (multi-mono-ubiquitination) to the same substrate or as ubiquitin chains. Ubiquitination is dependent on the interplay of multiple enzymes, which build a cascade to activate and transfer ubiquitin: a ubiquitin-activating enzyme (E1), a ubiquitin-conjugating enzyme (E2) and a ubiquitin-ligase complex (E3). Substrate specificity is created through the interplay of different enzymes, but it is mandatory to always have an E1, E2 and E3 for proper ubiquitination. E1 enzymes link a thiolester bond to the C-terminus of ubiquitin which is an energy-dependent reaction. The activated ubiquitin forms a thiolester bond with an E2 enzyme, which can interact with an E3 ligase. E2 and E3 together catalyze the formation of isopeptide bonds between the target substrate and ubiquitin (Hochstrasser et al., 1999). Although activating ubiquitination events were described, it is well established that ubiquitination marks proteins for their degradation via the 26S proteasome. The 26S proteasome consists of two parts, one catalytic unit called the 20S particle, which forms a cylindric core and two regulatory particles on both ends (Driscoll and Goldberg, 1990). Protein degradation is involved in many cellular processes like stress response, signal transduction or cell cycle control (Hochstrasser, 1996). Many isoforms of E2 and E3 enzymes exist, which create substrate specificity in cells, but the assembly and removal of ubiquitin to substrates depend on E3 ligase complexes. E3 ligase complexes that are involved in mitosis in budding yeast are for example Ubr2/Mub1, Psh1 or APC/C. The E3 ligase Ubr2 with its cofactor Mub1 interacts with the E2 enzyme Rad6 and regulate levels of the outer kinetochore subunit Dsn1 (Akiyoshi et al., 2013b). The local restriction of Cse4, an H3 variant that is incorporated in centromeric nucleosomes, to the centromere is regulated by the ubiquitin ligase Psh1 (Hewawasam et al., 2010; Ranjitkar et al., 2010). The largest known class of E3 ubiquitin ligases are Cullin-RING complexes. As they are of importance for this study, they will be discussed here in more detail.

They consist of a core subunit called Cullin (Cul1 in metazoans or Cdc53 in yeast), which can recruit a multi-subunit ligase complex (Petroski and Deshaies, 2005). The structure of this complex was determined in X-ray crystallographic analyses (Zheng et al., 2002). The core subunit Cdc53/Cul1 or subunits with Cullin-homology domains have a curved N-terminal stalk and a globular C-terminal domain, which interacts with the RING like subunit that binds to the C-terminal domain is also called Rbx1 in higher vertebrates or Hrt1 in budding yeast. This subunit further recruits the E2 enzyme (often Cdc34) with an activated ubiquitin molecule attached (Pickart, 2001). On the N-terminal site of the core subunit binds an adaptor subunit called Skp1, which is a global subunit of many E3 ligases. Binding of the F-Box protein to the complex generates substrate specificity, because it targets a limited number of specific substrates (Orlicky et al., 2003). F-Box proteins have a F-box motif, a substrate interaction domain on their C-terminus, a leucine rich repeat (LRR) domain and a WD40 repeat domain. The F-Box proteins Cdc4 and Grr1 in yeast recognize only phosphorylated substrates and hence bind them through either the WD40 domain like Cdc4 or through the LRR domain like Grr1 (Skowyra et al., 1997). One important example for Cullin-RING ligases is SCF, containing a Skp1, Cullin and F-Box protein. In Figure 1.4 a model of the Cullin-RING E3 ligase complex SCF with the F-Box protein Cdc4 in complex with a phosphorylated substrate peptide is shown. Its importance for mitotic division will be described later (Chapter 1.2.2). Structural analysis of both yeast and human subunits were combined to a composed structural model showing the whole complex (Orlicky et al., 2003). SCF has a C-shaped conformation, which is derived from binding of Skp1-Cdc4 and Rbx1-Ubc7 on both sides of Cul1. This modelling illustrates, that the cleft between the E2 enzyme and the substrate is about 59 Å, which fits to previous results (Zheng et al., 2000) and allows transfer of the ubiquitin to the substrate.

In the next section this E3 ligase complex is described in more detail, as SCF with the F-Box protein Cdc4 ubiquitinates phosphorylated substrates which will be important for this thesis.

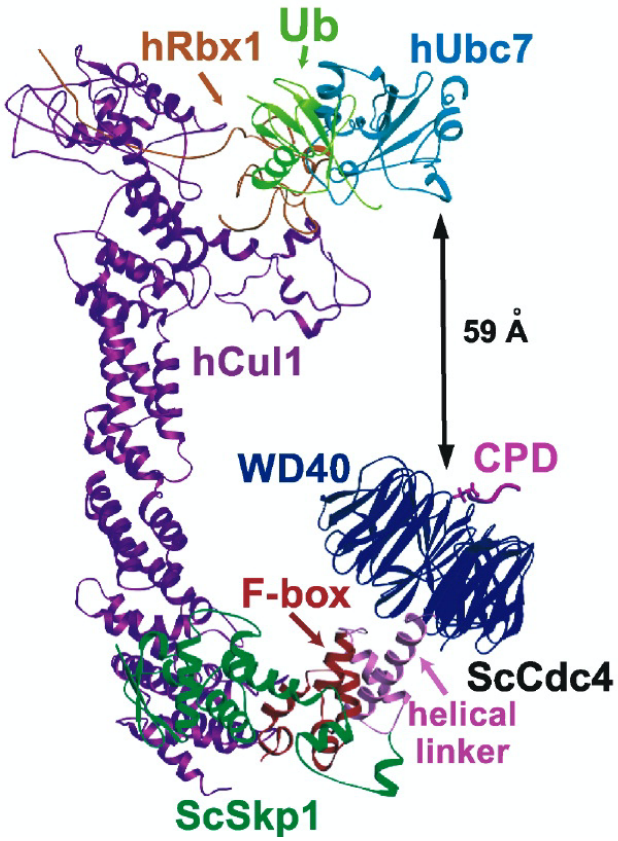

Figure 1.4: Model of SCF^{Cdc4} bound to a phosphorylated substrate. This composition of yeast and human structures shows the C-shaped form of the Cullin-RING E3 ligase SCF bound to the F-box protein Cdc4. The phosphorylated substrate (CPD) binds to the WD40 domain of Cdc4 and is in proximity to the E2 enzyme Ubc7 by 59Å, allowing ubiquitin transfer to substrates that bind to Cdc4 (adapted from (Orlicky et al., 2003)).

1.2.1 The E3 ubiquitin ligase complex SCF^{Cdc4} ubiquitinates phosphorylated target proteins

The E3 ligase SCF^{Cdc4} ubiquitinates substrates in a phosphorylation-dependent manner. Cdc4 recognizes substrates that harbor a specific high-affinity degron motif, also called Cdc4-phospho-degron (CPD), that is defined the consensus sequence I/L-I/L/P-pT-P-(K/R), where (K/R) are disfavored residues (Nash et al., 2001). The phosphorylated Threonine at position P0 and the following Proline at P+1 strongly resemble the CDK motif pS/pT-P-X-K/R and are essential for Cdc4 interaction. A less favorable Serine at position P0 is also detected and bound, but with less affinity. It was also shown, that additional phosphorylation events in close proximity of the CDK phosphorylation site positively effect Cdc4 binding, creating bi-phospho-degrons (Lyons et al., 2013). Already known and investigated targets for SCF^{Cdc4} are Cdc6, Cln2 or Eco1, which are all recognized in a phosphorylation-dependent manner (Lyons and Morgan, 2011; Patton et al., 1998).

Another well characterized substrate of SCF^{Cdc4} is the CDK inhibitory protein Sic1, which regulates the levels of S cyclins during cell cycle progression to avoid premature DNA replication (see section 1.2.2). Sic1 harbors nine CPD sites, of which at least six have to be phosphorylated in order to be recognized by Cdc4. Interestingly, not a single one of the nine CPD sites resemble the optimal sequence (Nash et al., 2001; Orlicky et al., 2003), making a multisite phosphorylation of one substrate even more important. To confirm that multiple low-affinity CPD sites of Sic1 act in concert to build a high-affinity binding site for Cdc4, an optimal CPD site was placed in Sic1 and all known sites were mutated. This Sic1 mutant was recognized and ubiquitinated by SCF^{Cdc4} *in vitro* and elimination was confirmed *in vivo* (Nash et al., 2001). Multisite phosphorylation of several suboptimal CPD sites has advantages over a single optimal CPD site. CDK phosphorylation and SCF^{Cdc4} mediated ubiquitination act antagonistically which is important to create a threshold of Sic1 destruction in order to allow S cyclin inhibition for the length of G1. A single optimal CPD site would lead to a too efficient degradation of Sic1 early in G1 and therefore to a too early initiation of S-Phase. Therefore, it is more feasible to have multiple suboptimal CPD sites present that need to be phosphorylated over time (Nash et al., 2001).

In this thesis we focus on CDK phosphorylation of kinetochore proteins and investigate a possible regulation of subunit levels through degradation that would affect assembly of

kinetochores. To further elucidate the importance of E3 ligase complexes during mitotic cell division, we will describe APC and SCF function in more detail in the next section.

1.2.2 E3 ubiquitin ligase complexes regulate protein levels during cell division

Two important E3 ligases in the cell division cycle are APC/C and SCF. Both are Cullin-RING E3 ligases and are important to maintain the balance of proteins for a correct progression through the cell cycle and can ubiquitinate multiple effectors of CDK/Cyclin complexes to finetune CDK/cyclin activities and hence cell cycle progression. The importance of E3 ligases for cell cycle control will be illustrated via three specific examples that are summarized in the following paragraphs.

When a new cell cycle begins, the budding yeast cell needs to switch from uniform to polar growth. The major drivers of bud emergence in budding yeast are the two G1 cyclins Cln1 and Cln2 in complex with Cdc28 (Howell and Lew, 2012). They act through activating the major regulator of cell polarization, which is the small Rho-GTPase Cdc42, that is important for establishment and maintenance of cell polarity (Simon et al., 1995). G1-CDK phosphorylates substrates that are important binding partners of Cdc42 and acts therefore at the levels of Cdc42 regulator activation to promote polarization. When stress occurs, the morphogenesis checkpoint delays nuclear division until the cell was able to properly form a bud (Lew, 2003). This delay in nuclear division is dependent on the CDK-inhibitory kinase Swe1, which is a Wee1 family kinase, that phosphorylates T19 on Cdc28 (Booher et al., 1993; Sia et al., 1996) and is therefore responsible for S-CDK inactivation. Phosphorylation of T19, which is located at the active site of CDK, leads to a reorientation of bound ATP and therefore to inhibition of substrate phosphorylation by CDK. For cell cycle progression, this inhibitory kinase Swe1 has to be degraded. In G1 this is mediated through APC/C, whereas another pool of Swe1 that is active in G2/M-Phase is degraded by the E3 ubiquitin ligase complex SCF^{Met30} (Kaiser et al., 1998). This degradation is induced through Cdc28/Clb1 and Polo-like kinase (Cdc5) phosphorylation of Swe1. Also, in mammalian cells, Cdk1 and the Polo-like kinase Plk1 create phospho-degrons on Wee1 (homolog of Swe1) for $SCF^{\beta TrPC}$ targeted degradation (Watanabe et al., 2005; Watanabe et al., 2004).

Another regulator of CDK that acts at G1- to S-Phase transition is the Cyclin-dependent Kinase Inhibitor (CKI) Sic1, that interacts with the CDK-Clb5/Clb6 complex in order to prevent premature S-Phase transition (Figure 1.5). The beginning of the cell cycle induces production not only of the G1 CDK complexes Cdc28/Cln1/2, but also the S-Phase CDK complexes Cdc28/Clb5/6. To ensure that only G1 CDK is active in G1, Sic1 binds to S CDK complexes and hence prevents premature S-Phase transition. When cells progress through G1, Cdc28/Cln2 and Cdc28/Clb5 complexes specifically phosphorylates this inhibitory protein Sic1, leading to its very efficient degradation by an E3 ubiquitin ligase complex called SCF^{Cdc4} and hence release of the CDK-Clb5/Clb6 complex from Sic1 for S-Phase initiation (Koivomagi et al., 2011a; Nash et al., 2001).

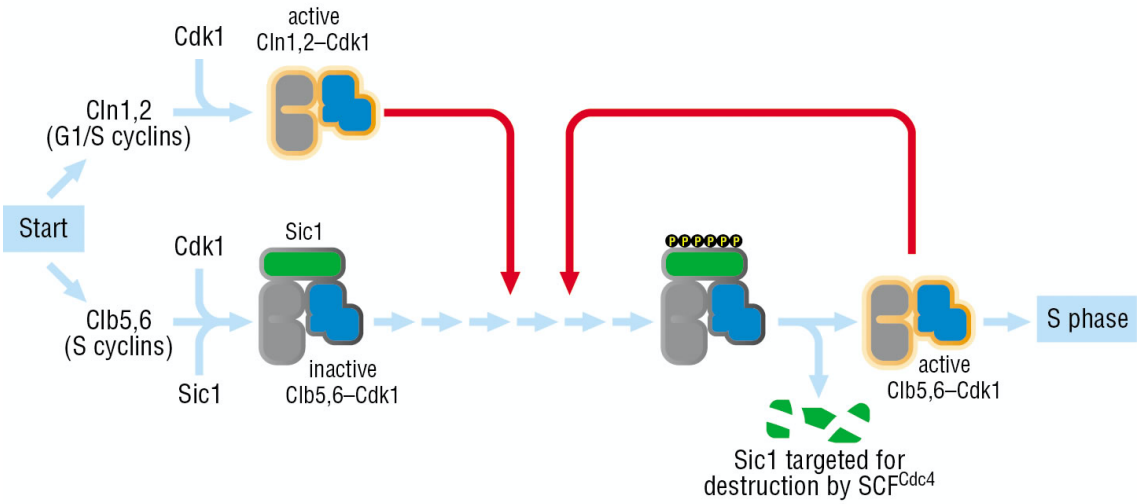

Figure 1.5: SCF degradation of Sic1 controls S-CDK activation. Entry into a new cell cycle requires increased expression of G1/S and S cyclins. The CKI protein Sic1 binds to S cyclins and prevents premature entry into S-Phase. Increased activity of G1/S cyclins leads to multisite phosphorylation of Sic1 and results in ubiquitination via SCF^{Cdc4} and degradation allows replication through activation of S cyclins (adapted from (Morgan, 2007)).

Another important E3 ligase complex is the previously mentioned APC/C. Its target binding is specified by two individual activator proteins called Cdc20 and Cdh1, which can bind to APC in different cell cycle stages (Figure 1.6). When the SAC is satisfied as a consequence of all chromosomes being properly aligned to the mitotic spindle, the phosphorylation of APC/C subunits by M-Phase CDK enhances the binding of the activator Cdc20. Once activated, APC/C-Cdc20 targets Securin and S/M-Phase cyclins for destruction, creating a negative feedback loop for M-Phase cyclins (Rudner and Murray, 2000) which in turn inactivates CDK and allows progression to anaphase, characterized by spindle elongation and chromosome segregation. Because the binding of Cdc20 is dependent on M-Phase CDK phosphorylation, Cdc20 detaches from APC/C once levels of M-Phase cyclins drop to a minimum. This drop in cyclin levels is achieved through the activation of the mitotic exit network (MEN) and the release of the antagonistic phosphatase Cdc14 from the nucleolus at anaphase transition (Yeong et al., 2002). Cdc14 is a phosphatase with dual specificity, that can remove phosphates from either pSer/pThr or pTyr residues, whereas pSer is preferred to pThr (Manzano-Lopez and Monje-Casas, 2020). Dimerization of Cdc14 is essential for efficient phosphatase activity and Cdc14 has a strong affinity for the full consensus motif of CDK (Kataria et al., 2018; Kobayashi and Matsuura, 2017). Cdc14 is important for dephosphorylation of multiple proteins like Sic1, Swe1, Ask1, Sli15, different kinetochore proteins and more (Manzano-Lopez and Monje-Casas, 2020), and for dephosphorylation of Cdc28/Clb2, which leads to degradation of Clb2 by APC/C and a drop of mitotic CDK levels and ultimate in mitotic exit (Visintin et al., 1998). Once cells completed mitosis, the second activator Cdh1 binds to APC/C. This binding is - unlike Cdc20 binding - not phosphorylation dependent, although Cdh1 phosphorylation by S/M-Phase CDK prevents premature binding before mitotic exit. APC/C-Cdh1 is therefore mainly active in G1 and is another mechanism to keep cyclin levels low and establish a stable G1 phase. During G1, APC/C-Cdh1 destruct S and M-Phase cyclins (Clb1,2 and Clb5,6) further, but the G1/S-Phase cyclins Cln1 and Cln2 are not detected to allow the beginning a new cell cycle, which in turn phosphorylate Cdh1 and lead to inactivation of the APC/C until the next anaphase (Peters, 2002).

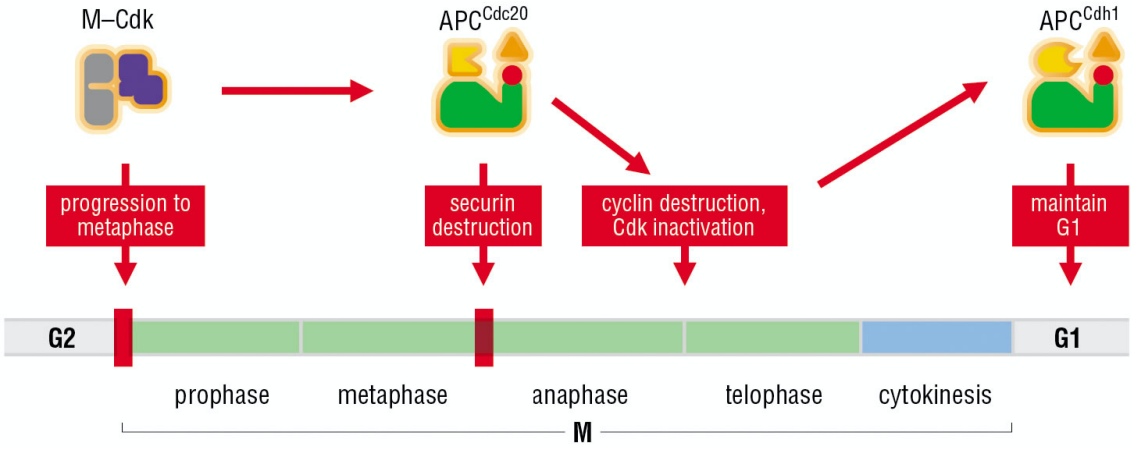

Figure 1.6: The E3 ligase APC/C with two activator proteins induces late mitosis. As entry of mitosis is controlled by M-CDK complexes, the APC/C with its coactivator Cdc20 induces late mitotic events when all chromosomes are correctly attached to the microtubules of the mitotic spindle. Binding of Cdc20 to APC/C is increased through M-CDK phosphorylation and leads to Securin and M cyclin destruction at the metaphase to anaphase transition. Inactivated CDK leads to APC/C binding to the second activator Cdh1, which is active during mitotic exit and in early G1, where it maintains low M-CDK levels (adapted from (Morgan, 2007)).

As described above, the interplay of multiple kinases, phosphatases and E3 ubiquitin ligases allows a switch-like progression through the mitotic cell division cycle. Kinetochores establish a regulated binding platform on chromosomes for dynamic spindle microtubules. So far, it is unknown if APC/Cs impact on level regulation of kinetochore subunits might explain how a spatially and timely restricted assembly and disassembly of the kinetochore is achieved. In favor of that hypothesis, it has already been shown that the restriction of Cse4 nucleosome incorporation to the centromeric region is regulated via the ubiquitin-proteasome system through different E3 ligases. We sought to investigate, if other E3 ligases are involved in the regulation of additional kinetochore proteins and whether this regulation is involved in safe-guarding kinetochore assembly. Understanding of how phosphorylation, dephosphorylation and ubiquitination of kinetochore proteins influences kinetochore assembly in time and space would lead to new insights of how kinetochore assembly regulation is realized.

1.3 Kinetochores are structural and regulatory complexes for correct chromosome segregation

For a correct segregation of sister chromatids during mitotic cell division, chromosomes have to be attached to dynamic microtubules in a way that resist pulling forces of the mitotic spindle. Responsible for establishing these load-bearing attachments are multiprotein complexes known as kinetochores, which are built on specialized locations of every chromatid, known as centromeric regions. Although general kinetochore architecture and function is conserved among all eukaryotes, centromere characteristics can largely differ between species. Apart from kinetochores' function in creating attachments with spindle microtubules, they are also responsible for detecting and correcting any false attachments such that the cell can proceed into anaphase. The architecture of budding yeast kinetochores as well as how they realize their different functions, will be discussed in detail in the following sections, as this is the basis of this study. Furthermore, it will be important to summarize what is known about how kinetochore assembly is restricted to the centromeric region, as this study contributes to the knowledge of how regulation of protein levels of single kinetochore components might contribute to the important mechanism of kinetochore localization. This is of uttermost importance for the cell, as formation of additional kinetochores on a single chromatid will cause segregation problems and will therefore be discussed in more detail here.

1.3.1 Centromeres – the basis for kinetochore assembly

DNA is the carrier of the genetic information in all organisms. Chromosomes comprise this genetic information in the form of DNA as well as DNA-associated proteins, including nucleosomes. DNA is wrapped around these nucleosomes in order to minimize the overall length (Richmond et al., 1984) and allow compaction of the DNA for transcriptional inactivation or condensation during mitosis. These nucleosomes consist of octameric histone protein complexes, including two molecules of four different histones, respectively: the histones of a canonical nucleosome are called H2A, H2B, H3 and H4 (Arents et al., 1991). However, there is a variety of specialized histone proteins, that are incorporated into the nucleosome under specific circumstances or at specific locations within the genome to fulfill specialized functions. Centromeres are special regions on the

chromosome, in which the nucleosome protein H3 is exchanged with a specialized histone that is called CENP-A in higher eukaryotes or Cse4 in the budding yeast *S. cerevisiae*. As this specialized nucleosome is recognized by a subset of kinetochore proteins, it has been largely accepted as being the epigenetic basis of kinetochore assembly only at the centromeric region, although many other mechanisms also contribute to the restriction of kinetochore assembly to centromeres. One of these mechanisms includes level regulation of free kinetochore proteins, which will be focus of this study.

Different types of centromeres in eukaryotes exist: point centromeres like in *S. cerevisiae*, where only a single nucleosome specifies this chromosomal locus (Fitzgerald-Hayes et al., 1982); regional centromeres like in human cells, where multiple CENP-A nucleosomes are incorporated into a 1- to 4- Mb region of the chromosomes that are composed of tandem repeats of alpha satellite DNA (Musacchio and Desai, 2017); or holo-centromeres in which centromeres are incorporated through the whole length of the chromosome, which can be found in the nematode *Caenorhabditis elegans*, or some insects (Albertson and Thomson, 1982; Drinnenberg et al., 2014). In budding yeast, a single Cse4 nucleosome is incorporated into a stretch of 125 bp centromeric DNA, that consists of a specific sequence comprising the centromeric determining elements (CDEI, II and III) on all of the 16 yeast chromosomes (Fitzgerald-Hayes et al., 1982; Fleig et al., 1995). CDEI and CDEIII are short and conserved through all 16 chromosomes, whereas CDEII only shares an AT-rich sequence of about 80-90 nucleotides (Yan et al., 2018). As kinetochore assembly is based on the incorporation of Cse4, it is of great importance to restrict Cse4 incorporation to the centromeric region, because positioning of Cse4 at chromosome arms leads to ectopic kinetochore assembly and hence mis-segregation or a halt of mitosis through the SAC (Foley and Kapoor, 2013; Lampson and Cheeseman, 2011). Cse4 overexpression has been shown to promote ectopic Cse4 incorporation at specific non-centromeric loci. Cse4 levels in cells are regulated through ubiquitin-mediated proteolysis (Collins et al., 2004), which will be further discussed later. In yeast, a protein complex called CBF3 is needed in order to load Cse4 nucleosomes to this specific stretch of centromeric DNA, which also helps restricting Cse4 incorporation to the centromeric region. This complex consists of four proteins namely Ndc10, Cep3, Skp1 and Ctf13. Together with Cbf1, a nonessential basic helix-loop-helix protein which also has DNA binding ability, the CBF3 complex detects and binds to CDEII and is the

first kinetochore protein complex at centromeric DNA. The recruitment of the inner kinetochore to centromeric DNA is the start of a hierarchical kinetochore assembly.

1.3.2 Kinetochores assemble on centromeric chromatin

As mentioned above, kinetochores are large multiprotein complexes that are assembled on centromeric chromatin and build a platform for dynamic microtubules to bind and segregate the duplicated chromosomes between mother and daughter cell. In Co-Immunoprecipitation experiments it was shown that most proteins are organized in subcomplexes, that can be isolated from lysates individually (Figure 1.7). In general, kinetochores consist of an inner DNA-binding and an outer microtubule-binding layer. The inner kinetochore is also referred to as the Constitutive Centromere Associated Network (CCAN) and is able to specifically assemble onto centromeric nucleosomes through specific interaction of some components with CENP-A/Cse4 nucleosomes. The CCAN (or Ctf19c in budding yeast) provides a platform for the microtubule binding outer kinetochore (Hinshaw and Harrison, 2019). Whereas in budding yeast and higher vertebrates the CCAN consists of up to 16 different proteins, in *Drosophila melanogaster* only a single protein called CENP-C is sufficient to fulfill its functions (Przewloka et al., 2011). The inner kinetochore is assembled in a hierarchical manner, where proteins directly binding to the Cse4 nucleosomes recruit additional components to create a platform for the outer kinetochore component recruitment. Three of the budding yeast CCAN proteins were shown to be essential in genetic experiments, including Mif2, Ame1 and Okp1. All three proteins have in common, that they are presumably mainly unstructured apart from their C-termini. Mif2 homodimerizes through a C-terminal cupin domain, whereas Ame1 and Okp1 contain coiled-coil regions at their C-termini, allowing them to form heterodimers. In this region the binding domain for another heterodimer was identified previously, allowing the interaction of Ame1/Okp1 with the two additional proteins Ctf19 and Mcm21, leading to formation of the tetrameric COMA complex (Schmitzberger et al., 2017). Ctf19 and Mcm21 are both non-essential proteins and bind to Okp1 via RWD domains in their C-terminal half (Schmitzberger and Harrison, 2012; Schmitzberger et al., 2017). In higher vertebrates, the homologous proteins form the CENP-PORQU complex (Pesenti et al., 2018). The homolog of human CENP-R has not been identified yet, although a small heterodimer called Nkp1/Nkp2 show homologous functions and also has a binding capacity for Ame1/Okp1 and might therefore be the functional equivalent of CENP-R.

A

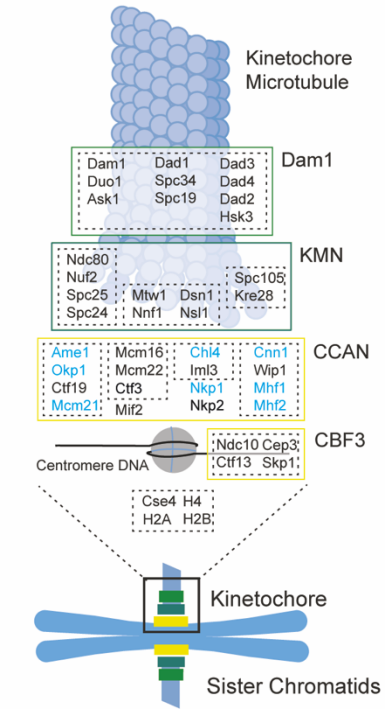

B

CCAN subunit	total P-sites detected	minimal Cdk1 (S/TP)	full Cdk1 (S/TP_K/R)
Ame1	8	4 (T31, S41, S45, S53)	--
Okp1	8	--	--
Mcm21	1	--	1 (S139)
Nkp1	3	--	1 (S222)
Cnn1	17	2 (T42, S192)	2 (T21, S177)
Chl4	3	1 (S281)	--
Mcm22	2	--	--
Mhf1	3	1 (T34)	--
Mhf2	1	1 (S60)	--
	70	9	4
	mapped P-sites in CCAN subunits		

Figure 1.7: Overview of the budding yeast kinetochore. (**A**) The budding yeast kinetochore is a multiprotein complex consisting of individual subcomplexes. The point centromere-binding subcomplexes are described as the Constitutive Centromere Associated Network (CCAN) and are shown together with the DNA binding complex CBF3 in yellow. The CCAN consists of 16 proteins, oh which only three proteins are essential namely Ame1, Okp1 and Mif2. The microtubule-binding subcomplexes are the Knl1/Spc105-Mtw1c-Ndc80c (KMN) and the Dam1 complex which forms rings around the dynamic microtubule, both shown in green. Highlighted in light blue in (**A**) and listed in (**B**) are the CCAN components that show a CDK phosphorylation motif in their amino acid sequence.

Another shared function of Ame1 and Mif2 is the recruitment of the outer kinetochore component Mtw1. Apart from this axis of Mtw1c and hence Ndc80c recruitment, another pathway to recruit Ndc80c molecules has been shown to involve the CCAN proteins Ctf3 complex, the heterodimer Cnn1/Wip1, Chl4/Iml3 and Ctf19 and Mcm21, which are all nonessential proteins (Lang et al., 2018; Pekgoz Altunkaya et al., 2016). Together these two pathways create a platform for outer kinetochore assembly. The outer layer of the kinetochore, also known as the KMN network, consists of three subcomplexes, termed Ndc80c, Mtw1c and Spc105 (Knl1 in higher vertebrates). The KMN network mediates the binding to a single microtubule in budding yeast or to 20-40 microtubules in higher vertebrates and is the stage for SAC function and error correction of false kinetochore microtubule attachments. Mtw1 forms a tetrameric complex together with Dsn1, Nnf1 and Nsl1. Mtw1 forms a heterodimer with Nnf1, whereas Dsn1 forms a heterodimer with

Nsl1. Both subcomplexes can bind to each other and form an elongated Y-shaped complex (Dimitrova et al., 2016). The Ndc80c is a long and flexible protein complex, consisting of four proteins organized in two heterodimers (Ndc80/Nuf2 and Spc24/Spc25). Spc105/Knl1 forms a heterodimer with Kre28 (Pagliuca et al., 2009). A yeast specific protein complex that binds directly to microtubules is the Dam1c, which consists of 10 subunits that assemble into a ring of 12-16 subcomplexes around a single microtubule (Westermann et al., 2006). Kinetochores are assembled from multiple subcomplexes as mentioned above. In Figure 1.8 the regulated assembly of multiple building blocks is shown. The KMN network and Dam1c are targets of different regulatory mechanisms and are involved in SAC recruitment and functioning. SAC function in error correction is of high importance, because unfaithful chromosome segregation will have major consequences for the cell or organism. Therefore, the SAC can halt mitosis in order to correct any false microtubule kinetochore interactions and avoid chromosome mis-segregation. A main binding interface for different SAC components is the Spc105/Kre28 subcomplex, but also the Ndc80c is involved in SAC function. The SAC, but also error correction of false microtubule attachments is largely based on posttranslational modifications. Apart from these two important mechanisms, posttranslational modifications are involved in proper kinetochore assembly and prevention of ectopic kinetochore assembly, which will be discussed in the following sections.

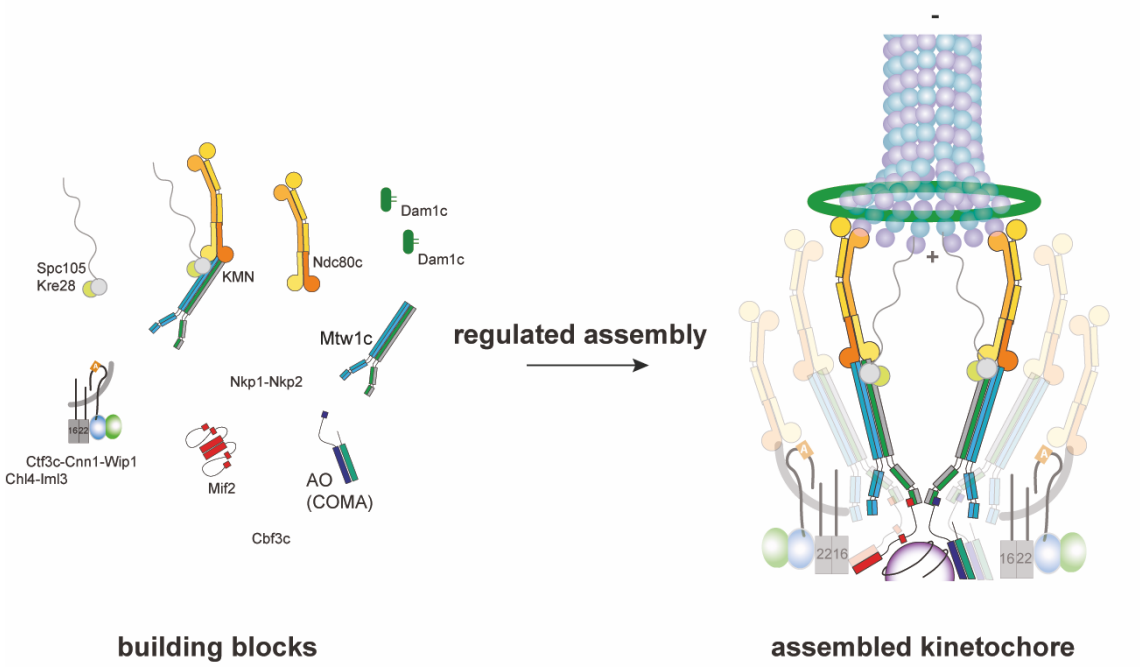

Figure 1.8: Kinetochores are assembled from individual building blocks. The budding yeast kinetochore is assembled from multiple building blocks, which can be purified as stable entities from yeast cells and from recombinant protein expression. A regulated

assembly into the proteinaceous complex is mandatory. On the left site the building blocks are shown, which assemble into the kinetochore in a regulated fashion. The CCAN subcomplexes shown here are: Mif2 homodimer, Ame1/Okp1 heterodimer/COMA, Ctf3c with Cnn1/Wip1, the Nkp1/Nkp2 dimer and the CBF3 complex. The KMN network is shown as individual subcomplexes (Spc105/Kre28, Mtw1c and Ndc80c) or together. In addition, Dam1c subcomplexes are shown, that form a ring after assembly (adapted from (Killinger et al., 2020)).

1.3.3 Posttranslational modifications allow SAC function and error correction

A very important and well characterized interplay of phosphorylation and ubiquitination is the regulation of kinetochore-microtubule interactions by the SAC and error-correction mechanisms in order to generate proper chromosome-microtubule attachments. Bi-orientation has to be achieved and monotelic, syntelic or merotelic attachments of kinetochores to microtubules have to be resolved and corrected. When cells have properly attached their chromosomes to microtubules of opposing spindle poles, tension within the kinetochore is created and a key player in tension-sensing is the kinase Ipl1/AuroraB, which phosphorylates subunits of the Ndc80c and Dam1c complexes (Cheeseman et al., 2002). These phosphorylation events lead to a reduction in microtubule binding, which hence leads to a release of false attachments. A current model suggests that correct kinetochore-microtubule attachments lead to a physical stretching of kinetochores due to spindle forces, which in turn leads to the incapability of lpl1 to phosphorylate its targets. Opposing phosphatases can then remove phosphates on Ndc80c and Dam1c which in turn leads to stabilization of correct attachments. As long as a single kinetochore is not properly attached to the mitotic spindle, the SAC will halt progression to anaphase by preventing the APC/C from being activated. One way to keep the APC/C inactive is to prevent its mitotic co-activator Cdc20 from binding to the complex, which is achieved through incorporation of Cdc20 into the mitotic checkpoint complex (MCC). The kinetochore associated proteins Mad2, Mad1, Mad3, Bub1 and Bub3 are members of the MCC together with the kinase Mps1 (Faesen et al., 2017). A conformational change in Mad2 is important for the binding of Cdc20 to the MCC. Mad1 binds to unattached kinetochores, through interactions with Spc105/Knl1. The N-terminal half of Spc105/Knl1 harbors multiple phosphorylated motifs that are targets for the kinase Mps1 and are binding sites for both Bub1 and Bub3, which are conserved from yeast to human cells. These motifs contain a consensus sequence [M/I/L/V]-[E/D]-[M/I/L/V]-T, which is also called MELT motif (Krenn et al., 2014). Recruitment of Mad1 to phospho-MELT

motifs relies on the kinase activity of Bub1. Mad2 in a so-called closed form can bind Mad1 at unattached kinetochores, which leads to a conformational change of Mad2 into its open form. This soluble open Mad2 can bind to Cdc20 and incorporate it into the MCC which in turn keeps APC/C inactive. Bub1 also phosphorylates Cdc20, which additionally inhibits Cdc20 binding to the APC/C (Vanoosthuyse and Hardwick, 2005). When the cell has achieved correction of all false kinetochore-microtubule attachments, Cdc20 is released from the MCC, which leads to activation of the E3 ligase APC/C. APC/C then ubiquitinates Securin and mitotic cyclins for degradation via the 26S proteasome. Securin destruction leads to the release of the protease Separase, which is responsible for cleavage of sister chromatid cohesion and therefore for chromosome segregation (Nasmyth, 2002). Apart from these well studied mechanisms of error-correction and SAC function, posttranslational modifications also play a role in kinetochore assembly. Well studied examples are the interaction of Mif2 to Mtw1c, which enhanced via phosphorylation of the Dsn1 component (Akiyoshi et al., 2013a), a mechanism shown to be conserved in human (Petrovic et al., 2016).

1.3.4 Posttranslational modifications of Cse4 avoid ectopic kinetochore assembly

Posttranslational modifications have also been implicated in restricting kinetochore assembly to the centromeric region. When Cse4 is overexpressed in cells, localization is not restricted to the centromere anymore, but Cse4 is also found in chromosome arms (Collins et al., 2004), which could lead to ectopic kinetochore assembly and can ultimately result in problems during mitosis and hence aneuploidy. This has to be prohibited in order to only assemble kinetochores on Cse4 at centromeres. Cse4/CENP-A is target of different PTMs which are mandatory to avoid chromosomal instability. In a brief summary, Cse4 is phosphorylated in yeast by Ipl1 (Zeitlin et al., 2001), phosphorylated by Cdc5/Plk1, which prevents instability of chromosomes (Mishra et al., 2019), methylated on Arg37 and acetylated on Lys49, which both negatively regulate binding of Ame1/Okp1 (Fischbock-Halwachs et al., 2019), sumyolated on several lysin residues (Ohkuni et al., 2020) and trimethylated on its N-terminus which is important for CENP-T and CENP-I recruitment in higher vertebrates (Bailey et al., 2013; Sathyan et al., 2017). Another important modification of Cse4 is ubiquitination, which leads ultimately to destruction via the 26S proteasome. Therefore, Cse4 is ubiquitinated in several ways. It contains 16 lysines, which could serve as ubiquitin conjugation sites. It

was shown that mutation of all 16 residues does lead to some stabilization of Cse4, but it is still degraded to some degree, therefore other mechanisms exist to additionally modify Cse4 and tag it for degradation (Collins et al., 2004). One E3 ligase that is responsible for ubiquitin-mediated degradation of Cse4 is Psh1, which leads to a similar phenotype when it is deleted (Au et al., 2013; Hewawasam et al., 2010). Another E3 ligase that restrict Cse4 localization to the centromere is the E3 ligase complex SCF with three different F-Box proteins. It was shown that the F-Box proteins Rcy1 (Cheng et al., 2016), Met30 and Cdc4 (Au et al., 2020) can bind to SCF and create three individual complexes for ubiquitination of Cse4. All follow the same goal, which is to inhibit the deposition of Cse4 to chromosome arms. Additional E3 ligases like Ubr1 and the Ubc4-dependent E3 complex composed of Slx5 and Slx8 promote Cse4 turnover as well and it was found that multiple E3 ligases can act in parallel to maintain Cse4 levels in budding yeast (Cheng et al., 2016). Besides regulation of Cse4 levels to avoid ectopic kinetochores, components of the inner kinetochore contribute to proper kinetochore localization.

1.3.5 Inner kinetochore components specify kinetochore localization

The initially identified direct Cse4 interactor is Mif2/CENP-C, which is essential and conserved from yeast to humans. It has been described as the blueprint of the kinetochore, as it directly associates with other CCAN components as well as the outer kinetochore. Mif2 forms homodimers through a cupin-fold domain at its C-terminus, the function of this being incompletely understood. Mif2 has been shown to be implicated in prevention of ectopic kinetochore formation through an auto-inhibitory mechanism that prevents its interaction with the outer kinetochore component Mtw1c away from centromeres (Killinger et al., 2020; Klare et al., 2015). A recently identified second interactor of Cse4 and centromeric DNA is the heterodimer Ame1/Okp1, both proteins being essential in budding yeast (Anedchenko et al., 2019; Fischbock-Halwachs et al., 2019). Ame1 has at its N-Terminus a stretch of 15 amino acids, which are highly conserved among different yeasts and is essential and sufficient to bind to Mtw1c, an outer kinetochore component, *in vitro* (Hornung et al., 2014). In near proximity to the very N-terminus, a cluster of seven phosphorylation sites is positioned in a presumably unstructured region. These seven sites were identified to be phosphorylated both *in vivo* and *in vitro*, four of them containing a minimal motif for CDK (see Figure 3.11). The C-Terminus contains a coiled-coil region, which is mainly responsible for heterodimerization with Okp1. Two

additional phosphorylation sites were identified at the very C-terminus of Ame1. As mentioned above, Ame1 and Mif2 can both bind to the outer kinetochore component Mtw1c/Mis12c which recruits Ndc80c molecules that are responsible for dynamic microtubule interactions. Mif2 and Ame1 interact with Mtw1c through their extreme N-termini, and this interaction was shown mutually exclusive, indicating their interaction with different Mtw1c molecules (Killinger et al., 2020). In this study we will focus on the inner kinetochore, especially on the essential CCAN protein Ame1 and its role in restricting kinetochore assembly to centromeric chromatin. Through its interactions with DNA, other CCAN components and the Mtw1c it contains the potential to assemble kinetochores away from the centromeric region. As described before, Mif2 that interacts with a similar subset of kinetochore proteins, prevents this ectopic kinetochore assembly at least in part through an autoinhibitory mechanism (Killinger et al., 2020). Therefore, it is reasonable to assume that also Ame1 is subject to some kind of regulatory mechanism to prevent kinetochore formation away from the centromere. In this study we will focus on Ame1 phosphorylation and degradation as a way to regulate Ame1 levels during kinetochore assembly and hence prevent ectopic kinetochore assembly.

1.4 Objectives

Posttranslational modifications of kinetochore proteins can have multiple effects on proper assembly and disassembly. They are needed for correct Cse4 positioning, they enable or prevent protein interactions and therefore promote correct assembly and they are needed for error-correction of kinetochore-microtubule interactions. In budding yeast, different from higher eukaryotes, no strict separation between S- and M-Phase exists and as soon as the centromeric region is replicated, kinetochores have to be assembled rapidly to ensure bi-oriented microtubule binding, which is a prerequisite for sister chromatid segregation. How efficient kinetochore assembly is regulated remains incompletely understood. Here, we focused on understanding the role of Ame1/CENP-U phosphorylation, an essential component of the inner kinetochore. Ame1 and other CCAN components were found to be phosphorylated in a cell cycle dependent manner by the major regulatory kinase CDK. We show that CDK phosphorylation on Ame1 creates phospho-degron motifs that is recognized by an E3 ligase called SCF^{Cdc4}. Biochemical and genetic experiments indicate that ubiquitination and proteasomal degradation affects excess kinetochore subunits that are not part of fully assembled kinetochores. These findings point towards the existence of a mechanism that removes additional subcomplexes that are not incorporated into the microtubule binding interface at the centromeric region. As a result, we reveal a novel mechanism in kinetochore subunit level regulation that functions by limiting the number of Ame1/Okp1 heterodimers and COMA complexes to avoid ectopic kinetochore assembly.

II. MATERIALS AND METHODS

2.1 Instrumentation and Software

Table 2.1: Instrumentation used in this study

Instrument	Type	Provider
Agarose gel chambers	Peqlab Mini S	Peqlab
Agarose gel documentation	Gel Doc XR+	Bio-Rad Laboratories, Inc.
Autoradiogram delevoping machine	CAWOMAT 200 IR	CAWO Photochemisches Werk GmbH
Balances	Pioneer PA4101C	Ohaus Corporation
	XS105 Dual Range Micro Scale	Mettler Toledo
Block heater	SBH 200D	Stuart
Blue Light LED Illuminator	BL Star 16	Biometra GmbH
Cell Sorter	MaxQuant VYB	Miltenyi Biotech B.V. & Co. KG
Centrifuges	5424 R	Eppendorf AG
	5810 R	Eppendorf AG
	Sorvall RC6 Plus + SS-34 Rotor	Thermo Fisher Scientific
	Avanti JXN-26 + JLA-8.1 Rotor	Beckman Coulter, Inc.
	Optima Ultracentrifuge 130,000 rpm	Beckman Coulter, Inc.
	MiniStar	VWR International
Columns for FPLC/Ettan System	HisTrap™ 5ml G HP	GE Healthcare Life Sciences
	SEC: Superdex 200 pg HiLoad 16/600 Superdex 200 10/300 GL Superose 6 Increase 3,2/300	GE Healthcare Life Sciences

Instrument	Type	Provider
Concentrators	Amicon Ultra	Merck Millipore
End-over-end rotator	Bio RS-24	Lab4you
Enviromental Shaker	Innova44	New Bruinswick Scientific
	Multitron Standard	Infors AG
Ettan system	Ettan LC + P-905 + UV900 + pH/C-900 + Box-900 + Frac-950 in Unichromat 1500	GE Healthcare Life Sciences
FPLC system	Amersham P-920 + UPC-900 + Frac-950 (GE Healthcare) in Unichromat 1500	GE Healthcare Life Sciences
Freezer Mill	Large Freezer Mill 6870	SPEX SamplePrep
Incubator	HeraTherm Incubator IGS60 and IGS100	Thermo Fisher Scientific
Laminar Flow	Nuaire Laminar Flow	IBS Integra Bioscience
Microscopes	Optical: Dissecting microscope MSM System 200 Primo Star	 Singer Instruments Carl Zeiss AG
	Fluorescence: Deltavision Elite Deconvolution IX-71 microscope (Olympus) + Plan Apochromat 100x or 60x 1.4 NA objective (Olympus) + Coolsnap HQ camera (Photometrics)	GE Healthcare Life Sciences
	Axio Imager.M1 + Plan Apochromat 100x or 60x 1.4 NA objective (Carl Zeiss) + camera	Carl Zeiss AG
Microwave		Samsung
Mini-Rocker Shaker	PMR-30	Grant Instruments™ Grant Bio™

Instrument	Type	Provider
NanoDrop	NanoDrop One	Thermo Fisher Scientific
pH Meter	Seven Compact	Mettler Toledo
Photometer	BioPhotometer	Eppendorf AG
Platform Incubator	Unimax 1010	Heidolph Instruments GmbH
Rotating wheel	TC-7 rotating wheel	New Bruinswick Scientific
Scanner	9000F Mark II	Canon
SDS-PAGE chamber	Novex™ Xcell*SureLock*™ Mini Cell	Invitrogen™
SDS-PAGE chambers	Bio-Rad Mini-Protean 3 Cell, Mini-Protean Tetra Cell, Criterion™ Cell or Criterion™ Blotter	Bio-Rad Laboratories, Inc.
Sonifier Unit	Branson Digital Sonifier 450 + Sonifier Sound Enclosure Unit + Microtip	Marshall Scientific LLC
Stirring plates	MR 3001	Heidolph Instruments GmbH
	Heat-stir SB162	Stuart
	C-MAG MS10	IKA
Thermal Cycler (PCR)	C1000 Touch Thermal Cycler	Bio-Rad Laboratories, Inc.
Thermomixer	Thermomixer C	Eppendorf AG
Ultrasonic waterbath	Ultrasonic Cleaner USC-TH	VWR International
Vacuum Pump	VacuSip	Integra Bioscience GmbH
Vortexer	Vortex Genie 2	Scientific Industries, Inc.
Waterbath	5A Waterbath	Julabo GmbH
Western Blot developing machine	Amersham 600 Imager	GE Healthcare Life Sciences

Table 2.2: Software used in this study

Software	Usage	Provider
A plasmid Editor	Plasmid construction, *in silico* cloning, oligonuncleotide design	By Wayne Davis
Axio Vision SE64	Software Axio Imager.M1	Carl Zeiss AG
FlowJo	Single-cell flow cytometry data analysis	Becton, Dickinson & Company (BD)
Illustrator CC 2018	Figure editing	Adobe
ImageJ 1.47v	Figure editing	National Institutes of Health
ImageQuant™ TL	Western Blot exposure	GE Healthcare Life Sciences
Microsoft Office	Text editing, data analysis	Microsoft
Photoshop CS5.1	Scanning of SDS-PAGEs and Coomassie stained agarose gels	Adobe
SnapGene Viewer	Plasmid construction, *in silico* cloning, oligonuncleotide design	GSL Biotech LLC.
SoftwoRx™	Software DeltaVision Elite microscope	GE Healthcare Life Sciences
Unicorn Control software	Software FPLC/Ettan System	GE Healthcare Life Sciences

2.2 Chemicals

Table 2.3: Chemicals used in this study

Chemical	Provider
β-Mercaptoethanol	Carl Roth
50 % (w/v) PEG 3350	Sigma Aldrich
Acetic Acid (AcOH)	VWR International
Acrylamid solution 30 %	AppliChem GmbH or Carl Roth
Adenine Sulfate (ADE)	Alfa Aesar
Amersham ECL Western Blotting Reagents	GE Healthcare Life Science

Chemical	**Provider**
Amersham Nitrocellulose Membrane	GE Healthcare Life Science
Ammonium Acetate (CH_3COONH_4)	Sigma Aldrich
Ammonium Sulfate ($(NH_4)_2SO_4$)	Carl Roth
Ampicillin	Carl Roth
Bacto Agar	Becton, Dickinson & Company (BD)
Bacto Peptone	Becton, Dickinson & Company (BD)
Bacto Yeast Extract	Becton, Dickinson & Company (BD)
Benomyl	Sigma Aldrich
Bis Tris propane	Fluka Chemika
Bovine Serum Albumin (BSA)	AppliChem GmbH
Bovine Serum Albumin Standard	Thermo Fisher Scientific
Bradford Reagent	Bio-Rad Laboratories, Inc.
Calcium Chloride ($CaCl_2$)	Sigma Aldrich
Concavalin A (ConA)	Sigma Aldrich
Coomassie Brilliant Blue R250	Sigma Aldrich
Cycloheximide (CHX)	Sigma Aldrich or Carl Roth
D-Dextrose	Carl Roth
D-Galactose	Sigma Aldrich
D-Raffinose	BioSynth
ddH_2O	ELGA system
Dimethyl pimelimidate (DMP)	Thermo Fisher (Pierce)
Di-Potassium hydrogenphosphate (K_2HPO_4)	Fluka Chemika
Di-Sodium hydrogenphosphate (Na_2HPO_4)	Merck Chemicals
Difco Yeast Nitrogen Base without amino acids	Becton, Dickinson & Company (BD)
Dimethylsulfoxid (DMSO)	Carl Roth
DNA 1 kb (Plus) ladder	Thermo Fisher Scientific
DNA loading dye	Thermo Fisher Scientific
Dynabeads Protein G (magnetic)	Invitrogen or Merck Millipore
Ethanol (EtOH)	Fisher Chemicals
Ethylenediaminetetraacetic acid (EDTA)	AppliChem GmbH

Chemical	**Provider**
Ethyleneglycol-bis(β-aminoethylether) (EGTA)	Fluka Analytical
Formaldehyde	Carl Roth
Gel Filtration Standard	GE Healthcare Life Science
Geniticin (G-418)	VWR International
Gluthathione Sepharose^{TM} 4B	GE Healthcare Life Science
Glycerol	Carl Roth
HEPES	Carl Roth
Hydroxyurea	US Biological Life Sciences
IgG Sepharose	GE Healthcare Life Science
Imidazole	Sigma Aldrich
IPTG	Thermo Fisher Scientific
Isopropanol	Fisher Chemical
L-Histidine (HIS)	Carl Roth
L-Leucin (LEU)	Carl Roth
L-Lysine (LYS)	Carl Roth
L-Tryptophan (TRP)	Carl Roth
Lithium Acetate (LiAc)	Alfa Aesar
M2 Flag Agarose	Sigma Aldrich
Magnesium Chloride ($MgCl_2$)	Fluka Chemika
Methanol (MeOH)	Fisher Chemical
Milk powder	Carl Roth
MOPS SDS running buffer NuPage	Invitrogen
NiNTA Sepharose	IBA Lifesciences
Nocodazole	Sigma Aldrich
Nourseothricin (Clonat)	Jena Bioscience
NP-40 Alternative	CalBiochem
PeqGreen DNA/RNA dye	Peqlab
Phenylmethylsulfonyl fluoride (PMSF)	Sigma
PhosTag reagent	Nard Institute, Ltd
Ponceau S	Serva Chemicals
Potassium Acetate (Kac)	Sigma Aldrich

Chemical	Provider
Potassium Chloride (KCl)	Sigma Aldrich
Protein Marker prestained or unstained	Thermo Fisher Scientific
Salmon sperm carrier DNA	AppliChem GmbH
Seakem LE Agarose	Lonza Group AG
Silver Nitrate ($AgNO_3$)	Sigma Aldrich
Sodium Acetate ($C_2H_3NaO_2$)	Sigma Aldrich
Sodium Borate ($Na_2B_4O_5(OH)_4$)	Sigma Aldrich
Sodium Carbonate (Na_2CO_3)	Merck Chemicals
Sodium Chloride (NaCl)	AppliChem GmbH
Sodium Tetraborate ($B_4Na_2O_7$ * 10 H_2O)	Sigma Aldrich
Sodium Thiosulfate ($Na_2S_2O_3$)	Sigma Aldrich
Sorbitol	Carl Roth
Sucrose	Carl Roth
Sytox Green	Invitrogen
Tris-(2-carboxyethyl)-phosphin (TCEP)	Carl Roth
Tris(hydroxymethyl)-aminomethan ($C_4H_{11}NO_3$)	AppliChem GmbH
Triton X-100	Sigma Aldrich
Tween-20	Sigma Aldrich
Uracil (URA)	Carl Roth
Zinc Chloride ($ZnCl_2$)	Sigma

2.3 Frequently used buffers and solutions

Table 2.4: Solutions and buffers used in this study

Buffer or Solution	Ingredients	Provider
10x PBS	80 g/l NaCl	AppliChem GmbH
	150 g/l KCl	Sigma Aldrich
	11,5 g/l N_2HPO_4	Merck
	2 g/l K_2HPO_4	Fluka Chemicals

Buffer or Solution	Ingredients	Provider
10x SDS	25 mM Tris-HCl 200 mM Glycin 3.5 mM SDS	AppliChem GmbH AppliChem GmbH Carl Roth
10x TAE	0.4 M Tris Base 48.4 g Acetic Acid 0.01 M EDTA	AppliChem GmbH VWR AppliChem GmbH
10x TBS	50 mM Tris-HCl pH 7.5 150 mM NaCl	AppliChem GmbH AppliChem GmbH
10x TE	10 mM Tris 100 mM EDTA	AppliChem GmbH AppliChem GmbH
10x Western Transfer Buffer	25 mM Tris 190 mM Glycin 1.75 mM SDS 10 % MeOH	AppliChem GmbH AppliChem GmbH Carl Roth Fisher Chemical
4x SDS separation buffer	1.5 M Tris-HCl 0.4 % SDS pH 8.8	AppliChem GmbH Carl Roth
4x Stacking buffer	0.5 M Tris-HCl 0.4 % SDS pH 6.8	AppliChem GmbH Carl Roth
6x SDS loading dye (40 ml)	12 ml β-Mercaptoethanol 23.2 ml 100 % Glycerol 4.8 g SDS 15 ml 0.25 M Tris pH 6.8	Carl Roth Carl Roth Carl Roth AppliChem GmbH
Buffer for analytical Size Exclusion Chromatography (SEC)	20 mM Hepes, pH 7.5 200 mM NaCl 25 % Glycerol 2 mM TCEP	Carl Roth AppliChem GmbH Carl Roth Carl Roth
Buffer for Electrophoretic Mobility Shift Assays (EMSA)	20 mM Hepes, pH 7.5 250 mM NaCl	Carl Roth AppliChem GmbH

Buffer or Solution	Ingredients	Provider
Coomassie staining solutions	Solution A:	
	25 % Isopropanol	Fisher Chemicals
	10% Acetic Acid	VWR International
	0.05 % Coomassie Brilliant Blue R250	Sigma Aldrich
	Solution B:	
	25 % Isopropanol	Fisher Chemicals
	10 % Acetic Acid	VWR International
	0.005 % Coomassie Brilliant Blue R250	Sigma Aldrich
	Solution D:	
	10 % Acetic Acid	VWR International
doADE solution	30 mg/l L-Leucine	Carl Roth
	20 mg/l L-Tryptophan	Carl Roth
	20 mg/l Uracil	Carl Roth
	30 mg/l L-Lysine	Carl Roth
	20 mg/l L-Histidine	Carl Roth
doHIS solution	20 mg/l Adenine Sulfate	Carl Roth
	30 mg/l L-Leucine	Carl Roth
	20 mg/l L-Tryptophan	Carl Roth
	20 mg/l Uracil	Carl Roth
	30 mg/l L-Lysine	Carl Roth
doLEU solution	20 mg/l Adenine Sulfate	Carl Roth
	20 mg/l L-Tryptophan	Carl Roth
	20 mg/l Uracil	Carl Roth
	30 mg/l L-Lysine	Carl Roth
	20 mg/l L-Histidine	Carl Roth
doLYS solution	20 mg/l Adenine Sulfate	Carl Roth
	30 mg/l L-Leucine	Carl Roth
	20 mg/l L-Tryptophan	Carl Roth
	20 mg/l Uracil	Carl Roth
	20 mg/l L-Histidine	Carl Roth

Buffer or Solution	Ingredients	Provider
doTRP solution	20 mg/l Adenine Sulfate	Carl Roth
	30 mg/l L-Leucine	Carl Roth
	20 mg/l Uracil	Carl Roth
	30 mg/l L-Lysine	Carl Roth
	20 mg/l L-Histidine	Carl Roth
doURA solution	20 mg/l Adenine Sulfate	Carl Roth
	30 mg/l L-Leucine	Carl Roth
	20 mg/l L-Tryptophan	Carl Roth
	30 mg/l L-Lysine	Carl Roth
	20 mg/l L-Histidine	Carl Roth
Elution buffer for purification of AO complexes	30 mM Hepes, pH 7.5	Carl Roth
	400 mM NaCl	AppliChem GmbH
	1 M Imidazole (Gradient)	Sigma Aldrich
	1 mM TCEP	Carl Roth
FACS buffer	5 mM Tris-HCl, pH 7.5	AppliChem GmbH
Gelfiltration buffer	30 mM Hepes, pH 7.5	Carl Roth
	250 mM NaCl	AppliChem GmbH
	5 % Glycerol	Carl Roth
	2 mM TCEP	Carl Roth
Lysis buffer for Co-Immunoprecipitation	25 mM Hepes, pH 8.0	Carl Roth
	150 mM $MgCl_2$	Fluka Chemicals
	0.1 mM EDTA, pH 8.0	AppliChem GmbH
	0.5 mM EGTA, pH 8.0	Fluka Analytical
	0.1 % NP-40 Alternative	CalBiochem
	150 mM KCl	Sigma Aldrich
	15 % Glycerol	Carl Roth
	1mM DTT	Serva
	1:100 protease inhibitor	Pierce, Sigma Aldrich
Lysis buffer for genomic DNA isolation	50 mM Tris-HCl pH 7.5	AppliChem GmbH
	20 mM EDTA pH 8.0	AppliChem GmbH
	1 % SDS	Carl Roth

Buffer or Solution	Ingredients	Provider
Lysis buffer for purification of AO complexes	30 mM Hepes, pH 7.5 400 mM NaCl 20 mM Imidazole 1 mM TCEP 5 % Glycerol	Carl Roth AppliChem GmbH Sigma Aldrich Carl Roth Carl Roth
Lysis buffer for whole cell extract preparation	25 mM Hepes, pH 8 150 mM NaCl 150 mM EDTA 1 mM DTT 5 % Glycerol 1:100 protease and phosphatase inhibitor	Carl Roth AppliChem GmbH AppliChem GmbH Serva Carl Roth Pierce
Lysogeny broth (LB) according to Lennox or Lysogeny broth (LB) + Amp	5 g/l Sodium Chloride 10 g/l Tryptone 5 g/l Yeast Extract Premixed LB-Medium powder 1.5 % (w/v) Bacto Agar 100 µg/ml Ampicillin	 AppliChem BD Carl Roth
Minimal Medium	1.7 g/l Difco Yeast Nitrogen Base without amino acids 5 g/l Ammonium Sulfate 0.05 g/l Adenine Sulfate 22 g/l Bacto Agar for plates 1.1 % (w/v) Dextrose (SD) 1.2 % (w/v) Raffinose + 2 % (w/v) Galactose (S-RG) 10 % amino acid drop out solution (either doHIS, doURA, doLEU, doLYS, doTRP, doADE)	BD Carl Roth Alfa Aesar BD Carl Roth BioSynth/Sigma Aldrich
Ponceau S solution	2.5 g/l Ponceau S 400 ml MeOH 150 ml Acetic Acid	Serva Chemicals Fisher Chemicals VWR International

Buffer or Solution	Ingredients	Provider
Protease and phosphatase inhibitor cocktail mix	EDTA-free tablets	Thermo Fisher (Pierce)
Protease and phosphatase inhibitor cocktail mix for yeasts and fungi		CalBiochem
Sporulation Medium	10 g/l Potassium Acetate 1 g/l Bacto Yeast Extract 0.5 g/ml Dextrose	Sigma Aldrich BD Carl Roth
Synthetic complete amino acid solution	20 mg/l Adenine Sulfate 30 mg/l L-Leucine 20 mg/l L-Tryptophane 20 mg/l Uracil 30 mg/l L-Lysine 20 mg/l L-Histidine	Carl Roth Carl Roth Carl Roth Carl Roth Carl Roth Carl Roth
Wash buffer for Co-Immunoprecipitation	25 mM Hepes, pH 8.0 150 mM KCl	Carl Roth Sigma Aldrich
Wash buffer for Co-Immunoprecipitation II	20 mM Hepes, pH 7.5 150 mM NaCl 2.5 % Glycerol 2 mM TCEP	Carl Roth AppliChem GmbH Carl Roth Carl Roth
Yeast Extract Peptone (YEP)	11 g/l Bacto Yeast Extract 22 g/l Bacto Peptone 0.05 g/l Adenine Sulfate 22 g/l Bacto Agar for plates 1.3 % (w/v) Dextrose (YEPD) 2 % (w/v) Raffinose + 2 % (w/v) Galactose (YEPRG)	BD BD Alfa Aesar BD Carl Roth BioSynth/Sigma Aldrich

2.4 Enzymes

Table 2.5: Enzymes used in this study

Enzyme family	Description	Provider
Ligase	T4 DNA Ligase	New England Biolabs
Phosphatase	Alkaline Phosphatase (CIP)	New England Biolabs
Polymerase	Q5 Hot Start Polymerase Ranger DNA Polymerase	New England Biolabs Bioline
Protease	Pronase	Roche
Protease/Glucanase	Zymolase 100 T	Carl Roth
Proteinase	Proteinase K	Carl Roth
Restriction Endonuclease	BamHI	New England Biolabs
Restriction Endonuclease	DpnI	Thermo Fisher Scientific
Restriction Endonuclease	HindIII	New England Biolabs
Restriction Endonuclease	NcoI	New England Biolabs
Restriction Endonuclease	NotI	New England Biolabs
Restriction Endonuclease	SalI	New England Biolabs
Restriction Endonuclease	XhoI	New England Biolabs
Restriction Endonuclease	XmaI	New England Biolabs
Ribonuclease	RNAse A	Sigma Aldrich

2.5 Kits

Table 2.6: Kits used in this study

Kit	Provider
NucleoSpin Plasmid Kit	Macherey & Nagel
FastGene Gel/PCR Extraction Kit	Nippon Genetics Co. Ltd
PureLink Quick PCR Purification Kit	Invitrogen by Thermo Fisher Scientific

2.6 *Saccharomyces cerevisiae* strains

All strains were derived from the wildtype strain S288C with Mat a/α; ade2-1, lys2-801am, ura3-52, his3Δ200, leu2-3,112, TRP1. If otherwise stated strains were derived from wildtype strain W303 with Mat a/α; ade2-1, ura3, his3-11,15, leu2-3, trp1-1, can1-100, psi+, ssd1-d2. The following table contains all background strains used in this study. An extended list can be found in the Supplementary data.

Table 2.7: *S. cerevisiae* background strains used in this study

Strain	Genotype	Reference
DDY902	Mat a, ade2-1, leu2-3,112, his3Δ200, ura3-52	Westermann lab
DDY904	Mat α, lys2-801am, leu2-3,112, his3Δ200, ura3-52	Westermann lab
DDY1102	Mat a/α Ade2/ade2-1, his3Δ200/ his3Δ200, leu2-3,112/leu2-3,112, ura3-52/ura3-52, Lys2/lys2-801	Westermann lab
DDY1944	Mat a, ura3-52, lys2-801, ade2-101, his3Δ200, trp1Δ63, leu2Δ1::skp1-3::LEU2	Westermann lab
DDY2270	Mat a, ade2, his3, trp1, ura3, leu2, can1 (W303)	Yanagida lab
SWY355	Mat α, his3Δ200, ura3-52, lys2-801am, tor1-1 fpr1::loxP-LEU2-loxP RPL13A-2xFKBP12::loxP-TRP1-loxP	Westermann lab

2.7 Generated and used plasmids

An extended list with all the used plasmids for genetic experiments in *S. cerevisiae* (Table 5.2) or expression in *E.coli* (Table 5.3) can be found in the supplementary data. Here, lists of the used plasmid backbones are presented.

Table 2.8: Plasmid backbones used for genetic experiments in *S. cerevisiae*

Plasmid	Characteristics	Reference
pRS305	Shuttle vector for yeast integration with marker gene LEU2	Sikorski and Hieter, 1989

pRS306	Shuttle vector for yeast integration with marker gene URA3	Sikorski and Hieter, 1989
pESC-HIS	pESC yeast epitope tagging vector with marker gene HIS3	Agilent Technologies
pESC-URA	pESC yeast epitope tagging vector with marker gene URA3	Agilent Technologies

Table 2.9: Plasmid backbones used for expression in *E. coli* or *S.cerevisiae*

Plasmid	**Characteristics**	**Reference**
Bacterial expression		
pET3aTr/pST39	Polycistronic cloning vector for expression in *E. coli*	Tan et al., 2005
pETDuet-1	Vector for co-expression of two target genes in *E. coli*	Novagen
Yeast expression		
pESC-URA	pESC yeast epitope tagging vector with marker gene URA3	Agilent Technologies

2.8 Antibodies

Table 2.10: Antibody solutions with the according dilution and incubation times used in this study.

Epitope Tag/Protein	**Dilution**	**Incubation time**	**% milk/BSA**	**Provider**
Flag	1:10000	1 h at RT or overnight at 4 °C	2.5 %	Sigma
Myc (clone 9E10)	1:1000	Overnight at 4 °C	2.5 %	BioLegend

Epitope Tag/Protein	Dilution	Incubation time	% milk/BSA	Provider
HA	1:1000-1:2000	3 h at RT or overnight at 4 °C	2.5 % for RT, 5 % for overnight at 4 °C	Covance
Tubulin	1:1000	1 h at RT or overnight at 4 °C	2.5 %	Santacruz Biotechnologies

2.9 Recombinant proteins

Table 2.11: Recombinant proteins generated and used in this study.

Protein	Construct	Mutation	Reference
Ame1-6xHis/Okp1	Full length	Wildtype	Hornung et al., 2011
Ame1-6xHis/Okp1	Full length	Ame1 T31A	This study
Ame1-6xHis/Okp1	Full length	Ame1 T31A S59A S101A	This study
Ame1-6xHis/Okp1	Full length	Ame1 S41A S45A	This study
Ame1-6xHis/Okp1	Full length	Ame1 S52A S53A	This study
Ame1-6xHis/Okp1	Full length	Ame1 S41A S45A S52A S53A	This study
Ame1-6xHis/Okp1	Full length	Ame1 T31A S41A S45A S52A S53A S59A S101A	This study
Ame1-6xHis/Okp1	Full length	Ame1 T31E S41E S45E S52E S53E S59E S101E	This study
Ame1-6xHis/Okp1	Ame1-1-256/Okp1 full length	Ame1 deletion of 257-324 aa	S. Westermann
Ame1-6xHis/Okp1	Ame1-1-256/Okp1-1-359	Ame1 deletion of 257-324 aa, Okp1 deletion of 360-406 aa	This study
Ame1-6xHis/Okp1	Ame1 full length/Okp1-1-359	Okp1 deletion 360-408 aa	S. Westermann

Protein	Construct	Mutation	Reference
Ame1-6xHis/Okp1	Full length	Okp1 S26A	This study
Ame1-6xHis/Okp1	Full length	Ame1 S41A S45A S52A S53A Okp1 S26A	This study
Ame1-6xHis/Okp1	Full length	Ame1 T31A S41A S45A S52A S53A S59A S101A + Okp1 S26A	This study
Ame1-6xHis/Okp1	Ame1-126-324/Okp1 full length	Ame1 deletion of 1-125 aa	S. Westermann
Ame1-6xHis/Okp1	Ame1 full length/Okp1-128-406	Okp1 deletion of 1-127 aa	S. Westermann
Nkp1-6xHis/Nkp2	Full length	Wildtype	This study
Mtw1/Dsn1-6xHis-Nnf1-Nsl1	Dsn1-172-576/Nsl1/Mtw1/Nnf1	Dsn1 deletion of 1-171 aa	Killinger et al., 2020
Mtw1/6xHis-Nnf1	Full length	Wildtype	Killinger et al., 2020
TEV-protease	Full length	S219V	Kapust et al., 2001

Standard methods used for *Escherichia coli* were modified after (Sambrook and Russell, 2001).

All methods for *Saccharomyces cerevisiae* were modified after Methods in Yeast Genetics: A Cold Spring Harbor Laboratory Course Manual 2005 Edition (Amberg et al., 2005).

2.10 Plasmid generation in *E. coli*

Plasmids were generated with either restriction based cloning methods or using a restriction free technique (van den Ent and Lowe, 2006).

The gene of interest and the vector backbone were digested using compatible restriction endonucleases and a ligation with T4 ligase was performed for 1 h at room temperature or with an incubation over night at 16 °C according to the protocols by New England Biolabs. Digested insert and vector backbone were purified from an agarose gel using the FastGene PCR/Gel extraction Kit from Nippon Genetics. Alternatively, the gene of interest was amplified with homologous overhangs to the vector backbone with specific oligonucleotides. The amplified DNA was purified from an agarose gel and used as a megaprimer on the vector backbone or used in a Gibson Assembly Reaction. For site directed mutagenesis of plasmids a single oligonucleotide was used that carries the mutated codon of the gene of interest using a specific PCR amplification according to the QuikChange Multi Site-Directed Mutagenesis Kit by Agilent Technologies. The following PCR program was used: 95 °C 5 minutes, 30 cycles of 95 °C 1 minute, 55 °C 1 minute, 68 °C 16 minutes, final annealing 55 °C 1 minute, final elongation 68 °C 30 minutes (QuikChangeKK). Afterwards parental DNA was digested at 37 °C for 1 hour and 10 minutes using the restriction endonuclease Dpn*I*.
3-5 µl of the ligated or Dpn*I* digested vector was transformed into either 50 µl XL10 Gold or DH5α *E. coli* cells using the standard protocol for chemically competent cells. The generated plasmids were selected via an ampicillin resistance on LB solid medium with 100 mg/ml ampicillin for 16 h at 37 °C. Plasmid DNA was isolated from single colonies using the NucleoSpin Plasmid Kit from Macherey & Nagel and verified by sequencing through Eurofins Genomics.

2.11 Bacterial expression in *E. coli*

Recombinant Ame1/Okp1, Nkp1/Nkp2 or Mtw1 (kindly provided by K. Killinger) complexes were expressed in BL21 Rosetta DE3 *E. coli* cells containing the plasmids of interest. Cultures of 2-5 l LB supplemented with 100 mg/ml ampicillin were grown to a logarithmic growing culture of an OD_{600} of 0.6 – 1 at 37 °C in an environmental shaker with 200-250 rpm, cooled down to 18 °C and induced with 0.5 mM IPTG. Cells were cultivated over night at 18 °C and 200-250 rpm for optimal expression of the proteins. For MNc expression cells were induced with 0,5 mM IPTG and incubated at 37 °C for 4 h (kindly provided by K. Killinger). Cells were harvested at 4800 x g at 20 °C for 15 minutes, washed once in 1xPBS and directly used for purification or stored at -20 °C.

2.11.1 Purification of recombinant Ame1/Okp1 complexes

Pellets were resuspended in lysis buffer (30 mM Hepes pH 7.5, 400 mM NaCl, 20 mM Imidazole, 1 mM TCEP, 5 % Glycerol) and treated with ultrasound to break cells using the Branson Digital Sonifier. Broken cells were pelleted at 18000 rpm and 4 °C for 20 minutes and clear lysates were either loaded onto a HisTrap HP 5 ml column or onto NiNTA sepharose beads. When the HisTrap HP 5 ml column was used, the lysate was loaded onto the column using the sample pump at the FPLC system. After loading, the column was washed with 6 CV lysis buffer and eluted with an Imidazole gradient (30 mM Hepes pH 7.5, 400 mM NaCl, 1 M Imidazole, 1 mM TCEP, 5 % Glycerol) at app. 300 mM. Protein elution was followed by absorbance measurements at 280 nm and peak fractions were analyzed on a 12 % SDS-PAGE. Fractions with high amounts of Ame1/Okp1 complexes were pooled and concentrated to the correct volume in order for the second step purification. When NiNTA sepharose beads were used, the clear lysate was incubated with equilibrated beads (washed first in water, second in lysis buffer) for 2-3 hours at 4 °C while rotating. Beads were washed with 50 CV lysis buffer and eluted in 4-6 ml elution buffer containing 300 mM Imidazole. The eluate was concentrated to the correct volume for the following second step purification.
In a second step the complex was purified over an analytical size exclusion chromatography using either a Superdex 200 10/300 GL or a Superdex 200 pg HiLoad 16/600 and eluted in 30mM Hepes pH 7.5, 250 mM NaCl, 5 % Glycerol and 2 mM TCEP. When the concentration was below 1 mg/ml measured with Bradford reagent or with the NanoDrop, Ame1/Okp1 complexes were concentrated using a Vivaspin Centrifugal Concentrator from Sartorius AG with a molecular weight cut off (MWCO) of 5 kDa. Recombinant proteins were frozen in liquid nitrogen and stored at -80 °C.

2.11.2 Purification of Nkp1/Nkp2 complex

Pellet of a 2 liter culture was lysed in the following buffer (30 mM Hepes, pH 7.5, 400 mM NaCl, 20 mM Imidazole, 1 mM TCEP, 5 % glycerol) and treated with ultrasound using the Branson Digital Sonifier. Opened cells were pelleted at 18000 rpm and 4 °C for 20 minutes and clear lysates were loaded onto a HisTrap 5 ml column using the sample pump at the FPLC system. The column was washed with 6 CV with lysis buffer and the

protein was eluted using an Imidazole gradient with 1 M Imidazole in the lysis buffer. Protein elution was followed by absorbance measurements at 280 nm and peak fractions were analyzed on a 12 % SDS-PAGE. Fractions containing the protein complex were pooled and concentrated for a second purification step. The subcomplex was purified further over an analytical Size Exclusion Chromatography using the Superdex 200 16/600 pg column and eluted in 30 mM Hepes, pH 7.5, 250 mM NaCl, 2 mM TCEP. Protein samples were flash frozen in liquid nitrogen and stored at -80 °C.

2.11.3 Purification of Mtw1c and Mtw1/Nnf1 complexes

Mtw1c and the Mtw1/Nnf1 complexes were kindly provided by K. Killinger, extended purification protocol can be found in Killinger et al., 2020. Both complexes were expressed in BL21 (DE3, Novagen) cells and purified using a multi-step purification protocol. Lysis buffer consists of 50 mM Tris-HCl, pH 7.5, 500 mM NaCl, 30 mM Imidazole, 10 % glycerol, 5 mM β-Mercaptoethanol as described previously (Maskell et al., 2010). Lysates were purified first via the 6xHIS Tag on either Dsn1 (Mtw1c) or on Nnf1 (Mtw1/Nnf1) using a HisTrap HP 5-ml column (GE Healthcare), washed and eluted with a buffer containing 250 mM Imidazole (30 mM Tris, pH 8.5, 80 mM NaCl, 10 % glycerol, 5 mM β-Mercaptoethanol, 250 mM Imidazole). For Mtw1c an anion exchange chromatography (HiTrap Q HP 5-ml column, GE Healthcare; 30 mM Tris-HCl, pH 8.5, 5 % glycerol from 80 mM (A) or 1 M NaCl (B)) and afterwards Size Exclusion Chromatography (HiLoad Superdex 200 16/600 pg, GE Healthcare; 30 mM Hepes pH 7.5, 250 mM NaCl, 5 % glycerol, 2 mM TCEP) was performed, whereas for Mtw1/Nnf1c the anion exchange column did not work and after concentration the eluate was loaded onto the Superdex 200 10/300 GL column (GE Healthcare) directly. Concentrated recombinant protein complexes were frozen in liquid nitrogen and stored at -80 °C.

2.12 Protein expression in *S. cerevisiae*

Recombinant yeast proteins were expressed in a protease deficient strain (DDY1810) from an inducible galactose promoter.

2.12.1 Purification of Cdc28/Clb2 kinase

Recombinant Cdc28/Clb2 kinase was expressed in yeast using a 2micron plasmid which holds Clb2-CBP-TEV-ZZ under the control of an inducible galactose promoter. In order to maintain the plasmid in all cells, cultures were incubated always under selective pressure. Cells were incubated first on a SD-doURA minimal medium plate and then grown in a 60 ml preculture in SD doURA (2 % dextrose) overnight at 30 °C and 180 rpm shaking. With that, another 600 ml SD-doURA preculture was incubated to saturation for 2 days at 30 °C and 180 rpm. Cells were then washed twice with 1x PBS and incubated in 6 l SR-doURA minimal medium (2 % raffinose) to an OD_{600} of 1. Expression was induced by adding galactose to a final concentration of 2 % and addition of 10x YEP solution and cells were incubated overnight at 30 °C and 180 rpm. Cells were harvested at 2500 rpm for 15 minutes and frozen down as droplets using liquid nitrogen, ground into powder using a large freezer mill and stored at -80 °C until further usage. 60 grams of grinded yeast powder were lysed in 60 ml 2x Hyman buffer (100 mM bis-Tris propane pH 7, 200 mM KCl, 10 mM EDTA, 10 mM EGTA, 20 % Glycerol) with additional protease inhibitors like Protease Inhibitor Cocktail tablet, 1 mM PMSF and Calbiochem Protease Inhibitor Cocktail Mix. Addition of the last one will stain the lysate red when lysis is complete. Before sonification, Triton X-100 was added for a final concentration of 1 %. The lysate was sonified for 30 sec with a 50 % amplitude with a pulse of 1 sec. After pelleting cell debris for 30 min at 4 °C, the supernatant was spun a second time under the same conditions in fresh tubes. A layer of lipids was removed and the clear lysate was transferred into falcons with 1 ml slurry IgG Sepharose pre-equilibrated as follows: 10 ml TST, 1 ml 0.5 M Ammonium Acetate (NH_4OAc), 5 ml TST, 1 ml 0.5 M NH_4OAc, 5 ml TST, 5 ml 1x Hyman buffer (50 mM bis-Tris propane pH 7, 100 mM KCl, 5 mM EDTA, 5 mM EGTA, 10 % Glycerol) (+300 mM KCl). The KCl concentration of the lysate had to be adjusted to 300 mM final for more stability. After incubating the lysate with the IgG Sepharose for 4 hours at 4 °C, beads were pelleted and washed with 15 ml 1x Hyman buffer (+300 mM KCl), washed with 25 ml 1x Hyman buffer (+300 mM KCl, 1 mM DTT, 0.1 % Tween 20) and resuspended in 1.5 ml 1x Hyman buffer (+300 mM KCl, 1 mM DTT, 0.1 % Tween 20) for TEV cleavage overnight at 4 °C. Here 2x50 µl TEV-protease were used. Recover TEV eluate and add 3 volumes of Calmodulin binding buffer (25 mM Tris-HCl pH 8, 150 mM NaCl, 0.02 % NP-40, 1 mM $MgCl_2$, 1 mM Imidazole, 2 mM $CaCl_2$, 1 mM DTT) and adjust the $CaCl_2$ concentration by adding 3 µl 1 M $CaCl_2$ per ml TEV eluate. Incubate with 400 µl slurry of preequilibrated

Calmodulin Sepharose 4B for 1.5 hours at 4 °C. Afterwards beads were washed twice with 8 ml Calmodulin binding buffer and eluted 5 times in 300 µl fractions using Calmodulin elution buffer (like binding buffer but with 20 mM EGTA instead of 2 mM $CaCl_2$). Fractions with highest protein concentration were frozen in 15 µl aliquots and 5 µl were used for one kinase reaction.

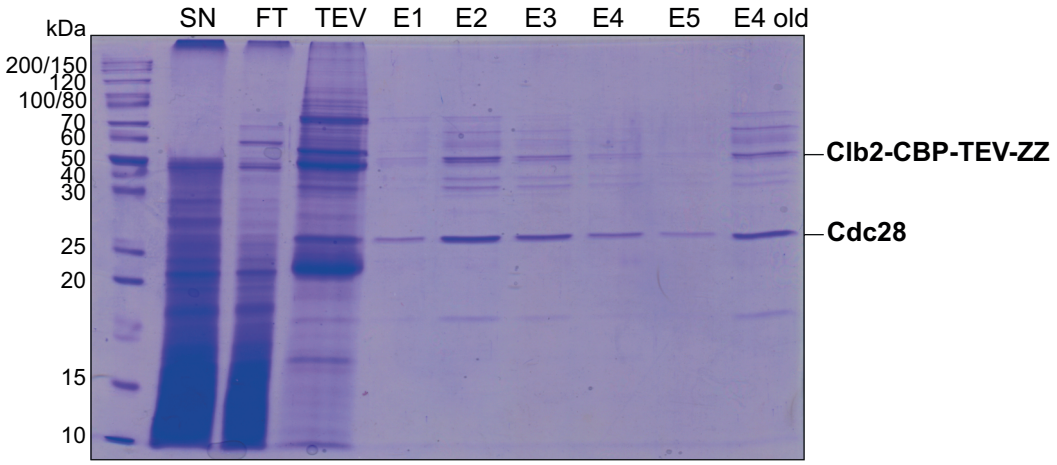

Figure 2.1: Purification of Cdc28/Clb2. SDS-PAGE stained with Coomassie showing the different elution fractions of new Cdc28/Clb2 purification. An established protocol was used and followed without any changes. SN = lysate after high speed spin; FT = lysate after bead incubation; TEV = eluate after TEV cleavage overnight; E1-E5 = elution fractions from beads; E4 old = elution fraction E4 from old purification for comparison of purity and concentration

2.13 Generation of *S. cerevisiae* strains

S. cerevisiae strains were either generated by transformation with the Lithium Acetate/PEG method or through genetic crossing.

2.13.1 Transformation of *S. cerevisiae*

For transformation of *S. cerevisiae,* a 50 ml liquid culture in YEPD was incubated to enrich logarithmic growing cells. Cells were pelleted by centrifugation at 2500 rpm for

3 minutes and washed twice in sterile ddH_2O. Yeast cells were taken up in 1.5 ml of a mixture containing 0.1 M LiAc, 1x TE in sterile ddH_2O and 200 µl cells were incubated with 200 µg *carrier* DNA, up to 5 µg transforming DNA and a mixture containing 0.1 M LiAc, 1x TE in 40 % PEG 3350 for 30 minutes with rotation, followed by a heat shock at 42 °C for 12 minutes. Pelleted cells were taken up in 150 µl sterile ddH_2O and plated on minimal medium plates containing the required amino acid dropout solution for 2-3 days at 30 °C, stated by the used auxotrophy marker (uracil, leucine, or histidine) or antibiotic resistance cassette (geniticin or nourseothricin).

Transforming DNA was either generated through a PCR after Longtine or Knop (Janke et al., 2004; Longtine et al., 1998) or by linearization of a yeast-bacterial shuttle vector (pRS based plasmids). To amplify DNA in order to integrate it into yeast for a homologous recombination, a PCR with following standard settings was used: 5 minutes denaturation at 95 °C, 30 cycles of 95 °C for 1 minute, 1 minute at 54 °C for annealing, 4 minutes of 68 °C for elongation, final elongation for 5 minutes at 68 °C. As a template either plasmid DNA or genomic DNA was used. Specific oligonucleotides that create a homologous overhang to the genomic locus of interest were utilized and the DNA was amplified in a 50 µl volume, from which 45 µl were transformed into yeast cells without further purification.

Yeast-bacterial shuttle vectors (for generation protocol see section 2.1) were linearized in a 50 µl volume with 500 ng of plasmid DNA with the according restriction endonuclease (Nco*I*, EcoR*I*, Xma*I*, Hind*III*) for 3 hours at 37 °C and 45 µl were transformed into yeast cells. 5 µl of each transformed DNA were tested in an agarose gel electrophoresis for the correct size and completeness of linearization.

Integration was achieved through homologous recombination by using homologous overhangs to the region of integration – the endogenous locus or exogenously at a locus from an auxotrophy marker gene.

For the generation of yeast overexpression strains, 2-3 µl of a yeast episomal plasmid (YEp) was transformed into yeast cells without digest. These plasmids carry the pUC ori and an ampicillin resistance cassette for replication and selection in *E. coli*, but also the yeast 2micron origin, which enables autonomous replication in *S. cerevisiae* (Agilent Technologies). Additionally, these plasmids contain one of four yeast auxotrophy marker genes for selection on minimal medium plate supplemented with the according drop out solution (here drop out histidine or uracil).

2.13.2 Genetic crossing and mating of *S. cerevisiae*

Genetic crossing was used to generate new strains. Therefore, two haploid strains of opposing mating types (a and alpha) were streaked on top of each other on a YEPD rich medium plate and incubated for 5 hours to overnight. To separate the diploid from the haploid parental strains either the formed zygotes were picked under a dissection microscope (Singer Instruments) and incubated at 30 °C on YEPD rich medium for 2-3 days or via a double drop out SD minimal medium plate. For this, SD plates with an amino acid solution was used, that lack two amino acids that are needed for selection of auxotrophy marker genes, which are provided by the parental strains. Because the diploid crossed strain has both auxotrophy marker genes, only the diploid strain can grow whereas the haploid parental strains are not able to. Minimal medium plates with parental and mated strains were incubated at 25 °C for 2-3 days.

After incubation of the diploids for 2-3 days on plate, a sporulation culture was inoculated with a saturated starting culture. Therefore, 1 ml of overnight culture was pelleted and washed once with sterile ddH_2O. 4 ml of sporulation medium with 1:300 amino acid solution SC were inoculated with the diploid cells and incubated at room temperature for 4-10 days on a rotating wheel.

The sporulation was examined under a light microscope where the product of meiosis could be observed: 4 haploid spores in an ascus. To mechanically separate these spores the ascus was removed upon Zymolase treatment: 37,5 µl prewarmed Zymolase 100 T (2 mg/ml in 1 M Sorbitol) for 250 µl sporulation culture, incubated for 3.5 minutes at 37 °C, reaction stopped on ice with 150 µl 1xPBS. For dissection, the Zymolase treated cell suspension was inoculated on a rich medium YEPD plate and separation of 16 tetrads per plate was performed at the dissection microscope (Singer Instruments). The YEPD plate was incubated for 2-3 days at 25 or 30 °C.

The haploid spores of 12 tetrads were spotted on different drop out minimal plates (SD-doHIS, LEU, URA, ADE, LYS, TRP) and on rich YEPD plates incubated at different temperatures (25, 30, 34, 37 °C) to examine the genotype. If necessary, spores were also spotted on YEPD with geneticin or nourseothricin. To determine the Mating type, two defined Mating type tester strains (DDY55 (a) + DDY56 (alpha)) were plated onto SD plates and haploid spores were spotted on top. A growth on the mating type tester plates was only observed, when the haploid spore could mate with the tester strain and therefor supplement all the nutrients for growth. Cells that could grow on the mating type tester DDY55 had to be alpha, whereas cells that grew on DDY56 had to be a.

2.13.3 Genomic DNA isolation from *S. cerevisiae*

To verify the correct integration of the transformed DNA by PCR the genomic DNA of the newly generated strains has to be isolated. Therefore, 1 ml of a saturated starting culture was pelleted and washed with sterile ddH_2O before incubated in a lysis buffer (50 mM Tris-HCl pH 7.5, 20 mM EDTA pH 8, 1 % SDS) with protease and phosphatase inhibitors (EDTA-free tablets from Pierce, Thermo Fisher Scientific). Yeast cells were disrupted through bead beating with 500 µl acid washed glass beads (Carl Roth) for 1.5 minutes at 4 °C. Nucleic acids were precipitated through addition of 0.5 M KAc and 0.5 M NaCl, and proteins were inactivated by high temperature (75 °C) for 10 minutes. Nucleic acids were pelleted and washed with EtOH abs. (100 % and 70 %) and taken up in 50 µl 1x TE with 200 µg/ml RNAse (Sigma Aldrich). 2 µl of genomic DNA were used in a PCR reaction to verify genomic integration or used as a template to amplify a megaprimer for restriction free cloning (van den Ent and Lowe, 2006).

2.13.4 Verification of newly generated strains

To verify different clones after transformation either a colony PCR or an amplification from genomic DNA was performed. In a colony PCR fresh cells from a selection plate were heated for 1 minute in a microwave, mixed with a PCR master mix (containing required oligonucleotides, dNTPs, buffer and polymerase) and incubated as described before.

If a sequencing of the PCR product is required, for example to check for amino acid substitutions, a PCR was performed with genomic DNA as a template. Program: 98 °C 3 minutes, 30 cycles of 98 °C 10 seconds, 54 °C 20 seconds, 72 °C 50 seconds, final elongation 72 °C 2 minutes (Q5 gDNA). For sequencing the amplified DNA has to be purified from an agarose gel. After agarose gel electrophoresis the DNA of the correct size was cut out of the gel using a blue light table to minimize the risk of UV radiation. For gel extraction the FastGene Gel/PCR Extraction Kit from Nippon Genetics Co. was used according to the manual and the purified DNA was sent to Eurofins Genomics for sequence verification.

2.14 Cell cycle arrests of *S. cerevisiae*

To arrest cells in a specific cell cycle stage different peptides and drugs can be used. Liquid cultures were inoculated from a saturated starting culture to an OD_{600} of 0.3 and let grow for 1-2 hours. To halt the cells in G1 phase, the yeast pheromone alpha factor was added to cells of the mating type a in a final concentration of 10 µg/ml (polar unbudded cells); For an arrest in synthesis phase Hydroxyurea was added in a final concentration of 0.2 M (large budded cells; depletion of dNTPs by inhibition of ribonucleotide reductase); For a metaphase arrest 15 µg/ml Nocodazole was added (large budded cells, microtubule depolymerization). Arrests were performed for 90-120 minutes and the cell shape was viewed under a light microscope.
For analysis of one complete cell cycle, cells were diluted in 80 ml of liquid YEPD with a starting OD_{600} = 0.2 and incubated for 1 hour at 30 °C and 180 rpm. Next, cells were arrested in a G1-like state with alpha-factor for 2 hours at 30 °C and 180 rpm. Afterwards, cells were washed extensively in YEPD + Pronase (100 µg/ml) and in YEPD to remove the alpha factor. Cells were than incubated in fresh YEPD in fresh flasks at 30 °C + 180 rpm and immediately and every 15 minutes cells were fixed for budding index, FACS staining and for cell extracts for Western Blotting analysis.

2.14.1 FACS analysis

Yeast cells were fixed in 95 % ethanol using the following protocol: 1 ml of cells with an OD_{600} of less than 1 were harvested and resuspended in 300 µl ddH_2O and 700 µl 95 % ethanol was added dropwise. Cells were stored at 4 °C until digest. Cells were digested and stained with Sytox Green following the protocol found in (Haase and Reed, 2002). Digested cells were sonicated and read out at the MaxQuant VJB machine. FACS profiles were generated using the FlowJo software.

2.15 GAL-Shift assay

For overexpression studies strains that contain 2micron plasmids were incubated overnight in YEPD. Next morning, cells were washed twice in YEP-Raffinose (2 %) and incubated in YEP+R for 3 hours at 30 °C and 180 rpm. Overexpression was induced with

the addition of 2 % Galactose, and timepoints were after 0, 3 and 5 hours in YEP+RG. Cell extracts for Western Blotting analysis were prepared for each timepoint.

2.16 Serial dilution of *S. cerevisiae*

In order to test the viability of mutated strains a serial dilution assay was performed. Therefore, a saturated overnight culture was diluted to an OD_{600} of 0.4-0.6 in 1 ml of minimal medium to wash out residual rich medium. Afterwards a serial dilution of 1:4 was performed 6 times in a 96well plate. With the use of a 48 pin-pinning tool up to 8 different strains/dilutions were transferred to different solid media, either rich medium (YEPD and YEP+RG) or minimal media (SD or S+RG) and incubated for 2-3 days at 25, 30, 34 and 37 °C.

2.16.1 The anchor-away technique

To investigate mutations that would cause lethality, the anchor-away technique is used to deplete an essential protein from its usual localization so that an introduced mutated protein version is the only present copy (Haruki et al., 2008). FRB-tagged Ame1 was anchored-away from the nucleus upon addition of Rapamycin in a final concentration of 1 µg/ml. In this thesis Rapamycin was added to YEPD rich medium plates and they were used in serial dilution assays. This method requires a specific genomic background, which can be seen in the strain list (Table 2.7 background strain SWY355).

2.17 Colony sectoring assay of *S. cerevisiae*

For a chromosome segregation fidelity experiment a system was used, that tracks the loss of a centromeric plasmid (mini chromosome) that is carrying a suppressor gene (SUP11) for a mutation in the adenine auxotrophy marker gene. Upon loss of *SUP11* yeast colonies turn red. Strains were incubated always under selective pressure (SD doHIS) to ensure maintenance of the plasmid. A saturated starting culture in SD doHIS was diluted back into YEPD to achieve a controlled loss of the mini chromosome for 4 hours, afterwards cells of an OD_{600} of 0.4 were washed once with 1 ml of SD doHIS, diluted 1:1000 in 1 ml SD doHIS and plated onto SD doHIS plates. Plates were incubated for 3 days at 30 °C

and 1 day at 4 °C to increase the red pigmentation. Red and red-sectored colonies were counted.

2.18 Preparation of whole cell lysates from *S. cerevisiae*

For strain verification or biochemical analysis whole cell lysates had to be prepared from different *S. cerevisiae* strains. Two different methods were used: either a quick and dirty method, in which the cells are boiled in SDS loading dye (storage at -20 °C), or a more extended method, in which a clear yeast cell extract was prepared, that can be stored at -80 °C.

2.18.1 Quick & Dirty method to prepare whole cell lysates

For checking different clones or to follow proteins with an epitope tag over the cell cycle, whole cell lysates with the Quick & Dirty method were prepared (Kushnirov, 2000). Therefore, cells with an equivalent of OD_{600} of 2 were pelleted and washed with 1x PBS to remove the growth medium. After that, cells were either mechanically disrupted by bead beating or treated with 200 µl 0.1 M NaOH to open the cells. Afterwards the broken cells were incubated in 1x SDS loading dye and boiled for 5 minutes at 95 °C. Cell debris was pelleted and the clear supernatant was loaded on a 12 % SDS-PAGE and further analyzed by Western Blotting.

2.18.2 Extended method to prepare clear yeast cell extracts

For immunoprecipitation experiments clear yeast cell extracts were prepared as following: 50 ml of a logarithmic growing culture were pelleted and washed with 1x PBS. Cells were taken up in 700 µl lysis buffer (25 mM Hepes pH 8, 150 mM NaCl, 2 mM EDTA, 1 mM DTT, 5 % glycerol, 1:100 protease and phosphatase inhibitor (EDTA-free tablets Pierce, Thermo Fisher Scientific)) and disrupted through bead beating with 500 µl acid washed glass beads for 1.5 minutes at 4 °C. After addition of 0.1 % NP-40 and an incubation for 20 minutes rotating at 4 °C cell debris was pelleted. The supernatant was spun at maximum speed and 4 °C for 10 minutes. Protein concentration of the clear

supernatant was measured with Bradford Reagent (Bio-Rad) and lysates were snap frozen in liquid nitrogen and stored at -80 °C. For immunoprecipitation assays 400 µl with a total amount of 200-300 mg protein were used, for SDS-PAGE and Western Blotting 30 µg in total was sufficient.

2.19 Biochemical analysis of yeast proteins

To investigate different kinetochore proteins and their binding properties, different biochemical analyses were used.

2.19.1 Polyacrylamide gel electrophoresis

To separate proteins according to their molecular weight a sodium dodecyl sulfate polyacrylamide gel electrophoresis (SDS-PAGE) was performed using the Bio-Rad Mini-PROTEAN Cell system. As a standard a molecular weight marker (PageRuler Plus from ThermoFisher; prestained for Western Blotting and unstained for SDS-PAGE), 1x SDS running buffer was used and the gels were run at 150-200 V. The polyacrylamide concentration was 10 or 12 %. Afterwards gels were stained with Coomassie Brilliant Blue in order to visualize the proteins, for example after a purification, or used for Western Blotting.
For better resolution of phosphorylated isoforms of proteins, the reagent PhosTag was added to the polyacrylamide gels at a concentration of 20 mM, next to 40 mM $ZnCl_2$. Polyacrylamid solution was filtered before pouring the SDS-PAGE gels. During SDS-PAGE gel loading, $ZnCl_2$ was added to every sample to avoid waviness. The SDS-PAGE gel was washed twice with 1x Western Transfer buffer containing 100 mM EDTA prior to Western Blotting.

2.19.2 Western Blotting

To transfer proteins from an SDS-PAGE onto a nitrocellulose membrane (GE Healthcare) in order to visualize proteins with a fluorescent tag, Western Blotting using the Bio-Rad Mini Trans-Blot Cell system was performed. Therefore, the Tank Blotting method with 1x Western Transfer Buffer was used and run for 90-120 minutes at 4 °C at 150 V or overnight at 4 °C and 30 V constant. After blotting the nitrocellulose membrane was stained with Ponceau S to document the correct transfer. After blocking the membrane in 5 % milk in 1x TBST (0.02 % Tween 20), it was incubated with an antibody solution in 2.5 % milk in 1x TBST for 1-3 hours at room temperature or overnight at 4 °C on a rocker. The used antibodies can be found in section 1.8. Except for the anti-Flag and the anti-Tubulin antibody which are HRP coupled directly, a secondary antibody is necessary to create a signal in chemiluminescence via an HRP tag. Therefore, an anti-mouse antibody was used in a 1:10000 dilution in 2.5 % milk for 1 h at room temperature. After washing 3x for 10 minutes with 1x TBST the membrane was exposed for 30 seconds or up to 12 minutes using the GE Healthcare Amersham Imager 600.

2.19.3 Electrophoretic mobility shift assay (EMSA)

To test the ability of recombinant proteins to bind to centromeric DNA, electrophoretic mobility shift assays (EMSAs) were performed. For that, increasing amounts of purified proteins (0 µg to 6 µg final protein; protein concentrations vary between 0.5 to 1.5 mg/ml) were incubated with constant volumes (150-400 ng, variation upon independent experiments) of purified DNA. To visualize the DNA-protein complex a 1.2 % agarose gel with 1x TAE buffer and PeqGreen in a 1:5000 dilution was prepared and run at 120 V for 45 minutes. Afterwards the agarose gel was stained with Solution A and B for 10 minutes and destained overnight in Solution D.

2.19.4 Analytical Size Exclusion Chromatography

For *in vitro* binding studies recombinant proteins were incubated at 4 °C for 15 minutes and loaded onto a Superose 6 3.2/30 column using the Ettan LC system from GE Healthcare. As controls, the protein complexes were also loaded onto the column

alone to compare elution profiles. SEC buffer contains 20 mM Hepes pH 7.5, 150 mM NaCl, 2.5 % Glycerol, 1mM TCEP and was used for all binding assays. Recombinant proteins that served as a binding partner to Ame1/Okp1 complex (Mtw1c and Mif2) were provided by lab members and not purified in this study. Elution profiles were monitored at 280 nm and 100 µl fractions were collected. Fractions with elution peaks were mixed with 1x loading dye and loaded onto an 12 % SDS-PAGE and polyacrylamide gels were stained with Coomassie Brilliant Blue. Overlaid curves of elution profiles were produced using the Unicorn software from GE Healthcare.

2.19.5 *In vitro* kinase assays

To test if Cdc28/Clb2 can phosphorylate Ame1/Okp1 complexes *in vitro*, kinase assays were performed. Therefore, recombinant Ame1/Okp1 complexes with different Ame1 phospho-preventing mutations (T31A, S41AS45A, S52AS53A, S41AS45AS52AS53A (4A) or T31AS41AS45AS52AS53AS59AS101A (7A)) with a final amount of 1 µg were incubated with 5 µl Cdc28/Clb2, 1 µl 1 mM cold ATP, 1 µl radioactive labeled ATP (10 µCi/µl) and 5 µl 4x kinase buffer (80 mM Hepes pH 7.5, 400 mM KCl, 40 mM $MgCl_2$, 40 mM $MnCl_2$, 100 mM β-Glycerolphosphate, 4 mM DTT) in a final volume of 20 µl. The reaction was incubated for 30 minutes at 30 °C and stopped by adding 6x SDS loading dye. 22 µl were loaded on a SDS-PAGE and stained with Coomassie Brilliant Blue. After destaining the gel overnight in Solution D an X-ray film was exposed for 5-20 minutes and developed with the CAWOMAT 200 IR machine. (Many thanks to A. Dudziak who performed the kinase assays for me!).

For kinase assays with Ame1/Okp1 complexes and Mtw1c complexes recombinant proteins were preincubated in a molar ratio of 2:1, where always 5 µM of AOc and 10 µM Mtw1c were used. Mixed protein samples were incubated on ice for 30 minutes, followed by adding all other components described above.

III. RESULTS

3.1 Biochemical analyses of Ame1-WT and phosphorylation mutants

The inner kinetochore component Ame1/CENP-U is essential for binding the outer kinetochore complex Mtw1c/Mis12c. It also has other binding partners within the inner kinetochore, as it is a member of the tetrameric complex called COMA (see introduction) and can interact with Mif2/CENP-C. In this study we analyze the role of Ame1 phosphorylation and its function in kinetochore assembly and cell cycle regulation using biochemical methods presented in this chapter and genetic studies described in later sections.

Based on Mass Spectrometry results described in the introduction, mutants of Ame1 were designed, that either eliminate or mimic phosphorylation on clustered residues in the N-terminal half. Seven previously identified amino acids (a single Threonine (T31) and six Serines (S41, S45, S52, S53, S59 and S101)) were mutated to either Alanine to prevent phosphorylation, or to Glutamic Acid to mimic phosphorylation. The mutations were introduced on a pST39 polycistronic plasmid, suitable for co-expression of Ame1 and Okp1 in *E.coli*.

3.1.1 Recombinant Ame1-WT and phosphorylation mutants have similar biochemical properties

In order to allow investigation of differences between Ame1-WT and the phosphorylation mutants in binding to established Ame1 interactors, Ame1/Okp1 (AOc) were produced recombinantly in *E. coli*. For the production of recombinant Ame1/Okp1 complexes an already established protocol was used, which is described in section 2.2.1. Briefly, Ame1/Okp1 was purified with a 2-step protocol including affinity chromatography based on a C-terminal 6xHis-tag on Ame1 followed by Size Exclusion Chromatography (SEC). For this study, a variety of different Ame1/Okp1 mutants were purified all in a similar fashion. To ensure that the mutations introduced into Ame1 do not interfere with overall protein folding, stability and properties, their behavior in analytical SEC was compared, as shown in Figure 3.1. As the elution profiles of Ame1-WT/Okp1 and Ame1-7A and 7E/Okp1 are nearly identical, we conclude that the mutants allow complex formation with Okp1 and do not interfere with overall protein structure or stability. In addition, their

behavior throughout the purification procedure was very similar. Coomassie stained SDS-PAGE gels of peak fractions show equal elution of all three complexes, whereas Ame1-7E shifts in SDS-PAGE to a higher molecular weight that is even bigger than Okp1. These purified AO complexes were further analyzed in protein binding assays with Mif2, the Mtw1 complex, the Nkp1/Nkp2 heterodimer or centromeric DNA.

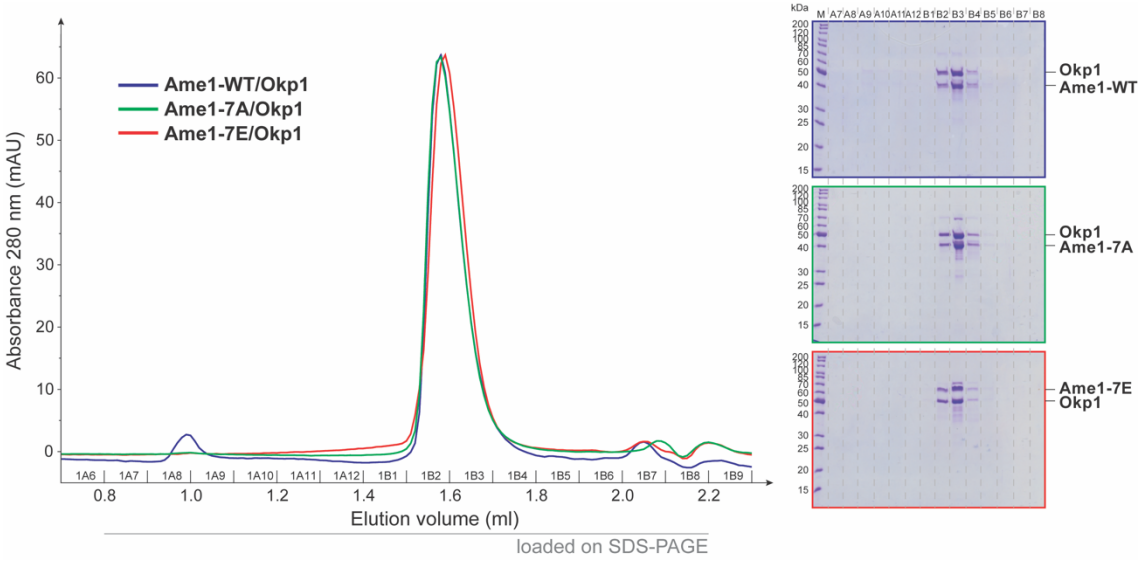

Figure 3.1: Ame1/Okp1 or Ame1 variants 7A and 7E behave similar in SEC. All AO complexes with either Ame1-WT, Ame1-7A or Ame1-7E were purified in an identical fashion and subjected to analytical size exclusion chromatography on a Superpose 6 increase 3.2/300 column. All samples were run at isocratic conditions. Samples of peak fractions were run on an SDS-PAGE and stained with Coomassie (indicated by grey line). Note that Ame1-7E runs higher in the Coomassie stained SDS-PAGE and the complex eluted slightly later from the column.

3.1.2 Ame1-WT/Okp1 and Ame1 mutants bind DNA in a similar manner

To test the aforementioned recombinant AO complexes in their ability to bind DNA, a stretch of centromeric DNA (CEN-DNA) that carries a stretch of centromeric DNA that represents 300 bp around of CEN3 of budding yeast was produced. Interaction of the complexes was than tested in an Electrophoretic Mobility Shift Assay (EMSA) as shown in Figure 3.2. In this assay the DNA amount was kept constant, whereas the protein amount was gradually increased, which should lead to a shift of free DNA to complex bound DNA with increasing concentration of protein, assuming the complex binds to DNA. As the shifts of free DNA to complex bound DNA look very similar in Ame1-WT/Okp1 as compared to Ame1-7A and Ame1-7E/Okp1, we conclude that all complexes bind equally well to CEN-DNA. Variation in the amount of AO complexes used do not mask possible differences in the binding, as protein amounts were evaluated through Coomassie staining of the agarose gel and adjusted equally. As no difference in the complexes interaction to DNA was found, other known binding partners were tested for their interaction to WT and mutant AO complexes.

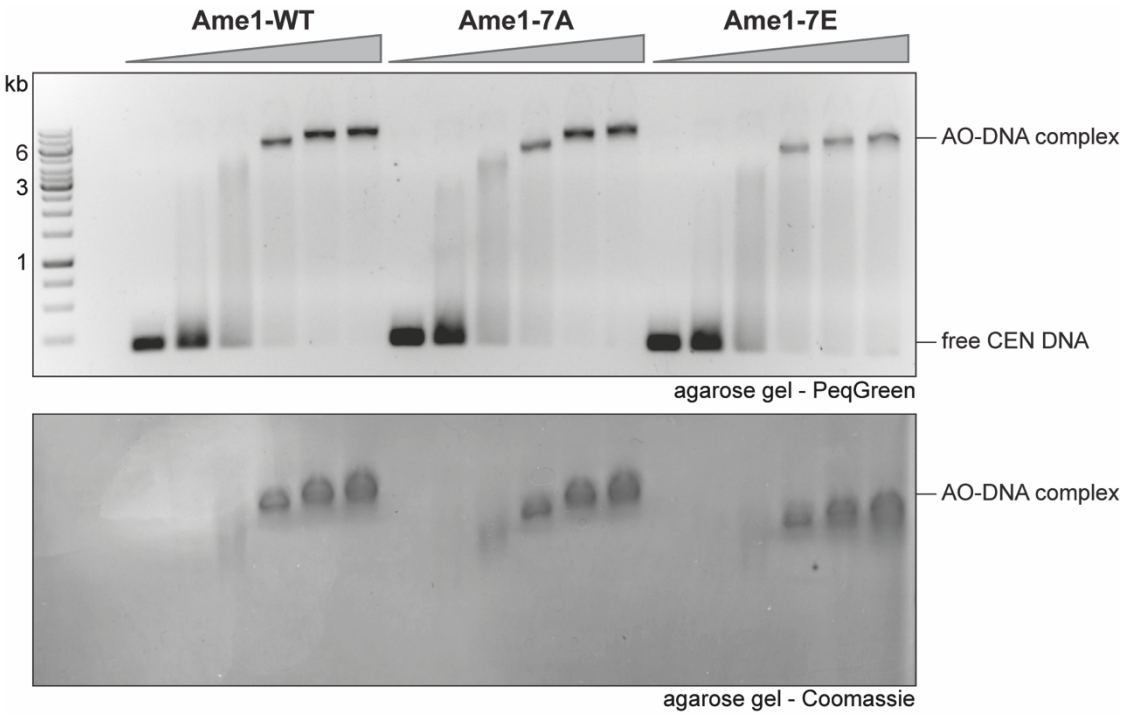

Figure 3.2: Electrophoretic Mobility Shift Assay of AO complexes reveals similar binding to DNA. Top agarose gel shows shift of free CEN DNA when it is bound to Ame1/Okp1 with gradually increasing concentration of AOc from left to right. Coomassie stained agarose gel indicates different amounts of Ame1/Okp1 complexes used in corresponding lanes. Both Ame1-WT and phospho-mutants are able to bind to centromeric DNA equally well.

3.1.3 Ame1/Okp1 wildtype and mutant complexes bind equally well to the outer kinetochore component Mtw1c in solution

As described in the introduction Ame1/Okp1 binds to Mtw1c through the N-terminus of Ame1. Because the phosphorylation cluster in Ame1 is relatively close to this interaction site, we tested if this posttranslational modification alters the binding capacity of Ame1 to Mtw1c.

To do so, Ame1-WT/Okp1 or mutant complexes were incubated with recombinant Mtw1c and the mixture was separated on an analytical SEC. As depicted in Figure 3.3, the binding of Ame1-7A/Okp1 and Ame1-7E/Okp1 to Mtw1c is comparable to the binding of Ame1-WT/Okp1 to Mtw1c as seen in a shift to an earlier elution volume in the chromatogram and of all proteins on the Coomassie stained SDS-PAGE gel of the peak fractions.

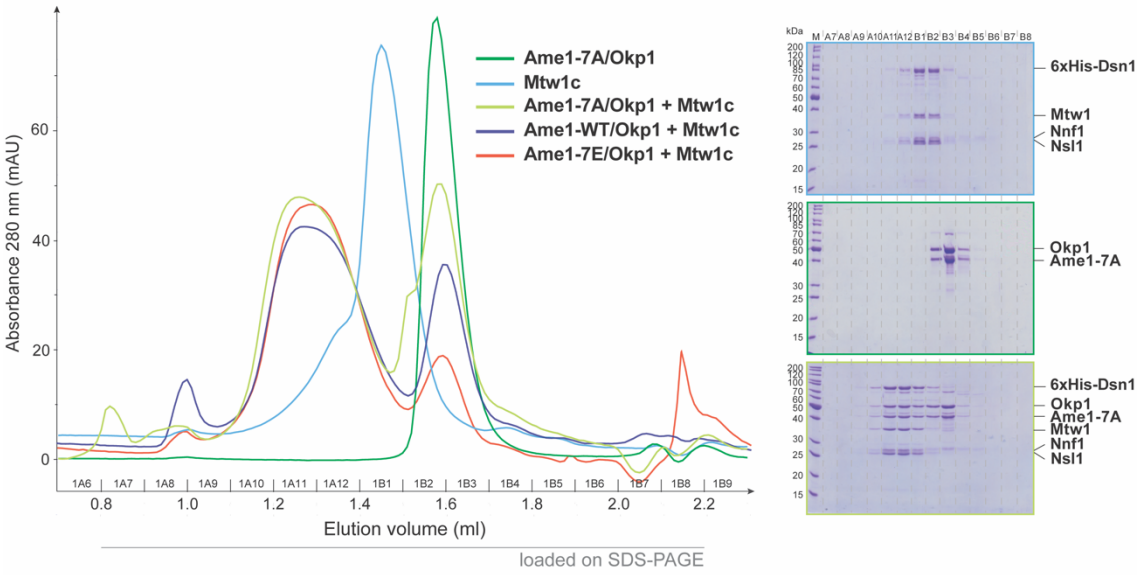

Figure 3.3: Ame1-WT/7A/7E/Okp1 complex binding to Mtw1c is similar in SEC. Analytical SEC chromatograms and corresponding Coomassie stained SDS-PAGE gels of AO-7A complex (green) with Mtw1c alone and in combination at 10 µM concentration. For AO-WT and AO-7E together with Mtw1c only chromatograms are shown (dark blue and red). All combinations were incubated for 1 hour at 4 °C prior to the run. Grey line indicates fractions loaded on SDS-PAGE. Mtw1c is depicted in light blue and Ame1-7A/Okp1 alone in dark green.

3.1.4 The Ame1/Okp1 complex binds to the main inner kinetochore component Mif2

Another known interaction partner of the AOs is Mif2/CENP-C (Hornung et al., 2014). To investigate if mutations in the phosphorylation cluster interfere with this binding, interaction of Mif2 purified from insect cells with different Ame1/Okp1 complexes was tested in SEC experiments. Ame1-WT as well as Ame1-7A/7E/Okp1 complexes were able to bind to Mif2 equally well in SEC. In Figure 3.4 SEC runs of Ame1-WT/7A/7E/Okp1 and Mif2 are shown together and in isolation. An interaction of these components was apparent from a shift in the elution profile to an earlier elution volume and from a shift of all proteins visible in Coomassie stained SDS-PAGE gels of the peak fractions. No difference in the interaction of Mif2 to WT or mutant AO complexes was detected in this assay. The peak at an elution volume of 2 ml corresponds to the Flag-Peptide used for Mif2 purification, which is still present in the Mif2 protein sample.
Taken together, Ame1/Okp1 complexes that are mutated in the seven residues of the phosphorylation cluster, are able to bind to the known interactors Mtw1c, Mif2 and to centromeric DNA similarly to the AO wildtype complex.

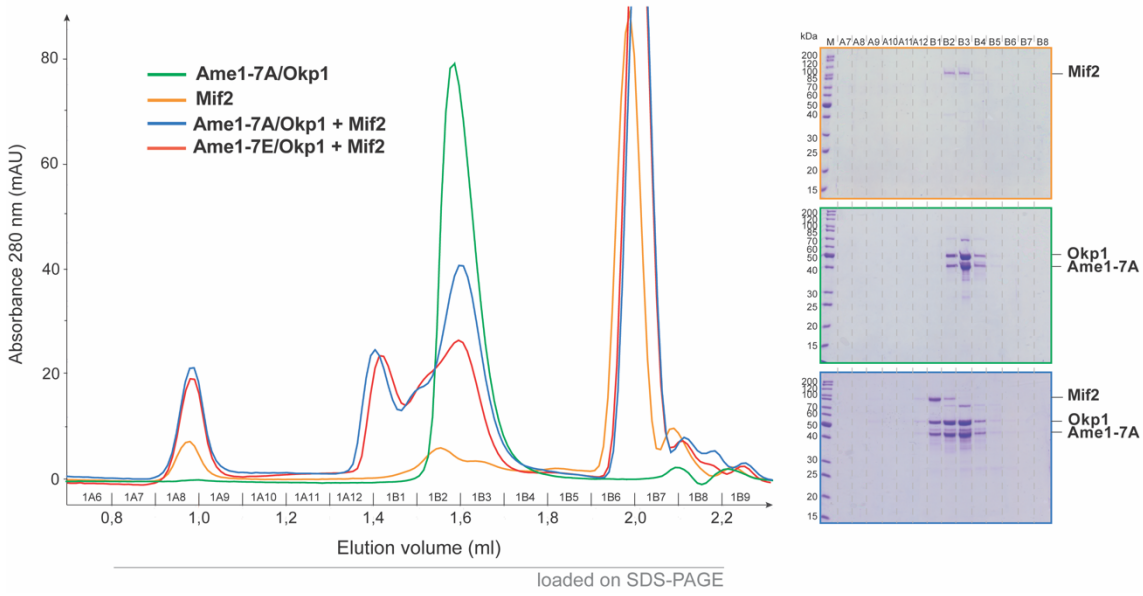

Figure 3.4: AO mutant complexes bind to Mif2 in SEC. Analytical SEC chromatograms and corresponding Coomassie stained SDS-PAGEs of Ame1-7A/Okp1 complex with Mif2 alone and in combination at 10 µM concentration (combination shown in blue). For the binding of Ame1-7E/Okp1 only the chromatogram is shown because they bind equally well (red). Both combinations were incubated for 1 h at 4 °C prior to the run. Mif2 is depicted in orange and Ame1-7A/Okp1 alone in green. The peak at an elution volume of 2.0 ml corresponds to the Flag-Peptide used for Mif2 purification.

3.1.5 Purification of N- and C-terminal truncation mutants of AOc

As none of the previously described interaction partners was affected by the phospho-mutations introduced into Ame1, the study was expanded to another set of kinetochore proteins, the Nkp1/Nkp2 (NNc) dimer. This heterodimer is not essential in yeast or higher vertebrates and might resemble CENP-R in the human kinetochore. Recombinant COMA complex from *K. lactis* forms a hexameric complex with Nkp1/Nkp2 (Schmitzberger et al., 2017). As the N-terminus of Ame1 binds to the Mtw1c and recent structural evidence indicates that the NN dimer is located to a different site of the CCAN (Yan et al., 2019), investigations concentrated on the C-terminus of Ame1. At the C-terminus of Ame1 a coiled-coil region is responsible for the dimerization with Okp1. Therefore, in this study recombinant proteins were produced in which the C-terminus of Ame1 was truncated only to a point to keep the AO heterodimer intact (Ame1 1-255). Additionally, the C-terminus of Okp1 was truncated until residue Okp1 1-359. An N-terminal truncation of Ame1 that eliminates the phospho-cluster was included to exclude the possibility of NNc binding to that region (Ame1 126-324). In addition to the C-terminal truncation mutants, N-terminal truncations of Ame1 and Okp1 were tested in DNA binding assays (EMSA). Figure 3.5 shows the different constructs that were used for the studies stated below. Note, that Ame1/Okp1 is always present as a heterodimer, which is also true for C- or N-terminal truncations.

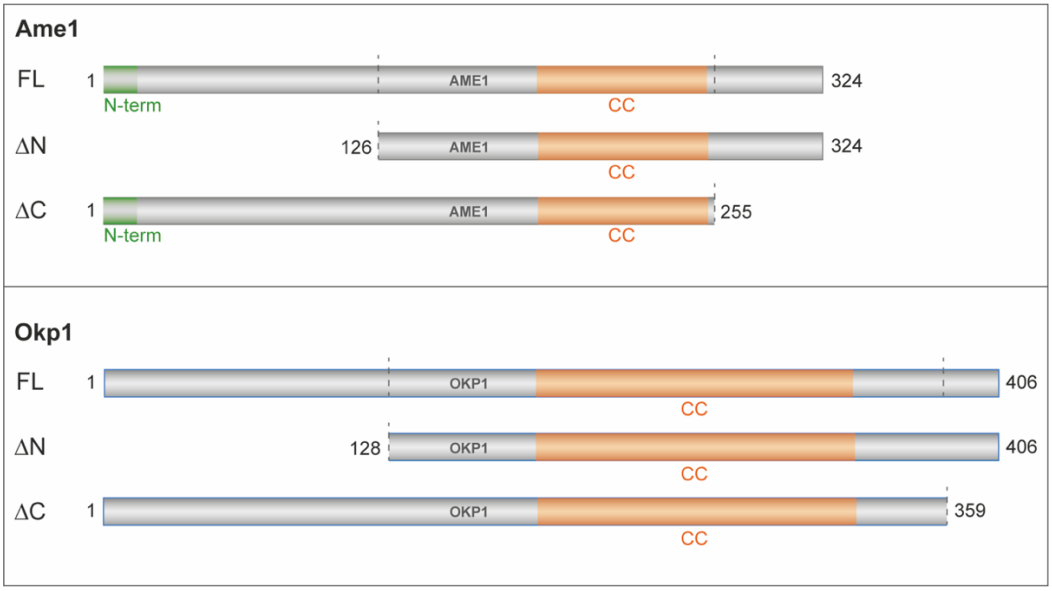

Figure 3.5: Purification of N- and C-terminal truncation mutants of Ame1/Okp1. Ame1 and Okp1 were truncated at either their C- or N-terminus in order to investigate the binding ability to either NNc (C-term) or to DNA (N-term). Both C-terminal truncations were constructed to keep the coiled-coil region intact, as it is necessary for heterodimerization. Note that for biochemical studies the heterodimer was always used, for simplification Ame1 and Okp1 truncations were shown solely.

To control for the integrity and heterodimer formation of all AO complexes mentioned above, they were tested for their biochemical behavior in analytical SEC. In Figure 3.6 chromatograms of the four different C-terminally truncated Ame1/Okp1 complexes in SEC and the accompanying Coomassie stained SDS-PAGE gels are shown. In dark blue AO-WT is depicted, which shows the typical two distinct bands for Okp1 and Ame1 on the SDS-PAGE gel. In light blue C-terminal deletions of either Ame1 alone or Ame1 and Okp1 in combination are shown, which both run similar, but not identical to the AO-WT complex. In both cases, separate bands for Ame1 and Okp1 are visible on the SDS-PAGE gel. In contrast, Ame1-WT/Okp1-ΔC is depicted in light green and shows a single band in SDS-PAGE, elutes at an early elution volume in a broad peak. As both Ame1 and Okp1 cannot be purified in isolation, we assume both proteins to be present in this complex. From this experiment, we conclude that all complexes shown here can be produced in sufficient amounts to perform biochemical experiments, but their properties in SEC slightly change. It is particularly noticeable that the simultaneous truncation of both C-termini leads to a complex that elutes clearly later than wildtype. As SEC is based on size and shape of a complex, it is feasible that truncated proteins show a slightly different behavior as compared to the WT complex. All complexes show a single peak in SEC and their proteins are visible on the SDS-PAGE gel. Therefore, we conclude that complex integrity is intact. To confirm functionality of the complexes, their binding to DNA was again tested in EMSAs.

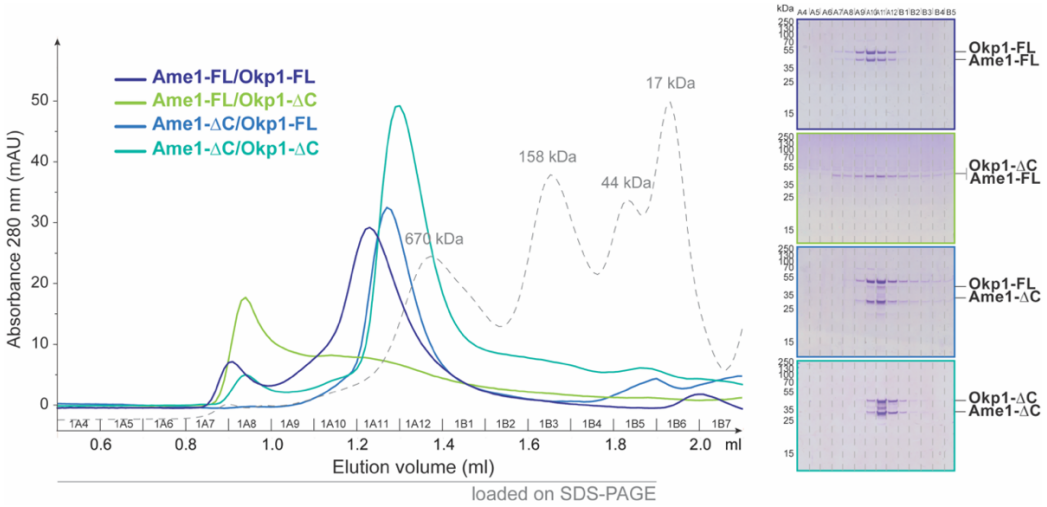

Figure 3.6: C- terminal truncation mutants of Ame1/Okp1 can be purified but show different behavior in SEC. Analytical SEC chromatograms and corresponding Coomassie stained SDS-PAGE gels of AO-WT full length, Ame1 or Okp1 truncations at 10 µM concentration. Grey dotted line indicates a gel filtration standard. (**A**) Ame1/Okp1-WT (dark blue), C-terminal truncation of Ame1 (light blue) and the double C-terminal truncation (dark green) show similar elution profiles. The C-terminal truncation of Okp1 (light green) elutes differently.

3.1.6 Ame1/Okp1 complexes with truncated proteins bind equally well to DNA

To evaluate if the functionality of C-and N-terminal truncations of Ame1 and Okp1, EMSAs were performed with centromeric DNA and recombinant AOc. In Figure 3.7A the N-terminal truncations of Ame1 and Okp1 are shown, both complexes can bind centromeric DNA properly as stated by a shift of DNA with increasing amounts of recombinant protein similar to the AO full length complex. Also, the C-terminal truncations in Figure 3.7B are able to bind to DNA similarly. With these assays we confirm that both truncation mutant variants of AOc are able to bind to centromeric DNA, a known and characterized binding partner of Ame1/Okp1 complexes. Therefore, although the elution profiles in SEC of the C-terminal truncation mutants, the C-terminal truncation mutants can be further used in analytical SEC experiments to test the binding of NNc.

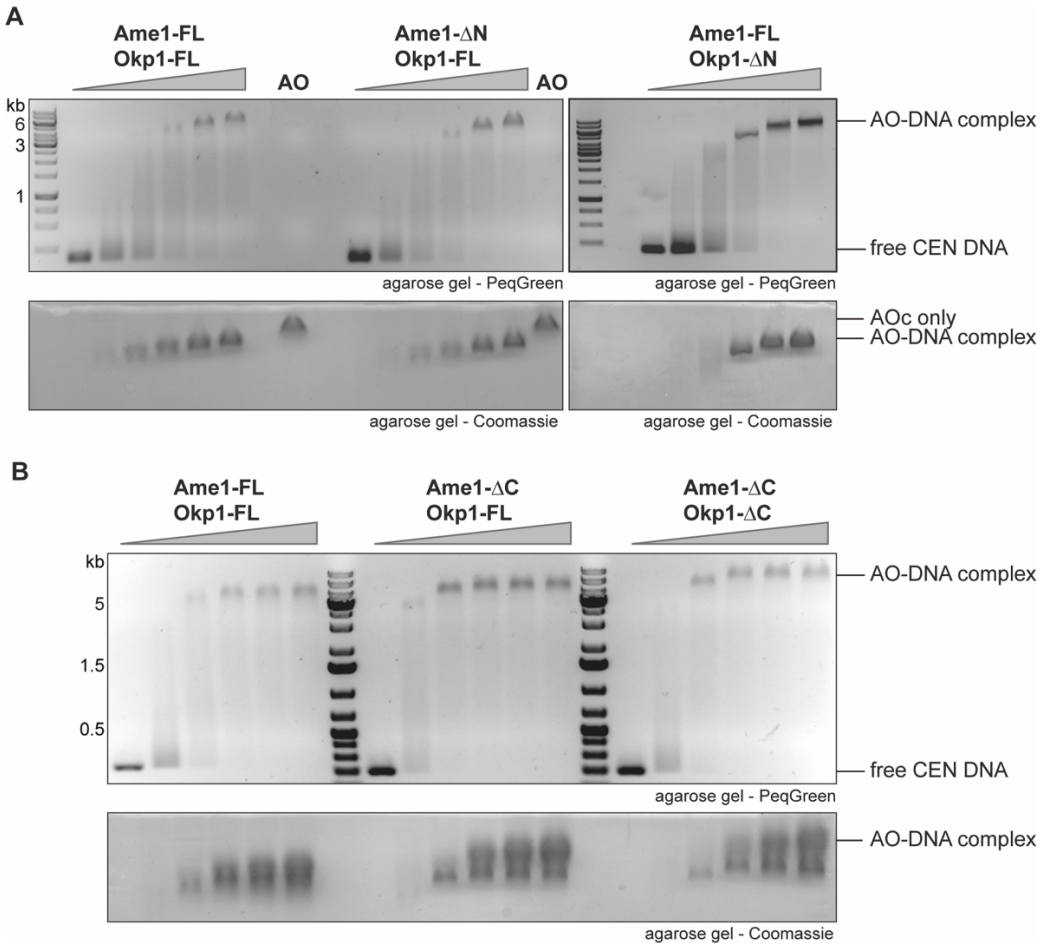

Figure 3.7: EMSAs of C- and N-terminal truncations of AOc reveal normal DNA-binding activity. DNA binding assays of centromeric DNA with recombinant C- and N-terminal truncation mutants of AOc. Proteins and DNA were incubated at room temperature for 15 minutes prior to run on an agarose gel. (**A**) shows EMSA of either AOc, Ame1-ΔN/Okp1 or Ame1/Okp1-ΔN. (**B**) shows EMSAs of either AOc, Ame1-ΔC/Okp1 or Ame1-ΔC/Okp1-ΔC.

3.1.7 Nkp1/Nkp2 binds to the C-termini of Ame1 and Okp1

The truncated AO complexes were tested for their interaction with Nkp1/Nkp2, as this interaction was shown for the *K. lactis* homologs *in vitro* (Schmitzberger et al., 2017). Additionally, if the interaction exists in *S. cerevisiae* and whether it is based in either Ame1, Okp1 or a combined interface remains unclear.

The binding of NNc to AOc with the *S. cerevisiae* homologs was confirmed with AO full length complex in SEC (Figure 3.8A). The combination of both complexes elutes at an earlier elution volume compared to the single complexes and shows the formation of a tetrameric complex in the Coomassie stained SDS-PAGE gel. Some residual NNc is still unbound, but this could be due to excess of the NN dimer. AOc with a C-terminal truncation in Okp1 showed reduced binding capability to NNc in SEC, seen in an incomplete tetrameric complex formation and only partial shift of the NN heterodimer in the chromatograms (Figure 3.8B). Since there is a shift in SDS-PAGE gel, we interpret that some interaction is maintained in this mutant, but weaker as compared to AO-WT full length complex. This might be due to direct interaction of the Okp1 C-terminus with NNc or stabilization of the Ame1 C-terminus through Okp1, as Ame1 C-terminal truncations have an even stronger effect on the NNc interaction, as described below (Figure 3.9).

Next, we tested if the C-terminal truncation of Ame1 influences the binding of the AO heterodimer to Nkp1/Nkp2. When Ame1-ΔC is in complex with either Okp1-full length (Figure 3.9A) or with Okp1-ΔC (Figure 3.9B) the binding to NNc is disrupted in solution. The elution profiles of the two individual peaks for AOc and NNc are unaltered and no complex formation can be seen in the corresponding SDS-PAGEs (Figure 3.9A and 3.9B). Taken together, both C-termini of Ame1 and Okp1 are essential for the binding of the heterodimer Nkp1/Nkp2, although it seems to be that Ame1 makes the more important contribution.

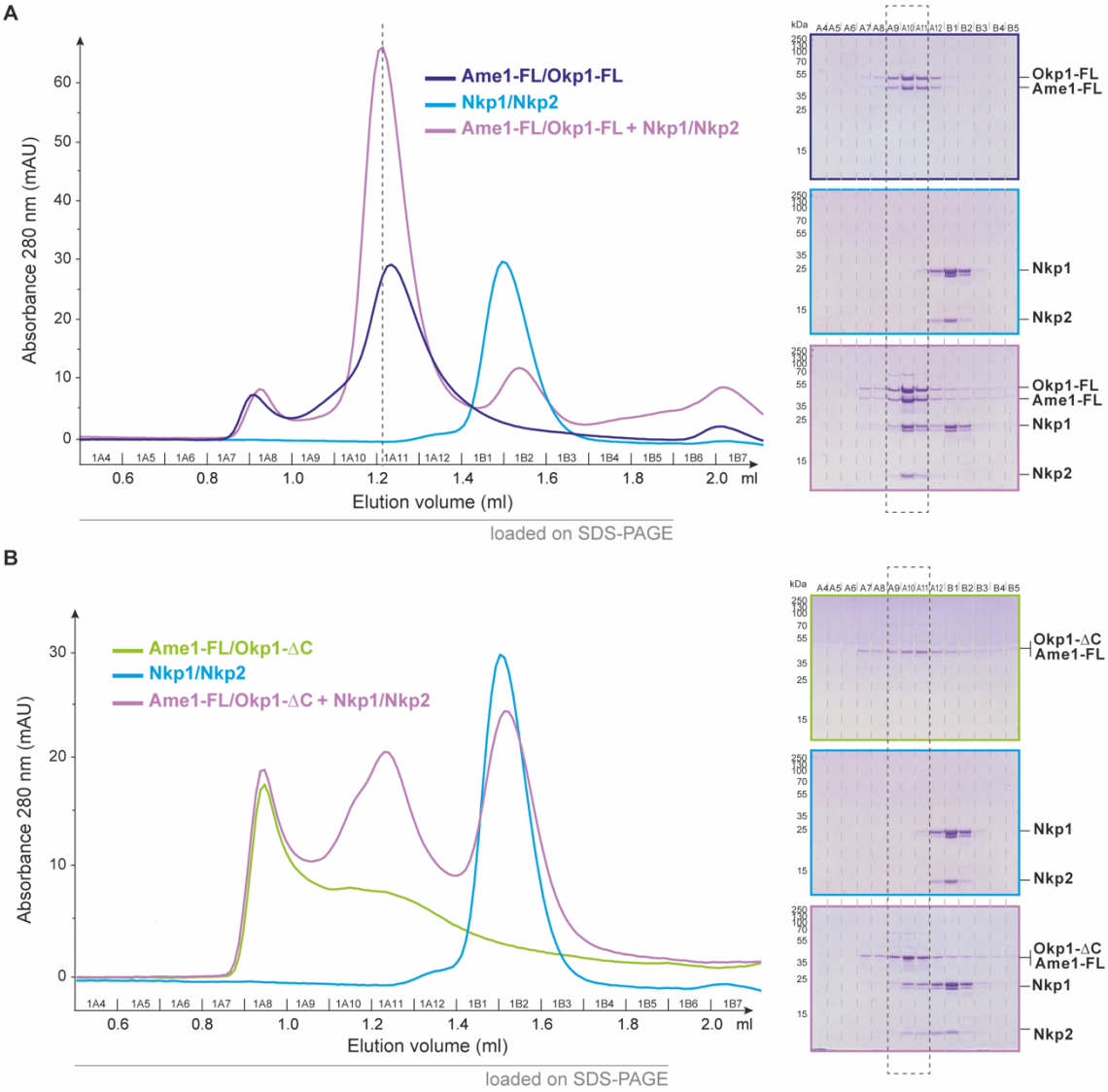

Figure 3.8: Okp1 C-terminus is partially responsible for interaction with Nkp1/Nkp2. Analytical SEC chromatograms and corresponding Coomassie stained SDS-PAGE gels of AO-WT or Ame1/Okp1-ΔC complexes with NN dimer alone and in combination at 10 µM concentration. All combinations were incubated for 1 h at 4 °C prior to the run. (**A**) AO full length complex is shown in dark blue, in light blue NNc and in purple the combination. Although the shift of the elution profile is only minimal, a clear binding is visible in SDS-PAGE gels where in two fractions all four proteins run together as a four-protein complex, see dashed box. (**B**) AO-ΔC is shown in light green, in light blue NNc and in purple the combination. A shift of the NN dimer in SDS-PAGE gel and chromatogram when combined with the AOc is visible, although not as prominent as with full length AOc, indicating a weaker binding (dashed box).

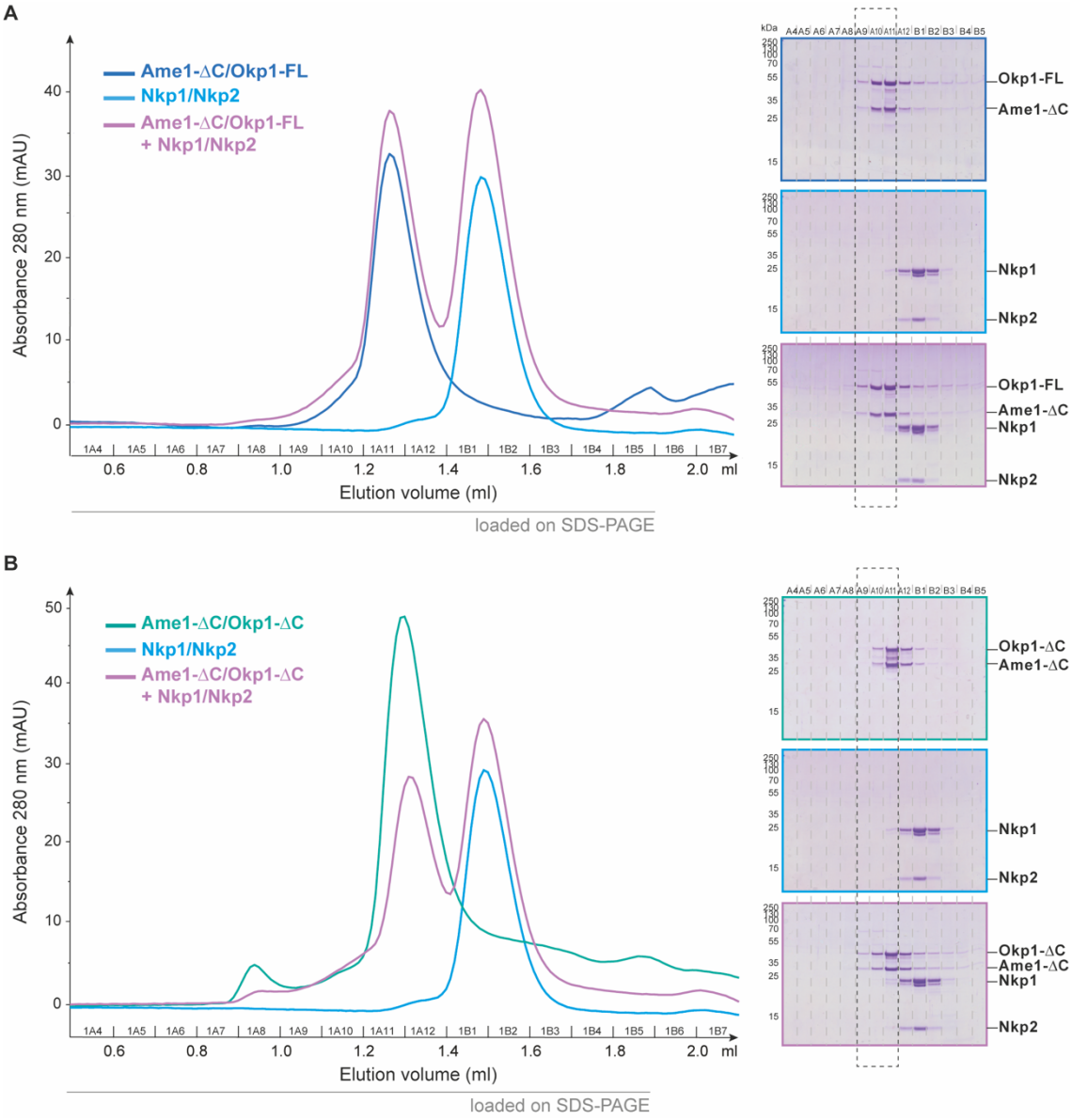

Figure 3.9: The C-terminus of Ame1 is essential for NNc interaction. Analytical SEC chromatograms and corresponding Coomassie stained SDS-PAGE gels of AO-WT or Ame1/Okp1-ΔC complexes with NN dimer alone and in combination at 10 µM concentration. All combinations were incubated for 1 h at 4 °C prior to the run. (**A**) Ame1-ΔC/Okp1-FL is shown in dark blue, in light blue NNc and in purple the combination. When the C-terminus of Ame1 is missing, no binding can be observed as seen in two distinct peaks in the chromatogram and no coelution on the SDS-PAGE gel. (**B**) Ame1-ΔC/Okp1-ΔC is shown in turquoise, NNc in light blue and the combination in purple. Similar to the binding of only C-terminally truncated Ame1, no binding can be observed if Okp1 is C-terminally truncated in addition as seen by two distinct peaks in the chromatogram and no coelution on SDS-PAGE. Dashed box shows fractions of AOc bound to NNc in Figure 3.8.

3.1.8 Nkp1/Nkp2 and DNA bind to Ame1/Okp1 competitively

As shown above, AOc can efficiently bind to centromeric DNA (Figure 3.2). It was also demonstrated, that the C-termini of Ame1 and Okp1 are responsible for the formation of a four-protein complex with the NN dimer (Figure 3.8 and 3.9). Therefore, we decided to test whether AOc can bind to DNA and NNc simultaneously in an EMSA (Figure 3.10). Centromeric DNA was used at a concentration known to efficiently bind to AOc in all samples. The concentration of NNc was gradually increased. With increasing concentration of NNc, increasing amounts of free centromeric DNA was observed. This can only be seen when AO is present as a full length complex, when one or both C-termini are truncated, no free DNA can be detected, which we interpret as the in ability of NNc to bind to the AOc and therefore no competition between DNA and NNc binding to the AOc. Ame1/Okp1 has a higher affinity to the Nkp1/Nkp2 heterodimer as to DNA, which means a higher specificity to protein-protein interaction.

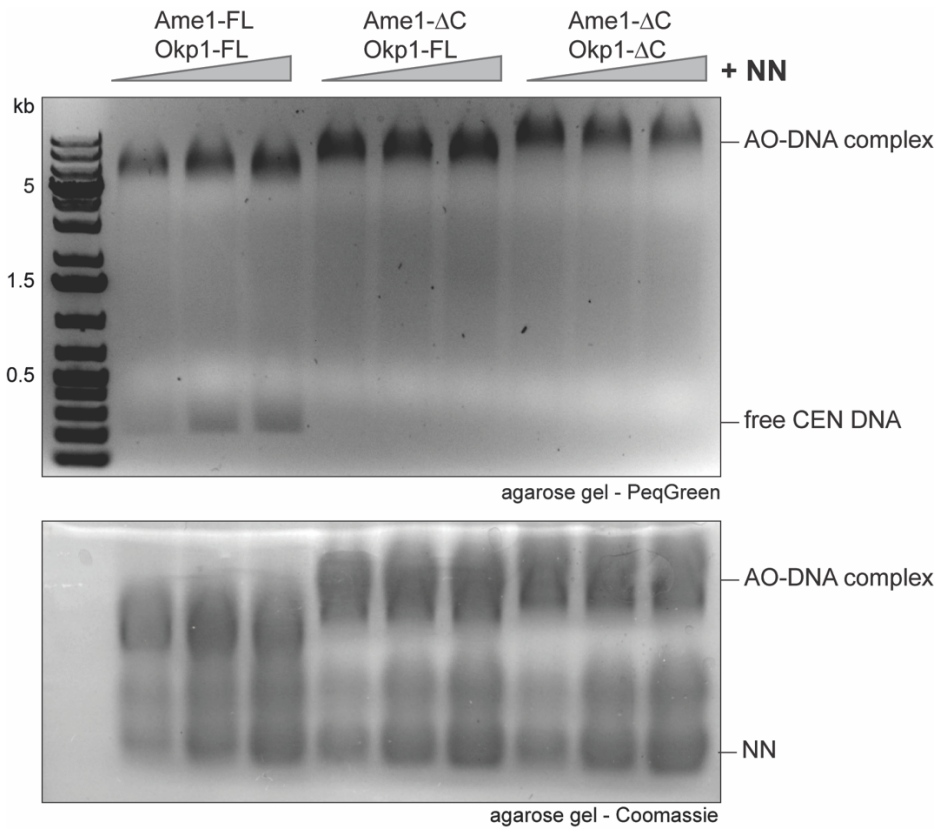

Figure 3.10: In EMSA NNc and DNA bind competitively to AOc full length but not to C-terminal truncation mutants. Top agarose gel shows competition of free centromeric DNA with NN cin AOc binding. Concentrations of centromeric DNA and AOc were the same, only increasing amounts of NNc were used. Next to the full length AOc also C-terminal truncations of only Ame1 or both Ame1 and Okp1 are shown in the same assay. The lower agarose gel is stained with Coomassie to show proteins.

3.2 Ame1 is a target for the cyclin dependent kinase (CDK) *in vivo*

After analyzing the domain structure and the phosphorylation cluster of Ame1 *in vitro*, in vivo approaches were pursued to analyze the role of Ame1 phosphorylation in cells.

3.2.1 Generation of a non-phosphorylatable mutant of the essential CCAN component Ame1

The N-terminal half of Ame1 contains seven phosphorylated residues (T31, S41, S45, S52, S53, S59, S101) from which five residues follow a minimal substrate motif for CDK. In order to analyze which effect Ame1 phosphorylation might have on yeast viability, all seven residues were mutated to alanine or glutamic acid to prevent or mimic phosphorylation, respectively.

To examine the effect that these alterations might have on yeast cells, pRS plasmids were generated, that allow Ame1-6xFlag integration, either at the endogenous or exogenous locus in *S. cerevisiae* for *in vivo* analyses.

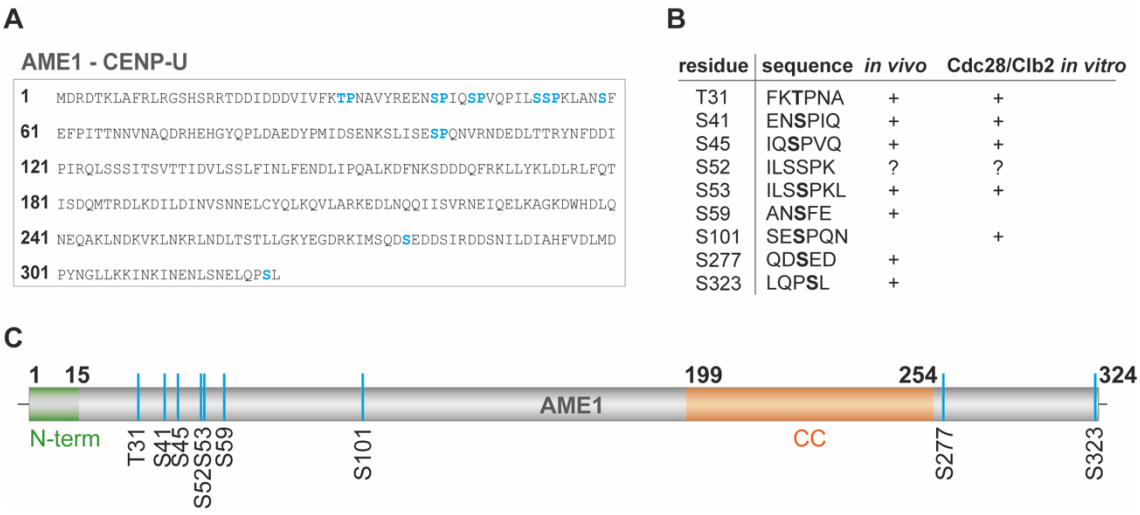

Figure 3.11: Domain organization and mapped phosphorylation sites of the essential CCAN protein Ame1. (**A**) Sequence of Ame1. Residues that were identified as phosphorylated *in vivo* and in *in vitro* kinase assays with Cdc28/Clb2 are highlighted in blue (Hornung and Westermann, unpublished observations). (**B**) Overview of nine phosphorylated residues and how they were identified. (**C**) Schematic overview of the domain organization of Ame1 drawn to scale: N-terminal 15 aa that are essential for binding the KMN component Mtw1 and C-terminal coiled-coil region that is required for dimerization with Okp1 are highlighted in green and orange.

Because of the essentiality of Ame1 in cells, two different yeast background strains were used to generate strains that provide an unaltered copy of Ame1 to keep cells alive: a diploid heterozygous deletion strain in which one endogenous allele of Ame1 is replaced with a HIS3 auxotrophy marker gene or a haploid strain in which the endogenous Ame1 allele is fused to an FRB tag to use it in an anchor away approach (Haruki et al., 2008). Here, the ribosomal anchor Rpl13-FKBP2 was used, that anchors Ame1-FRB out of the nucleus to ribosomes after rapamycin addition. After sporulating and dissection of the diploid strains, haploid strains that carry the integrated Ame1-6xFlag version as the only present copy were viable and used for genetic studies.

3.2.2 Ame1 phosphorylation mutants do not alter the growth phenotype of budding yeast

To investigate the growth phenotype of Ame1 phosphorylation mutants, the wildtype and mutant proteins were integrated into yeast cells, carrying an FRB tag on the endogenous Ame1 protein, that is removed from the nucleus upon the addition of rapamycin to the medium, so that the only present copy in the cell is the introduced mutated version of Ame1. As described in section 2.5 strains with different Ame1 mutants in the FRB strain background were spotted onto solid media YEPD plates with and without rapamycin and incubated at different temperatures to compare their growth (Figure 3.12). While cells lacking a rescue allele failed to proliferate in the presence of rapamycin, both phosphorylation mutants Ame1-7A and Ame1-7E were viable at all tested temperatures and showed little to no difference in their growth in comparison to Ame1-WT. In order to sensitize the strains further, two non-essential CCAN components were deleted in the Ame1-FRB background strains: Ctf19/CENP-P and Cnn1/CENP-T. Previously it was shown, that both deletions increase the temperature sensitivity of a Mif2 N-terminal deletion mutant (Killinger et al., 2020). As shown in Figure 3.12 both deletions don't alter the growth behavior of Ame1-7A nor Ame1-7E. From the plates it seems that the mutants, compared to the integrated wildtype, confer a slight growth advantage in the deletion mutants. In addition, a deletion of Mad1, which results in a nonfunctional Spindle Assembly Checkpoint (SAC), was introduced in order to test the effect of the Ame1 mutants. A nonfunctional SAC did not create any growth defect of both mutants.
Because the phosphorylation mutants do not cause an obvious growth phenotype in the FRB system, haploid strains in which Ame1-WT, Ame1-7A or Ame1-7E represent the

only copy in the cell were generated. In serial dilution assays with these strains the same results were obtained, although clonal differences were higher (Supplementary figure 1).

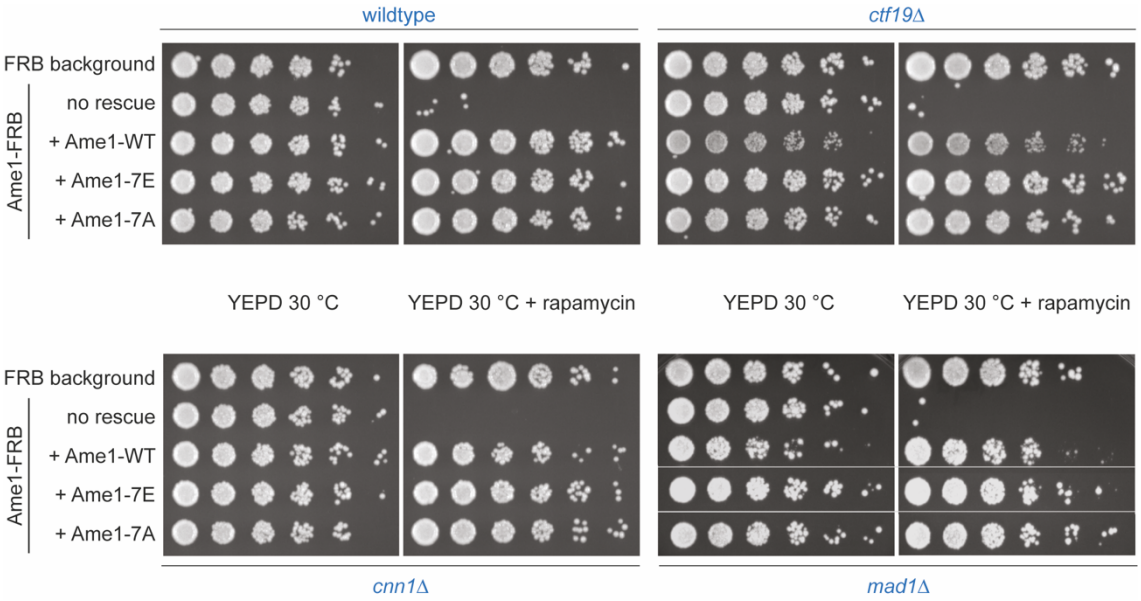

Figure 3.12: Phosphorylation mutants in Ame1 do not have a major effect on cell growth. Indicated strains were plated in serial dilution onto YEPD or YEPD + 1 µg/ml rapamycin and incubated at 30 °C. Ame1-7A and Ame1-7E are viable upon rapamycin addition and are comparable to Ame1-WT in their growth behavior. Ame1-7A and Ame1-7E were combined with deletions of *ctf19*, *cnn1* or *mad1* and plated in serial dilution onto YEPD and YEPD + rapamycin at 30 °C. The indicated deletion mutants do not change the growth phenotype of Ame1-7A or Ame1-7E profoundly.

3.2.3 Manipulation of the Ame1 phosphorylation status in cells

In order to exclude altered expression levels for being the reason of unaltered cell growth, lysates of strains expressing different Ame1 versions were analyzed by SDS-PAGE followed Western Blotting using the C-Terminal 6xFlag-Tag on the used Ame1 constructs (Method described in section 2.19.1). Interestingly, all Ame1 versions show a different behavior in an SDS-PAGE analysis. Ame1-WT shows slow migrating forms, that are fully eliminated when phosphorylation is prevented in the Ame1-7A mutant. The Ame1-7E mutant displays reduced mobility in SDS-PAGE, as it seems that the signal is on the same height as the slowest migration form of Ame1-WT. The expression level overall was similar and clones that expressed similar levels of the wildtype or mutant proteins were chosen for further analyses. (Figure 3.13).

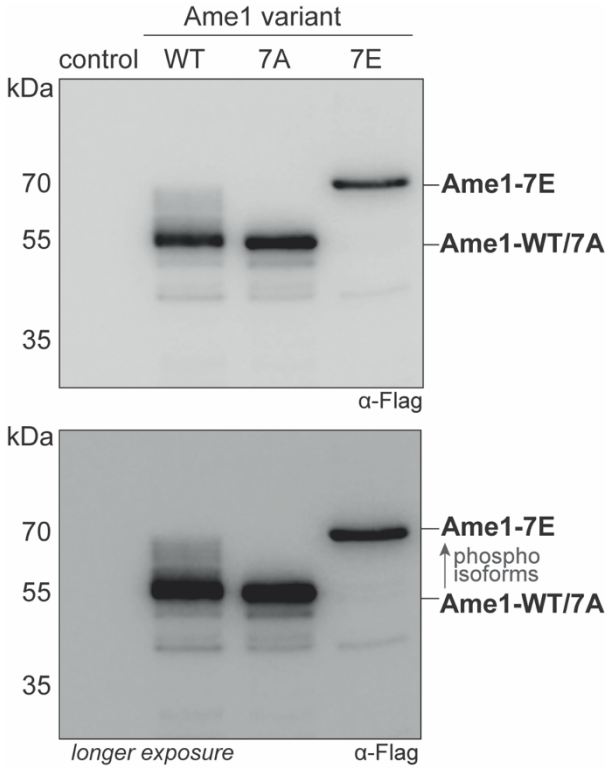

Figure 3.13: Ame1 phospho-mutants display different migration behavior in SDS-PAGE. Cell lysates of logarithmically growing cultures expressing 6xFlag-tagged Ame1-WT, -7A or -7E were analyzed in Western Blotting. Ame1-WT shows slowly migrating forms, that are eliminated in the Ame1-7A mutant. Ame1-7E runs more slowly than Ame1-WT and Ame1-7A and matches in height with one of the most slowly migrating forms in Ame1-WT. The lower panel shows a longer exposure of the same western blot.

3.2.4 Cdc28 is at least partially responsible for the phosphorylation of Ame1

In order to understand the basis of this unusual migration pattern of Ame1 in SDS-PAGE, the change of the Ame1 phosphorylation pattern was analyzed at a mitotic arrest using Nocodazole. The effect of the mitotic arrest compared to logarithmically growing cells on Ame1 is shown in Figure 3.14A. In a logarithmically growing culture one prominent band for Ame1 is visible at 55 kDa, and additionally two distinct slowly migrating forms. This pattern is also visible in a mitotic arrest although the slowly migrating forms are weaker. To confirm that the slow migration forms of Ame1-WT are different phosphorylation isoforms, a lambda phosphatase treatment of the Nocodazole-treated lysate was performed. The negative control for the phosphatase experiment shows less distinct bands as compared to untreated M-Phase lysates, which is probably due to DMSO in the buffer. Nonetheless, the slowly migrating forms disappear due to phosphatase treatment, confirming phosphorylation being the basis of the unusual behavior of Ame1 during SDS-PAGE. In order to investigate which kinase is responsible for the modification of Ame1, a temperature sensitive mutant of Cdc28 was used. In Figure 3.14B Ame1-WT was analyzed in a *cdc28-13* background strain. A visible reduction in slowly migrating forms could be seen with the temperature-sensitive *cdc28-13* allele. Although not all slow migrating forms are eliminated as seen with an Ame1-7A mutant, we conclude that Ame1 is phosphorylated by CDK *in vivo*. Therefore, Ame1 phosphorylation over the cell cycle was explored in more detail.

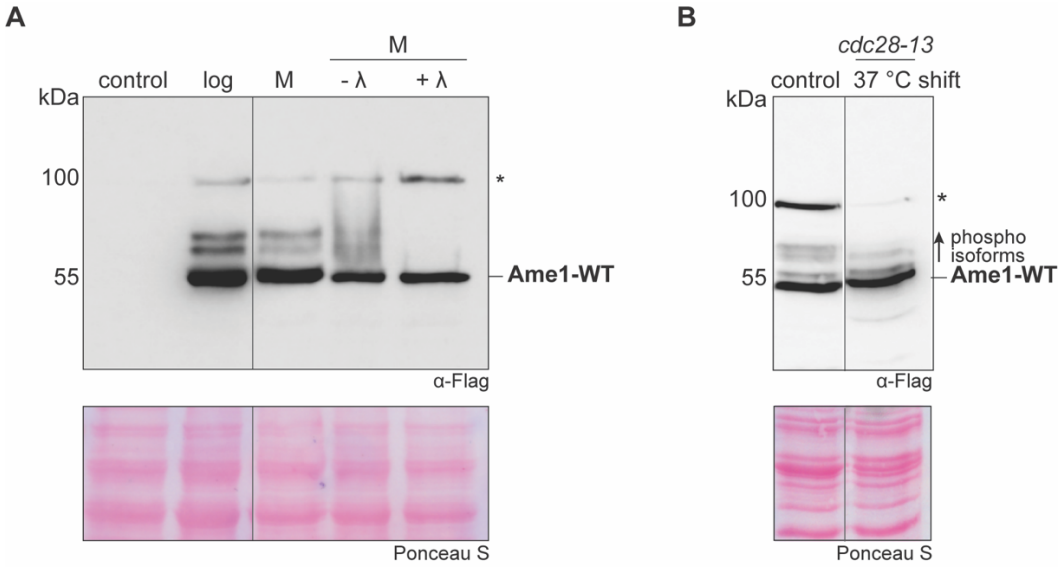

Figure 3.14: Ame1-WT phosphorylation is at least partially dependent on CDK. (**A**) Cells expressing Ame1-WT-6xFlag were arrested in mitosis using Nocodazole and lysates were subjected to Western Blotting. The slowly migrating forms are removed upon Lambda phosphatase treatment. (**B**) Ame1-WT-6xFlag was analyzed by Western Blotting in strains carrying *cdc28-13* and logarithmically growing cells were shifted to

the restricted temperature of 37 °C. In the *cdc28-13* mutant a simpler pattern of slowly migrating forms of Ame1-WT was present when CDK-phosphorylation was inhibited through a shift to 37 °C. Although logarithmically growing cells were used, it cannot be excluded that treatment of cells leads to an arrest in a certain cell cycle stage.

3.2.5 Phosphorylation of Ame1 changes during cell cycle progression

As Ame1 was shown to be phosphorylated by Cdc28, the question came up whether Ame1 is phosphorylated in a cell cycle dependent manner by this kinase. Therefore, the Ame1 protein was followed over a complete cell cycle and the phosphorylation status was observed by Western Blotting in Ame1-WT and Ame1-7A expressing strains (Figure 3.15). Cells were arrested with α-factor in a G1-like state and released into fresh medium. After 65 minutes a second round of α-factor was added, to stop the cells from entering a second cell cycle. In these strains, Pds1/Securin was Myc tagged to follow anaphase onset. In later experiments it was shown that it is better to add the second α factor earlier, because cells that already entered mitosis will not arrest sufficiently and proceed into a second cell cycle. This can also be seen in the later timepoints where Pds1-Myc signal is still visible. Ame1-WT is again present as differently phosphorylated isoforms, that accumulate as cells progress into S-Phase and mitosis. Interestingly, coincident with a decline of Pds1 levels, the level of phosphorylated Ame1 is slightly reduced after mitosis has started (60 minutes, less Pds1), which is not an artefact, because it is seen in successive experiments respectively, and will be explained in the upcoming chapters. Ame1-7A shows no slowly migrating forms as seen before and protein levels appear equal throughout the cell cycle.

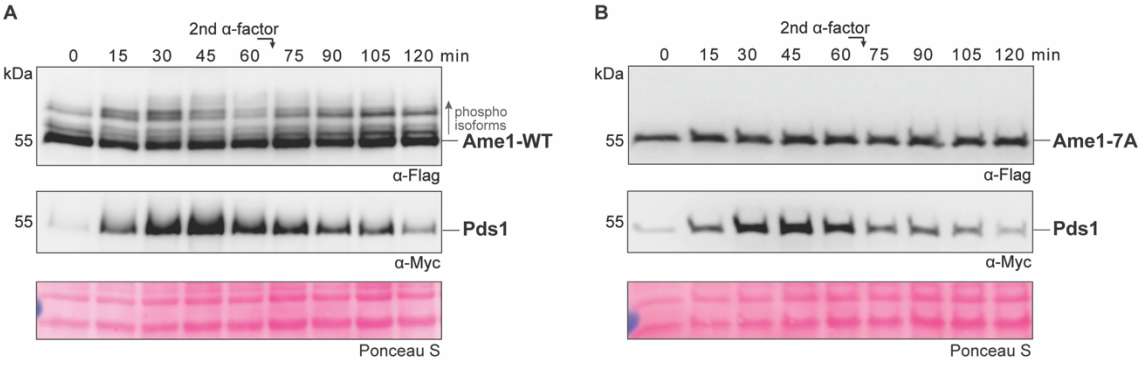

Figure 3.15: The phosphorylation pattern of Ame1-WT changes over the cell cycle. Release of Ame1-WT (**A**) or Ame1-7A (**B**) after α-factor arrest into fresh medium shows gradual accumulation of Ame1-WT phospho-isoforms in Western Blotting. These forms are eliminated in Ame1-7A. Additionally, Pds1 was detected to show cell cycle progression, which is unaltered in Ame1 mutant cells.

3.2.6 Ame1 phosphorylation mutants display similar localization in cells

To investigate whether introduction of phosphorylation mutants into Ame1 changes its recruitment or localization at the kinetochore, we subjected cells to microscopic analysis. To do so, GFP-tagged Ame1-WT, Ame1-7A or Ame1-7E was introduced into haploid cells under its own endogenous promoter as the only present copy of Ame1 in the cell. Logarithmically growing cultures of these three strains were analyzed by fluorescence microscopy with the help of a Delta Vision Elite Microscope. As seen in Figure 3.16 all three strains show Ame1 fluorescence confined to one or two dots per cell, which is a typical indication for kinetochore recruitment throughout the cell cycle. A single Ame1 signal corresponds to a cluster of all 16 kinetochores of a G1 cell, whereas spindle forces in mitosis separate the two kinetochore clusters of sister chromatids, so two green fluorescent dots are visible. Brightfield images are shown to appraise the cell cycle stage of a respective cell. The kinetochore localization was comparable in all strains, therefore a change in protein availability can be ruled out as a consequence for the effects seen in further experiments.

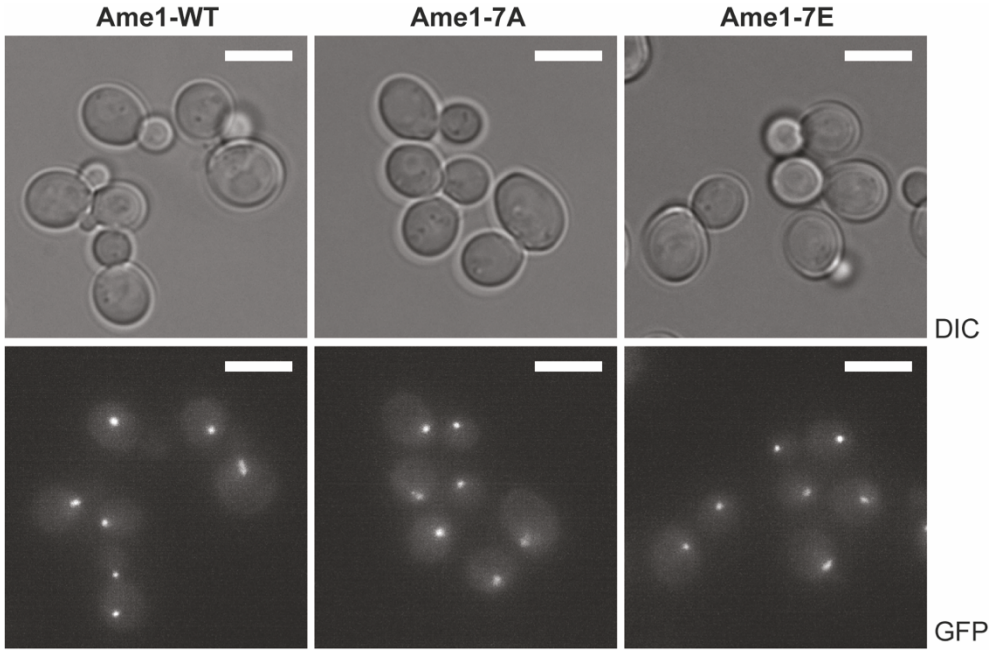

Figure 3.16: Ame1-WT and mutant proteins localize to kinetochore in a similar fashion. Ame1 was tagged with GFP to visualize its localization in logarithmically growing cells. Intensities are equal in mutant variants compared to Ame1-WT for all cell cycle stages (G1 = single dot; mitotic = two dots). Scale bar represents 5 µm. Brightfield images are shown to interpret cell cycle stages of the respective cells.

3.2.7 Purification of Ame1/Okp1 complexes from budding yeast

As the kinetochore is a multi-proteinaceous network, biochemically stable subcomplexes can be extracted from yeast cells by pulling on one of its components, as shown in previous studies (Schleiffer et al., 2012). Here, purification of 6xFlag-tagged Ame1 phospho-mutants from a wildtype strain background (DDY904) were compared to Ame1-WT, in order to detect possible differences in their interaction with other proteins. To this end, soluble yeast lysates were prepared and incubated with anti-Flag antibody immobilized on magnetic beads. The beads were then washed multiple times and bound proteins were eluted by the addition of 3xFlag peptide. Elution fractions and remaining beads were loaded on a 4-12 % gradient SDS-PAGE and stained with silver nitrate as shown in Figure 3.17. Two elution fractions from magnetic α-Flag beads (E1 and E2) and the bead fraction after elution (beads) were loaded. Overall, the pattern of eluted proteins looks similar, although Ame1-7A shows in E1 a bit more total protein, whereas Ame1-7E has less compared to Ame1-WT. Therefore, we conclude that the mutant and Ame1-WT bind the same set of proteins, possibly in different quantities. As this experimental approach only gives a limited picture of protein interactions, one would need to perform more specific analyses to confirm this interpretation (e.g., Mass Spectrometry approaches). However, the similarity of the pattern in SDS-PAGEs did not encourage us to investigate this question any further. Alternatively, Ame1-WT and phospho-mutants can be tested for differences in their binding of known interaction partners *in vivo* by alteration of the expression levels, as described below (see section 3.4).

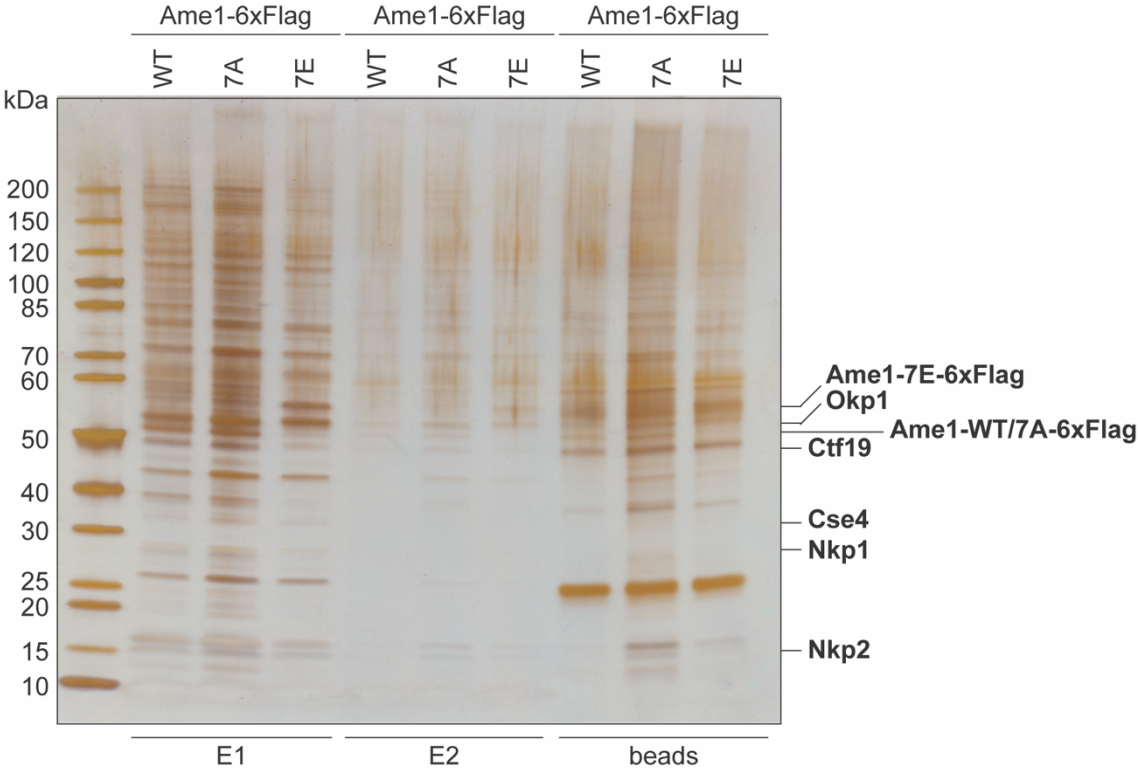

Figure 3.17: Ame1-WT and phospho-mutants copurify a similar set of proteins. Silver stained gel of purified Ame1-6xFlag variant extraction from yeast lysate. Bands that were assigned as specific kinetochore components based on their molecular weight are labeled. In Ame1-7A overall protein levels seem to be elevated as compared to Ame1-WT, whereas in Ame1-7E levels were slightly reduced. In both cases, the general pattern of copurified proteins is largely unaltered. We conclude that Ame1 phospho-mutants can copurify with the same set of proteins as Ame1-WT.

3.2.8 The Ame1-7A mutant displays slightly reduced chromosome transmission fidelity

To analyze the effects of Ame1 phospho-mutants in more detail a chromosome loss assay was performed (for method see section 2.17). In this assay, the mitotic transmission of a linear chromosome fragment carrying a selectable marker and a reporter gene (SUP11) is scored. Two control strains were included every time, a positive control in which all colonies should turn red (*ctf19* deletion) and the background strain where all colonies should stay white. In this background strain the endogenous Ame1-WT allele was exchanged with either Ame1-WT or Ame1-7A. Figure 3.18 shows the results of such a chromosome loss experiment with both controls. The presence of Ame1-7A in the cell leads to more cells that have problems in chromosome maintenance, which could be counted in more colonies that turned red, compare 19.4 % to 16.2 % in Ame1-WT.

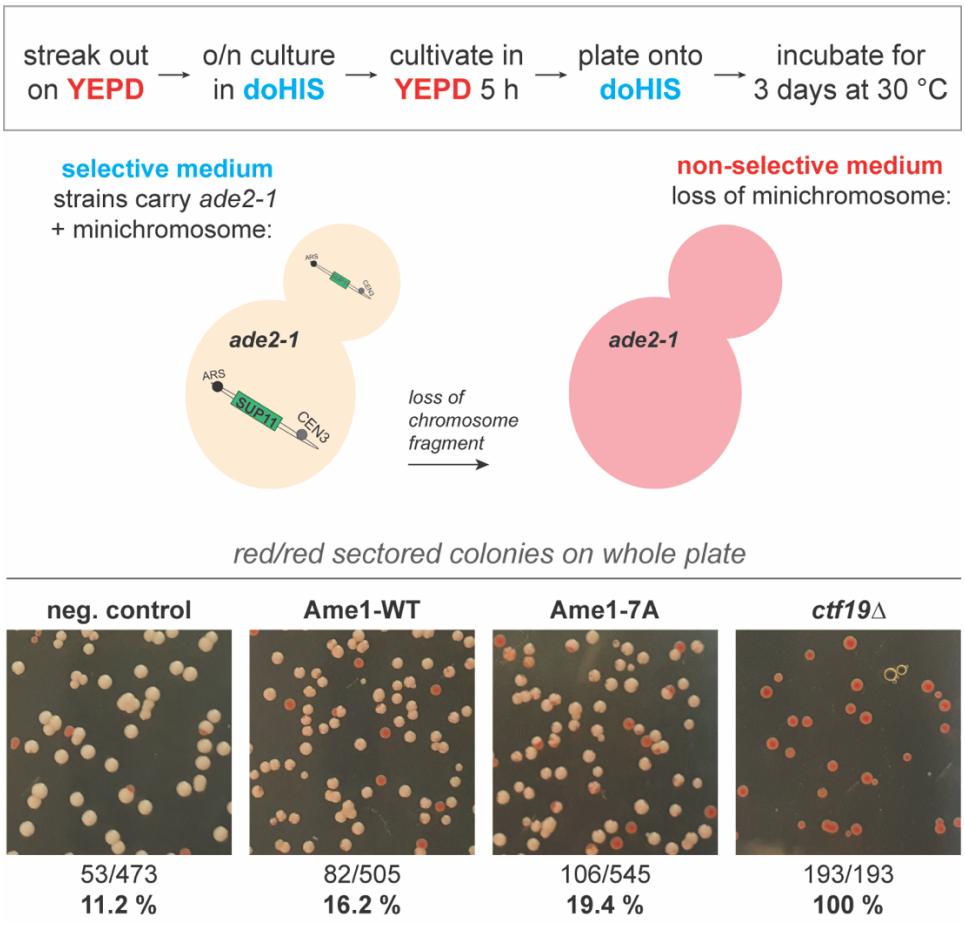

Figure 3.18: Chromosome transmission fidelity experiment with Ame1-WT and Ame1-7A. Ame1-WT or Ame1-7A were introduced into a background strain (SWY2328) at the endogenous locus. As controls, this background strain and also a positive control for the sectoring (SWY2329) are shown. After the strains were incubated in rich medium for 5 hours (loss of plasmid), they were plated onto selection medium SD doHIS with low Adenine to increase the red pigmentation.

3.2.9 Internal truncations of the Ame1 N-terminus compromise cell viability

As in all experiments shown above no significant growth difference in Ame1 with mutated phosphorylation cluster was detected, a more pronounced mutation in which the whole region including these phosphorylation sites is deleted, was applied. The region of interest lies in between the conserved coiled-coil region (CC), which is important for heterodimerization with Okp1 and the N-terminus, which is essential for binding Mtw1c and is predicted to be unstructured. As it is known that the N-terminus is essential for viability, we left the first 30 amino acids untouched. As it was hypothesized that shortening Ame1 possibly leads to a compromised cell viability, as Ame1 might not be able to reach to its interaction partners within the outer kinetochore, several Ame1 deletion constructs were subjected for further analyses using the Ame1-FRB strains. If deleting only the phosphorylation cluster leads to a growth phenotype that is not progressively worsening upon deletion of further residues, the effect seen is likely to be based on the loss of the phosphorylation cluster. In Figure 3.19B all used constructs are depicted. With the first two truncations six out of the seven residues from the phosphorylation cluster were eliminated, and the seventh one with the truncation up to amino acid 116. The longest truncation of Ame1 included the residues 31-187. As shown in Figure 3.19A, Ame1-Δ31-116 is slightly diminished in its growth as compared to shorter truncations or Ame1-WT. Interestingly, shorter Ame1 versions show a progressively stronger growth phenotype which seems to be independent from loss of the phosphorylation cluster. Therefore, we interpret this result as a consequence of Ame1 not being able to reach its targets rather than a non-phosphorylatable Ame1. Note however, that Ame1-Δ31-116 is the first to show a single band (probably meaning not phosphorylated) and the first to show a phenotype. Therefore, overall integrity of the Ame1 N-terminus is important for cell viability, most probably because of the essentiality of its N-terminus to reach its binding partner Mtw1c. To exclude this phenotype being a consequence of the reduced expression of the truncated proteins, cell extracts were prepared and protein levels were checked in Western Blotting. All Ame1 variants are expressed to a similar amount and comparable to Ame1-WT levels. Unfortunately, the Ame1-Δ1-15 variant was not expressed in this experiment, although it was used and characterized in previous experiments (Hornung et al., 2014).

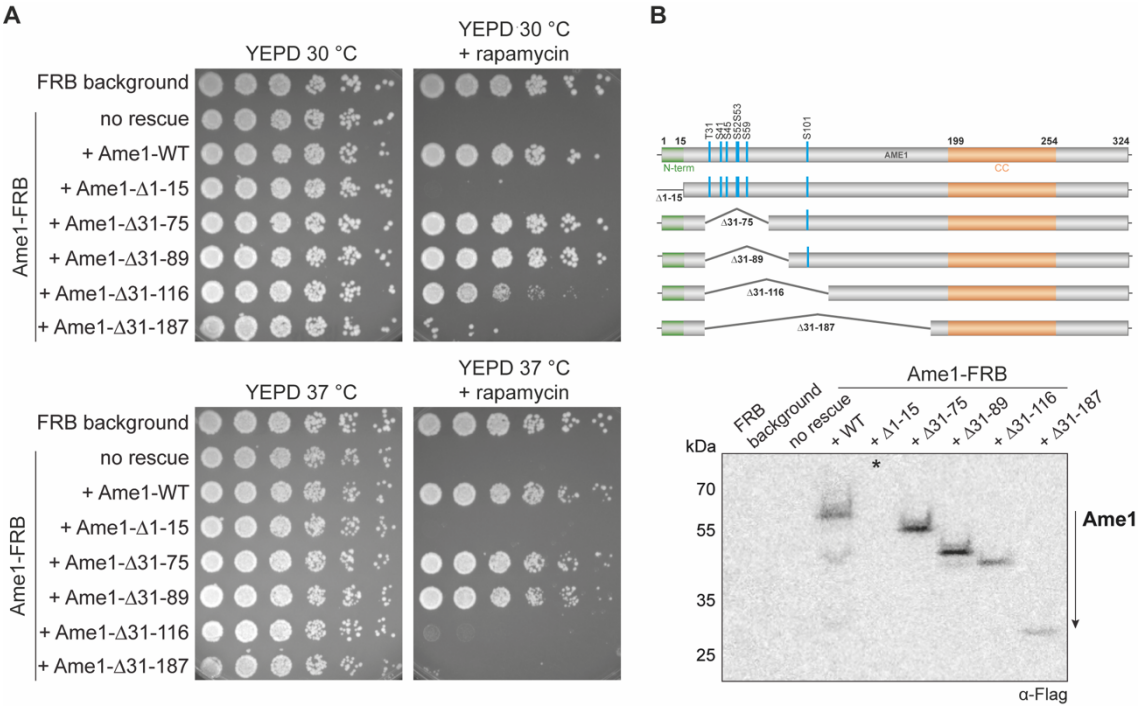

Figure 3.19: Ame1 truncation mutants show that protein length is important for viability. (**A**) Serial dilution assay of Ame1-FRB strains with different rescue alleles of Ame1. Cells were spotted on YEPD or YEPD + rapamycin and incubated at 30 °C and 37 °C. (**B**) Overview of the different truncation mutants used in the serial dilution assay and Western Blotting. Lysates of strains from (**A**) were subjected to western blot analysis and show expression of all used Ame1-variants, except Ame1-Δ1-15, which was previously characterized to be lethal.

As shown above, the Ame1 phospho-mutants expressed under the control of the endogenous promotor did not cause any obvious phenotype in all the conditions tested. However, this does not exclude these residues from playing a regulatory role within the kinetochore, which is implemented into a regulatory network of several proteins and therefore only produces a very subtle phenotype on its own. Therefore, the effect of the phospho-mutations on Ame1 in an overexpression system where tested again *in vivo*.

3.3 Analyzing CDK phosphorylation of Ame1 in more detail using an overexpression system

For further investigations Ame1 and its interaction partner Okp1 were overexpressed from a Galactose-inducible promoter in yeast to analyze the consequences of elevated levels of these proteins in cells.

3.3.1 Ame1 phospho-mutants accumulate to increased protein levels after overexpression

To investigate possible phenotypes in an overexpression system, Ame1-WT and phospho-mutants were expressed from an inducible GAL promoter. As Ame1 occurs in a heterodimeric complex with Okp1, both proteins were placed under the control of a bidirectional GAL promoter using specific 2micron plasmids which allow expression of two genes from the same plasmid to ensure the same expression conditions (pESC-HIS and derivates). Strains with either AO-WT or A-7A/7E/O were shifted to YEP+RG and expression of both proteins was evaluated by Western Blotting of the lysate after defined times in Galactose-containing medium (Figure 3.21A). As expected, expression of Ame1 and Okp1 was increased over time in galactose. While the expression of Okp1 is similar in all strains independent of the Ame1 version expressed, the expression level of the phosphorylation mutants was elevated in comparison to Ame1-WT as shown in Figure 3.20A. We conclude that the accumulation of Ame1-7A or Ame1-7E is based on the altered ability to be phosphorylated, because otherwise expression levels of Okp1 would also differ between these strains. This accumulation effect of Ame1 upon overexpression was observed in multiple different strain backgrounds including a *mad1* deletion strain, although the overall protein levels here were somewhat reduced. The overexpression of Ame1/Okp1 either in wildtype or mutant form did not produce a strong growth phenotype, although viability was compromised at elevated temperature in the presence of Galactose in an otherwise wildtype or *mad1* background as seen when plated in serial dilution on YEPD or YEPRG plates (Figure 3.20B**)**.

In order to investigate which residues are responsible for this accumulation of Ame1, single mutated residues or combinations were tested using the GAL shift assay. As shown in Figure 3.20C the residues S41, S45, S52 and S53 seem to be most important, as – when mutated to alanine - they all cause a strong accumulation of Ame1 in the cell as compared to wildtype Ame1.

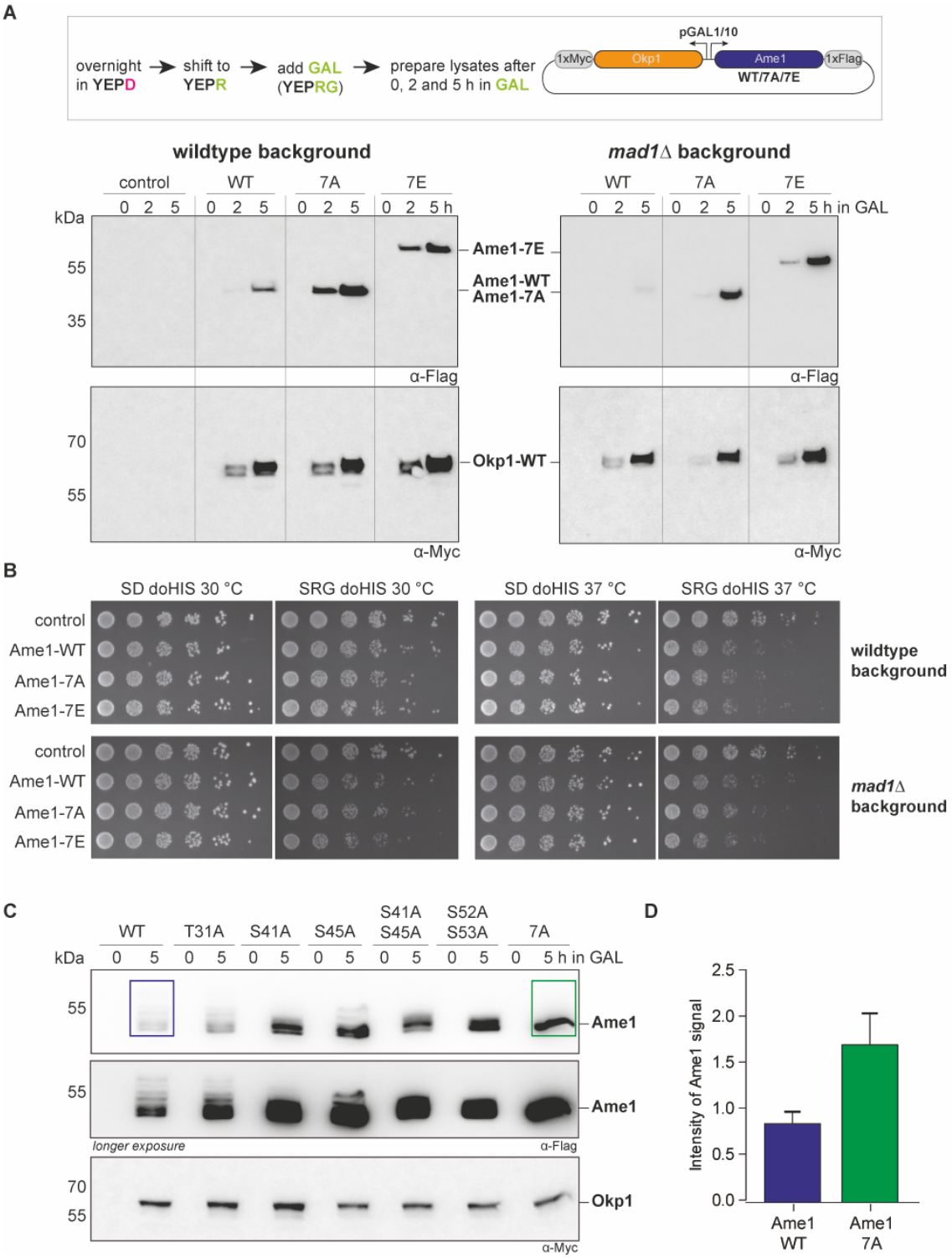

Figure 3.20: Overexpression of Ame1 leads to an accumulation of the phosphorylation mutants relative to the wildtype protein. (**A**) Western Blot analysis of Ame1-WT and Ame1-7A/7E in an overexpression system using 2micron plasmid before and 2 or 5 hours after shift to Galactose. An empty vector was added as a control in the wildtype background. The Ame1 and Okp1 signals increase over time in GAL, but Ame1-7A and 7E accumulate to a higher extent than Ame1-WT. Deletion of *mad1* in these strains does not change the outcome of the experiment. (**B**) Strains from (**A**) were spotted in serial dilution on either SD doHIS or SRG doHIS. (**C**) Western blot of Ame1 single residue mutations overexpression. The residues S41+S45 and S52+S53 increase the amount of Ame1 similar to Ame1-7A. (**D**) Quantification of mean (+/- SEM) signal

intensities of Ame1-WT and Ame1-7A with ImageJ. Signals were normalized to corresponding Okp1 signals. n= 7 technical replicates.

Because Ame1-7A and Ame1-7E behave exactly in the same manner in all described assays here, we assume that Ame1-7E does not mimic Ame1 phosphorylation. Instead, it probably behaves as a phospho-null mutant Ame1-7A. Therefore, we decided to compare only Ame1-WT and Ame1-7A in further experiments. Figure 3.20D shows a quantification of Ame1-WT and Ame1-7A levels based on the western blot in Figure 3.20C. Ame1-7A levels are twice as high compared to Ame1-WT in this experiment. Values were normalized to the corresponding Okp1 signals.

3.3.2 The E3 ubiquitin ligases Psh1 and Mub1 are not responsible for Ame1 protein level regulation

As Ame1-WT and mutants were expressed under the same promoter, an accumulation of the different Ame1 phosphorylation mutants is interpreted as a lack of degradation rather than being an effect of different rates of the overproduction of protein. There are different E3 ubiquitin ligases that were shown previously to regulate the protein level of different kinetochore proteins. Psh1 is a ubiquitin ligase that is important for the restriction of the H3 variant Cse4 to centromeres (Collins et al., 2004). Ubr2/Mub1 is another ubiquitin ligase that regulates the levels of Dsn1 (Akiyoshi et al., 2013b). If one of these ubiquitin ligases is responsible for the accumulation of Ame1-7A, a deletion of such ligase should also lead to an accumulation of Ame1-WT to levels comparable to those of Ame1-7A. As shown in Figure 3.21, deletions of either *psh1* or *mub1* did not change the expression levels of Ame1-WT, which indicates that probably a different E3 ubiquitin ligase is responsible for this phenotype.

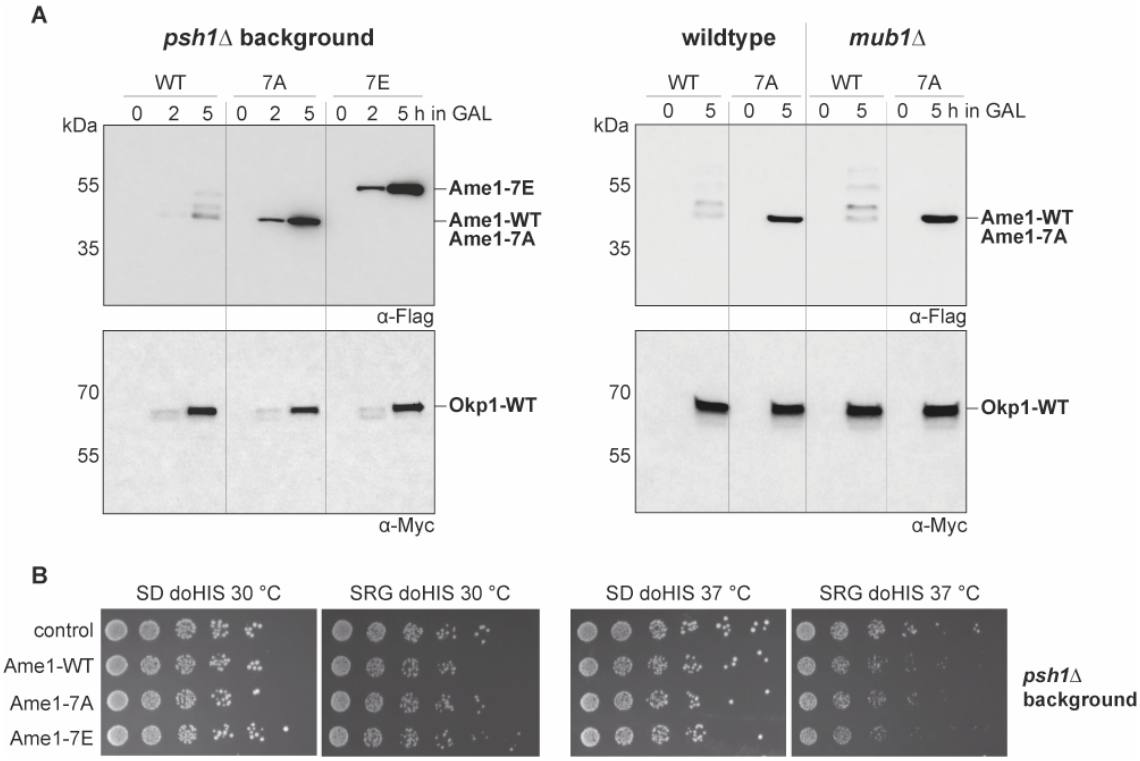

Figure 3.21: Comparison of Ame1 expression levels in two E3 ubiquitin ligase complex mutants. (**A**) Western Blot analysis of Ame1-WT and mutants in two different E3 ligase deficient strains: *psh1* deletion and *mub1* deletion. In both deletion mutants Ame1-7A/7E levels accumulate, whereas Ame1-WT levels are unaltered. Okp1 levels are also unchanged. (**B**) Serial dilution growth assay of overexpressed Ame1-WT, Ame1-7A and Ame1-7E in a *psh1* deletion background. Higher levels of Ame1 and Okp1 decrease the growth minimally, although no difference between WT and mutant Ame1 can be observed.

3.3.3 Identification of phospho-degron motifs in Ame1

From the previous experiment it was apparent that accumulation of Ame1 is based on its inability to be phosphorylated at specific residues. In the cell cycle, phosphorylation is typically linked to the E3 Ubiquitination pathway via so-called phospho-degrons. Therefore, the protein sequence of Ame1 was analyzed for the presence of specific degrons, that would support this hypothesis. Two different potential phospho-degrons that are specific for the SCF^{Cdc4} E3 ubiquitin ligase were identified at the residues Ser41/Ser45 (motif 2) and Ser52/Ser53 (motif 1). Motif 2 resembles a di-phospho-degron that shows similarities to the ones found in Cyclin E. These residues showed an accumulation effect comparable to Ame1-7A (which contains mutations of these 4 residues as well) (Figure 3.20). Figure 3.22 shows the protein structure of Ame1 and two potential Cdc4-phospho-degron (CPD) motifs. Both motifs cover two minimal motifs for CDK, which further strengthens the hypothesis of Ame1 being under the control of a phospho-degron, because they often contain CDK sites. To further validate these findings, two additional Ame1 variants were generated: an Ame1-4A strain = CPD null mutation preventing motif 1+2 phosphorylation or an Ame1-3A strain = CPD only, allowing motif 1+2 phosphorylation and in which all other potentially phosphorylated residues outside the CPD are mutated.

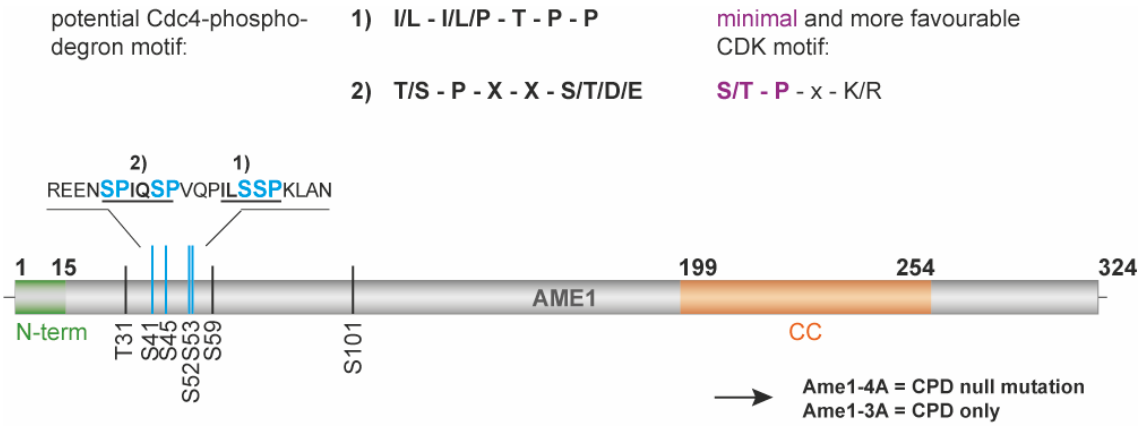

Figure 3.22: Identification of SCF^{Cdc4} phospho-degrons in Ame1. Two phospho-degrons were identified that resemble the docking sites for the E3 ubiquitin ligase complex SCF with its cofactor Cdc4. One is a bi-phospho-degron that includes the residues Ser41 and Ser45 of Ame1, and the second one includes the residues Ser52 and Ser53. For further analyses an Ame1-4A (CPD null; S41A, S45A, S52A, S53A) and an Ame1-3A (CPD only; T31A, S59A, S101A) are used for a more specific analysis.

3.3.4 The E3 ubiquitin ligase SCF^{Cdc4} initiates Ame1 degradation

As stated in the introduction, the E3 ligase SCF is an important regulator of many different proteins. Therefore, it was speculated that it could be responsible for the degradation of Ame1. Importantly, the function of SCF and its cofactor Cdc4 is dependent on pre-phosphorylation of its targets. SCF is a polyprotein complex consistent of Skp1, a Cullin (Cdc53 in yeast) and an F-Box protein (Cdc4 or Grr1, often phospho-dependent). Together with an E2 enzyme (here Cdc34) it specifically detects target proteins and ubiquitinates them for further degradation by the 26S proteasome (Figure 3.23A). Since Ame1 was shown to be phosphorylated, its levels are likely to be regulated via SCF^{Cdc4}. Interestingly, Ame1's protein sequence shows two potential phospho-degrons that indicate SCF^{Cdc4} being involved in Ame1 regulation (Figure 3.22). To investigate this hypothesis further, a *skp1* ts-mutant, which is part of the SCF complex, was analyzed in the established GAL shift assay. If SCF was involved in regulating Ame1 level upon overexpression, then it would be predicted that the wildtype protein and not just the phospho-mutant should accumulate. Interestingly, in this SCF mutant strain Ame1-wildtype and Okp1-wildtype accumulate to a higher level as compared to a wildtype background. Levels are now comparable to Ame1-7A, which is also elevated in its levels (Figure 3.23B). Based on the migration pattern, Ame1 wildtype phosphorylation is preserved in the *skp1-3* mutant. Taken together, this suggests that Ame1 is phosphorylated at the identified sites, which regulates its levels through SCF^{Cdc4} ubiquitination. To investigate this further, mutants of other SCF components were tested using the same assay (Figure 3.23C). The effect of Ame1-WT accumulation in *skp1-3* was also seen in the other tested mutants, a quantification of the overexpression is shown above the lanes. Pixel intensity of corresponding lanes were compared to wildtype background (set to 100 %). In all SCF mutants, levels of Ame1 were increased at least to 200 % in *cdc53-1* or up to 500 % in *cdc34-2*. Okp1 levels were also increased in the tested SCF mutants independent on Ame1-WT or Ame1-7A. Only in the *cdc34-2* mutant background Okp1 levels vary between Ame1-WT and Ame1-7A. When the cytoplasmic F-Box protein Grr1 is deleted, levels of Ame1-WT and Ame1-7A were even decreased to 63 %, whereas Okp1 levels were increased compared to the wildtype background.

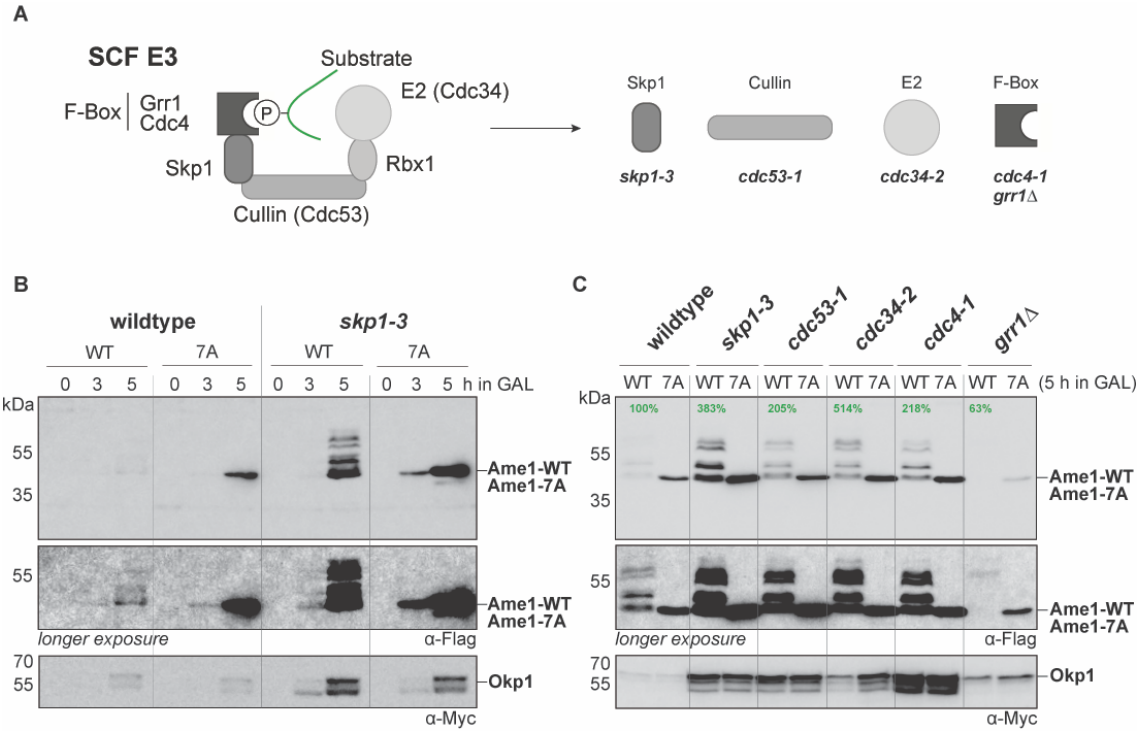

Figure 3.23: SCF^{Cdc4} complex is responsible for Ame1 protein level regulation. Western Blot analysis of overexpressed Ame1-WT or Ame1-7A in SCF^{Cdc4} complex mutant strains. Cells were grown for 5 hours at 30 °C in YEPRG and lysates were prepared after 0, 3 and 5 h and samples were analyzed for protein amounts in Western Blotting. In (**A**) a schematic overview of a phosphorylated substate bound to SCF is shown with two F-Box proteins, Cdc4 and Grr1. On the righthand site the temperature sensitive mutant strains are shown that are used in the GAL shift assay in (**B**) and (**C**). (**B**) Comparison of wildtype background and *skp1-3* used at the permissive temperature of 30 °C. Ame1-WT accumulates to similar levels like Ame1-7A in wildtype conditions. (**C**) Additional strains with SCF^{Cdc4} complex mutants were analyzed in the same way and confirm the previous result. A deletion of a cytoplasmic F-Box protein (*grr1*) does not increase the levels of Ame1-WT, the expression of Ame1-WT and Ame1-7A is even lower, although Okp1 signals increase minimally. In green: percentage of Ame1-WT signal intensity, when wildtype background is set to 100 %.

3.3.5 Overexpression of Ame1 compromises the growth of SCF mutants

To test the effect of Ame1 overexpression in cells, a serial dilution assay on synthetic medium was performed, to maintain the selective pressure for the pESC plasmid, because on full YEP medium the effect was very subtle, possibly due to the loss of the plasmids during longer incubation times. In addition, to the Ame1 mutants already investigated, we checked Okp1 for the presence of any potential CDK sites, that might contribute to phospho-regulation, as multiple degrons are often found in SCF substrates. A candidate full CDK site in Okp1 (S26) was mutated to alanine in order to test the potential growth phenotypes within the cell. In Figure 3.25 the overexpression of AOc-WT was compared with either Ame1-7A/Okp1-WT or Ame1-7A/Okp1-1A. These three individual mutants were overexpressed in either a wildtype background strain or in two SCF mutant strains: *skp1-3* or *cdc34-2*. In Figure 3.24A strains expressing the different AO versions can be compared in a WT or *skp1-3* background at different temperatures. As *skp1-3* is a temperature sensitive mutation, growth phenotypes are expected at elevated temperatures. In *skp1* strains, no growth difference was observed between wildtype Ame1 and Okp1 and their phospho-mutants, although all strains grew slightly slower at higher temperatures. In the *skp1-3* mutant strain, growth of all strains is compromised at 34 °C and completely abolished at 37 °C. Interestingly, the overexpression of any AOc, either in wildtype or phospho-mutant form, aggravates the growth defect of *skp1-3*, an effect most clearly seen at 34 °C. For this reason, the *skp1-3* mutant was used at 34 °C in further experiments.

Besides being part of the SCF complex, Skp1 is also a subunit of the CBF3 complex that is essential for proper kinetochore assembly. To exclude the possibility that the result observed in the *skp1-3* strain is specific for this mutation, another SCF mutant was tested for its behavior under conditions of AOc overexpression. A serial dilution assay in the *cdc34-2* background recapitulated the result seen in A (Figure 3.24B). The overexpression of Ame1 and Okp1 diminishes the growth of all strains, although an effect can already be seen at 30 °C, which might be due to a stronger temperature sensitivity of the background strain (compare 3.25B, 30 °C and 34 °C).

Overall, it can be concluded that the overexpression of the Ame1/Okp1 complex leads to a growth defect in SCF mutant strains, This is consistent with AOc being a physiologically relevant substrate of SCF. Presumably, SCF can only bind and ubiquitinate a limited amount of protein at a time and the overexpression of key substrates

leads to problems in the ubiquitination pathway and hence efficient degradation by the 26S proteasome.

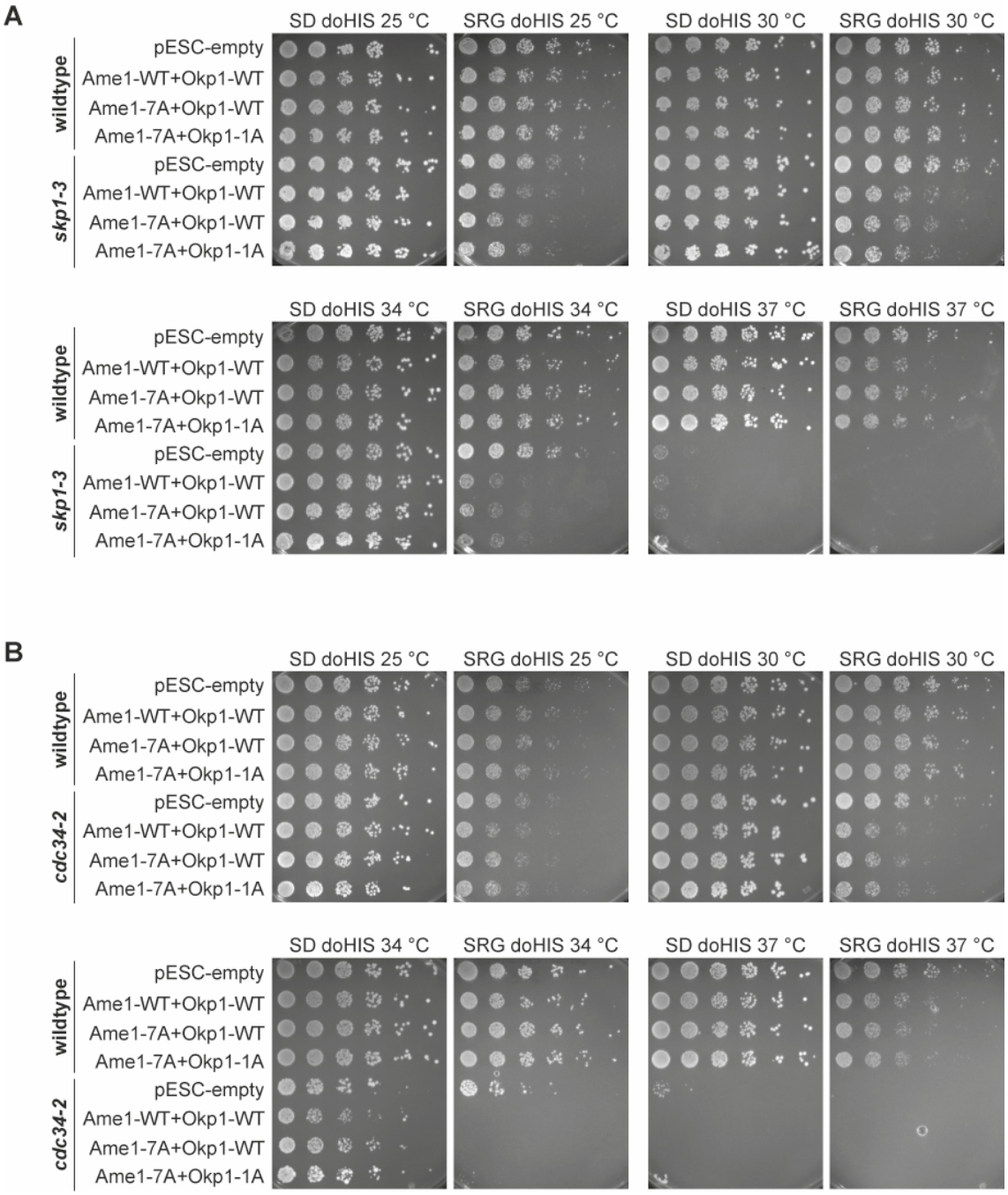

Figure 3.24: AOc overexpression inhibits growth in *skp1-3* or *cdc34-2* backgrounds. In *skp1-3* (**A**) and *cdc34-2* (**B**) strains, Ame1 and Okp1 overexpression was introduced from a 2µ plasmid through the addition of galactose to the medium and spotting the strains in a serial dilution on SD doHIS or SRG doHIS at various temperatures. The overexpression of introduced AO variants diminishes the growth in the *skp1-3* and *cdc34-2* strains at elevated temperatures.

3.3.6 Optimizing the phospho-degron sequence on Ame1 enhances its degradation via SCF^{Cdc4}

As shown above, Ame1 degradation is dependent on the phosphorylation at the previously identified residues S41, S45, S52 and S53, which resemble two phospho-degrons (Figure 3.20). As both of these degrons do not represent an optimal Cdc4-phospho-degron (CPD), we decided to mutate one (motif 1) of these two degrons into an optimal CPD motif by changing the sequence from ILSSP to ILTPP (Figure 3.25A). This would make Ame1 motif 1 more similar to the classical CyclinE-type degron. In particular, phospho-Threonine should provide a higher affinity for Cdc4 compared to phospho-Serine (Nash et al., 2001). According to the hypothesis that Ame1 levels are controlled via Cdc4-dependent degradation, optimizing the phospho-degron sequence should further improve its degradation and this effect should be reversible in a *cdc4* mutant strain. Indeed, overexpression of this Ame1-CPD^{ILTPP} variant was not detectable in a western blot of cell lysates after expression in the GAL shift assay in two independent clones (Figure 3.25B, lanes 5-8). Interestingly, also Okp1 expressed from the same plasmid, was undetectable by western blot. Additionally, Ame1 level regulation via SCF was confirmed in the *cdc4-1* mutant strain, because Ame1-CPD^{ILTPP} and Okp1 expressed at the permissive temperature, was restored to levels comparable to the wildtype background (Figure 3.25B, lanes 9-12).

To explore the functional relationship between the Ame1-CPD^{ILTPP} allele and the *cdc4-1* mutant by a different approach, yeast strains were generated in which either Ame1-WT or Ame1-CPD^{ILTPP} expressed from its own promoter was combined with *cdc4-1*. In Figure 3.25C a serial dilution assay of the resulting strains is depicted. Interestingly, Ame1-CPD^{ILTPP} grows more poorly than Ame1-WT in a wildtype strain background, most clearly seen in the presence of benomyl or at elevated temperature. By contrast, Ame1-CPD^{ILTPP} can restore, to a certain extent, the temperature- and benomyl-hypersensitivity of a *cdc4-1* mutant strain. In particular at 34 °C, expression of Ame1-CPD^{ILTPP} partially rescued the lethality of *cdc4-1* and also improved growth in the presence of benomyl. Ame1 and Okp1 are both target to degradation when they are phosphorylated by CDK and ubiquitylated by SCF^{Cdc4} at this specific docking motif. The identified native phospho-degrons on Ame1 (and Okp1) are non-optimal, probably because otherwise this machinery would be working too well and level regulation may not be proper.

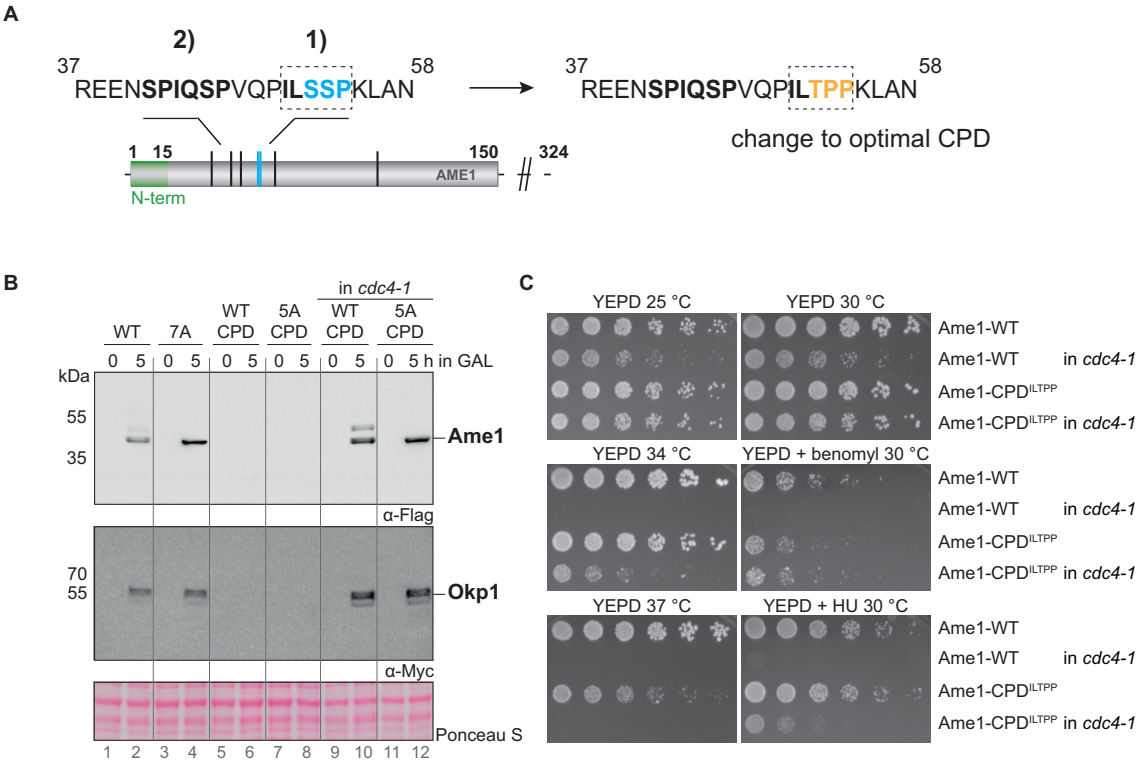

Figure 3.25: Placing an optimal CPD into Ame1 counteracts the *cdc4-1* mutant. (**A**) Schematic overview of mutating the first phospho-degron into an optimal CPD^{ILTPP}. (**B**) Western blot analysis of different Ame1 strains, lysates were prepared immediately or after 5 h of overexpression. Lanes 1-4: repetition of overexpressing Ame1-WT and Ame1-7A together with Okp1. Lanes 5-12: Ame1-CPD^{ILTPP} was tested in two independent clones in either wildtype or *cdc4-1* mutant background. Whereas the signal is below the detection limit in a wildtype background, signals are restored in mutant background. (**C**) Serial dilution assay of endogenously expressed Ame1 variants spotted on YEPD or YEPD + benomyl or hydroxyurea, incubated at different temperatures. Combination of Ame1-CPD^{ILTPP} and *cdc4-1* partially restores growth and hypersensitivity of *cdc4-1*.

3.4 Phosphorylated forms of endogenous Ame1 accumulate over S-Phase and start to disappear in mitosis

In the previously described experiments, it was shown that motif 1 and motif 2 in the Ame1 phosphorylation cluster seem to be most important for the accumulation in the cell in the overexpression experiment – which was shown to be a consequence of impaired degradation through the SCF^{Cdc4} complex. To reveal a possible relationship between Ame1 phosphorylation and cell cycle dependent degradation for endogenous Ame1, its levels of Ame1 and its phosphorylation status during the cell cycle were investigated in different strain backgrounds.

3.4.1 Stepwise phosphorylation of endogenous Ame1 occurs at the identified phospho-degron sequences

Some of the seven potentially phosphorylated Ame1 residues that are investigated in this study are characterized CDK sites, as described above. Therefore, a change in the phosphorylation pattern of Ame1 is likely to occur over the cell cycle. The four CDK phosphorylatable residues (S41, S45, S52 and S53), also resemble Cdc4 Phospho-degrons that are recognized by SCF^{Cdc4} (CPD). As in the assays used, it can only be observed whether Ame1 is phosphorylated or not, a simplified mutant was generated, in which the residues T31, S59 and S101 were mutated to alanine, so that only the motif 1 and motif 2 CPD sites are phosphorylatable. This Ame1-3A (= CPD only) mutant was introduced into yeast as the only present copy at an exogenous locus, but under endogenous expression conditions. A control strain in which the four CPD residues are mutated to alanine was also generated, so that CDK phosphorylation cannot take place (Ame1-4A = CPD null). Schematic overviews of both mutants are shown in Figure 3.26A. Cells expressing either Ame1-3A or Ame1-4A were arrested in different cell cycle stages and cell extracts were analyzed in a western blot detecting Ame1 (Figure 3.26B). In a logarithmic growing culture Ame1-3A consists of a main band and two phospho-isoforms, whereas Ame1-4A does not show any phospho-bands at any cell cycle stage. Ame1-3A shows also two distinct slowly migrating forms in mitotic cells, but in G1 and replicating cells only one of these forms is visible. This could be due to a cell cycle dependent phosphorylation of Ame1 by CDK. The Ame1-3A mutant is easier to analyze due to a limited number of its slowly migrating forms and was therefore further used in cell cycle regulation studies

instead of Ame1-WT in which a more complex pattern of phospho-bands was detected (see Figure 3.15).

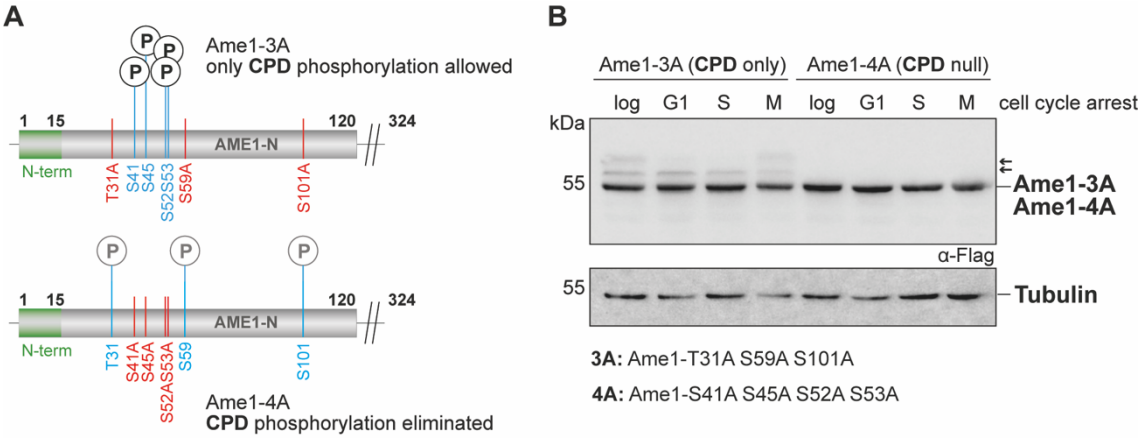

Figure 3.26: Two new Ame1 variants allow to follow CPD phosphorylation over the cell cycle. In (**A**) a schematic overview of both mutants is shown. Ame1-3A allows phosphorylation at residues S41, S45, S52 and S53 (motif 1+2), whereas Ame1-4A prevents phosphorylation of these sites. In (**B**) cells with Ame1-3A or 4A were arrested in different cell cycle stages and cell extracts were prepared. In Western blot Ame1-3A shows one main band besides two distinct phosphorylated isoforms in a logarithmically growing culture, that is also visible in mitotic cells. In G1 and replicating cells only a single phospho-isoform is visible. Ame1-4A shows only the main band, as no slowly migrating bands are visible. The arrows indicate the different phospho-isoforms.

3.4.2 Ame1 phosphorylation patterns change during the cell division cycle

The phosphorylation pattern of Ame1-3A was analyzed over the complete cell cycle by arresting cells in a G1 like state with α factor and releasing them into the cell cycle. Cell extracts were prepared every 15 minutes starting at the release and phosphorylation of Ame1 was followed via Western Blotting and progression through the cell cycle via FACS analysis. Another addition of alpha factor at 38 minutes after release prevents cells from entering another cell cycle. The phosphorylation of Ame1 changes gradually over the cell cycle, it increases when cells enter S phase (as seen in FACS analysis (Figure 3.27B)) and reaches its maximum when cells enter mitosis after about 30 min (when correlating phospho-bands with the FACS analysis (Figure 3.27A and 3.27B). When cells progress through mitosis as judged by FACS (30-75 minutes), suddenly the phosphorylated forms disappear (see dashed box, 45 and 60 minutes) and only the unphosphorylated main band of Ame1 is present, similar to Ame1-4A, where no CDK phosphorylation can take place.

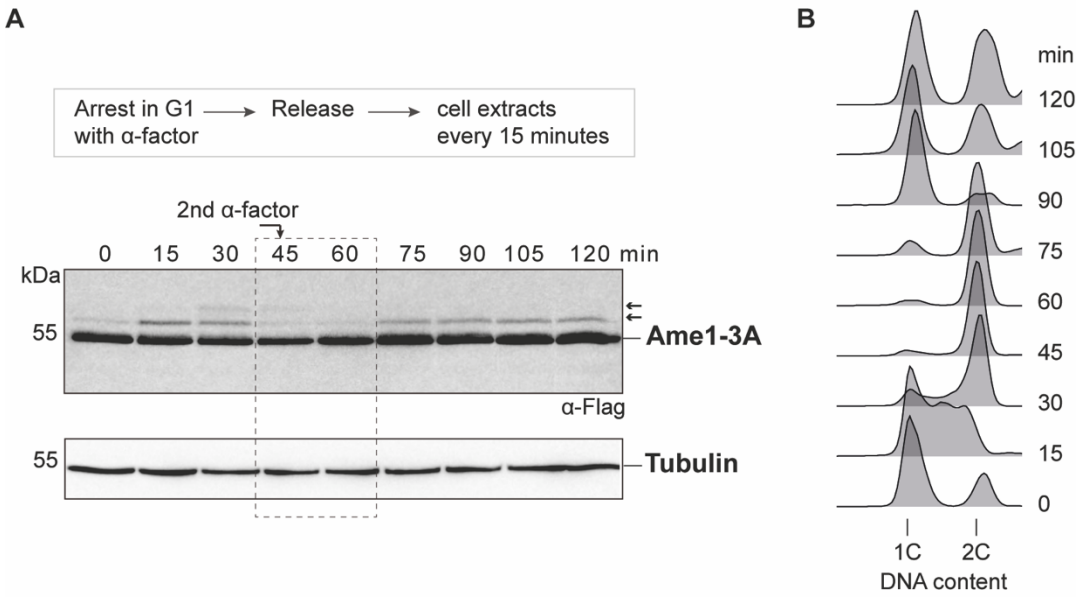

Figure 3.27: Phosphorylated Ame1-3A appears at entry of S-Phase and disappears during mitosis as seen in western blot and FACS profiles. (**A**) Ame1-3A expressing cells were arrested in a G1 like state using α factor and released into the cell cycle. Additional alpha factor after 38 minutes prevents cells from entering another cell cycle. Ame1-3A gets phosphorylated in a cell cycle dependent manner, as isoforms appear gradually when cells proceed from G1 to replication and mitosis, judged by FACS in (**B**). The arrows indicate the different phospho-isoforms. (**B**) FACS analysis of Ame1-3A. Apart from cell extracts also cells were fixed for FACS staining every 15 minutes after release and read out. Phosphorylated isoforms disappear rapidly when cells enter mitosis (dashed box in (**A**)), when cells divide, a residual phosphorylation takes place that will stay until 2 hours after release.

3.4.3 Phosphorylated forms of Ame1 disappear in mitosis

From the previous experiment, it was concluded that Ame1 gets phosphorylated upon S-Phase entry, phosphorylated isoforms of Ame1 disappear in mitosis and Ame1 gets re-phosphorylated after reentering G1. As judgement of the cell cycle stage from FACS analysis is limited and the removal of phosphorylated isoforms of Ame1 in mitosis is potentially very interesting, we aimed for another readout to evaluate the cell cycle stage instead of FACS analysis. Therefore, Pds1-Myc was introduced in the strains used in the previous experiment. Pds1 secures cohesion attachment of the sister chromatids after replication until all chromosomes are aligned properly and attached to microtubules from opposing spindle poles. Hence, Pds1 gets degraded once cells proceed to anaphase onset and can be used as marker to observe anaphase onset in Western Blotting, Figure 3.28A shows a repetition of the previous experiment, only that it includes Pds1-Myc detection. Ame1-3A phosphorylation is again gradually increasing over the cell cycle and Pds1-Myc confirms the rapid disappearance of phosphorylated isoforms at anaphase onset, probably as a result of its degradation. This could be stated because Pds1 signals vanish slowly around the same time (Figure 3.28A). Ame1-4A again shows only a single band in Western Blotting throughout the cell cycle (Figure 3.28B). The Pds1 signal is the same in both cases, which means that the missing phosphorylation at these four residues does not significantly delay mitosis. Two more strains were generated as described before: One strain where only the phosphorylation of S52 and S53 (motif 1) is allowed (Ame1-5A1) or of residues S41 and S45 (motif 2) (Ame1-5A2). When only motif 1 is phosphorylated, a very residual phosphorylation can be observed in a long exposure of a Western Blot. When only motif 2 can be phosphorylated, no obvious slow migrating forms can be seen (Supplementary figure 2).

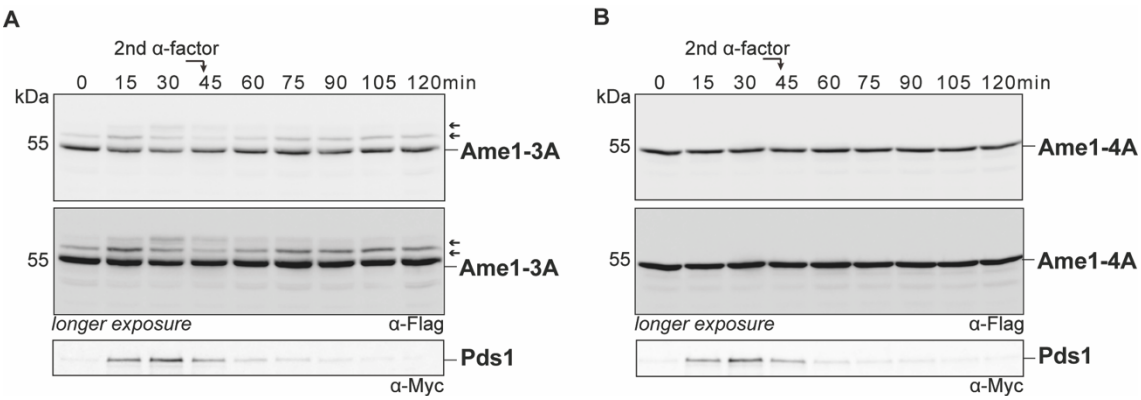

Figure 3.28: Pds1-Myc staining reveals disappearance of Ame1 phospho-forms at anaphase onset. (**A**) Cell cycle progression of cells carrying Ame1-3A and Pds1-Myc is shown. Ame1-phosphorylation appears gradually when cells transit from S-Phase to mitosis. Pds1 confirms that mitotic cells lack any phosphorylated isoforms of Ame1. The

arrows indicate the different phospho-isoforms. (**B**) Ame1-4A is combined with Pds1-Myc. The inability to phosphorylate Ame1 at its phospho-degron sites does not delay the cell cycle progression.

3.4.4 SCF^{Cdc4} is responsible for degradation of phosphorylated Ame1 in mitosis

The CDK phosphorylated residues within the phospho-degron (S41, S45, S52 and S53) are potential binding sites for the E3 ubiquitin ligase complex SCF^{Cdc4}. One key component of SCF is Skp1, a mediator for different F-Box proteins like Cdc4 that can bind to specific targets like phosphorylated proteins. As stated above, we hypothesize that the rapid disappearance of phosphorylated Ame1 during the cell cycle experiment is due to degradation mediated by SCF^{Cdc4}. This is an interesting idea, as it would indicate Ame1 degradation at a time where it fulfills its main function within the cell. In order to test this hypothesis, we checked if phosphorylated isoforms of Ame1 persist through the cell cycle in a *skp1-3* mutant. As in the two experiments above, Ame1-3A phosphorylation was observed over a complete cell cycle. At the permissive temperature of 30 °C the mutant *skp1-3* allele is still functional, which leads to an Ame1 phosphorylation pattern similar to wildtype background strains. Different from a wildtype background, the degradation of phosphorylated Ame1 isoforms in mitosis is delayed by 15 minutes as the bands disappear only at 60 minutes not at 45 minutes after release as shown before (compare Figures 3.28A and 3.29A). However, FACS analysis does not detect differences in cell cycle progression between these two strains (Figure 3.29D, first and second profiles). At the semi-permissive/restrictive temperatures of 34 °C and 37 °C the mutant *skp1-3* allele displays different degrees of functionality. In order to allow cells to proliferate and arrest properly in G1 with alpha factor, cells were pre-incubated at the permissive temperature. This is necessary, because Skp1 is generally required for cell cycle progression by allowing entry into S-Phase via degradation of the CDK inhibitor Sic1. Shifting cells to 34 °C at the time of cell cycle release, results in a normal cell cycle progression until mitosis, which seems to be perturbed, judged by FACS analysis, Ame1 phosphorylation is gradually increasing starting from S-Phase entry as seen in a wildtype background, but isoforms are not degraded upon mitotic entry in the *skp1-3* mutant at 34 °C until the end of the experiment (Figure 3.29B and third FACS profile in 3.29D). When cells were shifted to 37 °C however, cells have serious problems to even proceed to replication as stated by FACS which reveals a greatly delayed appearance of a 2C DNA peak

(Figure 3.29B, fourth FACS profile in 3.29D). In addition, phosphorylation of Ame1 only appears with a great delay while 34 °C allows replication but inhibits the mitotic function specifically. Therefore, 34 °C was used for further experiments.

From this experiment we conclude that rapid removal of phosphorylated isoforms of endogenous Ame1 in mitosis is indeed mediated via SCF^{Cdc4}. It has to be said, that combination of Ame1-3A already decreases the cell cycle progression of *skp1-3*, as the same mutant combined with e.g., Mcm21-WT only shows a minor cell cycle delay (see Figure 3.33).

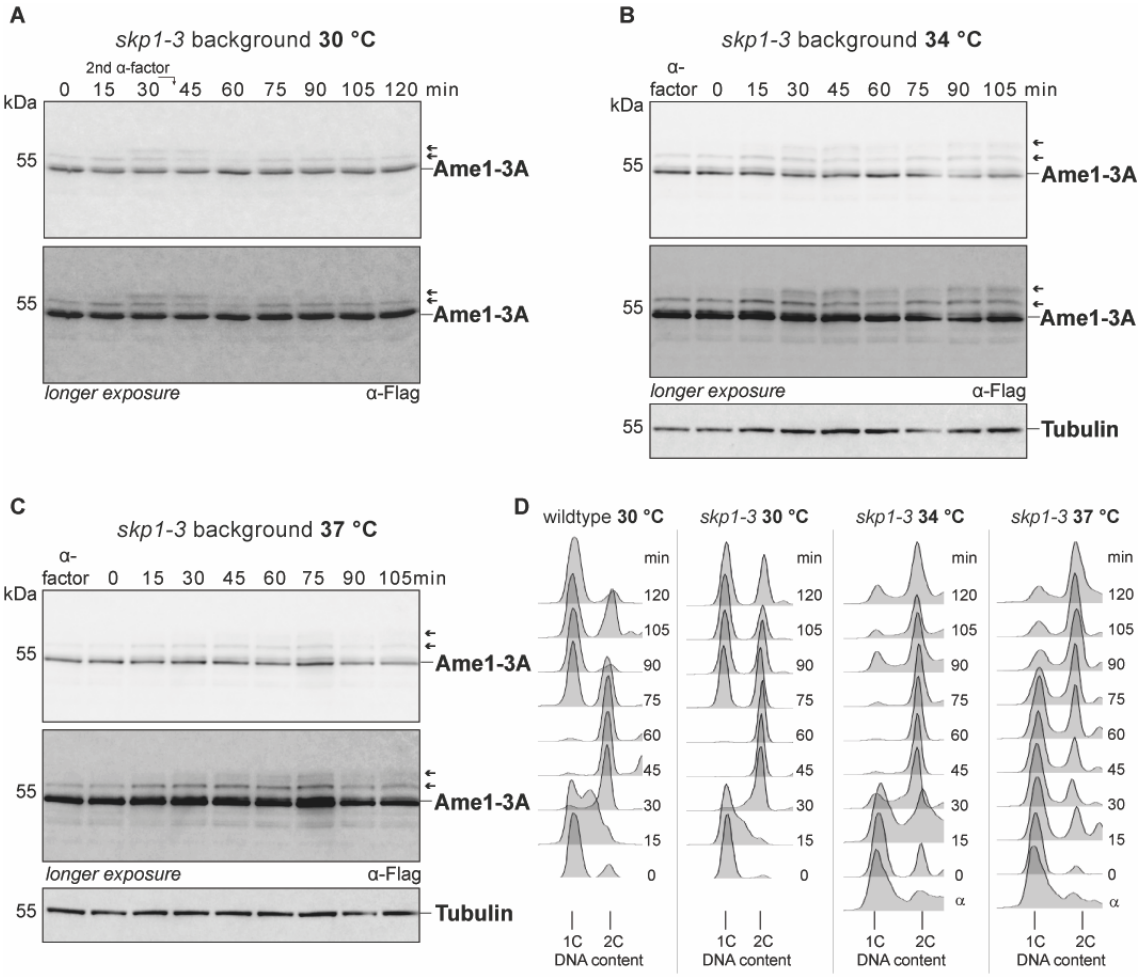

Figure 3.29: Skp1 is necessary for Ame1 degradation in mitosis. (**A**) Cell cycle analysis Ame1-3A in a *skp1-3* mutant strain background at 30 °C. Ame1 phosphorylation appears gradually as seen in previous experiments. Another addition of α factor after 38 minutes prevents cells from entering another cell cycle. (**B**) Cell cycle analysis of Ame1-3A in a *skp1-3* mutant at semi-permissive temperature of 34 °C. Phosphorylation appears gradually again but does not disappear as seen in (**A**). (**C**) Cell cycle progression of Ame1-3A in *skp1-3* mutant at the restrictive temperature of 37 °C, cells do not even enter S-Phase as stated from FACS (**D**), phosphorylation does not appear to full extent as seen in (**A**). (**D**) FACS analysis of cell cycles seen in (**A**), (**B**) and (**C**) and additionally from Ame1-3A in a wildtype background. The arrows indicate the different phospho-isoforms.

3.5 *In vitro* kinase assays with Cdc28/Clb2 reveal an Mtw1c binding-sensitive phosphorylation of Ame1 and Okp1

To gain further insights into the role of Ame1 phosphorylation, *in vitro* kinase assays were performed using purified Cdc28/Clb2, an M-Phase CDK-cyclin complex from budding yeast (Loog and Morgan, 2005). This complex was purified in this study from yeast using a 2-step purification of Clb2-TAP (for method see section 2.12.1). Different recombinant Ame1/Okp1 complexes (Figure 3.30) were subjected to phosphorylation via Cdc28/Clb2 *in vitro* and their phosphorylation statues compared in autoradiograms. Also, the effect of AOc interaction with known binding partners on its phosphorylation was tested by pre-incubating Ame1/Okp1 complexes with known binding partners prior to *in vitro* phosphorylation. All purified variants show a similar behavior in SDS-PAGE gels. Schematic overviews show mutated residues. Next to Ame1/Okp1 wildtype, nine different phospho-preventing mutants were generated, from which three also carry a mutation on Okp1.

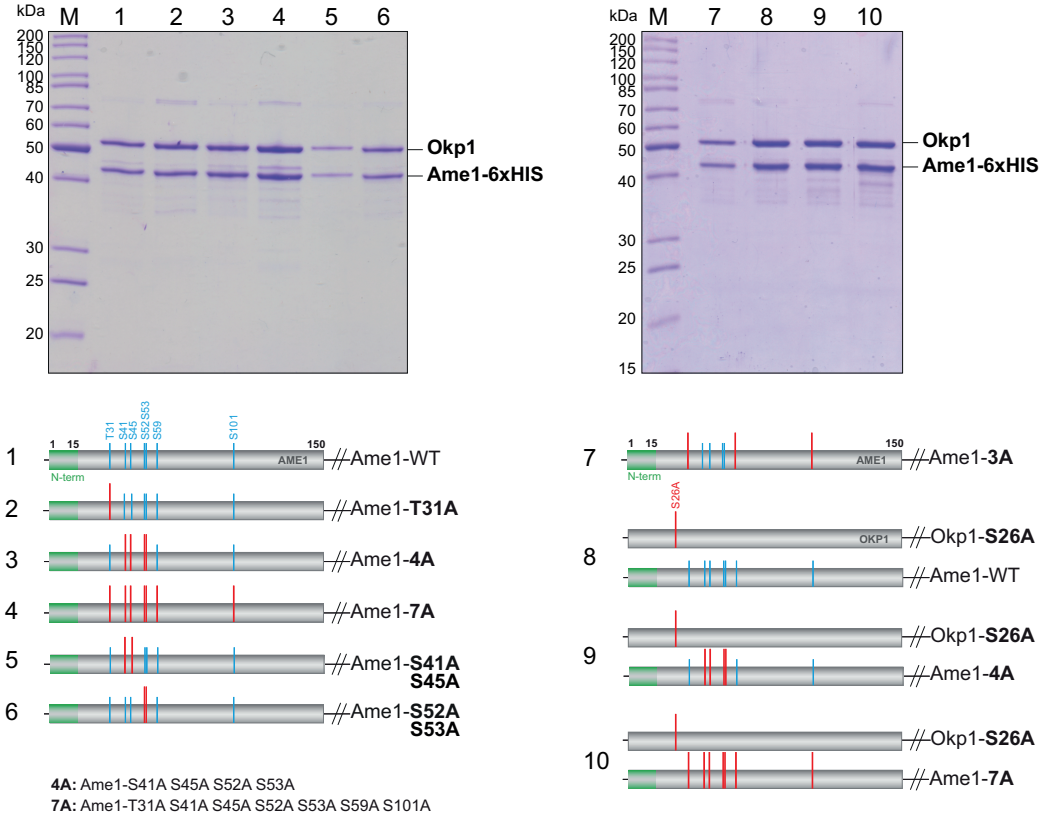

Figure 3.30: Overview of recombinant Ame1/Okp1 complexes. SDS-PAGE gels show all recombinant Ame1/Okp1 variants that were purified for this project. All subcomplexes show similar behavior in SDS-PAGE gel as two distinct bands for Ame1 and Okp1. On the left site, Ame1/Okp1 wildtype is shown at position 1 with seven phosphorylatable residues in blue. Mutated residues of corresponding mutants are shown in red (2-10). Three subcomplexes were purified and used that also have Ser26 of Okp1 mutated to alanine (8-10).

3.5.1 Ame1's seven-residue phosphorylation cluster is a target for Cdc28/Clb2

It was previously shown that Ame1 is a target for CDK *in vivo* and *in vitro* (Figures 3.10 and 3.14). In this kinase assay recombinant Ame1/Okp1 complexes were phosphorylated by Cdc28/Clb2 with radioactively labelled γ-^{32}P-ATP for visualization. Briefly, Ame1/Okp1 complexes were incubated with kinase for 30 minutes and loaded on SDS-PAGE gels. SDS-PAGE gels were exposed to films and developed for visualization of phosphorylated proteins. Both Ame1 and Okp1 were clearly phosphorylated by Cdc28/Clb2 (see Figure 3.31A, compare lanes 2 and 3). Ame1 again shows different phosphorylated isoforms, running as two distinct bands in the SDS-PAGE gel. When Ame1 is mutated at either T31 (lane 4), CPD sites (S41 + S45 (lane 7) or S52 + S53 (lane 8) or together (lane 5)) or at all seven CDK residues (lane 6), the number of phosphorylated isoforms of Ame1 is reduced. When only a single residue (T31, lane 4) is mutated, Ame1 can be phosphorylated to a similar extent than Ame1-WT. When the phospho-degron motifs for SCF^{Cdc4} are mutated (Ame1-4A, lane 5), only a single band for phosphorylated Ame1 is visible. When all seven residues are mutated to alanine (Ame1-7A, lane 6) phosphorylation is completely prohibited. In lanes 7+8 the individual phospho-degron motifs were mutated to alanine (S41+45A or S52+53A), which resembles the same effect as already seen in lane 5, phosphorylation of Ame1 is diminished.

Ame1-3A, which only allows phosphorylation at the phospho-degron motifs, is also phosphorylated *in vitro* and shows only a single band in the autoradiogram (Figure 3.31B, lane 4). Okp1 also harbors a single full CDK site at the residue S26 which also resembles a potential phospho-degron motif. Mutation of this site to alanine was combined with Ame1-WT, 4A or 7A (lanes 7-9). This leads to unphosphorylated Okp1, which results in a completely unphosphorylated AOc in combination with the Ame1-7A mutant (lane 9). The phosphorylation status of Ame1-WT or Ame1-4A is not changed when combined with Okp1-1A (lanes 7+8). We conclude that Ame1 and also Okp1 are both phosphorylated by Cdc28/Clb2 in vitro at SCF^{Cdc4} phospho-degron motifs, which is in line with our previous experiments, because this would explain a cell cycle dependent degradation of AOc in mitosis, where Cdc28/Clb2 becomes active.

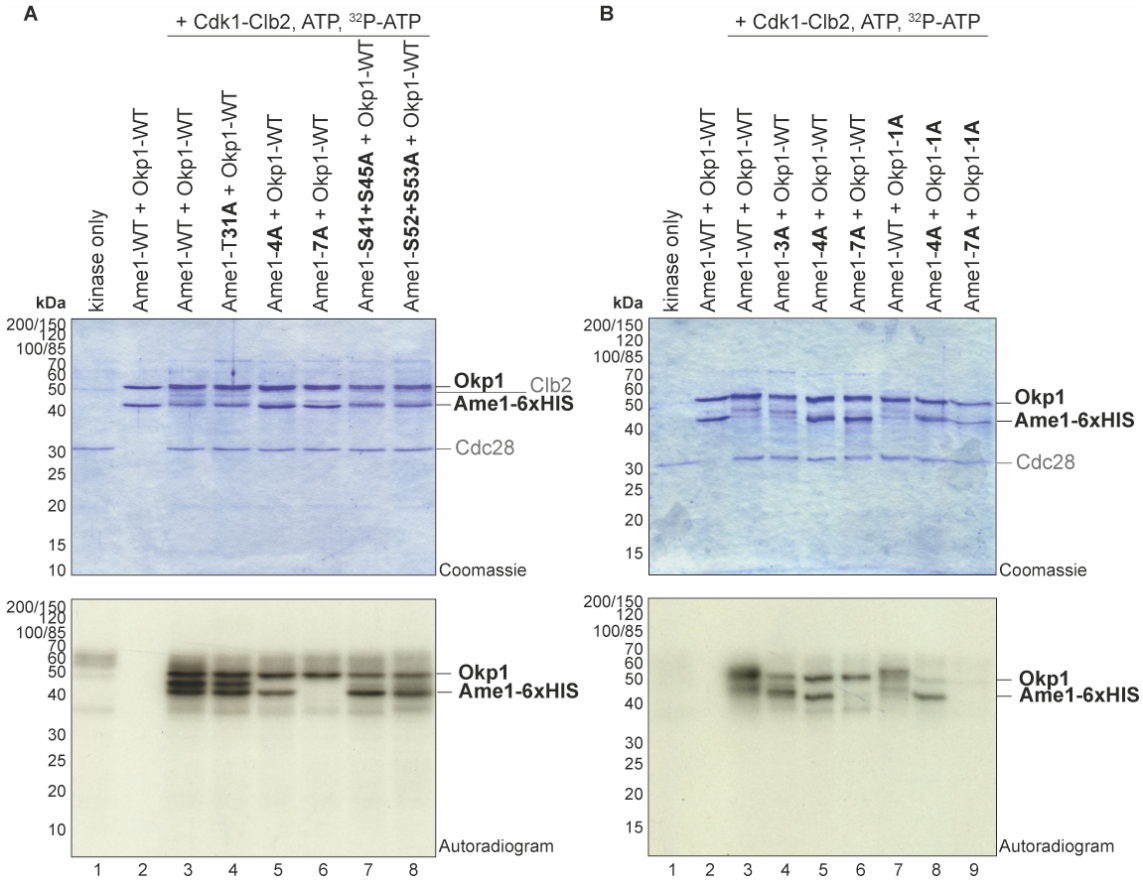

Figure 3.31: Ame1 and Okp1 are phosphorylated by Cdc28/Clb2 *in vitro*. (**A**) Different Ame1/Okp1 complexes containing Ame1 phospho-mutants were incubated with recombinant Cdc28/Clb2. Cdc28/Clb2 was purified from yeast in a 2-step protocol. (A) shows different Ame1-variants in complex with Okp1. Lane 1: kinase only, lane 2: AOc only, lane 3: AOc wildtype with kinase, lane 4: Ame1-T31A/Okp1 with kinase, lane 5: Ame1-4A/Okp1 with kinase, lane 6: Ame1-7A/Okp1 with kinase, lane 7: Ame1-S41A+S45A/Okp1 with kinase, lane 8: Ame1-S52A+S53A/Okp1 with kinase. (**B**) shows Ame1 phospho-mutants in combination with Okp1-1A. Lane 1: kinase only, lane 2: AOc wildtype only, lane 3: AOC with kinase, lane 4: Ame1-3A/Okp1 with kinase, lane 5: Ame1-4A/Okp1 with kinase, lane 6: Ame1-7A/Okp1 with kinase, lane 7: Ame1-WT/Okp1-1A with kinase, lane 8: Ame1-4A/Okp1-1A with kinase, lane 9: Ame1-7A/Okp1-1A. When Ame1-7A is combined with Okp1-1A, phosphorylation is completely eliminated.

3.5.2 Ame1 phosphorylation by Cdc28/Clb2 is sensitive to Mtw1c binding

As shown above, the phospho-degron motifs in Ame1 and Okp1 are targets of Cdc28/Clb2 phosphorylation. Ame1 phosphorylation *in vivo* was shown to be incomplete throughout the cell cycle as only a small fraction is phosphorylated at any given time, as judged from the appearance of only a small fraction of Ame1 as a shifted isoform in Western Blotting (e.g. Figure 3.13). From this, it can be assumed that only a fraction of the Ame1 pool in the cell is phosphorylated in order to be removed from the cell. This could be a way to eliminate excessive complexes that are not needed for kinetochore incorporation. If this was correct, phosphorylation of AOc may decrease upon binding to Mtw1c. Mtw1c is a likely candidate to influence Ame1 phosphorylation, as the binding is mediated by the N-terminus, in the close proximity to the phospho-cluster. Indeed, kinase assays reveal a diminished phosphorylation of AOc when bound to Mtw1c (Figure 3.32A) or only Mtw1/Nnf1 dimer (Figure 3.32B). Under identical conditions, Ame1-WT was still phosphorylated in the presence of Mtw1c or MNc, but to a much lesser extent as compared to AOc in isolation (Figure 3.32A). Ame1/Okp1 in isolation is phosphorylated very prominently (lane 3), although the two separate signals that were visible in Figure 3.31 now run together as one. Interestingly, when Mtw1c was phosphorylated alone, it revealed that also Dsn1 is also a substrate of Cdc28/Clb2 (lane 5).

For further studying the previously introduced phospho-mutants of Ame1, AOc was incubated with MN, as this bears the advantage that the phosphorylation status of Okp1 is not masked by Dsn1 phosphorylation, which runs at the same height (Figure 3.32B). Supporting the previous result, Ame1/Okp1-WT that was preincubated with MNc showed reduced phosphorylation as compared to AOc without binding partner (compare lanes 1+2). A similar effect can be seen when Ame1-3A + Okp1 is used (lanes 3+4). When the phospho-degron motifs are mutated (Ame1-4A), the phosphorylation of both Ame1 and Okp1 is not changing upon binding to MNc (lanes 5+6), again confirming Ame1 phosphorylation by Cdc28/Clb2 at the phospho-degrons. As a control for this binding-sensitive effect on Ame1 phosphorylation, a reaction was used in which Ame1/Okp1 complex was preincubated with NNc (a heterodimer that binds to the C-terminus of Ame1), before being phosphorylated via Cdc28/Clb2. We interpret the reduced phosphorylation of Ame1 as a consequence of the shielding of the phospho-cluster by binding to Mtw1c, and this should not be the case when AOc is bound to NNc, which binds to the C-terminus (see Figure 3.8). Although the autoradiogram is a bit weak at this

site and the intensity of Ame1 and Okp1 is weaker than in lane 1, it seems as if Ame1 and Okp1 are phosphorylated normally, which would indeed indicate that Ame1 phosphorylation is specifically inhibited upon Mtw1c binding.

Taken together we conclude that Ame1 phosphorylation at the phosphorylation cluster near the essential N-terminus is prevented when Ame1 is bound to the Mtw1 subunit of the Mtw1c *in vitro*, thus when it is incorporated in the kinetochore.

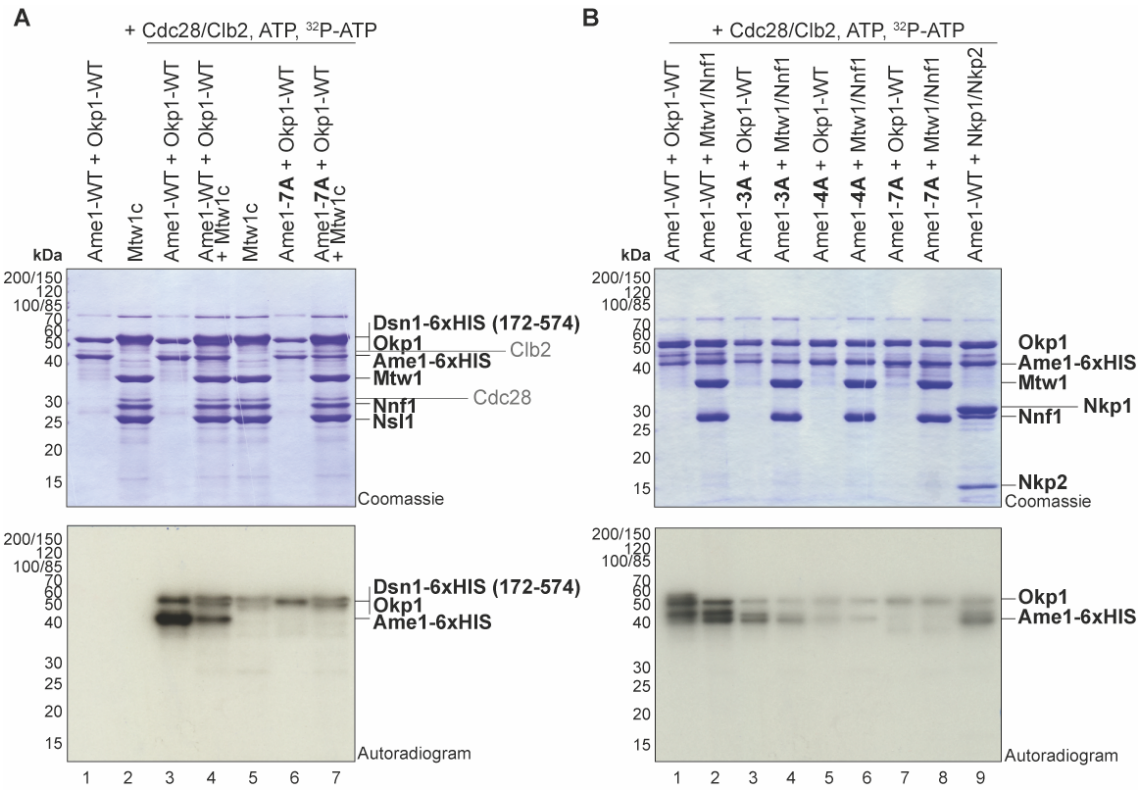

Figure 3.32: *In vitro* kinase assays of Ame1 reveal binding-sensitive phosphorylation of Ame1/Okp1. *In vitro* kinase assay with Ame1/Okp1 complexes bound to recombinant Mtw1c. (**A**) shows Ame1-WT/Okp1 compared to Ame1-7A/Okp1, both preincubated with Mtw1c. Lane 1: AOc without kinase, lane 2: Mtw1c without kinase, lane 3: AOc with kinase, lane 4: AOc-WT plus Mtw1c, lane 5: Mtw1c with kinase, lane 6: AOc-7A with kinase, lane 7: AOc-7A with Mtw1c. Ame1 phosphorylation is reduced, when AOc is preincubated with Mtw1c. Dsn1 is phosphorylated by Cdc28/Clb2 as well. (**B**) AOc phospho-mutants preincubated with MNc. Lane 1: AOc alone, lane 2: AOc + MNc, lane 3: Ame1-3A/Okp1 alone, lane 4: Ame1-3A/Okp1 with MNc, lane 5: Ame1-4A/Okp1 alone, lane 6: Ame1-4A/Okp1 with MNc, lane 7: Ame1-7A/Okp1 alone, lane 8: Ame1-7A/Okp1 with MNc, lane 9: AOc with NN. Whereas phosphorylation of Ame1 is reduced as seen in (**A**) when preincubated with MNc, the phosphorylation of Ame1 is not reduced upon NNc binding.

3.6 The COMA complex is a better target for SCF^{Cdc4}

As Ame1 and Okp1 can also bind to another heterodimer called Ctf19/Mcm21 at the inner kinetochore and form a stable tetrameric complex (COMA), we intend to analyze also these other two components and their phosphorylation status *in vivo*. As Ctf19 has no predicted CDK motifs and was not identified as a phosphorylated protein in previous proteomic studies, the focus lay on Mcm21. It was previously shown, that SCF^{Cdc4} can bind to and ubiquitinate substrates that are phosphorylated by CDK at multiple sites. As Ame1/Okp1 often is in complex with Ctf19/Mcm21 as COMA, there might be the possibility that not only Ame1 and Okp1 are phosphorylated by CDK and ubiquitinated by SCF^{Cdc4}, but also the whole COMA complex. Therefore, we analyzed Mcm21 with regard to phosphorylation and ubiquitination.

3.6.1 Mcm21 is phosphorylated by CDK *in vivo* and *in vitro*

Mcm21 is a nonessential component of the inner kinetochore and forms a stable heterodimer with Ctf19. Both together form the tetramer COMA with Ame1 and Okp1, but Ctf19 and Mcm21 are also part of the CENP-T pathway in budding yeast, which is one way to recruit two Ndc80 complexes for microtubule binding (Pekgöz Altunkaya et al., 2016). In *in vitro* studies Mcm21 was also identified to be phosphorylated at the residues T88, T138, S139 and S141. In Figure 3.33A the phosphorylated residues are shown in a schematic overview of Mcm21. T88 and S139 both resemble both a CDK site, of which S139 shows a full CDK phosphorylation motif. Additionally, in *in vitro* studies mentioned before also the residues T138 and S141 were found to be phosphorylated by CDK. Interestingly, the residues around T138 and S139 strongly resemble the optimal CPD site that we created in Ame1-CPD^{ILTPP} and that was empirically determined (Figure 3.23), except basic amino acid residues at position +3 to +6, which could possibly reduce the ability to bind Cdc4 (Nash et al., 2001). This sequence is also well conserved among different yeast species and is a good candidate for our investigations.
A schematic overview of the assembled COMA complex is shown in Figure 3.33B and would allow the combination of phosphorylation o multiple subunits which could lead to a higher affinity for SCF^{Cdc4}.

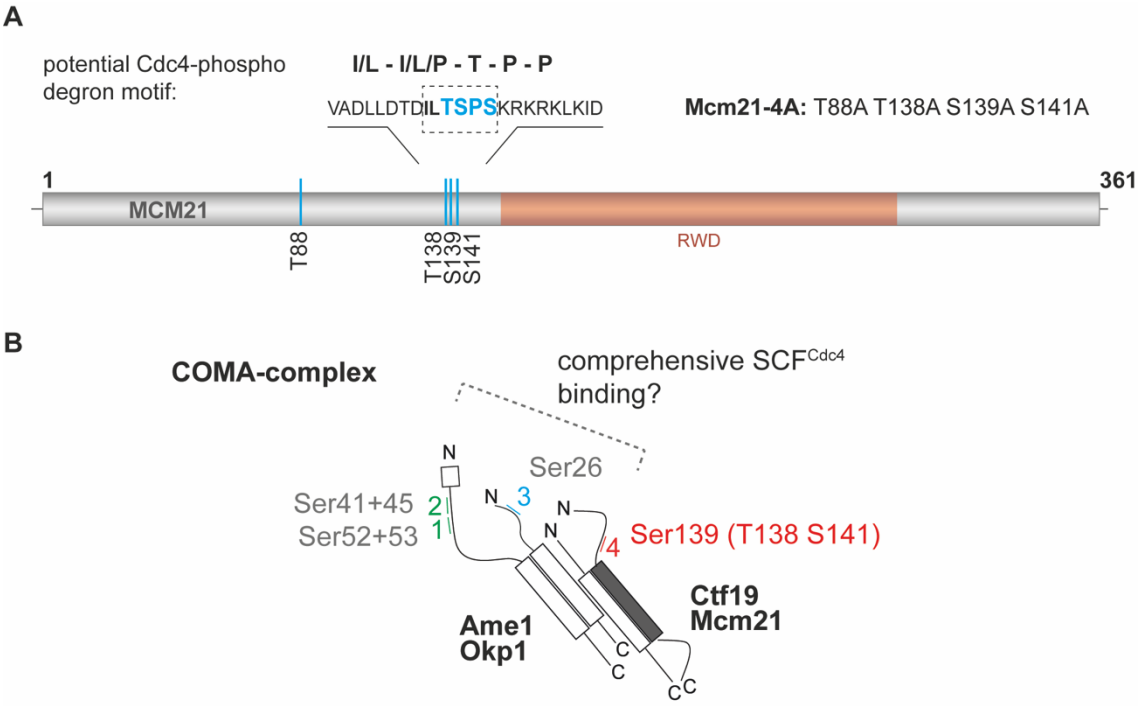

Figure 3.33: Domain organization of Mcm21 and COMA complex formation. (**A**) shows the domain structure of Mcm21. This protein contains at the C-terminus an RWD domain, which is responsible for binding to Ctf19 and Okp1. Four residues were found to be phosphorylated by CDK, although only T88 and T139 show the CDK motif. (**B**) shows a scheme of COMA, were the N-termini of Ame1, Okp1 and Mcm21 are phosphorylated by CDK and could potentially form a platform for a comprehensive SCF^{Cdc4} binding. Numbers 1-4 indicate phospho-degrons on different COMA subunits, whereas on Mcm21 only Ser139 and Ser138 show sequence similarity.

3.6.3 Mcm21 is phosphorylated in a cell cycle dependent manner

To analyze the phosphorylation of Mcm21 *in vivo*, we introduced a 6xFlag-tag on endogenous Mcm21, combined this mutant with the *skp1-3* allele and followed Mcm21 over one complete cell cycle. Cells were arrested in G1 using alpha-factor, released and simultaneously shifted to the restrictive temperature of 34 °C. In Figure 3.34 is shown, that Mcm21 is phosphorylated in a cell cycle dependent manner, as a slowly migrating from appears when cells enter S-Phase. The slow migration form vanishes rapidly during mitosis, as stated by FACS analysis. In a *skp1-3* mutant background, accumulated Mcm21 phosphorylation is comparable to a wildtype background (compare Figure 3.34A and B), although cells are delayed for 15 minutes as seen in FACS analysis. The disappearance of the slow migrating form is delayed as well. In order to make the slowly migrating form of Mcm21 visible, the PhosTag reagent was used in SDS-PAGE gels, because without it Mcm21-6xFlag was only visible as a single distinct band. Mcm21 is phosphorylated during the cell cycle in a similar manner as Ame1. Next, we would like to test if overexpression of COMA creates a growth phenotype in cells using the established GAL shift assay.

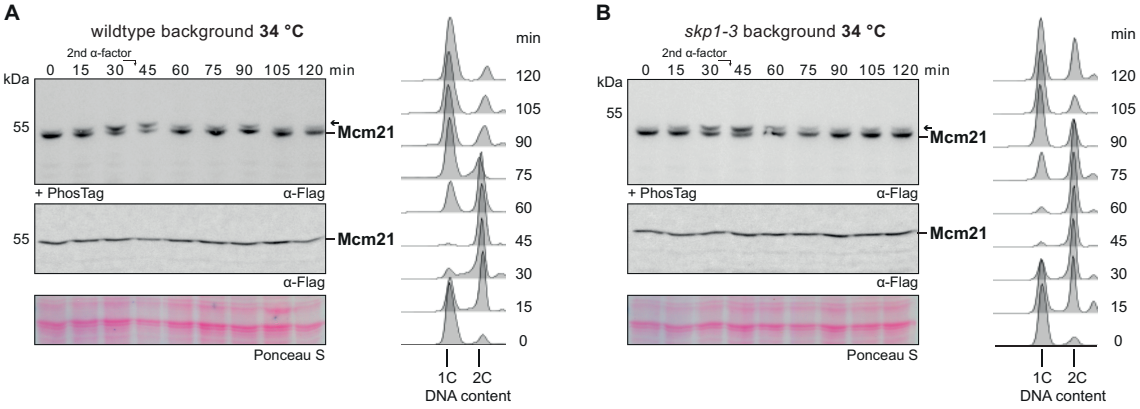

Figure 3.34: Mcm21-6xFlag is phosphorylated in a cell cycle dependent manner. Cells containing Mcm21-6xFlag were arrested in G1 using α-factor at 30 °C for 2 hours and released into a 34 °C temperature shift. Samples were taken every 15 minutes and loaded onto an SDS-PAGE gel. Mcm21-6xFlag in a wildtype background (**A**) or *skp1-3* mutant background (**B**) on either a normal SDS-PAGE (lower gel) or + PhosTag reagent (upper gel). A shift of Mcm21 was only seen in PhosTag SDS-PAGE gels. FACS analysis revealed a phosphorylation in S- and early M-Phase, similar to Ame1 (see Figure 3.28). The arrows indicate the phospho-isoform of Mcm21.

3.6.4 Increased levels of COMA are toxic to yeast cells

To overexpress Ame1/Okp1 together with Ctf19/Mcm21, an additional 2micron plasmid was introduced in strains that already contain the overexpression plasmid with Ame1 and Okp1 as described before. Overexpression of both heterodimers in cells were either investigated in a wildtype or *skp1-3* mutant background. As it was described before, incubating the *skp1-3* mutant at 34 °C leads to a partially restricted activity of SCF, whereas incubation at 37 °C completely abolishes cell growth. In Western Blotting analysis, the overexpressed levels can be compared as shown in Figure 3.35. Logarithmic growing cultures were shifted to full medium containing galactose to induce overexpression and samples were taken immediately or after 3 and 5 hours. Ame1 and Okp1, when overexpressed, accumulate over time as seen before, and show an increased level in the *skp1-3* mutant background. Only Mcm21 is detectable, but Ctf19 should also be expressed similarly, because it is under the control of the same promoter as Mcm21. As seen before, not only Ame1 and Okp1 but also Mcm21 accumulates to higher protein levels in a *skp1-3* mutant strain background. For Ame1 and Okp1 a shift in SDS-PAGE gels is visible, which is reduced when Ame1 is mutated at the phosphorylation cluster. Although the CDK site in Okp1 is also mutated in AO-8A, a slowly migrating form is still present even if it is weaker. Interestingly, Ame1 levels are higher when all identified CDK sites on COMA are mutated to alanine (COMA-12A) in a *skp1-3* mutant strain background, which in turn leads to compromised growth.

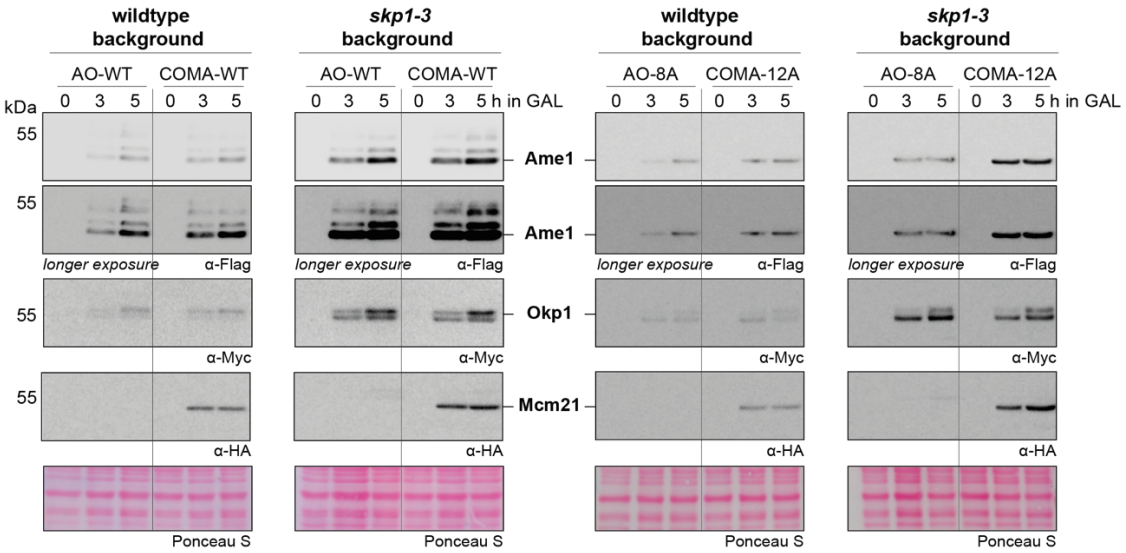

Figure 3.35: Overexpression of either COMA wildtype or COMA phospho-mutants. Ctf19/Mcm21 and Ame1/Okp1 were overexpressed from 2micron plasmids in either wildtype or *skp1-3* mutant background. In the *skp1-3* mutant, Ame1, Okp1 and Mcm21 accumulate to higher levels. Whereas the phosphorylation mutant of Okp1 together with Ame1 (AO-8A) does not change protein levels of Ame1, the overexpression of COMA-12A leads to an accumulation of Ame1 in *skp1-3* mutant background. Okp1 is phosphorylated to a higher extend in COMA and still phosphorylated in COMA-12A, which eliminates also a CDK site in Okp1.

To analyze the effect of COMA overexpression on cell viability, serial dilution assays were performed with strains that either contained the overexpression plasmids with Ame1/Okp1, Ctf19/Mcm21 or both together. In Figure 3.36 the overexpression of Ame1/Okp1 is compared to Ctf19/Mcm21 or COMA either as wildtype or as CDK null mutants (AO-8A, CM-4A or COMA-12A). In a wildtype strain background, increased levels of Ame1/Okp1 diminish cell viability only slightly compared to Ctf19/Mcm21, whereas overexpression of the tetrameric complex COMA shows a clear growth defect. These effects are even stronger in a *skp1-3* mutant background (Figure 3.36B) especially at 30 °C and 34 °C. The CDK null mutants of Ame1/Okp1, Ctf19/Mcm21 or COMA only slightly increase the growth defects seen with the wildtype versions. The results indicate that controlling the protein levels of COMA is a much more critical task for the cell, compared to the levels of individual AO or CM subcomplexes. This is clearly indicated by the observation that overexpression of COMA, but not of AO or CM is toxic, both in wildtype and in *skp1-3* mutant backgrounds. On the other hand, COMA might be a better target for SCF^{Cdc4} and comprehensive phosphorylation creates a stronger phospho-degron, which in turn is most-likely ubiquitinated more efficiently.

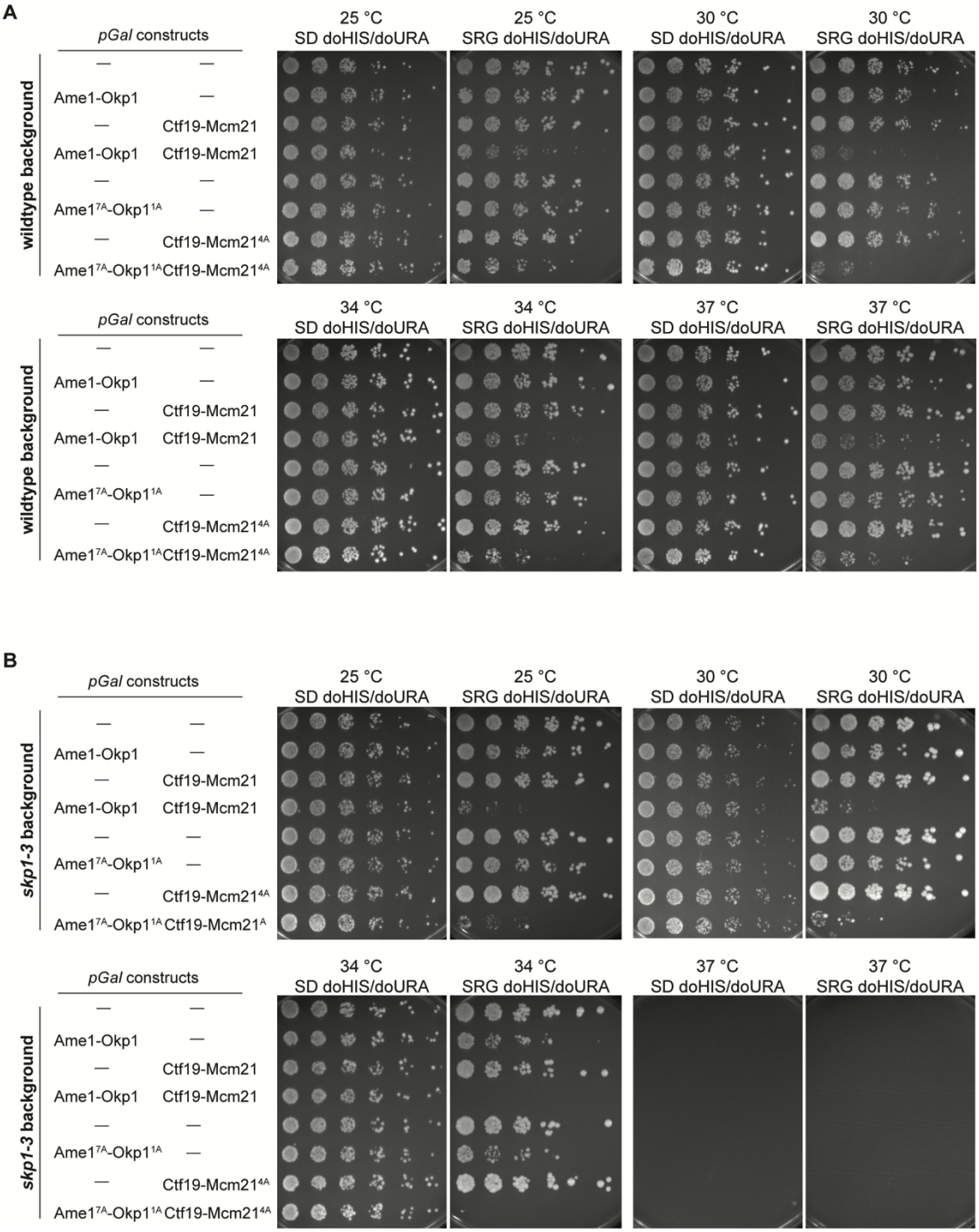

Figure 3.36: Overexpression of COMA diminishes growth in a wildtype and *skp1-3* mutant background. Serial dilution assay of Ame1/Okp1, Ctf19/Mcm21 or both together. Dilutions were spotted on both synthetic medium with glucose or galactose and incubated at different temperatures. Individual overexpression of Ame1/Okp1 or Ctf19/Mcm21 leads only to a minor growth defect in both wildtype (**A**) and *skp1-3* mutant strain (**B**) background, whereas overexpression of COMA diminishes the growth almost completely.

IV. DISCUSSION

In this thesis *S. cerevisiae* was used as a model organism to explore new aspects of the posttranslational regulation of the essential kinetochore protein Ame1. It was established that the essential subcomplex Ame1/Okp1 is phosphorylated in a cell cycle dependent manner at specific residues by the CDK complex Cdc28/Clb2. This phosphorylation event was excluded from being involved in Ame1/Okp1 heterodimeric complex formation or its binding to known interactors including Mif2, Mtw1c or to DNA. We also demonstrate a novel interaction between Ame1/Okp1 and Nkp1/Nkp2, which is mediated through the Ame1 C-terminus and does not require CDK phosphorylation. Instead, Ame1 is phosphorylated in a cell cycle dependent manner and a phosphorylated pool of Ame1 is ubiquitinated by SCF^{Cdc4}, which targets it for its degradation via the proteasome. The cell cycle dependent disappearance of phosphorylated Ame1 detected by Western Blotting is interpreted here as degradation rather than simple dephosphorylation. This is partly due to its observed timing, which appears to be prior to anaphase onset, when CDK opposing phosphatases such as Cdc14 would become active. This degradation is more efficient when assembled COMA complexes and not only Ame1 are phosphorylated by CDK, which leads to a multisite phosphorylation on different polypeptides and therefore to high affinity SCF^{Cdc4} binding. Also, it was shown, that the incorporation of Ame1/Okp1 into the kinetochore shields the subcomplex from efficient CDK phosphorylation and hence ubiquitination-driven degradation. In order to restrict degradation of Ame1/Okp1 to only those subcomplexes that are not needed for kinetochore assembly, it was shown that binding of the Mtw1c complex shields neighboring degron sequence from effective phosphorylation by CDK. In summary, a novel mechanism for a restricting kinetochore assembly to the centromeric region via CDK-mediated phosphorylation and ubiquitination was identified, which will be discussed here in detail.

4.1 A new role for the Ame1 C-terminus within kinetochore architecture

Apart from the various established functions of the Ame1/Okp1 dimer, the role of their potentially unstructured C-termini is largely unknown. Here we show that truncations of both C-termini alone or in combination does not hinder heterodimerization of the complex. This was expected, because the truncations did not include the coiled-coil region that was already established as the region responsible for dimer formation (Schmitzberger et al., 2017). Interestingly, as seen in Figure 3.6, we noticed that the truncation of both C-termini leads to a remarkable shift in its SEC elution to a smaller molecular weight as compared to wildtype. This shift might be too pronounced to be simply explained by truncating a complex by 115 amino acids which leads to decreasing the molecular weight of the complex from approximately 85 to 72 kDa. Therefore, the shift can be interpreted as an incapability of Ame1/Okp1 to form higher-order structures. Conversely, this means that Ame1/Okp1 full length might form multimers of dimers, e.g., tetramers. In SEC, these tetramers would elute at an earlier elution volume, which could be the case for Ame1/Okp1 full length. Future experiments using precise determination of the molecular weight by analytical ultracentrifugation of SEC coupled with multi-angle laser light scattering (SEC-MALLs) can help to shed light on this issue. How this formation of multimers might relate to the situation in the cell, especially in the context of the whole kinetochore, is not clear yet. There is evidence, that the number of Ame1/Okp1 molecules in a kinetochore might exceed that of COMA. It is possible that oligomeric assemblies of Ame1/Okp1 could be important for this particular pool of the complex. Nevertheless, our finding reveals the C-termini of Ame1/Okp1 as a novel interaction site for dimerization of the heterodimer. Furthermore, we characterize the C-terminus of Ame1 as a binding platform for the known CCAN components Nkp1/Nkp2. (Figure 3.8+3.9). This interaction to Ame1/Okp1 was already mapped before (Schmitzberger et al., 2017), but here we identify the Ame1 C-terminus as being the critical binding hub for this protein complex. The role of this interaction and the function of the non-essential heterodimer Nkp1/Nkp2 needs to be determined. This finding of Ame1 C-terminus being responsible for Nkp1/Nkp2 recruitment is confirmed by a recently published cryo-electron microscopy structure, that identifies the heterodimer at the very carboxyterminal end of the Ame1 protein (Yan et al., 2019). Interestingly, also the binding interface for Ctf19/Mcm21 was previously identified at the C-terminus of Okp1 (amino acids Asp320-Ile340). Therefore, the C-termini of Ame1 and Okp1 can be

defined as an interaction hub for other heterodimeric kinetochore proteins (including Ame1/Okp1, Ctf19/Mcm21 and Nkp1/Nkp2).

We were able to improve the functional map of the essential kinetochore protein Ame1 by another interaction partner (Figure 4.1). In summary, Ame1 binds Mtw1c at its very N-terminus, interacts with Okp1 via its coiled-coil region and Nkp1/Nkp2 through its C-terminal region. Apart from these known functions of Ame1, it comprises a region within its N-terminal half that harbors several CDK phosphorylation sites of unknown function, which was further characterized in this study.

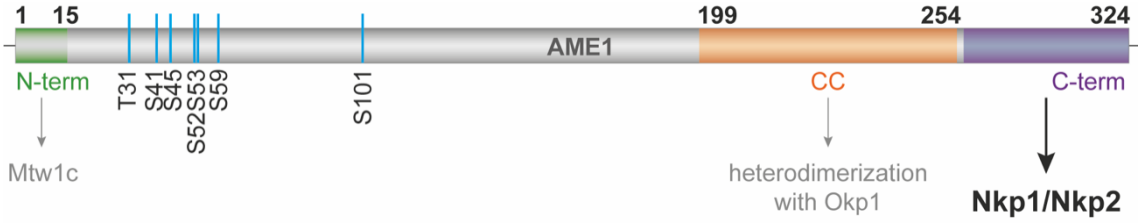

Figure 4.1 A new Ame1 structure highlighting the C-terminus as an interaction hub. Domain structure of Ame1 with highlighted regions important for interaction. The essential N-terminus is necessary and sufficient for Mtw1c binding, whereas the coiled-coil (CC) region is important for heterodimerization. A novel interaction hub at the C-terminus was identified here to be responsible for the interaction with Nkp1/Nkp2.

4.2 Ame1 can assemble into the kinetochore independently of its phosphorylation status

Here we show that the essential CCAN component Ame1 is phosphorylated in a cell cycle dependent manner as seen in a shift to a higher molecular weight in SDS-PAGE/Western Blotting. This phosphorylation was shown here to be at least partly mediated by CDK but may also involve additional kinases. We found no evidence that this phosphorylation is responsible for influencing the protein-protein interactions of Ame1 with its known kinetochore binding partners. This is interesting because many phosphorylation events of kinetochore proteins either lead to enhanced binding (e.g. binding of Mif2 to Mtw1c after phosphorylation of Dsn1 (Dimitrova et al., 2016)) or prevents binding (e.g., error correction of Ndc80c microtubule interactions upon phosphorylation of Ndc80c, as well as Ndc80-Dam1 interactions (Lampert et al., 2010)). In contrast, phosphorylation of Ame1 does not alter its interaction with Okp1, as Ame1-WT, Ame1-7A or Ame1-7E co-purified efficiently with Okp1, which confirms that heterodimerization with Okp1 is still intact when these seven residues of Ame1 are altered (see Figure 3.1). In addition, in binding assays using recombinant Mif2 or Mtw1c the Ame1 phosphorylation mutants were both able to bind as efficiently as the wildtype Ame1/Okp1 complex (see Figures 3.3 and 3.4), again showing that phosphorylation does not have a strong effect on the interaction. Furthermore, it was shown here that both phospho-mutants of Ame1 together with Okp1 are able to bind to centromeric DNA in EMSAs (see Figure 3.2), again confirming that phosphorylation of Ame1 does not alter its incorporation into the kinetochore. This leads to formulation of the interesting question as to the role of Ame1 phosphorylation. As it was characterized before, Cse4 deposition is restricted to centromeres with the help of degradation by different E3 ubiquitin ligases like Psh1 and SCF. This is of great importance, as it was shown that Cse4 overexpression leads to mis-incorporation into chromosome arms and hence ectopic kinetochore assembly away from centromeres. It seems likely that also other kinetochore components are regulated in their protein level, therefore Ame1 was analyzed for this possibility.

4.3 An overexpression system to study the consequences of increased AO/COMA levels in the cell

To study the consequences of elevated AO/COMA levels in the cells, an overexpression system was used which allowed Galactose-induced expression of either AOc or CMc

from individual 2micron (pESC) vectors, or the combined expression of all four subunits of the COMA complex from two vectors. The effect of increased levels of either the two subcomplexes, or the entire COMA complex could be followed in serial dilution assays. It was found that wildtype cells tolerate increased levels either AOc or CMc relatively well, with no strong effects being observable in bulk growth assays. Increased levels of COMA, however, appeared to be much more problematic for the cell, as viability was clearly decreased. Why is overexpression of COMA so much worse than overexpression of AOc, even though only AOc makes essential contacts to the outer kinetochore and therefore may pose a threat to titrate outer kinetochore components away from the centromere? It is conceivable that COMA poses a greater threat to the cell, because of its ability to form additional protein-protein interactions with other CCAN components. Especially Ctf19 is required for additional interactions with Iml3/Chl4, Ctf3 and others. This may lead to an increased capacity to form ectopic kinetochores, a situation that the cell needs to avoid. Increased protein levels of COMA may be worse than the effects of Cse4 overexpression, as this has been shown to be lethal only when Psh1 is deleted, but not in wildtype strain background (Collins et al., 2004; Hewawasam et al., 2010). Future experiments will have to characterize the functional consequences of increased COMA levels in more detail. For example, ChIP-qPCR or ChIP-seq could be used to test for the association of COMA with non-centromeric loci under conditions of overexpression. The pronounced effects of increased levels of COMA make it necessary for the cell to develop mechanisms that prevent toxic accumulation.

4.4 Ame1 phosphorylation by CDK promotes degradation via the E3 ligase SCF^{Cdc4}

Analyzing endogenous Ame1 over the cell cycle showed that it is subjected to phosphorylation throughout the whole cell cycle, as seen in the presence of slowly migrating forms in SDS-PAGE followed by Western Blotting. Interestingly, 15 to 30 minutes after releasing cells from a G1 arrest, which corresponds to S-Phase as seen by FACS analysis (see Figure 3.27), phospho-forms of Ame1 appeared, which persisted throughout the entire cell cycle with a small exception at the onset of M-Phase (45 minutes after release), where phospho-bands largely disappeared. This disappearance of phosphorylated Ame1 could be interpreted as dephosphorylation of this protein at mitotic onset, but there are several arguments that speak against this hypothesis. First, dephosphorylation of Ame1 would lead to a slow and gradual disappearance of slowly

migrating forms in Western Blotting, similar to the gradual accumulation of phosphorylation. In contrast, here we found a more rapid disappearance and also reappearance of phosphorylated Ame1 isoforms, speaking against dephosphorylation of Ame1 being the cause for this observation. Second, during early M-Phase, which is a time where Ame1 phospho-bands start to disappear, mainly kinases are active including Cdc28, Cdc5 and Swe1. On the contrary, the most prominent phosphatases involved in mitotic division are Cdc55 and Cdc14, which are both become active not before mitotic exit. Cdc14 has a preference for pThr or pSer residues and would therefore be the most likely candidate for Ame1 dephosphorylation. From FACS analysis, mitotic exit was determined to be around 60-75 minutes after release, but the disappearance of phosphorylated Ame1 is occurring with the onset of M-Phase (after 45 minutes) which excludes Cdc14 as the reason for Ame1 dephosphorylation. Therefore, a more feasible explanation is that a pool of phosphorylated Ame1 is degraded presumably at a very specific time window during cell cycle progression, which was shown to be the case for Ame1 as described below.

The expression of phosphorylation mutants of Ame1 in wildtype cells showed no obvious growth phenotypes in bulk assays. However, we could show an effect of Ame1 phospho-mutants, as we observed that an Ame1-7A mutant protein which cannot be phosphorylated, strongly accumulates in an overexpression setting compared to Ame1-WT (Figure 3.20). This was the first direct evidence that phosphorylation of Ame1 is important for regulation of its protein levels. A straightforward explanation for accumulation of the Ame1-7A mutant is the inability, or decreased ability, of cells to degrade this mutant protein. As stated in the introduction, proteins can be primed by CDK phosphorylation for their degradation via the ubiquitination pathway. Therefore, Ame1 might be degraded through an E3 ligase complex, which often is mediated by CDK phosphorylation as shown with other targets like Sic1 or Cdc6 (Al-Zain et al., 2015; Nash et al., 2001). In order to test this hypothesis for the role of Ame1 phosphorylation by CDK, Ame1 phosphorylation mutants were genetically combined with mutants of different ubiquitin ligases (see Figure 3.21). If Ame1 is a target for ubiquitination by one of the ubiquitin ligases tested, the protein levels of Ame1-WT should increase to comparable levels of Ame1-7A in the respective mutant strain upon overexpression. Indeed, Ame1-WT accumulated like Ame1-7A when cells carried mutations in several subunits of the E3 ligase complex SCF^{Cdc4} (Figure 3.23). Therefore, we not only reveal a mechanism for regulating protein levels of Ame1, but also identify the specific E3 ligase

responsible. Level regulation of kinetochore proteins is a highly important topic and will therefore be further discussed in the following sections.

4.5 CDK phosphorylation is required for regulation of Ame1 protein levels away from kinetochores

It was shown here that Ame1 is phosphorylated at specific times during the cell cycle, that a non-phosphorylatable form accumulates in the cell and that a non-functional SCF leads to accumulation of Ame1-WT to similar levels. This led to the interpretation that Ame1 is degraded via SCF^{Cdc4} during mitosis. A well characterized example of protein degradation mediated through CDK-phosphorylation is the degradation of Sic1 by SCF^{Cdc4}, described in detail in section 1.2.1. The E3 ligase SCF with the F-box protein Cdc4 is responsible for degradation of Ame1 as well, as seen in Figure 3.23. To elucidate the mechanism of CDK phosphorylation of Ame1 and Okp1 in more detail, in co-operation with the Loog lab in Estonia Ame1 and Okp1 were analyzed with regard to docking motifs for either Cdc28/Clb5 (S-Phase) or Cdc28/Clb2 (M-Phase). It was previously determined that cyclins can bind to specific motifs, that are often positioned downstream of the residues phosphorylated by CDK (Ord and Loog, 2019). Interestingly, Okp1 harbors two such sites that resemble the Clb5 docking motif (residues following K63 (KSLF) and residues following K95 (KQLRF)) and there is also evidence from quantitative kinase assays that identified Okp1 as a preferred target for S-Phase CDK, rather than M-Phase CDK (Figure 4.2). Ame1 does not show any obvious docking motifs for cyclin binding and is phosphorylated more efficiently by the M-Phase CDK complex Cdc28/Clb2, but also to a lesser degree by the S-Phase CDK complex (data provided by M. Örd). This could be interpreted as a timely regulated phosphorylation of Ame1/Okp1, in which S-Phase CDK is recruited to the subcomplex first via Okp1 and phosphorylating the subunits respectively. As S-Phase and M-Phase are not completely separated in budding yeast and M-Phase CDK already becomes active during S-Phase, the specificity of Ame1 for M-Phase CDK could be a hint for co-operative phosphorylation of Ame1/Okp1 that would favor degradation via SCF^{Cdc4}, through multisite phosphorylation of multiple phospho-degrons. Another regulatory mechanism for CDK activity is the binding of the phospho-adaptor protein Cks1 to phosphorylated TP sites, which can potentiate low affinity CDK binding (Koivomagi and Loog, 2011; Koivomagi et al., 2011b; McGrath et al., 2013). Ame1 harbors one such TP site (T31) which is the first

phosphorylated residue of the phosphorylation cluster and could possibly prime for CDK binding at the identified CPD sites (Figure 4.2). Taken together, this would mean, that Ame1 and Okp1 are phosphorylated by CDK during S- and M-Phase, which leads to binding of SCF^{Cdc4} in a phosphorylation dependent manner. Ubiquitination and degradation of free Ame1/Okp1 subcomplexes after proper kinetochore assembly would lead to a clearance of unused subcomplexes, that would otherwise favor ectopic kinetochore formation.

Taken together, we propose a mechanism in which Ame1 is phosphorylated via CDK which leads to its degradation via the ubiquitin-proteasome system. This is of importance for the cell, as high levels of kinetochore proteins are only needed for efficient assembly at S-Phase but is potentially dangerous for the cell and therefore is avoided at other times of the cell cycle, as we will discuss in the next chapter.

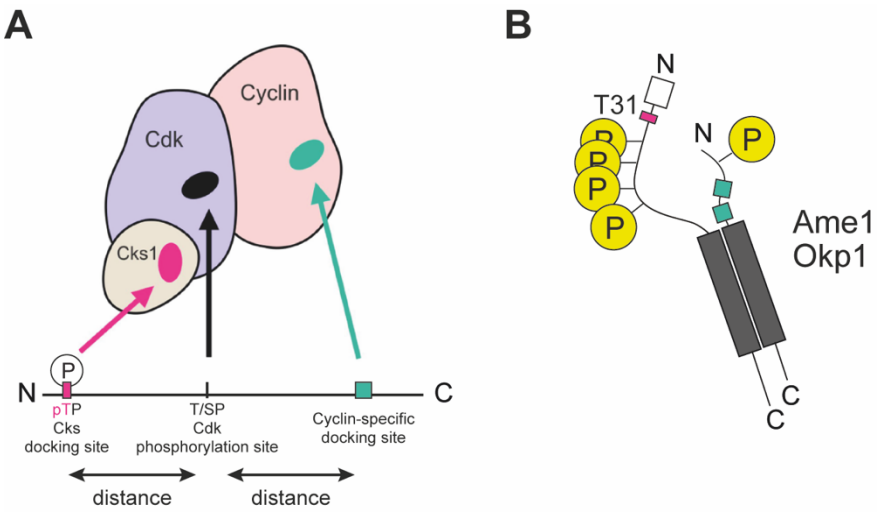

Figure 4.2: Ame1 and Okp1 are phosphorylated by CDK and show specific docking sites. CDK phosphorylation is enhanced through docking of either the phospho-adapter protein Cks1 or cyclins. (**A**) demonstrates the orientation of both docking sites respectively to CDK phosphorylation on proteins. (**B**) shows the Ame1/Okp1 heterodimer with phosphorylated residues (yellow), a potential Cks1 docking site at the phosphorylated residue T31 in Ame1 (magenta box) and two identified S-Phase cyclin docking motifs in Okp1 (green boxes) (data from Mihkel Örd) (adapted from (Örd and Loog, 2019), with changes).

4.6 Kinases other than CDK might also be involved in COMA phospho-regulation

As seen in Figure 3.14, Ame1 is not only phosphorylated by CDK, because when an Ame1-WT strain is combined with a *cdc28-13* temperature sensitive mutant, slowly migrating forms did not disappear completely, but one single band was still present under endogenous expression conditions. With the Ame1-7A mutation, where no slowly migrating forms are visible, all phosphorylated residues are mutated, not only the CDK sites. In addition, not all identified phosphorylation sites in the Ame1 N-terminal half follow the CDK consensus. The identified phospho-degron motif 1 SSP (Ser52+Ser53) follows a Polo-box binding domain consensus (Elia et al., 2003), and it is very likely that Ame1 gets phosphorylated by this additional kinase during cell division. It was also previously shown that the homolog of Ame1 in higher vertebrates CENP-U interacts with Plk1 and recruits Plk1 to centromeres until mitotic exit (Kang et al., 2011), which could also be the case in budding yeast. This is very interesting, as the generation of phospho-degrons often involves additional kinases as characterized for Sic1 or Eco1 (Lyons et al., 2013; Nash et al., 2001). This could also explain, why the mutation of this motif 1 into an optimal CPD^{ILTPP} leads to the dramatic changes in protein level as seen in Figure 3.25 using the overexpression system. However, to analyze this further, Ame1 mutants can be combined with *Cdc5* mutant strains, which is the Polo-like kinase in budding yeast, to gain insights in a combinatorial phosphorylation of Ame1 together with Cdc28, which would lead to a multisite phosphorylation by multiple kinases. Next to the experiment with *cdc28-13* mutant, also in the cell cycle experiments performed with Ame1-3A, which can only be phosphorylated at motif 1 (Ser52Ser53) and motif 2 (S41S45), a residual phosphorylated isoform can be detected in later timepoints (Figure 3.27). In these experiments, Ame1 gets phosphorylated gradually and two distinct isoforms appear, which we assume are phosphorylated subcomplexes of Ame1/Okp1, that get rapidly ubiquitinated by SCF^{Cdc4} and degraded via the proteasome. After disappearance of these slowly migrating forms, one single slow migration form reappears, that is present for the rest of the cell cycle and this could be additionally phosphorylated Ame1 by Cdc5. Interestingly, this slow migration form that is present just above the main band visible for Ame1, is also present in a cell cycle arrest using alpha factor, which halts cells in a G1-like state (Figure 3.26). These findings could be interpreted as motif 1 being phosphorylated by Polo-like kinase, that is present from S-Phase until cytokinesis (Lee et al., 2005). This phosphorylation of Cdc5 and Cdc28 would lead to multisite

phosphorylation and therefore creating of phospho-degron motifs in Ame1 that can be bound to SCF^{Cdc4} and lead to subsequent degradation of unused Ame1/Okp1 complexes.

4.7 Kinetochore assembly is restricted to centromeres

It is of great importance that kinetochore assembly is temporally and spatially restricted to centromeric regions, because formation of kinetochores outside centromeres will inevitably lead to segregation problems during mitosis, which will have fatal consequences for the cell. Compared to other higher eukaryotes, budding yeast does not have a clear separation between S- and M-Phase through a G2 phase, and the nucleus stays intact throughout the whole mitotic division. Because no real G2 exists, mitotic division already starts when S-Phase is still ongoing. Supporting this, centromeres are the earliest replicating loci on the chromosomes, allowing kinetochore assembly and start of bi-orientation even before replication has been completed. The dynamic microtubules are attached to chromosomes almost all the time, and this attachment is only shortly disrupted when centromeric regions are duplicated during the beginning of S-Phase. This is also the time when kinetochores have to be detached at least for that time window, to allow the replication fork to pass through the centromeres. It is still a matter of debate, if the existing kinetochore is completely disassembled, detached from the centromere or partially disassembled into subcomplexes. However at least a second kinetochore has to be assembled from scratch very quickly and efficiently to provide a binding interface for dynamic microtubules to allow bi-orientation as soon as possible. In addition, to ensure a prompt assembly of kinetochores, the expression of kinetochore proteins and subcomplexes is increased before S-Phase, to avoid protein levels being the limiting factor and allow rapid assembly of this multiprotein complex. How excess or redundant proteins that are not incorporated into kinetochores are removed, is not understood. Interestingly, Skp1 is also a member of the essential CBF3 complex, which binds to centromeric DNA and nucleates kinetochores on Cse4 nucleosome particles. Two decades ago, it was already hypothesized, that the CBF3 complex possibly functions as an E3 ligase because of its member Skp1 which is also found in all SCF complexes together with Sgt1 (Kitagawa et al., 1999). Skp1's localization to centromeres would allow a rapid switch of its function from kinetochore assembly to ubiquitination of substrates in complex with SCF^{Cdc4}. What can be stated is that the excess subcomplexes bear a potential threat for the cell as they could form ectopic kinetochores in either

chromosome arms or free kinetochore particles in the nucleoplasm. Both would have major consequences for the cell, as already stated above. Therefore, a mechanism that regulates kinetochore protein levels to restricted kinetochore assembly is crucial, but yet undefined. In addition, such a mechanism would need to be accurately regulated in time, because premature activation of kinetochore protein degradation would lead to hindrance in kinetochore assembly, when high amounts of such proteins are crucial.

However, other mechanisms to restrict kinetochore assembly to centromeres have already been described. These include conformational changes of kinetochore components allowing their interaction with other proteins only when bound to the kinetochore or when being phosphorylated by kinases at the kinetochore, posttranslational modifications that enhance binding between components at the kinetochore and the degradation of Cse4 that is not incorporated into the centromeric region. In more detail, the essential CCAN component Mif2 folds back into an auto-inhibitory conformation, which only allows Mtw1c binding upon Cse4 interaction (Killinger et al., 2020). A similar mechanism was also shown for the Ndc80c (Kudalkar et al., 2015) upon binding to Mtw1c. A conformational change also supports Mtw1c interaction with Mif2. Dsn1 harbors a flexible loop, which masks the Mif2 binding site on the Mtw1/Nnf1 heterodimer and is only released upon Ipl1/AuroraB phosphorylation (Akiyoshi et al., 2013a; Dimitrova et al., 2016; Petrovic et al., 2016). Other subcomplexes are stabilized in their binding upon phosphorylation, like Cnn1 to Ndc80c (Pekgoz Altunkaya et al., 2016). Additionally, regulation of Cse4 protein levels are of high importance as overexpression of Cse4 leads to ectopic kinetochore formation. It was shown that Cse4 is removed via ubiquitination mediated proteolysis, a mechanism that is shown here to be also responsible for Ame1 level regulation. For this thesis it is important to point out, that during metaphase four subcomplexes of COMA were detected, whereas in anaphase only three complexes were measured (Joglekar et al., 2006). And also, other subcomplexes vary in their numbers between metaphase and anaphase suggesting for a protein level regulation during mitosis, but most of them increase (Dhatchinamoorthy et al., 2017). Phosphorylation is one of the major posttranslational modifications in eukaryotes and it sometimes mediates its effect through ubiquitination, which regulates protein levels. Ame1 is phosphorylated via CDK, which leads to its ubiquitination via SCF and hence degradation, but also many other kinetochore components have been described as substrates for CDK as seen in Figure 1.7 and might therefore also be regulated by a similar mechanism. Generally speaking, the role of CDK phosphorylation of kinetochore proteins is insufficiently understood. The

fact that phosphorylation of Ame1 is not essential for viability speaks for the idea that additional proteins might be regulated via a similar pathway. Combination of phospho-mutants of several kinetochore proteins might lead to a more complete picture and confirm this hypothesis. So far, we know that Dsn1 is phosphorylated at six residues and Cnn1 is phosphorylated at five residues by CDK, but when both are substituted with alanine, overall growth is not diminished and interaction with known binding partners is not disturbed (S. Westermann, personal note). Interestingly, however, mutation of Dsn1 Ser264, a CDK site, to alanine increases the protein levels of Dsn1 and can suppress the lethal Dsn1 Ser240A Ser250A mutation (Akiyoshi et al., 2013b). However, combination of either Dsn1-6A or Cnn1-5A with Ame1-7A does not change the growth behavior when the proteins were expressed from their endogenous promoters using the anchor away technique (Supplementary Figure 3). Furthermore, Ame1 mutants either preventing or mimicking phosphorylation did not compromise growth when combined with other mutants like a complete deletion of *cnn1* or deletion of *ctf19* (Figure 3.12), which strengthens the idea that a more global phosphorylation of multiple CCAN components is needed for the described regulatory mechanism to work efficiently. Several kinetochore proteins are present in excess amounts when compared to their actual copy number at assembled kinetochores. Presumably this allows efficient and rapid assembly of new kinetochores in S-Phase and makes it likely that regulated degradation not only of Ame1 but also of other proteins occurs. Here we provide evidence that CDK phosphorylation of Ame1 (and Okp1) does not directly regulate kinetochore assembly e.g., by altering affinities for Ame1 interactors but leads to a regulation of protein levels through CDK-mediated degradation at a specific time of the cell cycle. This dependency on CDK phosphorylation for its degradation allows timely regulation of protein degradation, which is crucial to allow efficient kinetochore assembly first, before unused components are removed.

4.8 COMA complex formation might create a high affinity binding interface for SCF^{Cdc4}

SCF^{Cdc4} binding to substrates is often mediated through multisite phosphorylation of the substrate, involving several phosphorylation sites in unstructured regions of the target protein. This was characterized in great detail for the regulated destruction of the CDK inhibitor Sic1. Sic1 contains nine potential CPD sites, of which at least six have to be phosphorylated in order to bind to Cdc4 and be targeted for ubiquitin-transfer. As mentioned before in section 3.6.1, also Okp1 and Mcm21 are targets for CDK phosphorylation and not only Ame1 but the whole COMA complex could possibly be a target for SCF^{Cdc4}. The CDK sites T138, S139 and S141 identified on Mcm21 are positioned in the RWD domain, whereas the residue T88 is positioned on an extruded loop that was not ordered in the crystal structure from the recombinant Ctf19/Mcm21 heterodimer from *K. lactis*, but it is known that this loop is reaching out of the "V" shaped Ctf19/Mcm21 dimer (Schmitzberger et al., 2017), which makes it accessible for CDK phosphorylation. This could be a possibility to enhance degradation of this complex. The hypothesis is that Ame1 contains two potential CPD sites, which by themselves might not provide sufficient binding affinity for SCF, so that the additional CPD sites on Okp1 and Mcm21 would be crucial for high-affinity binding to Cdc4 in cells, employing a multisite phosphorylated substrate on several polypeptides. In cells, Ame1 is mostly assembled into COMA complexes (Hornung et al., 2014). This potential involvement of several proteins within the complex might allow fine tuning of degradation of the complex, which is only possible because none of the CPD sites within the complex consist of an optimal sequence. Optimal sequence here means the sequence that provides the maximum affinity for Cdc4 and thereby leads to the most effective degradation. Interestingly, the optimal CPD^{ILTPP} placed in Ame1 was sufficient to drastically decrease Ame1 levels to a minimum in the overexpression setting, to the degree that it was no longer detectable in SDS-PAGE followed Western Blotting (Figure 3.25), confirming that the CPD sites in Ame1 and probably also in Okp1 and Mcm21 are suboptimal (as seen as well in sequence analyses) and create a low affinity for SCF^{Cdc4} binding of both heterodimers. As seen in Sic1 however, suboptimal CPD sites are critical to create a switch-like degradation, as too early degradation would also lead to problems in cell cycle progression (Nash et al., 2001). Consistent with this Ame1-CPD^{ILTPP} displayed reduced fitness in a wildtype strain background but was able to partially suppress the temperature sensitivity of a *cdc4-1* mutant (Figure 3.25). Here, too efficient degradation of

Ame1/Okp1 or COMA complexes could lead to failures or delays in kinetochore assembly and hence to incorrect chromosome segregation. Therefore, suboptimal CPD sites that are distributed on different subunits of COMA, regulate the CDK-mediated ubiquitination and degradation of additional proteins, so that only subcomplexes that are not needed for kinetochore assembly are degraded. We propose that complex formation of Ame1/Okp1 and Ctf19/Mcm21, which both contain low-affinity CPD sites, creates a high-affinity binding site for Cdc4 as shown in Figure 4.3, which allows very specific regulation of its degradation.

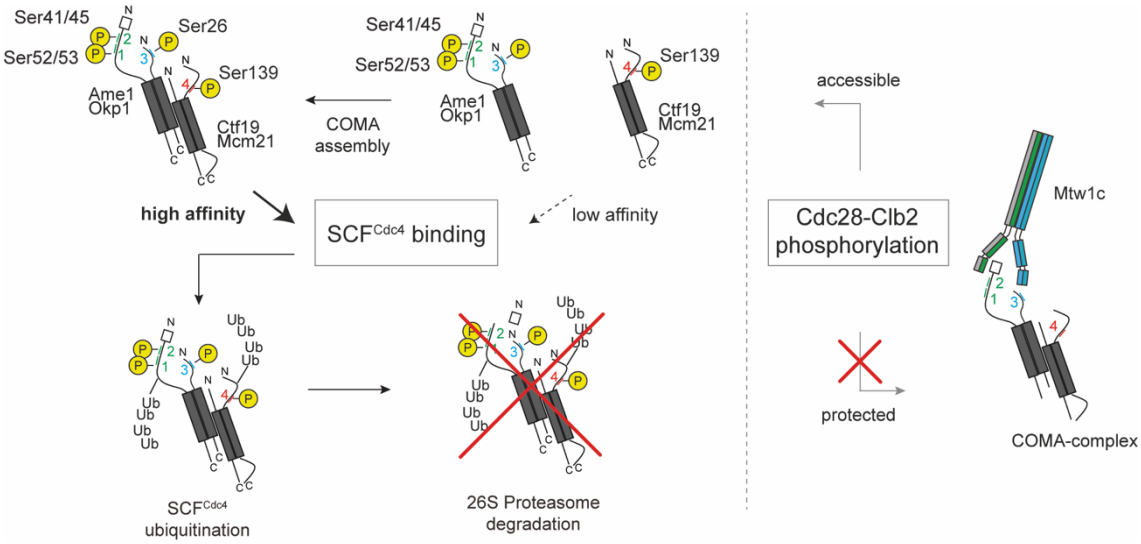

Figure 4.3: The COMA complex is only accessible for CDK-mediated ubiquitination when it is not incorporated into the kinetochore. The two heterodimers Ame1/Okp1 and Ctf19/Mcm21 each only harbor low affinity binding sites for SCF^{Cdc4}, whereas the formation of the COMA complex leads to a high affinity binding through combination of phosphorylation sites (marked in yellow). Ame1 harbors two CPD sites (green), Okp1 (blue) and Mcm21 (red) only a single CPD site. After ubiquitination via SCF^{Cdc4}, COMA is degraded through the 26S proteasome. The COMA complex is only accessible for phosphorylation by Cdc28/Clb2, when it is soluble in the nucleoplasm and not bound to the Mtw1c and therefore incorporation into the kinetochore shields COMA from CDK phosphorylation.

4.9 Incorporation into kinetochores prevents Ame1 degradation

An important and interesting question that arises when thinking about degradation mechanisms for excess kinetochore components is how the cell distinguishes between free proteins and proteins incorporated into the kinetochore. A straightforward and intuitive explanation would be that incorporation of proteins, which is always accompanied by binding of additional components, will prevent their accessibility by kinases or E3 ligases and thus hinder their degradation. In this thesis it is shown, that binding to the outer kinetochore component Mtw1c shields Ame1 phosphorylation and hence degradation, as it was shown that this binding decreases CDK phosphorylation in *in vitro* kinase assays (Figure 3.32). Therefore, incorporation of Ame1/Okp1 into the assembled kinetochore would hinder CDK phosphorylation through binding to Mtw1c, although other components might also take part in this. In addition, in these kinase assays phosphorylation was only decreased and not completely abolished (Figure 3.32). This could be explained by the fact that an excess of Ame1/Okp1 was preincubated with Mtw1c or the heterodimer Mtw1/Nnf1, that binds to Ame1 directly before Cdc28/Clb2 was added. As complexes have a specific association and disassociation constant, defining the thermodynamic equilibrium of the complex formation, some AOc will dissociate from Mtw1c/MNc. This probably provides a fraction of unbound AOc complexes left for Cdc28/Clb2 phosphorylation. As in this assay we cannot distinguish between bound and unbound Ame1, this will be seen in only a reduction in the phosphorylation of Ame1 bound to Mtw1c. Additionally, for further experiments the recombinant COMA complex can be used in kinase assays together with Mtw1c or MNc and the kinetics of phosphorylation could be monitored in a more precise manner. While biochemical and genetic evidence is provided here that ties Ame1 (COMA) phosphorylation to ubiquitination and hence degradation, it would be important to fully reconstitute the ubiquitination reaction *in vitro* with purified components (Swaney et al., 2013). This would allow to fully establish the molecular requirements for SCF recognition and ubiquitination in a defined setting, similar to what has been achieved for Sic1 (Petroski and Deshaies, 2005). Taken together, the mechanism described here could specifically allow the cell to provide of enough Ame1/Okp1 heterodimers or COMA complexes to efficiently assemble the kinetochore, but to reduce the level of free subcomplexes that bear a potential threat of ectopic kinetochore formation.

4.10 CDK-mediated ubiquitination via SCF^{Cdc4} as a novel mechanism for a regulated kinetochore assembly

Assuming that CDK-mediated degradation of CCAN components restrict kinetochore assembly, it does not play a direct role in the assembly process itself, as it was shown that preventing phosphorylation of Ame1 does not inhibit kinetochore incorporation of Ame1/Okp1. Most probably, phosphorylation of Ame1 is also not directly needed for kinetochore disassembly, as Ame1/Okp1 that is bound to Mtw1c is not accessible for phosphorylation at least by CDK, anymore, but still the components interact efficiently. Therefore, CDK phosphorylation of Ame1/Okp1 is not only directly important for stabilization of the assembled kinetochore, instead CDK-mediated degradation of excess subcomplexes is needed to avoid ectopic kinetochore assembly or prevent reduction of accessible kinetochore components due to their binding to free kinetochore particles. The model in Figure 4.4 shows how different E3 ligase complexes regulate kinetochore function during the mitotic cell cycle. In S-Phase, where a high abundance of kinetochore proteins is present in the cell, COMA complexes are phosphorylated by CDK only in a less efficient way, as only Okp1 is a better target for S-Phase CDK (M. Örd, personal note). This moderate CDK phosphorylation allows COMA complexes (apart from other kinetochore proteins) to be assembled into the kinetochore which ensures a rapid nucleation of this large molecular machinery. After kinetochores have efficiently assembled and the cells enter mitosis, M-Phase CDK complexes become active, COMA complexes that were not incorporated into the kinetochore are now a better target for CDK phosphorylation and degron sequences become fully phosphorylated. As COMA complexes within the kinetochore are prevented from being phosphorylated, only the soluble and free subcomplexes are targeted by the kinase. These heavily phosphorylated free subcomplexes create a high-affinity binding to the E3 ligase SCF^{Cdc4} which leads to degradation of this pool of complexes via the 26S proteasome. The efficient assembly of kinetochores and prevention of ectopic kinetochores via degradation of accessible components, allows chromosomes to achieve bi-orientation and cells to proceed from metaphase to anaphase. SCF^{Cdc4} has so far only been implicated in the regulation of the G1-S transition via degradation of Sic1. However, even in cells lacking Sic1, Cdc4 and the other subunits are essential proteins. In *sic1* deletion cells, Cdc4 mutants do not arrest at G1-S, but instead in M-Phase with a short spindle and a single undivided nucleus (Goh and Surana, 1999). The E3 ligase responsible for this transition to anaphase is the APC/C,

which inactivates M-Phase CDK complexes and destruction of Securin, leading to chromosome segregation.

Taken together, evidence is provided here, that a global phosphorylation of CCAN components allows ubiquitination via SCF^{Cdc4} and hence a clearance of unused, soluble kinetochore subcomplexes. This degradation is a novel mechanism that restricts kinetochore assembly to centromeres in budding yeast. Mediation of the phosphorylation through Cdc28/Clb2 allows timely regulation of this process, which is of high importance, because premature degradation of free kinetochore components would lead to a lack of these components to efficiently assemble kinetochores at the beginning of S-Phase. After these kinetochores assembled it becomes crucial to remove unused proteins, as access of these might lead to ectopic kinetochore formation or presence of free kinetochore particles, which are both obstacles during the next mitosis. We therefore not only proposed a mechanism of how free kinetochore components are removed from the cell, but also showed how this important process is restricted to a specific window during the cell cycle.

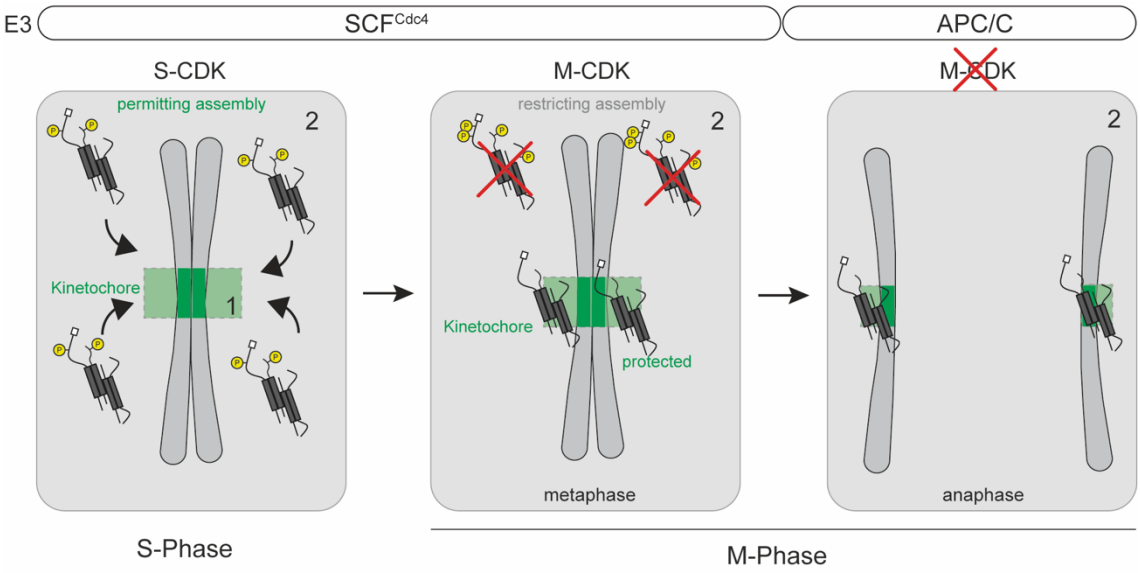

Figure 4.4: Different E3 ligases regulate kinetochore function during cell division. Kinetochore incorporation of the COMA complex is temporally and spatially regulated through CDK-mediated ubiquitination. The E3 ligase complex SCF^{Cdc4} is always active, but the phosphorylation of substrates changes mainly in S-Phase and early M-Phase, whereas the APC/C is active from anaphase until next G1, depending on which Co-activator protein, Cdc20 or Cdh1, is active. During S-Phase, assembly into kinetochores is permitted due to low CDK phosphorylation of COMA. In early M-Phase, COMA is heavily phosphorylated via CDK which leads to a high affinity binding interface for SCF^{Cdc4} interaction and hence to degradation via the 26S proteasome. Already incorporated COMA complexes are shielded from phosphorylation through binding to Mtw1c. In anaphase, M-Phase CDK complexes are degraded via the APC/C when bi-orientation occurs, which leads to chromosome segregation.

V. SUPPLEMENTARY DATA

Table S1: Extended list of all *S. cerevisiae* strains used in this study

Strain	Genotype	Reference
MLY2	Mat α, his3Δ200, ura3-52, lys2-801am, tor1-1 fpr1::loxP-LEU2-loxP RPL13A-2xFKBP12::loxP-TRP1-loxP, Ame1-FRB::KanMX, Δctf19(1-1021)::NatNT2	This study
MLY3	Mat α, his3Δ200, ura3-52::Ame1-WT-6xFlag::URA3, lys2-801am, tor1-1 fpr1::loxP-LEU2-loxP RPL13A-2xFKBP12::loxP-TRP1-loxP, Ame1-FRB::KanMX	This study
MLY5	Mat α, his3Δ200, ura3-52::Ame1-7A-6xFlag::URA3, lys2-801am, tor1-1 fpr1::loxP-LEU2-loxP RPL13A-2xFKBP12::loxP-TRP1-loxP, Ame1-FRB::KanMX	This study
MLY6	Mat α, his3Δ200, cnn1Δ::HIS3, ura3-52::Ame1-WT-6xFlag::URA3, lys2-801am, tor1-1 fpr1::loxP-LEU2-loxP RPL13A-2xFKBP12::loxP-TRP1-loxP, Ame1-FRB::KanMX	This study
MLY8	Mat α, his3Δ200, cnn1Δ::HIS3, ura3-52::Ame1-7A-6xFlag::URA3, lys2-801am, tor1-1 fpr1::loxP-LEU2-loxP RPL13A-2xFKBP12::loxP-TRP1-loxP, Ame1-FRB::KanMX	This study
MLY9	Mat α, his3Δ200, ura3-52::Ame1-WT-6xFlag::URA3, lys2-801am, tor1-1 fpr1::loxP-LEU2-loxP RPL13A-2xFKBP12::loxP-TRP1-loxP, Ame1-FRB::KanMX, Δctf19(1-1021)::NatNT2	This study
MLY11	Mat α, his3Δ200, ura3-52::Ame1-7A-6xFlag::URA3, lys2-801am, tor1-1 fpr1::loxP-LEU2-loxP RPL13A-2xFKBP12::loxP-TRP1-loxP, Ame1-FRB::KanMX, ctf19(1-1021)Δ::NatNT2	This study
MLY12	Mat a/α Ade2/ade2-1, his3Δ200/his3Δ200, ame1Δ::HIS3, leu2-3,112/leu2-3,112, ura3-52/ura3-52::Ame1-WT-6xFlag::URA3, Lys2/lys2-801	This study
MLY14	Mat a/α Ade2/ade2-1, his3Δ200/ his3Δ200, ame1Δ::HIS3, leu2-3,112/leu2-3,112, ura3-52/ura3-52::Ame1-7A-6xFlag::URA3, Lys2/lys2-801	This study
MLY15	Mat a, ade2-1, leu2-3,112, his3Δ200, ame1Δ::HIS3, ura3-52::Ame1-WT-6xFlag::URA3	This study

Strain	Genotype	Reference
MLY16	Mat α, ade2-1, leu2-3,112, his3Δ200, ame1Δ::HIS3, ura3-52::Ame1-WT-6xFlag::URA3	This study
MLY18	Mat a, ade2-1, leu2-3,112, his3Δ200, ame1Δ::HIS3, ura3-52::Ame1-5E-6xFlag::URA3	This study
MLY19	Mat a, ade2-1, leu2-3,112, his3Δ200, ame1Δ::HIS3, ura3-52::Ame1-7A-6xFlag::URA3	This study
MLY22	Mat α, leu2-3,112, his3Δ200, ame1Δ::HIS3, ura3-52::Ame1-WT-6xFlag::URA3	This study
MLY24	Mat α, leu2-3,112, his3Δ200, ame1Δ::HIS3, ura3-52::Ame1-7A-6xFlag::URA3	This study
MLY25	Mat a, ade2-1, leu2-3,112, Pds1-13xMyc::LEU2, his3Δ200, ame1Δ::HIS3, ura3-52::Ame1-WT-6xFlag::URA3	This study
MLY27	Mat a, ade2-1, leu2-3,112, Pds1-13xMyc::LEU2, his3Δ200, ame1Δ::HIS3, ura3-52::Ame1-7A-6xFlag::URA3	This study
MLY28	Mat a, ade2-1, leu2-3,112, Pds1-13xMyc::LEU2, his3Δ200, ura3-52	This study
MLY31	Mat α, his3Δ200, ura3-52::Ame1-7E-6xFlag, lys2-801am, tor1-1 fpr1::loxP-LEU2-loxP RPL13A-2xFKBP12::loxP-TRP1-loxP, Ame1-FRB::KanMX	This study
MLY32	Mat α, his3Δ200, cnn1Δ::HIS3, ura3-52::Ame1-7E-6xFlag, lys2-801am, tor1-1 fpr1::loxP-LEU2-loxP RPL13A-2xFKBP12::loxP-TRP1-loxP, Ame1-FRB::KanMX	This study
MLY33	Mat α, his3Δ200, ura3-52::Ame1-7E-6xFlag, lys2-801am, tor1-1 fpr1::loxP-LEU2-loxP RPL13A-2xFKBP12::loxP-TRP1-loxP, Ame1-FRB::KanMX, ctf19(1-1021)Δ::NatNT2	This study
MLY34	Mat a/α Ade2/ade2-1, his3Δ200/his3Δ200, ame1Δ::HIS3, leu2-3,112/leu2-3,112, ura3-52/ura3-52::Ame1-7E-6xFlag::URA3, Lys2/lys2-801	This study
MLY40	Mat a, ade2-1, leu2-3,112, his3Δ200, ame1Δ::HIS3, ura3-52::Ame1-7E-6xFlag::URA3	This study
MLY41	Mat α, lys2-801am, leu2-3,112, his3Δ200, ame1Δ::HIS3, ura3-52::Ame1-7E-6xFlag::URA3	This study
MLY52	Mat a/α Ade2/ade2-1, his3Δ200/his3Δ200, ame1Δ::HIS3, leu2-3,112/leu2-3,112, Ame1-	This study

Strain	Genotype	Reference
	7E-3xHA (endo)::LEU2, ura3-52/ura3-52, Lys2/lys2-801	
MLY53	Mat a/α Ade2/ade2-1, his3Δ200/his3Δ200, ame1Δ::HIS3, leu2-3,112/leu2-3,112, Ame1-7A-3xHA (endo)::LEU2, ura3-52/ura3-52, Lys2/lys2-801	This study
MBY54	Mat a, ade2-1, his3Δ200, ura3-52, Ame1-7E-3xHA(endo)::LEU2	This study
MBY56.1	Mat a, ade2-1, his3Δ200, ura3-52, leu2-3,112, Ame1-7A-3xHA (endo)::LEU2	This study
MBY70.1	Mat a, ade2-1, his3Δ200, dsn1Δ::HIS, ura3-52::Dsn1-6A::URA, leu2-3,112::Ame1-WT-3xHA (endo)::LEU2	This study
MBY71.1	Mat a, ade2-1, his3Δ200, dsn1Δ::HIS, ura3-52::Dsn1-6A::URA, leu2-3,112, Ame1-7E-3xHA (endo)::LEU2	This study
MBY72.1	Mat a, ade2-1, his3Δ200, dsn1Δ::HIS, ura3-52::Dsn1-6A::URA, leu2-3,112, Ame1-7A-3xHA (endo)::LEU2	This study
MBY79	Mat a, ade2-1, his3Δ200, ame1Δ::HIS3, leu2-3,112, ura3-52::Ame1-WT-6xFlag::URA3, Cse4-13xMyc::KanMX	This study
MBY81	Mat a, ade2-1, his3Δ200, ame1Δ::HIS3, leu2-3,112, ura3-52::Ame1-7E-6xFlag::URA3, Cse4-13xMyc::KanMX	This study
MBY83	Mat a, ade2-1, his3Δ200, ame1Δ::HIS3, leu2-3,112, ura3-52::Ame1-7A-6xFlag::URA3, Cse4-13xMyc::KanMX	This study
MBY87	Mat a/α Ade2/ade2-1, his3Δ200/ his3Δ200, ame1Δ::HIS3, leu2-3,112/leu2-3,112, ura3-52/ura3-52, Ame1-7E-3xHA (endo)::URA3, Lys2/lys2-801	This study
MBY88	Mat a/α Ade2/ade2-1, his3Δ200/ his3Δ200, ame1Δ::HIS3, leu2-3,112/leu2-3,112, ura3-52/ura3-52, Ame1-7A-3xHA (endo)::URA3, Lys2/lys2-801	This study
MBY89	Mat a, his3Δ200, leu2-3,112, ura3-52, Ame1-7E-3xHA (endo)::URA3	This study
MBY90	Mat α, his3Δ200, leu2-3,112, lys2-801am, ura3-52::Ame1-7E-3xHA (endo)::URA3	This study
MBY91	Mat a, his3Δ200, leu2-3,112, ura3-52, Ame1-7A-3xHA (endo)::URA3	This study
MBY92	Mat α, his3Δ200, leu2-3,112, lys2-801, ura3-52, Ame1-7A-3xHA (endo)::URA3	This study
MBY93	Mat a/α Ade2/ade2-1, his3Δ200, ame1Δ::HIS3, leu2-3,112/leu2-3,112, ura3-52/ura3-52, Ame1-WT-3xHA (endo)::URA3, Lys2/lys2-801	This study

Strain	Genotype	Reference
MBY96	Mat a, lys2-801am, ura3-52, Ame1-7E-3xHA (endo)::URA3, his3Δ200, cnn1Δ::HIS3, leu2-3,112::Cnn1-5A::LEU2	This study
MBY98	Mat a, ade2-1, his3Δ200, cnn1Δ::HIS3, leu2-3,112::Cnn1-5A::LEU2, ura3-52, Ame1-7A-3xHA (endo)::URA3	This study
MBY100	Mat a, his3Δ200, leu2-3,112, ura3-52, Ame1-WT-3xHA (endo)::URA3	This study
MBY106	Mat a, lys2-801am, ura3-52, Ame1-WT-3xHA (endo)::URA3, his3Δ200, cnn1Δ::HIS3, leu2-3,112::Cnn1-5A::LEU2	This study
MBY115.1	Mat α, his3Δ200, ame1Δ::HIS3, ura3-52::Ame1-WT-GFP::URA3, lys2-801am, leu2-3,112	This study
MBY117.1	Mat α, his3Δ200, ame1Δ::HIS3, ura3-52::Ame1-7E-GFP::URA3, lys2-801am, leu2-3,112	This study
MBY119.1	Mat α, his3Δ200, ame1Δ::HIS3, ura3-52::Ame1-7A-GFP::URA3, lys2-801am, leu2-3,112	This study
MBY152	Mat α, lys2-801am, leu2-3,112, his3Δ200, ura3-52, psh1Δ::NatNT2	This study
MBY153	Mat α, lys2-801am, leu2-3,112, his3Δ200, ura3-52, (2micron-pGAL::HIS3)	This study
MBY155	Mat α, lys2-801am, leu2-3,112, his3Δ200, ura3-52, (2micron-pGAL-Ame1-WT-1xFlag+Okp1-WT-1xMyc::HIS)	This study
MBY156	Mat α, lys2-801am, leu2-3,112, his3Δ200, ura3-52, (2micron-pGAL-Ame1-7A-1xFlag+Okp1-WT-1xMyc::HIS3)	This study
MBY157	Mat α, lys2-801am, leu2-3,112, his3Δ200, ura3-52, (2micron-pGAL-Ame1-7E-1xFlag+Okp1-WT-1xMyc::HIS3)	This study
MBY158	Mat α, lys2-801am, leu2-3,112, his3Δ200, ura3-52, psh1Δ::NatNT2, (2micron-pGAL::HIS3)	This study
MBY160	Mat α, lys2-801am, leu2-3,112, his3Δ200, ura3-52, psh1Δ::NatNT2, (2micron-pGAL-Ame1-WT-1xFlag+Okp1-WT-1xMyc::HIS3)	This study
MBY161	Mat α, lys2-801am, leu2-3,112, his3Δ200, ura3-52, psh1Δ::NatNT2, (2micron-pGAL-Ame1-7A-1xFlag+Okp1-WT-1xMyc::HIS3)	This study
MBY162	Mat α, lys2-801am, leu2-3,112, his3Δ200, ura3-52, psh1Δ::NatNT2, (2micron-pGAL-Ame1-7E-1xFlag+Okp1-WT-1xMyc::HIS3)	This study

Strain	Genotype	Reference
MBY163	Mat α, lys2-801am, leu2-3,112, his3Δ200, ura3-52, mad1Δ::KanMX, (2micron-pGAL::HIS3)	This study
MBY165	Mat α, lys2-801am, leu2-3,112, his3Δ200, ura3-52, mad1Δ::KanMX, (2micron-pGAL-Ame1-WT-1xFlag+Okp1-WT-1xMyc::HIS3)	This study
MBY166	Mat α, lys2-801am, leu2-3,112, his3Δ200, ura3-52, mad1Δ::KanMX, (2micron-pGAL-Ame1-7A-1xFlag+Okp1-WT-1xMyc::HIS3)	This study
MBY167	Mat α, lys2-801am, leu2-3,112, his3Δ200, ura3-52, mad1Δ::KanMX, (2micron-pGAL-Ame1-7E-1xFlag+Okp1-WT-1xMyc::HIS3)	This study
MBY209	Mat a/α Ade2/ade2-1, his3Δ200/ his3Δ200, ame1Δ::HIS3, leu2-3,112/leu2-3,112, ura3-52::Ame1-TM3-6xFlag::URA3, Lys2/lys2-801	This study
MBY210	Mat a/α Ade2/ade2-1, his3Δ200, ame1Δ::HIS3, leu2-3,112/leu2-3,112, ura3-52::Ame1-TM4-6xFlag::URA3, Lys2/lys2-801	This study
MBY211	Mat a/α Ade2/ade2-1, his3Δ200/ his3Δ200, ame1Δ::HIS3, leu2-3,112/leu2-3,112, ura3-52/ura3-52::Ame1-TM5-6xFlag::URA3, Lys2/lys2-801	This study
MBY212	Mat a/α Ade2/ade2-1, his3Δ200/ his3Δ200, ame1Δ::HIS3, leu2-3,112/leu2-3,112, ura3-52::Ame1-TM1-6xFlag::URA3, Lys2/lys2-801	This study
MBY213	Mat a/α Ade2/ade2-1, his3Δ200/his3Δ200, ame1Δ::HIS3, leu2-3,112/leu2-3,112, ura3-52::Ame1-TM2-6xFlag::URA3, Lys2/lys2-801	This study
MBY224	Mat α, his3Δ200, ura3-52::Ame1-TM1-6xFlag::URA3, lys2-801am, tor1-1 fpr1::loxP-LEU2-loxP RPL13A-2xFKBP12::loxP-TRP1-loxP, Ame1-FRB::KanMX	This study
MBY225	Mat α, his3Δ200, ura3-52::Ame1-TM2-6xFlag::URA3, lys2-801am, tor1-1 fpr1::loxP-LEU2-loxP RPL13A-2xFKBP12::loxP-TRP1-loxP, Ame1-FRB::KanMX	This study
MBY226	Mat α, his3Δ200, ura3-52::Ame1-TM3-6xFlag::URA3, lys2-801am, tor1-1 fpr1::loxP-LEU2-loxP RPL13A-2xFKBP12::loxP-TRP1-loxP, Ame1-FRB::KanMX	This study
MBY227	Mat α, his3Δ200, ura3-52::Ame1-TM4-6xFlag::URA3, lys2-801am, tor1-1 fpr1::loxP-	This study

Strain	Genotype	Reference
	LEU2-loxP RPL13A-2xFKBP12::loxP-TRP1-loxP, Ame1-FRB::KanMX	
MBY228	Mat α, his3Δ200, ura3-52::Ame1-TM5-6xFlag::URA3, lys2-801am, tor1-1 fpr1::loxP-LEU2-loxP RPL13A-2xFKBP12::loxP-TRP1-loxP, Ame1-FRB::KanMX	This study
MBY241	Mat α, lys2-801am, leu2-3,112, his3Δ200, ura3-52, (2micron-pGAL-Ame1-2A*-1xFlag+Okp1-WT-1xMyc::HIS3)	This study
MBY255	Mat α, lys2-801am, leu2-3,112, his3Δ200, ura3-52, (2micron-pGAL-Ame1-WT+ILTPP-1xFlag-Okp1WT-1xMyc::HIS3)	This study
MBY256	Mat α, lys2-801am, leu2-3,112, his3Δ200, ura3-52, (2micron-pGAL-Ame1-5A+ILTPP-1xFlag+Okp1-WT-1xMyc::HIS3)	This study
MBY275	Mat α, lys2-801am, leu2-3,112, his3Δ200, ura3-52, (2micron-pGAL-Ame1-T31A-1xFlag+Okp1WT-1xMyc::HIS3)	This study
MBY276	Mat α, lys2-801am, leu2-3,112, his3Δ200, ura3-52, (2micron-pGAL-Ame1-S45A-1xFlag+Okp1-WT-1xMyc::HIS3)	This study
MBY278	Mat α, lys2-801am, leu2-3,112, his3Δ200, ura3-52, (2micron-pGAL-Ame1-S41AS45A-1xFlag+Okp1-WT-1xMyc::HIS3)	This study
MBY279	Mat α, lys2-801am, leu2-3,112, his3Δ200, ura3-52, (2micron-pGAL-Ame1-S41A-1xFlag+Okp1-WT-1xMyc::HIS3)	This study
MBY292	Mat a, ura3-52, lys2-801, ade2-101, his3Δ200, trp1Δ63, leu2Δ1, skp1-3::LEU2, (2micron-pGAL-Ame1-WT-1xFlag+Okp1-WT-1xMyc::HIS3)	This study
MBY293	Mat a, ura3-52, lys2-801, ade2-101, his3Δ200, trp1Δ63, leu2Δ1, skp1-3::LEU2, (2micron-pGAL-Ame1-7A-1xFlag+Okp1-WT-1xMyc::HIS3)	This study
MBY308	Mat α, lys2-801am, leu2-3,112, his3Δ200, ura3-52, (2micron-pGAL-Ame1-3A-1xFlag+Okp1-WT-1xMyc::HIS3)	This study
MBY309	Mat α, lys2-801am, leu2-3,112, his3Δ200, ura3-52, (2micron-pGAL-Ame1-4A-1xFlag+Okp1-WT-1xMyc::HIS3)	This study
MBY310	Mat a, cdc53-1, ade2-1, trp1-1, can1-100, leu2-3,112, his3-11,15, ura3, psi+, ssd1-d2, (2micron-pGAL-Ame1-WT-1xFlag+Okp1-WT-1xMyc::HIS3)	This study
MBY311	Mat a, cdc53-1, ade2-1, trp1-1, can1-100, leu2-3,112, his3-11,15, ura3, psi+, ssd1-d2,	This study

Strain	Genotype	Reference
	(2micron-pGAL-Ame1-7A-1xFlag+Okp1-WT-1xMyc::HIS3)	
MBY312	Mat a, cdc34-2, ade2-1, trp1-1, can1-100, leu2-3,112, his3-11,15, ura3, psi+, ssd1-d2, (2micron-pGAL-Ame1-WT-1xFlag+Okp1-WT-1xMyc::HIS3)	This study
MBY313	Mat a, cdc34-2, ade2-1, trp1-1, can1-100, leu2-3,112, his3-11,15, ura3, psi+, ssd1-d2, (2micron-pGAL-Ame1-7A-1xFlag+Okp1-WT-1xMyc::HIS3)	This study
MBY314	Mat α, cdc4-1, ade2-1, trp1-1, can1-100, leu2-3,112, his3-11,15, ura3, psi+, ssd1-d2, (2micron-pGAL-Ame1-WT-1xFlag+Okp1-WT-1xMyc::HIS3)	This study
MBY315	Mat α, cdc4-1, ade2-1, trp1-1, can1-100, leu2-3,112, his3-11,15, ura3, psi+, ssd1-d2, (2micron-pGAL-Ame1-7A-1xFlag+Okp1-WT-1xMyc::HIS3)	This study
MBY316	Mat a, ade2-1, his3Δ200, trp1-1, ura3-52, leu2-3,112, grr1Δ::LEU2, lys2-801, (2micron-pGAL-Ame1-WT-1xFlag+Okp1-WT-1xMyc::HIS3)	This study
MBY317	Mat a, ade2-1, his3Δ200, trp1-1, ura3-52, leu2-3,112, grr1Δ::LEU2, lys2-801, (2micron-pGAL-Ame1-7A-1xFlag+Okp1-WT-1xMyc::HIS3)	This study
MBY318	Mat a/α Ade2/ade2-1, his3Δ200/his3Δ200, ame1Δ::HIS3, leu2-3,112/leu2-3,112, ura3-52/ura3-52::Ame1-3A-6xFlag::URA3, Lys2/lys2-801	This study
MBY319	Mat a/α Ade2/ade2-1, his3Δ200/his3Δ200, ame1Δ::HIS3, leu2-3,112/leu2-3,112, ura3-52/ura3-52::Ame1-4A-6xFlag::URA3, Lys2/lys2-801	This study
MBY322	Mat a, ade2-1, leu2-3,112, his3Δ200, ura3-52, mub1Δ::natNT2, (2micron-pGAL-Ame1-WT-1xFlag-Okp1-WT-1xMyc::HIS3)	This study
MBY323	Mat a, ade2-1, leu2-3,112, his3Δ200, ura3-52, mub1Δ::natNT2, (2micron-pGAL-Ame1-7A-1xFlag-Okp1-WT-1xMyc::HIS3)	This study
MBY324	Mat a, his3Δ200, ame1Δ::HIS3, ura3-52::Ame1-3A-6xFlag::URA3, leu2-3-112	This study
MBY327	Mat a, his3Δ200, ame1Δ::HIS3, ura3-52::Ame1-4A-6xFlag::URA3, leu2-3,112	This study
MBY330	Mat α, lys2-801am, leu2-3,112, his3Δ200, ura3-52, (2micron-pGAL-Ame1-WT-1xFlag+Okp1-1A-1xMyc::HIS3)	This study

Strain	Genotype	Reference
MBY331	Mat α, lys2-801am, leu2-3,112, his3Δ200, ura3-52, (2micron-pGAL-Ame1-7A-1xFlag+Okp1-1A-1xMyc::HIS3)	This study
MBY332	Mat a, ura3-52, lys2-801, ade2-101, his3Δ200, trp1Δ63, leu2Δ1, skp1-3::LEU2, (2micron-pGAL-Ame1-WT-1xFlag+Okp1-1A-1xMyc::HIS3)	This study
MBY333	Mat a, ura3-52, lys2-801, ade2-101, his3Δ200, trp1Δ63, leu2Δ1, skp1-3::LEU2, (2micron-pGAL-Ame1-7A-1xFlag+Okp1-1A-1xMyc::HIS3)	This study
MBY341	Mat a/α Ade2/ade2-1, his3Δ200/ his3Δ200, ame1Δ::HIS3, leu2-3,112/leu2-3,112, ura3-52/ura3-52::Ame1-5A1-6xFlag::URA3, Lys2/lys2-801 (only S52S53)	This study
MBY342	Mat a/α Ade2/ade2-1, his3Δ200/ his3Δ200, ame1Δ::HIS3, leu2-3,112/leu2-3,112, ura3-52/ura3-52::Ame1-5A1-6xFlag::URA3, Lys2/lys2-801 (only S41S45)	This study
MBY345	Mat a, his3Δ200, ame1Δ::HIS3, ura3-52::Ame1-5A1-6xFlag::URA3, ade2-3, leu2-3,112	This study
MBY347	Mat a, his3Δ200, ame1Δ::HIS3, ura3-52::Ame1-5A2-6xFlag::URA3, ade2-3, leu2-3,112	This study
MBY360	Mat α, cdc4-1, ade2-1, trp1-1, can1-100, leu2-3,112, his3-11,15, ura3, psi+, ssd1-d2, (2micron-pGAL-Ame1-WT+ILTPP-1xFlag+Okp1-WT-1xMyc::HIS3)	This study
MBY361	Mat α, cdc4-1, ade2-1, trp1-1, can1-100, leu2-3,112, his3-11,15, ura3, psi+, ssd1-d2, (2micron-pGAL-Ame1-5A+ILTPP-1xFlag-Okp1-WT-1xMyc::HIS3)	This study
MBY371	Mat a, his3Δ200, ame1Δ::HIS3, ura3-52::Ame1-3A-6xFlag::URA3, leu2-3,112, Pds1-13xMyc::LEU2	This study
MBY372	Mat α, his3Δ200, ame1Δ::HIS3, ura3-52::Ame1-4A-6xFlag::URA3, leu2-3,112, Pds1-13xMyc::LEU2	This study
MBY373	Mat a, his3Δ200, ame1Δ::HIS3, ura3-52::Ame1-5A1::URA3, ade2-3, leu2-3,112, Pds1-13xMyc::LEU2	This study
MBY374	Mat a, his3Δ200, ame1Δ::HIS3, ura3-52::Ame1-5A2::URA3, ade2-3, leu2-3,112, Pds1-13xMyc::LEU2	This study
MBY378	Mat a/α, ura3-52/ura3-52::Ame1-3A-6xFlag::URA3, Lys2/lys2-801, Ade2/ade2-	This study

Strain	Genotype	Reference
	101, his3Δ200/his3Δ200, ame1Δ::HIS3, Trp1/trp1Δ63, leu2Δ1, skp1-3::LEU2	
MBY379	Mat a/α, ura3-52/ura3-52::Ame1-4A-6xFlag::URA3, Lys2/lys2-801, Ade2/ade2-101, his3Δ200/his3Δ200, ame1Δ::HIS3, Trp1/trp1Δ63, leu2Δ1, skp1-3::LEU2	This study
MBY380	Mat a, his3Δ200, ame1Δ::HIS3, ura3-52::Ame1-3A-6xFlag::URA3, lys2-801, trp1-1, leu2-3,112, skp1-3::LEU2	This study
MBY382	Mat a, his3Δ200, ame1Δ1::HIS3, ura3-52::Ame1-4A-6xFlag::URA3, ade2-3, lys2-801, trp1-1, leu2-3,112, skp1-3::LEU2	This study
MBY400	Mat a, ura3-52, lys2-801, ade2-101, his3Δ200, trp1Δ63, leu2Δ1, skp1-3::LEU2, (2micron-pGAL-empty::HIS3)	This study
MBY407	Mat α, lys2-801am, leu2-3,112, Pds1-13xMyc::LEU2, his3Δ200, ura3-52	This study
MBY411	Mat a, cdc34-2 , ade2-1, trp1-1, can1-100, leu2-3,112, his3-11,15, ura3, psi+, ssd1-d2, (2micron-pGAL-Ame1-WT-1xFlag + Okp1-1A-1xMyc::HIS3)	This study
MBY412	Mat a, cdc34-2, ade2-1, trp1-1, can1-100, leu2-3,112, his3-11,15, ura3, psi+, ssd1-d2, (2micron-pGAL-Ame1-7A-1xFlag + Okp1-1A-1xMyc::HIS3)	This study
MBY429	Mat a, ade2-1, leu2-3,112, his3Δ200, ura3-52, (2micron-SUP11 (pSW1455))	This study
MBY430	Mat a, ade2-1, his3Δ200, ura3-52, leu2-3,112, Ame1-WT-3xHA (endo)::LEU2, (2micron-SUP11 (pSW1455))	This study
MBY431	Mat a, ade2-1, his3Δ200, ura3-52, leu2-3,112, Ame1-7A-3xHA (endo)::LEU2, (2micron-SUP11 (pSW1455))	This study
MBY432	Mat a, ade2-1, his3Δ200, leu2-3,112, ura3-52, ctf19(1-1021)Δ::NatNT2	This study
MBY434	Mat a, ade2-1, leu2-3,112, his3-11-15, ame1Δ::HIS3, ura3-52::Ame1-WT+ILTPP-6xFlag::URA3, psi1x, ssd1-d2, cdc4-1	This study
MBY438	Mat a, ade2-1, leu2-3,112, his3-11-15, ame1Δ::HIS3, ura3-52::Ame1-5A+ILTPP-6xFlag::URA3, psi1x, ssd1-d2, cdc4-1	This study
MBY447	Mat a, ade2-1, his3Δ200, leu2-3,112, ura3-52, ctf19(1-1021)Δ::NatNT2, (2micron-SUP11 (pSW1455))	This study
MBY456	Mat α, lys2-801am, leu2-3,112, his3Δ200, ura3-52, (2micron-pGAL::HIS3), (2micron-pGAL::URA3)	This study

Strain	Genotype	Reference
MBY457	Mat α, lys2-801am, leu2-3,112, his3Δ200, ura3-52, (2micron-pGAL::HIS3), (2micron-pGAL-Mcm21-WT-3xHA+Ctf19-WT-1xMyc::URA3)	This study
MBY459	Mat a, ura3-52, lys2-801, ade2-101, his3Δ200, trp1Δ63, leu2Δ1, skp1-3::LEU2, (2micron-pGAL-empty::HIS3), (2micron-pGAL::URA3)	This study
MBY460	Mat a, ura3-52, lys2-801, ade2-101, his3Δ200, trp1Δ63, leu2Δ1, skp1-3::LEU2, (2micron-pGAL-empty::HIS3), (2-micron-pGAL-Mcm21-WT-3xHA+Ctf19-WT-1xMyc::URA3)	This study
MBY462	Mat α, lys2-801am, leu2-3,112, his3Δ200, ura3-52, (2micron-pGAL-Ame1-WT-1xFlag+Okp1-WT-1xMyc::HIS3), (2micron-pGAL::URA3)	This study
MBY463	Mat α, lys2-801am, leu2-3,112, his3Δ200, ura3-52, (2micron-pGAL-Ame1-WT-1xFlag+Okp1-WT-1xMyc::HIS3), (2micron-pGAL-Mcm21-WT-3xHA+Ctf19-WT-1xMyc::URA3)	This study
MBY464	Mat a, ura3-52, lys2-801, ade2-101, his3Δ200, trp1Δ63, leu2Δ1, skp1-3::LEU2, (2micron-pGAL-Ame1-WT-1xFlag+Okp1-WT-1xMyc::HIS3), (2micron-pGAL-Mcm21-WT-3xHA+Ctf19-WT-1xMyc::URA3)	This study
MBY465	Mat a, ura3-52, lys2-801, ade2-101, his3Δ200, trp1Δ63, leu2Δ1, skp1-3::LEU2, (2micron-pGAL-Ame1-WT-1xFlag+Okp1-WT-1xMyc::HIS3), (2micron-pGAL::URA3)	This study
MBY466	Mat α, lys2-801am, leu2-3,112, his3Δ200, ura3-52, (2micron-pGAL-Ame1-7A-1xFlag+Okp1-1A-1xMyc::HIS3), (2micron-pGAL::URA3)	This study
MBY468	Mat a, ura3-52, lys2-801, ade2-101, his3Δ200, trp1Δ63, leu2Δ1, skp1-3::LEU2, (2micron-pGAL-Ame1-7A-1xFlag+Okp1-1A-1xMyc::HIS3), (2micron-pGAL::URA3)	This study
MBY470	Mat α, lys2-801am, leu2-3,112, his3Δ200, ura3-52, (2micron-pGAL::HIS3), (2micron-pGAL-Mcm21-4A-3xHA+Ctf19-WT-1xMyc::URA3)	This study
MBY471	Mat a, ura3-52, lys2-801, ade2-101, his3Δ200, trp1Δ63, leu2Δ1, skp1-3::LEU2, (2micron-pGAL-empty::HIS3), (2micron-pGAL-Mcm21-4A-3xHA+Ctf19-WT-1xMyc::URA3)	This study

Strain	Genotype	Reference
MBY472	Mat α, lys2-801am, leu2-3,112, his3Δ200, ura3-52, (2micron-pGAL-Ame1-7A-1xFlag+Okp1-1A-1xMyc::HIS3), (2micron-pGAL-Mcm21-4A-3xHA+Ctf19-WT-1xMyc::URA3)	This study
MBY473	Mat a, ura3-52, lys2-801, ade2-101, his3Δ200, trp1Δ63, leu2Δ1, skp1-3::LEU2, (2micron-pGAL-Ame1-7A-1xFlag+Okp1-1A-1xMyc::HIS3), (2micron-pGAL-Mcm21-4A-3xHA+Ctf19-WT-1xMyc::URA3)	This study
DDY1502	Mat a, his3Δ200, mad1Δ::HIS3, leu2-3,112, ura3-52, ade2-101	Westermann lab
KKY31.1	a, ade2-1, his3Δ200, ura3-52, leu2-3, Ame1-WT-3xHA (endo)::LEU2	K. Killinger
SWY333	Mat α, ade2-1, leu2-3,112, his3Δ200, dsn1Δ::HIS3, ura3-52::Dsn1-6A::URA3	Westermann lab
SWY637	Mat a, leu2-3,112::Cnn1-5A-6xFlag::LEU2, ura3-52, ade2-1, his3Δ200, cnn1Δ::HIS3	Westermann lab
SWY383	MAT a; leu2, ura3-52, trp1, prb1-1122, pep4-3, pre1-451, Ame1-6xHis-6xFlag::KanMX	Westermann lab
SWY355	Mat a tor1-1 fpr1::loxP-LEU2-loxP RPL13A-2xFKBP12::loxP-TRP1-loxP	Westermann lab
SWY397	Mat a/α Ade2/ade2-1, his3Δ200/ his3Δ200, ame1Δ::HIS3, leu2-3,112/leu2-3,112, ura3-52/ura3-52, Lys2/lys2-801	Westermann lab
SWY536	Mat α, his3Δ200, ura3-52, lys2-801am, Ame1-FRB::KanMX	Westermann lab
SWY541	Mat α, his3Δ200, cnn1Δ::HIS3, leu2-3,112, ura3-52, lys2-801am, Ame1-FRB::KanMX,	Westermann lab
SWY926	Mat α, cdc28-13, ade1, his2, leu2-3, 122, trp1-1	Westermann lab
SWY2265	Mat α, lys2-801am, leu2-3,112, his3Δ200, mad1Δ::KanMX, ura3-52,	Westermann lab
SWY2335	Mat a, cdc53-1, ade2-1, trp1-1, can1-100, leu2-3,112, his3-11,15, ura3, psi+, ssd1-d2	Westermann lab
SWY2336	Mat a, cdc34-2, ade2-1, trp1-1, can1-100, leu2-3,112, his3-11,15, ura3, psi+, ssd1-d2	Westermann lab
SWY2337	Mat α, cdc4-1, ade2-1, trp1-1, can1-100, leu2-3,112, his3-11,15, ura3, psi+, ssd1-d2	Westermann lab
SWY2338	Mata, ade2-1, his3Δ200, trp1-1, ura3-52, leu2-3,112, grr1Δ::LEU2, lys2-801	Westermann lab

Table S2: Extended list of plasmids used for genetic experiments in *S. cerevisiae*

Plasmid	Characteristics	Reference
pMLU13	Ame1-7A-6xFlag in pRS306 (T31A, S41A, S45A, S52A, S53A, S59A, S101A)	This study
pMLU17	Ame1-7E-6xFlag in pRS306 (T31E, S41E, S45E, S52E, S53E, S59E, S101E)	This study
pMLU19	Ame1-7E-3xHA in pKK3	This study
pKK3	Ame1-WT-3xHA in pRS305	K. Killinger
pMLU20	Ame1-7A-3xHA in pKK3	This study
pMB29	Ame1-WT-GFP	This study
pMB30	Ame1-7E-GFP	This study
pMB31	Ame1-7A-GFP	This study
pMB53	Okp1-WT-1xMyc in pESC-HIS	This study
pMB54	Ame1-WT-1xFlag + Okp1-WT-1xMyc in pESC-HIS	This study
pMB55	Ame1-7A-1xFlag + Okp1-WT-1xMyc in pESC-HIS	This study
pMB56	Ame1-7E-1xFlag + Okp1-WT-1xMyc in pESC-HIS	This study
pMB64	Ame1-TM3-6xFlag in pRS306 (Δ31-89)	This study
pMB65	Ame1-TM4-6xFlag in pRS306 (Δ31-116)	This study
pMB66	Ame1-TM5-6xFlag in pRS306 (Δ31-187)	This study
pMB67	Ame1-TM1-6xFlag in pRS306 (Δ31-55)	This study
pMB68	Ame1-TM2-6xFlag in pRS306 (Δ31-75)	This study
pMB72	Ame1-S41A, S45A-1xFlag + Okp1-WT-1xMyc in pESC-HIS	This study
pMB73	Ame1-S52A, S53A-1xFlag + Okp1-WT-1xMyc in pESC-HIS	This study
pMB82	Ame1-WT-ILTPP-6xFlag in pRS306 (optimal CPD)	This study
pMB83	Ame1-5A-ILTPP-6xFlag in pRS306 (only optimal CPD)	This study
pMB84	Ame1-WT-ILTPP-1xFlag + Okp1-WT-1xMyc in pESC-HIS (optimal CPD)	This study
pMB85	Ame1-5A-ILTPP-1xFlag + Okp1-WT-1xMyc in pESC-HIS (only optimal CPD)	This study
pMB86	Ame1-T31A-1xFlag + Okp1-WT-1xMyc in pESC-HIS	This study
pMB87	Ame1-S45A-1xFlag + Okp1-WT-1xMyc in pESC-HIS	This study

Plasmid	Characteristics	Reference
pMB90	Ame1-S41A-1xFlag + Okp1-WT-1xMyc in pESC-HIS	This study
pMB95	Ame1-4A-1xFlag + Okp1-WT-1xMyc in pESC-HIS (S41A, S45A, S52A, S53A)	This study
pMB98	Ame1-3A-6xFlag in pRS306 (T31A, S59A, S101A)	This study
pMB99	Ame1-4A-6xFlag in pRS306	This study
pMB103	Ame1-WT-1xFlag + Okp1-S26A-1xMyc in pESC-HIS	This study
pMB104	Ame1-7A-1xFlag + Okp1-S26A-1xMyc in pESC-HIS	This study
pMB113	Ame1-5A1-6xFlag in pRS306 (T31A, S41A, S45A, S59A, S101A) (only S52 + S53)	This study
pMB114	Ame1-5A2-6xFlag in pRS306 (T31A, S52A, S53A, S59A, S101A) (only S41 + S45)	This study
pMB120	Mcm21-WT-3xHA + Ctf19-WT-1xMyc in pESC-URA	This study
pMB141	Mcm21-4A-3xHA + Ctf19-WT-1xMyc in pESC-URA (T88A, S138A, S139A, S141A)	This study
pSW39	Dsn1-6A in pRS306 (T12A, S69A, T162A, S170A), T198A, S264A)	Westermann lab
pSW125	Cnn1-5A in pRS305 (T3A, T21A, T42A, S177A, S192A)	Westermann lab
pSW731	Ame1-WT-6xFlag in pRS306	Westermann lab
pSW747	Ame1-WT-eGFP in pRS306	Westermann lab
pSW1455	pYCF1-CEN3; Sup11 on mini chromosome	Hieter et al., 1985
pDD526	Pds1-13xMyc in pRS305	Westermann lab

Plasmids, if not otherwise stated, originate from pRS plasmids (genomic integration) or pESC plasmids (2micron overexpression).

Table S3: Extended list of plasmids used for expression in *E. coli*

Plasmid	Characteristics	Reference
pMLU16	Ame1-7A-6xHis/Okp1-WT (T31A, S41A, S45A, S52A, S53A, S59A, S101A)	This study
pMLU18	Ame1-7E-6xHis/Okp1-WT (T31E, S41E, S45E, S52E, S53E, S59E, S101E)	This study
pMB43	Ame1-1-256-6xHis/Okp1-WT	This study
pMB44	Ame1-1-256-6xHis/Okp1-1-359	This study
pMB91	Ame1-2A1-6xHis/Okp1-WT (S52A, S53A)	This study
pMB92	Ame1-T31A-6xHis/Okp1-WT	This study
pMB93	Ame1-2A2-6xHis/Okp1-WT (S41A, S45A)	This study
pMB94	Ame1-4A-6xHis/Okp1-WT (S41A, S45A, S52A, S53A)	This study
pMB109	Ame1-WT-6xHis/Okp1-S26A	This study
pMB110	Ame1-4A-6xHis/Okp1-S26A	This study
pMB111	Ame1-7A-6xHis/Okp1-S26A	This study
pMB112	Ame1-3A-6xHis/Okp1-WT (T31A, S59A, S101A)	This study
pSW698	pST39-Mtw1/Nsl1/Nnf1/6xHis-Dsn1	Hornung et al., 2014
pSW785	pETDuett-6xHis-Nnf1/Mtw1	Hornung et al., 2014
pSW900	Ame1-WT-6xHis/Okp1-wWT	Hornung et al., 2014
pSW916	Ame1-126-324-6xHis/Okp1-WT	Westermann lab
pSW918	Ame1-WT-6xHis/Okp1-128-406	Westermann lab
pSW1409	Ame1-WT-6xHis/Okp1-1-359	Westermann lab
pSW1414	Nkp1-WT-6xHIS/Nkp2	Westermann lab

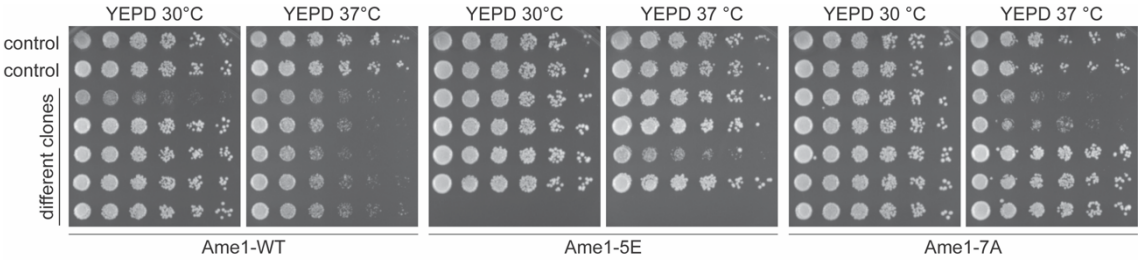

Figure S1: Serial dilution assay of integrated Ame1 phosphorylation mutants. Growth assay of Ame1-WT and phosphorylation mutants in serial dilution on YEPD. Plates were incubated at different temperatures and the corresponding plates of 30 °C and 37 °C are shown. For Ame1-WT and Ame1-7A five different clones are shown, from Ame1-5E only four different clones. The two control strains are the wildtype background strain DDY902 and a *mad1* deletion strain. No clear difference can be seen between Ame1-WT and the Ame1 phosphorylation mutants, as clonal differences are too high.

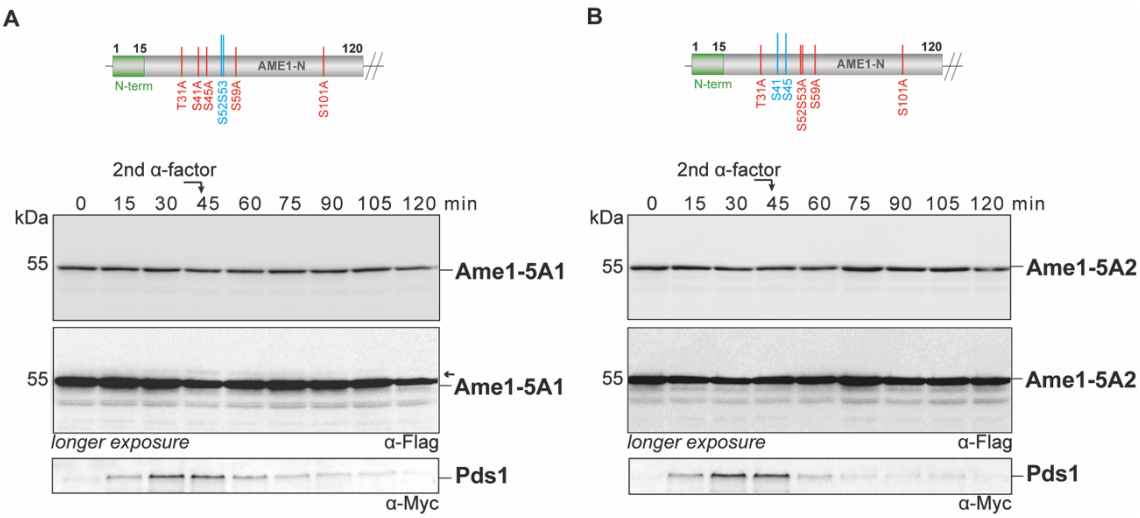

Figure S2: Cell cycle experiments with two additional Ame1 phosphorylation mutants to narrow down the important residues for slow migration forms. (**A**) Cell cycle progression of cells carrying Ame1-5A1 and Pds1-Myc is shown. In this mutant only S52 and S53 can be phosphorylated. Ame1-phosphorylation is only visible in a longer exposure and only a single slowly migrating form appears at 45 minutes (see arrow), which disappears around 75 minutes. Pds1 confirms that mitotic cells lack any phosphorylated isoforms of Ame1. The arrow indicates a phospho-isoform of Ame1-5A1. (**B**) Ame1-5A2 is combined with Pds1-Myc. Ame1-5A2 allows phosphorylation only at S41 and S45. No slowly migrating forms are visible, but the inability to phosphorylate Ame1 at its phospho-degron sites does not delay the cell cycle progression.

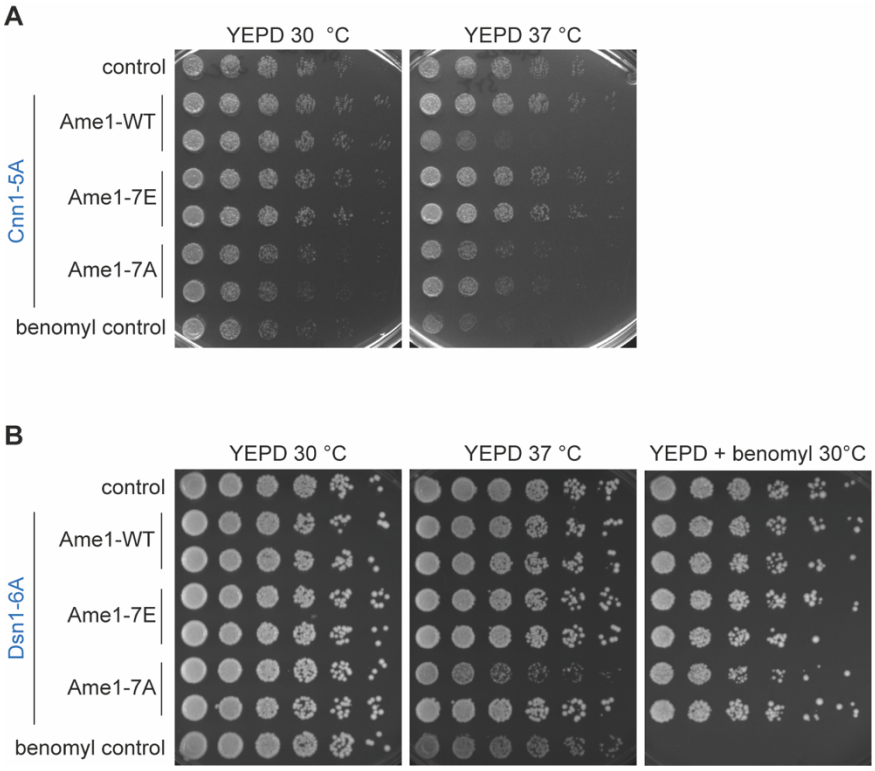

Figure S3: Combination of Ame1-WT or phosphorylation mutants with Cnn1-5A or Dsn1-6A does not compromise the growth. In (**A**) Ame1-WT/7A/7E are combined with a Cnn1-5A mutant strain, which has five previously identified CDK phosphorylation sites mutated to alanine. The combination does not have an effect on growth in serial dilution assays, although clonal differences exist. As controls in (**A**) and in (**B**) the wildtype background strain DDY904 and a *mad1* deletion strain is loaded. (**B**) shows a serial dilution assay of Ame1-WT/7A/7E combined with a Dsn1-6A mutant strain, which has six previously identified CDK phosphorylation sites mutated to alanine. Again, growth is not diminished in all tested mutants.

VI. REFERENCES

Akiyoshi, B., Nelson, C.R., and Biggins, S. (2013a). The aurora B kinase promotes inner and outer kinetochore interactions in budding yeast. Genetics *194*, 785-789.

Akiyoshi, B., Nelson, C.R., Duggan, N., Ceto, S., Ranish, J.A., and Biggins, S. (2013b). The Mub1/Ubr2 ubiquitin ligase complex regulates the conserved Dsn1 kinetochore protein. PLoS Genet *9*, e1003216.

Al-Zain, A., Schroeder, L., Sheglov, A., and Ikui, A.E. (2015). Cdc6 degradation requires phosphodegron created by GSK-3 and Cdk1 for SCFCdc4 recognition in Saccharomyces cerevisiae. Mol Biol Cell *26*, 2609-2619.

Albertson, D.G., and Thomson, J.N. (1982). The kinetochores of Caenorhabditis elegans. Chromosoma *86*, 409-428.

Amberg, D.C., Burke, D.J., and Strathern, J.N. (2005). Methods in Yeast Genetics. A Cold Spring Harbor Course Manual (Cold Spring Harbor, New York: Cold Spring Harbor Laboratory Press).

Anedchenko, E.A., Samel-Pommerencke, A., Tran Nguyen, T.M., Shahnejat-Bushehri, S., Popsel, J., Lauster, D., Herrmann, A., Rappsilber, J., Cuomo, A., Bonaldi, T.*, et al.* (2019). The kinetochore module Okp1(CENP-Q)/Ame1(CENP-U) is a reader for N-terminal modifications on the centromeric histone Cse4(CENP-A). EMBO J *38*.

Arents, G., Burlingame, R.W., Wang, B.C., Love, W.E., and Moudrianakis, E.N. (1991). The nucleosomal core histone octamer at 3.1 A resolution: a tripartite protein assembly and a left-handed superhelix. Proc Natl Acad Sci U S A *88*, 10148-10152.

Au, W.C., Dawson, A.R., Rawson, D.W., Taylor, S.B., Baker, R.E., and Basrai, M.A. (2013). A novel role of the N terminus of budding yeast histone H3 variant Cse4 in ubiquitin-mediated proteolysis. Genetics *194*, 513-518.

Au, W.C., Zhang, T., Mishra, P.K., Eisenstatt, J.R., Walker, R.L., Ocampo, J., Dawson, A., Warren, J., Costanzo, M., Baryshnikova, A.*, et al.* (2020). Skp, Cullin, F-box (SCF)-Met30 and SCF-Cdc4-Mediated Proteolysis of CENP-A Prevents Mislocalization of CENP-A for Chromosomal Stability in Budding Yeast. PLoS Genet *16*, e1008597.

Bailey, A.O., Panchenko, T., Sathyan, K.M., Petkowski, J.J., Pai, P.J., Bai, D.L., Russell, D.H., Macara, I.G., Shabanowitz, J., Hunt, D.F.*, et al.* (2013). Posttranslational modification of CENP-A influences the conformation of centromeric chromatin. Proc Natl Acad Sci U S A *110*, 11827-11832.

Bertoli, C., Skotheim, J.M., and de Bruin, R.A. (2013). Control of cell cycle transcription during G1 and S phases. Nat Rev Mol Cell Biol *14*, 518-528.

Biggins, S. (2013). The composition, functions, and regulation of the budding yeast kinetochore. Genetics *194*, 817-846.

Booher, R.N., Deshaies, R.J., and Kirschner, M.W. (1993). Properties of Saccharomyces cerevisiae wee1 and its differential regulation of p34CDC28 in response to G1 and G2 cyclins. EMBO J *12*, 3417-3426.

Bornens, M. (2002). Centrosome composition and microtubule anchoring mechanisms. Curr Opin Cell Biol *14*, 25-34.

Breitschopf, K., Bengal, E., Ziv, T., Admon, A., and Ciechanover, A. (1998). A novel site for ubiquitination: the N-terminal residue, and not internal lysines of MyoD, is essential for conjugation and degradation of the protein. EMBO J *17*, 5964-5973.

Cadwell, K., and Coscoy, L. (2005). Ubiquitination on nonlysine residues by a viral E3 ubiquitin ligase. Science *309*, 127-130.

Cahill, D.P., Lengauer, C., Yu, J., Riggins, G.J., Willson, J.K., Markowitz, S.D., Kinzler, K.W., and Vogelstein, B. (1998). Mutations of mitotic checkpoint genes in human cancers. Nature *392*, 300-303.

Cheeseman, I.M., Anderson, S., Jwa, M., Green, E.M., Kang, J., Yates, J.R., 3rd, Chan, C.S., Drubin, D.G., and Barnes, G. (2002). Phospho-regulation of kinetochore-microtubule attachments by the Aurora kinase Ipl1p. Cell *111*, 163-172.

Cheng, H., Bao, X., and Rao, H. (2016). The F-box Protein Rcy1 Is Involved in the Degradation of Histone H3 Variant Cse4 and Genome Maintenance. J Biol Chem *291*, 10372-10377.

Collins, K.A., Furuyama, S., and Biggins, S. (2004). Proteolysis contributes to the exclusive centromere localization of the yeast Cse4/CENP-A histone H3 variant. Curr Biol *14*, 1968-1972.

De Bondt, H.L., Rosenblatt, J., Jancarik, J., Jones, H.D., Morgan, D.O., and Kim, S.H. (1993). Crystal structure of cyclin-dependent kinase 2. Nature *363*, 595-602.

Dhatchinamoorthy, K., Shivaraju, M., Lange, J.J., Rubinstein, B., Unruh, J.R., Slaughter, B.D., and Gerton, J.L. (2017). Structural plasticity of the living kinetochore. J Cell Biol *216*, 3551-3570.

Dimitrova, Y.N., Jenni, S., Valverde, R., Khin, Y., and Harrison, S.C. (2016). Structure of the MIND Complex Defines a Regulatory Focus for Yeast Kinetochore Assembly. Cell *167*, 1014-1027 e1012.

Drinnenberg, I.A., deYoung, D., Henikoff, S., and Malik, H.S. (2014). Recurrent loss of CenH3 is associated with independent transitions to holocentricity in insects. Elife *3*.

Driscoll, J., and Goldberg, A.L. (1990). The proteasome (multicatalytic protease) is a component of the 1500-kDa proteolytic complex which degrades ubiquitin-conjugated proteins. J Biol Chem *265*, 4789-4792.

Duina, A.A., Miller, M.E., and Keeney, J.B. (2014). Budding yeast for budding geneticists: a primer on the Saccharomyces cerevisiae model system. Genetics *197*, 33-48.

Elia, A.E., Rellos, P., Haire, L.F., Chao, J.W., Ivins, F.J., Hoepker, K., Mohammad, D., Cantley, L.C., Smerdon, S.J., and Yaffe, M.B. (2003). The molecular basis for phosphodependent substrate targeting and regulation of Plks by the Polo-box domain. Cell *115*, 83-95.

Endicott, J.A., Noble, M.E., and Tucker, J.A. (1999). Cyclin-dependent kinases: inhibition and substrate recognition. Curr Opin Struct Biol *9*, 738-744.

Faesen, A.C., Thanasoula, M., Maffini, S., Breit, C., Muller, F., van Gerwen, S., Bange, T., and Musacchio, A. (2017). Basis of catalytic assembly of the mitotic checkpoint complex. Nature *542*, 498-502.

Fischbock-Halwachs, J., Singh, S., Potocnjak, M., Hagemann, G., Solis-Mezarino, V., Woike, S., Ghodgaonkar-Steger, M., Weissmann, F., Gallego, L.D., Rojas, J.*, et al.* (2019). The COMA complex interacts with Cse4 and positions Sli15/Ipl1 at the budding yeast inner kinetochore. Elife *8*.

Fitzgerald-Hayes, M., Clarke, L., and Carbon, J. (1982). Nucleotide sequence comparisons and functional analysis of yeast centromere DNAs. Cell *29*, 235-244.

Fleig, U., Beinhauer, J.D., and Hegemann, J.H. (1995). Functional selection for the centromere DNA from yeast chromosome VIII. Nucleic Acids Res *23*, 922-924.

Foley, E.A., and Kapoor, T.M. (2013). Microtubule attachment and spindle assembly checkpoint signalling at the kinetochore. Nat Rev Mol Cell Biol *14*, 25-37.

Goh, P.Y., and Surana, U. (1999). Cdc4, a protein required for the onset of S phase, serves an essential function during G(2)/M transition in Saccharomyces cerevisiae. Mol Cell Biol *19*, 5512-5522.

Haase, S.B., and Reed, S.I. (2002). Improved flow cytometric analysis of the budding yeast cell cycle. Cell Cycle *1*, 132-136.

Haruki, H., Nishikawa, J., and Laemmli, U.K. (2008). The anchor-away technique: rapid, conditional establishment of yeast mutant phenotypes. Mol Cell *31*, 925-932.

Hershko, A., Ciechanover, A., Heller, H., Haas, A.L., and Rose, I.A. (1980). Proposed role of ATP in protein breakdown: conjugation of protein with multiple chains of the polypeptide of ATP-dependent proteolysis. Proc Natl Acad Sci U S A *77*, 1783-1786.

Herskowitz, I. (1988). Life cycle of the budding yeast Saccharomyces cerevisiae. Microbiol Rev *52*, 536-553.

Hewawasam, G., Shivaraju, M., Mattingly, M., Venkatesh, S., Martin-Brown, S., Florens, L., Workman, J.L., and Gerton, J.L. (2010). Psh1 is an E3 ubiquitin ligase that targets the centromeric histone variant Cse4. Mol Cell *40*, 444-454.

Hieter, P., Mann, C., Snyder, M., and Davis, R.W. (1985). Mitotic stability of yeast chromosomes: a colony color assay that measures nondisjunction and chromosome loss. Cell *40*, 381-392.

Hinshaw, S.M., and Harrison, S.C. (2019). The structure of the Ctf19c/CCAN from budding yeast. Elife *8*.

Hochstrasser, M. (1996). Ubiquitin-dependent protein degradation. Annu Rev Genet *30*, 405-439.

Hochstrasser, M., Johnson, P.R., Arendt, C.S., Amerik, A., Swaminathan, S., Swanson, R., Li, S.J., Laney, J., Pals-Rylaarsdam, R., Nowak, J.*, et al.* (1999). The Saccharomyces cerevisiae ubiquitin-proteasome system. Philos Trans R Soc Lond B Biol Sci *354*, 1513-1522.

Hornung, P., Maier, M., Alushin, G.M., Lander, G.C., Nogales, E., and Westermann, S. (2011). Molecular architecture and connectivity of the budding yeast Mtw1 kinetochore complex. J Mol Biol *405*, 548-559.

Hornung, P., Troc, P., Malvezzi, F., Maier, M., Demianova, Z., Zimniak, T., Litos, G., Lampert, F., Schleiffer, A., Brunner, M.*, et al.* (2014). A cooperative mechanism drives budding yeast kinetochore assembly downstream of CENP-A. J Cell Biol *206*, 509-524.

Howell, A.S., and Lew, D.J. (2012). Morphogenesis and the cell cycle. Genetics *190*, 51-77.

Janke, C., Magiera, M.M., Rathfelder, N., Taxis, C., Reber, S., Maekawa, H., Moreno-Borchart, A., Doenges, G., Schwob, E., Schiebel, E.*, et al.* (2004). A versatile toolbox for PCR-based tagging of yeast genes: new fluorescent proteins, more markers and promoter substitution cassettes. Yeast *21*, 947-962.

Jaspersen, S.L., and Winey, M. (2004). The budding yeast spindle pole body: structure, duplication, and function. Annu Rev Cell Dev Biol *20*, 1-28.

Jeffrey, P.D., Russo, A.A., Polyak, K., Gibbs, E., Hurwitz, J., Massague, J., and Pavletich, N.P. (1995). Mechanism of CDK activation revealed by the structure of a cyclinA-CDK2 complex. Nature *376*, 313-320.

Joglekar, A.P., Bouck, D.C., Molk, J.N., Bloom, K.S., and Salmon, E.D. (2006). Molecular architecture of a kinetochore-microtubule attachment site. Nat Cell Biol *8*, 581-585.

Kadura, S., and Sazer, S. (2005). SAC-ing mitotic errors: how the spindle assembly checkpoint (SAC) plays defense against chromosome mis-segregation. Cell Motil Cytoskeleton *61*, 145-160.

Kaiser, P., Sia, R.A., Bardes, E.G., Lew, D.J., and Reed, S.I. (1998). Cdc34 and the F-box protein Met30 are required for degradation of the Cdk-inhibitory kinase Swe1. Genes Dev *12*, 2587-2597.

Kang, Y.H., Park, C.H., Kim, T.S., Soung, N.K., Bang, J.K., Kim, B.Y., Park, J.E., and Lee, K.S. (2011). Mammalian polo-like kinase 1-dependent regulation of the PBIP1-CENP-Q complex at kinetochores. J Biol Chem *286*, 19744-19757.

Kapust, R.B., Tozser, J., Fox, J.D., Anderson, D.E., Cherry, S., Copeland, T.D., and Waugh, D.S. (2001). Tobacco etch virus protease: mechanism of autolysis and rational design of stable mutants with wild-type catalytic proficiency. Protein Eng *14*, 993-1000.

Kataria, M., Mouilleron, S., Seo, M.H., Corbi-Verge, C., Kim, P.M., and Uhlmann, F. (2018). A PxL motif promotes timely cell cycle substrate dephosphorylation by the Cdc14 phosphatase. Nat Struct Mol Biol *25*, 1093-1102.

Killinger, K., Bohm, M., Steinbach, P., Hagemann, G., Bluggel, M., Janen, K., Hohoff, S., Bayer, P., Herzog, F., and Westermann, S. (2020). Auto-inhibition of Mif2/CENP-C ensures centromere-dependent kinetochore assembly in budding yeast. EMBO J *39*, e102938.

Kitagawa, K., Skowyra, D., Elledge, S.J., Harper, J.W., and Hieter, P. (1999). SGT1 encodes an essential component of the yeast kinetochore assembly pathway and a novel subunit of the SCF ubiquitin ligase complex. Mol Cell *4*, 21-33.

Kitamura, E., Tanaka, K., Kitamura, Y., and Tanaka, T.U. (2007). Kinetochore microtubule interaction during S phase in Saccharomyces cerevisiae. Genes Dev *21*, 3319-3330.

Klare, K., Weir, J.R., Basilico, F., Zimniak, T., Massimiliano, L., Ludwigs, N., Herzog, F., and Musacchio, A. (2015). CENP-C is a blueprint for constitutive centromere-associated network assembly within human kinetochores. J Cell Biol *210*, 11-22.

Kobayashi, J., and Matsuura, Y. (2017). Structure and dimerization of the catalytic domain of the protein phosphatase Cdc14p, a key regulator of mitotic exit in Saccharomyces cerevisiae. Protein Sci *26*, 2105-2112.

Koivomagi, M., and Loog, M. (2011). Cdk1: a kinase with changing substrate specificity. Cell Cycle *10*, 3625-3626.

Koivomagi, M., Valk, E., Venta, R., Iofik, A., Lepiku, M., Balog, E.R., Rubin, S.M., Morgan, D.O., and Loog, M. (2011a). Cascades of multisite phosphorylation control Sic1 destruction at the onset of S phase. Nature *480*, 128-131.

Koivomagi, M., Valk, E., Venta, R., Iofik, A., Lepiku, M., Morgan, D.O., and Loog, M. (2011b). Dynamics of Cdk1 substrate specificity during the cell cycle. Mol Cell *42*, 610-623.

Krenn, V., Overlack, K., Primorac, I., van Gerwen, S., and Musacchio, A. (2014). KI motifs of human Knl1 enhance assembly of comprehensive spindle checkpoint complexes around MELT repeats. Curr Biol *24*, 29-39.

Kudalkar, E.M., Scarborough, E.A., Umbreit, N.T., Zelter, A., Gestaut, D.R., Riffle, M., Johnson, R.S., MacCoss, M.J., Asbury, C.L., and Davis, T.N. (2015). Regulation of outer kinetochore Ndc80 complex-based microtubule attachments by the central kinetochore Mis12/MIND complex. Proc Natl Acad Sci U S A *112*, E5583-5589.

Kushnirov, V.V. (2000). Rapid and reliable protein extraction from yeast. Yeast *16*, 857-860.

Lampert, F., Hornung, P., and Westermann, S. (2010). The Dam1 complex confers microtubule plus end-tracking activity to the Ndc80 kinetochore complex. J Cell Biol *189*, 641-649.

Lampson, M.A., and Cheeseman, I.M. (2011). Sensing centromere tension: Aurora B and the regulation of kinetochore function. Trends Cell Biol *21*, 133-140.

Lang, J., Barber, A., and Biggins, S. (2018). An assay for de novo kinetochore assembly reveals a key role for the CENP-T pathway in budding yeast. Elife *7*.

Lee, K.S., Park, J.E., Asano, S., and Park, C.J. (2005). Yeast polo-like kinases: functionally conserved multitask mitotic regulators. Oncogene *24*, 217-229.

Lew, D.J. (2003). The morphogenesis checkpoint: how yeast cells watch their figures. Curr Opin Cell Biol *15*, 648-653.

Longtine, M.S., McKenzie, A., 3rd, Demarini, D.J., Shah, N.G., Wach, A., Brachat, A., Philippsen, P., and Pringle, J.R. (1998). Additional modules for versatile and economical PCR-based gene deletion and modification in Saccharomyces cerevisiae. Yeast *14*, 953-961.

Loog, M., and Morgan, D.O. (2005). Cyclin specificity in the phosphorylation of cyclin-dependent kinase substrates. Nature *434*, 104-108.

Lyons, N.A., Fonslow, B.R., Diedrich, J.K., Yates, J.R., 3rd, and Morgan, D.O. (2013). Sequential primed kinases create a damage-responsive phosphodegron on Eco1. Nat Struct Mol Biol *20*, 194-201.

Lyons, N.A., and Morgan, D.O. (2011). Cdk1-dependent destruction of Eco1 prevents cohesion establishment after S phase. Mol Cell *42*, 378-389.

Malumbres, M. (2014). Cyclin-dependent kinases. Genome Biol *15*, 122.

Manzano-Lopez, J., and Monje-Casas, F. (2020). The Multiple Roles of the Cdc14 Phosphatase in Cell Cycle Control. Int J Mol Sci *21*.

Maskell, D.P., Hu, X.W., and Singleton, M.R. (2010). Molecular architecture and assembly of the yeast kinetochore MIND complex. J Cell Biol *190*, 823-834.

Matellan, L., and Monje-Casas, F. (2020). Regulation of Mitotic Exit by Cell Cycle Checkpoints: Lessons From Saccharomyces cerevisiae. Genes (Basel) *11*.

McGrath, D.A., Balog, E.R., Koivomagi, M., Lucena, R., Mai, M.V., Hirschi, A., Kellogg, D.R., Loog, M., and Rubin, S.M. (2013). Cks confers specificity to phosphorylation-dependent CDK signaling pathways. Nat Struct Mol Biol *20*, 1407-1414.

Mishra, P.K., Olafsson, G., Boeckmann, L., Westlake, T.J., Jowhar, Z.M., Dittman, L.E., Baker, R.E., D'Amours, D., Thorpe, P.H., and Basrai, M.A. (2019). Cell cycle-dependent association of polo kinase Cdc5 with CENP-A contributes to faithful chromosome segregation in budding yeast. Mol Biol Cell *30*, 1020-1036.

Morgan, D.O. (1997). Cyclin-dependent kinases: engines, clocks, and microprocessors. Annu Rev Cell Dev Biol *13*, 261-291.

Morgan, D.O. (2007). The Cell Cycle. Principles of Control (New Science Press Ltd).

Musacchio, A., and Desai, A. (2017). A Molecular View of Kinetochore Assembly and Function. Biology (Basel) *6*.

Nash, P., Tang, X., Orlicky, S., Chen, Q., Gertler, F.B., Mendenhall, M.D., Sicheri, F., Pawson, T., and Tyers, M. (2001). Multisite phosphorylation of a CDK inhibitor sets a threshold for the onset of DNA replication. Nature *414*, 514-521.

Nasmyth, K. (2002). Segregating sister genomes: the molecular biology of chromosome separation. Science *297*, 559-565.

Ohkuni, K., Suva, E., Au, W.C., Walker, R.L., Levy-Myers, R., Meltzer, P.S., Baker, R.E., and Basrai, M.A. (2020). Deposition of Centromeric Histone H3 Variant CENP-A/Cse4 into Chromatin Is Facilitated by Its C-Terminal Sumoylation. Genetics *214*, 839-854.

Ord, M., and Loog, M. (2019). How the cell cycle clock ticks. Mol Biol Cell *30*, 169-172.

Orlicky, S., Tang, X., Willems, A., Tyers, M., and Sicheri, F. (2003). Structural basis for phosphodependent substrate selection and orientation by the SCFCdc4 ubiquitin ligase. Cell *112*, 243-256.

Pagliuca, C., Draviam, V.M., Marco, E., Sorger, P.K., and De Wulf, P. (2009). Roles for the conserved spc105p/kre28p complex in kinetochore-microtubule binding and the spindle assembly checkpoint. PLoS One *4*, e7640.

Pardo, B., Crabbe, L., and Pasero, P. (2017). Signaling pathways of replication stress in yeast. FEMS Yeast Res *17*.

Patton, E.E., Willems, A.R., Sa, D., Kuras, L., Thomas, D., Craig, K.L., and Tyers, M. (1998). Cdc53 is a scaffold protein for multiple Cdc34/Skp1/F-box proteincomplexes that regulate cell division and methionine biosynthesis in yeast. Genes Dev *12*, 692-705.

Pekgoz Altunkaya, G., Malvezzi, F., Demianova, Z., Zimniak, T., Litos, G., Weissmann, F., Mechtler, K., Herzog, F., and Westermann, S. (2016). CCAN Assembly Configures Composite Binding Interfaces to Promote Cross-Linking of Ndc80 Complexes at the Kinetochore. Curr Biol *26*, 2370-2378.

Pesenti, M.E., Prumbaum, D., Auckland, P., Smith, C.M., Faesen, A.C., Petrovic, A., Erent, M., Maffini, S., Pentakota, S., Weir, J.R.*, et al.* (2018). Reconstitution of a 26-Subunit Human Kinetochore Reveals Cooperative Microtubule Binding by CENP-OPQUR and NDC80. Mol Cell *71*, 923-939 e910.

Peters, J.M. (2002). The anaphase-promoting complex: proteolysis in mitosis and beyond. Mol Cell *9*, 931-943.

Petroski, M.D., and Deshaies, R.J. (2005). In vitro reconstitution of SCF substrate ubiquitination with purified proteins. Methods Enzymol *398*, 143-158.

Petrovic, A., Keller, J., Liu, Y., Overlack, K., John, J., Dimitrova, Y.N., Jenni, S., van Gerwen, S., Stege, P., Wohlgemuth, S.*, et al.* (2016). Structure of the MIS12 Complex and Molecular Basis of Its Interaction with CENP-C at Human Kinetochores. Cell *167*, 1028-1040 e1015.

Pickart, C.M. (2001). Mechanisms underlying ubiquitination. Annu Rev Biochem *70*, 503-533.

Przewloka, M.R., Venkei, Z., Bolanos-Garcia, V.M., Debski, J., Dadlez, M., and Glover, D.M. (2011). CENP-C is a structural platform for kinetochore assembly. Curr Biol *21*, 399-405.

Ranjitkar, P., Press, M.O., Yi, X., Baker, R., MacCoss, M.J., and Biggins, S. (2010). An E3 ubiquitin ligase prevents ectopic localization of the centromeric histone H3 variant via the centromere targeting domain. Mol Cell *40*, 455-464.

Richmond, T.J., Finch, J.T., Rushton, B., Rhodes, D., and Klug, A. (1984). Structure of the nucleosome core particle at 7 A resolution. Nature *311*, 532-537.

Rudner, A.D., and Murray, A.W. (2000). Phosphorylation by Cdc28 activates the Cdc20-dependent activity of the anaphase-promoting complex. J Cell Biol *149*, 1377-1390.

Salama, S.R., Hendricks, K.B., and Thorner, J. (1994). G1 cyclin degradation: the PEST motif of yeast Cln2 is necessary, but not sufficient, for rapid protein turnover. Mol Cell Biol *14*, 7953-7966.

Sambrook, J., and Russell, D.W. (2001). Molecular Cloning. A Laboratory Manual, Vol 3 (Cold Spring Harbor, New York: Cold Spring Harbor Laboratory Press).

Sathyan, K.M., Fachinetti, D., and Foltz, D.R. (2017). alpha-amino trimethylation of CENP-A by NRMT is required for full recruitment of the centromere. Nat Commun *8*, 14678.

Sato, N., Mizumoto, K., Nakamura, M., Maehara, N., Minamishima, Y.A., Nishio, S., Nagai, E., and Tanaka, M. (2001). Correlation between centrosome abnormalities and chromosomal instability in human pancreatic cancer cells. Cancer Genet Cytogenet *126*, 13-19.

Saunders, W.S., Shuster, M., Huang, X., Gharaibeh, B., Enyenihi, A.H., Petersen, I., and Gollin, S.M. (2000). Chromosomal instability and cytoskeletal defects in oral cancer cells. Proc Natl Acad Sci U S A *97*, 303-308.

Sazer, S. (2005). Nuclear envelope: nuclear pore complexity. Curr Biol *15*, R23-26.

Schleiffer, A., Maier, M., Litos, G., Lampert, F., Hornung, P., Mechtler, K., and Westermann, S. (2012). CENP-T proteins are conserved centromere receptors of the Ndc80 complex. Nat Cell Biol *14*, 604-613.

Schmitzberger, F., and Harrison, S.C. (2012). RWD domain: a recurring module in kinetochore architecture shown by a Ctf19-Mcm21 complex structure. EMBO Rep *13*, 216-222.

Schmitzberger, F., Richter, M.M., Gordiyenko, Y., Robinson, C.V., Dadlez, M., and Westermann, S. (2017). Molecular basis for inner kinetochore configuration through RWD domain-peptide interactions. EMBO J *36*, 3458-3482.

Sherman, F. (2002). Getting started with yeast. Methods Enzymol *350*, 3-41.

Sia, R.A., Herald, H.A., and Lew, D.J. (1996). Cdc28 tyrosine phosphorylation and the morphogenesis checkpoint in budding yeast. Mol Biol Cell *7*, 1657-1666.

Sikorski, R.S., and Hieter, P. (1989). A system of shuttle vectors and yeast host strains designed for efficient manipulation of DNA in Saccharomyces cerevisiae. Genetics *122*, 19-27.

Simon, M.N., De Virgilio, C., Souza, B., Pringle, J.R., Abo, A., and Reed, S.I. (1995). Role for the Rho-family GTPase Cdc42 in yeast mating-pheromone signal pathway. Nature *376*, 702-705.

Skowyra, D., Craig, K.L., Tyers, M., Elledge, S.J., and Harper, J.W. (1997). F-box proteins are receptors that recruit phosphorylated substrates to the SCF ubiquitin-ligase complex. Cell *91*, 209-219.

Swaney, D.L., Beltrao, P., Starita, L., Guo, A., Rush, J., Fields, S., Krogan, N.J., and Villen, J. (2013). Global analysis of phosphorylation and ubiquitylation cross-talk in protein degradation. Nat Methods *10*, 676-682.

Tan, S., Kern, R.C., and Selleck, W. (2005). The pST44 polycistronic expression system for producing protein complexes in Escherichia coli. Protein Expr Purif *40*, 385-395.

Tanaka, T.U., Stark, M.J., and Tanaka, K. (2005). Kinetochore capture and bi-orientation on the mitotic spindle. Nat Rev Mol Cell Biol *6*, 929-942.

Touati, S.A., and Uhlmann, F. (2018). A global view of substrate phosphorylation and dephosphorylation during budding yeast mitotic exit. Microb Cell *5*, 389-392.

van den Ent, F., and Lowe, J. (2006). RF cloning: a restriction-free method for inserting target genes into plasmids. J Biochem Biophys Methods *67*, 67-74.

Vanoosthuyse, V., and Hardwick, K.G. (2005). Bub1 and the multilayered inhibition of Cdc20-APC/C in mitosis. Trends Cell Biol *15*, 231-233.

Visintin, R., Craig, K., Hwang, E.S., Prinz, S., Tyers, M., and Amon, A. (1998). The phosphatase Cdc14 triggers mitotic exit by reversal of Cdk-dependent phosphorylation. Mol Cell *2*, 709-718.

Vleugel, M., Hoogendoorn, E., Snel, B., and Kops, G.J. (2012). Evolution and function of the mitotic checkpoint. Dev Cell *23*, 239-250.

Watanabe, N., Arai, H., Iwasaki, J., Shiina, M., Ogata, K., Hunter, T., and Osada, H. (2005). Cyclin-dependent kinase (CDK) phosphorylation destabilizes somatic Wee1 via multiple pathways. Proc Natl Acad Sci U S A *102*, 11663-11668.

Watanabe, N., Arai, H., Nishihara, Y., Taniguchi, M., Watanabe, N., Hunter, T., and Osada, H. (2004). M-phase kinases induce phospho-dependent ubiquitination of somatic Wee1 by SCFbeta-TrCP. Proc Natl Acad Sci U S A *101*, 4419-4424.

Weinert, T.A., and Hartwell, L.H. (1993). Cell cycle arrest of cdc mutants and specificity of the RAD9 checkpoint. Genetics *134*, 63-80.

Westermann, S., Cheeseman, I.M., Anderson, S., Yates, J.R., 3rd, Drubin, D.G., and Barnes, G. (2003). Architecture of the budding yeast kinetochore reveals a conserved molecular core. J Cell Biol *163*, 215-222.

Westermann, S., Drubin, D.G., and Barnes, G. (2007). Structures and functions of yeast kinetochore complexes. Annu Rev Biochem *76*, 563-591.

Westermann, S., Wang, H.W., Avila-Sakar, A., Drubin, D.G., Nogales, E., and Barnes, G. (2006). The Dam1 kinetochore ring complex moves processively on depolymerizing microtubule ends. Nature *440*, 565-569.

Wilkinson, K.D., Urban, M.K., and Haas, A.L. (1980). Ubiquitin is the ATP-dependent proteolysis factor I of rabbit reticulocytes. J Biol Chem *255*, 7529-7532.

Winey, M., and Bloom, K. (2012). Mitotic spindle form and function. Genetics *190*, 1197-1224.

Yan, K., Yang, J., Zhang, Z., McLaughlin, S.H., Chang, L., Fasci, D., Ehrenhofer-Murray, A.E., Heck, A.J.R., and Barford, D. (2019). Structure of the inner kinetochore CCAN complex assembled onto a centromeric nucleosome. Nature *574*, 278-282.

Yan, K., Zhang, Z., Yang, J., McLaughlin, S.H., and Barford, D. (2018). Architecture of the CBF3-centromere complex of the budding yeast kinetochore. Nat Struct Mol Biol *25*, 1103-1110.

Yeong, F.M., Lim, H.H., and Surana, U. (2002). MEN, destruction and separation: mechanistic links between mitotic exit and cytokinesis in budding yeast. Bioessays *24*, 659-666.

Zeitlin, S.G., Shelby, R.D., and Sullivan, K.F. (2001). CENP-A is phosphorylated by Aurora B kinase and plays an unexpected role in completion of cytokinesis. J Cell Biol *155*, 1147-1157.

Zheng, N., Schulman, B.A., Song, L., Miller, J.J., Jeffrey, P.D., Wang, P., Chu, C., Koepp, D.M., Elledge, S.J., Pagano, M.*, et al.* (2002). Structure of the Cul1-Rbx1-Skp1-F boxSkp2 SCF ubiquitin ligase complex. Nature *416*, 703-709.

Zheng, N., Wang, P., Jeffrey, P.D., and Pavletich, N.P. (2000). Structure of a c-Cbl-UbcH7 complex: RING domain function in ubiquitin-protein ligases. Cell *102*, 533-539.

AKNOWLEDGEMENTS

First of all, I would like to thank my supervisor Prof. Dr. Stefan Westermann for all his support during my PhD, for all the kind words and for always believing in me and this project. The last five years have taught me so much about myself and that would not have been possible without his kind, supportive and funny nature. I would also like to thank Prof. Dr. Doris Hellerschmied-Jelinek for taking over the second evaluation of my thesis. I also have to thank Dr. Delia Cosgrove for organizing the BIOME Graduate School of Biomedical Science, which brought me to many kind people in the core "genetics and cell biology" and trained my ability to present my data in presentations and poster sessions.

Next, I would like to thank all the current and former lab members for endless support, always helping out with lab materials and performing some lab work for or with me. In addition, I am very thankful for many fruitful discussions in our lab meetings and journal clubs together with Prof. Dr. Dominik Boos and his group. I also have to thank our collaboration partner Prof. Mart Loog and Mihkel Örd, who helped with some experiments regarding the phosphorylation of Ame1 and Okp1.

I am very thankful for my colleague Alex, who performed important *in vitro* kinase assays for this study and also for being the best practical course and seminar supervisor I could wish for. Without Sharvari, some experiments would have taken much longer, because she helped me a lot in the lab especially during the last months. I am also very happy to call her a friend, who taught me so much about India and its culture and the delicious food! Both Alex and Sharvari made the meetings we attended so much fun and never boring. Without our british mum Rita, our present secretary Stephi and our lab manager Simone the organization of the lab and of additional bureaucracy would not have been possible! I am happy that Simone helped me a lot with some of the Mcm21 experiments for this thesis. I also would like to thank Prof. Christian Johannes and Anika, Verena and Milena from AG Boos for many conversations and for their never-ending support. I am also thankful for meeting Jonas, Jenny and Nick together with all former lab members, who always gave constructive criticism during lab meetings, for a lot of laughter during coffee breaks, joyful Christmas parties and creating a good working atmosphere.

But most thankful am I for getting two best friends for life, Kerstin and Karo! These two are my heroes, my anchors, shoulders to cry on and the ones who always made me laugh, no matter how dark my mind was. Thank you for being my lab-friends, always and

forever! Both of them taught me a lot of important methods in the lab, helped me with a lot of biochemical and genetic experiments and always supported me.
My dearest sister-chromatid Kerstin is my lifesaver and partner in crime! No matter what challenge we had to face in the beginning with establishing the lab, we made it through all of them. Without her, I would have been lost so many times during the last five years.
My dearest Karo always showed me how to celebrate my results and myself! I loved chatting with her about everything, but most thankful am I for her support in the lab, without her, important experiments like the many cell-cycle analyses would be missing!
Thank you. Thank you both, for always believing in me at work or in our private lives, and always standing by my site.

Meiner gesamten Familie, insbesondere meinen Eltern Michael und Petra und meiner Schwester Jana, sowie meinen Freunden danke ich zutiefst, da sie immer an mich glauben und mich auf meinem Weg hierher und in den letzten 29 Jahren immer unterstützt haben. Sie waren in allen Lebenslagen an meiner Seite und haben mich immer auf den richtigen Weg zurückgeführt. Ohne euch, wäre ich nicht die Person, die ich heute bin.
Meine letzten Worte gehen an meinen wundervollen Ehemann Frederik, der immer an meiner Seite ist, an mich glaubt, mich immer unterstützt! DU bist mein größter Held! Danke, dass es dich gibt, ohne dich wäre das Leben nur halb so schön.

CURRICULUM VITAE

Der Lebenslauf ist in der Online-Version aus Gründen des Datenschutzes nicht enthalten.

Der Lebenslauf ist in der Online-Version aus Gründen des Datenschutzes nicht enthalten.

DECLARATIONS

Hiermit erkläre ich, gem. § 7 Abs. (2) d) + f) der Promotionsordnung der Fakultät für Biologie zur Erlangung des Dr. rer. nat., dass ich die vorliegende Dissertation selbständig verfasst und mich keiner anderen als der angegebenen Hilfsmittel bedient, bei der Abfassung der Dissertation nur die angegeben Hilfsmittel benutzt und alle wörtlich oder inhaltlich übernommenen Stellen als solche gekennzeichnet habe.

Essen, den _____ _____
Unterschrift des Doktoranden

Hiermit erkläre ich, gem. § 7 Abs. (2) e) + g) der Promotionsordnung der Fakultät für Biologie zur Erlangung des Dr. rer. nat., dass ich keine anderen Promotionen bzw. Promotionsversuche in der Vergangenheit durchgeführt habe und dass diese Arbeit von keiner anderen Fakultät/Fachbereich abgelehnt worden ist.

Essen, den _____ _____
Unterschrift des Doktoranden

Hiermit erkläre ich, gem. § 6 Abs. (2) g) der Promotionsordnung der Fakultät für Biologie zur Erlangung der Dr. rer. nat., dass ich das Arbeitsgebiet, dem das Thema „Regulation of the $Ctf19^{CCAN}$ protein complex at the budding yeast kinetochore“ zuzuordnen ist, in Forschung und Lehre vertrete und den Antrag von Miriam Böhm befürworte und die Betreuung auch im Falle eines Weggangs, wenn nicht wichtige Gründe dem entgegenstehen, weiterführen werde.

Essen, den _____ _____
Unterschrift eines Mitglieds der Universität Duisburg-Essen

Hiermit erkläre ich, gemäß § 6 Abs. (2) f) der Promotionsordnung der Fakultät für Biologie, dass mir die Gelegenheit zum vorliegenden Promotionsverfahren nicht kommerziell vermittelt worden ist. Insbesondere habe ich keine Organisation eingeschaltet, die gegen Entgelt Betreuerinnen und Betreuer für die Anfertigung von Dissertationen sucht oder die mir obliegenden Pflichten hinsichtlich der Prüfungsleistungen für mich ganz oder teilweise erledigt. Hilfe Dritter wurde bis jetzt und wird auch künftig nur in wissenschaftlich vertretbarem und prüfungsrechtlich zulässigem Ausmaß in Anspruch genommen.
Mir ist bekannt, dass Unwahrheiten hinsichtlich der vorstehenden Erklärung die Zulassung zur Promotion ausschließen bzw. später zum Verfahrensabbruch oder zur Rücknahme des Titels führen können.

Essen, den _____ _____

Unterschrift des Doktoranden